

Sheffield Hallam University

Study of surface modifications for improved selected metal (II-VI) semiconductor based devices.

BLOMFIELD, Christopher James.

Available from the Sheffield Hallam University Research Archive (SHURA) at:

<http://shura.shu.ac.uk/19362/>

A Sheffield Hallam University thesis

This thesis is protected by copyright which belongs to the author.

The content must not be changed in any way or sold commercially in any format or medium without the formal permission of the author.

When referring to this work, full bibliographic details including the author, title, awarding institution and date of the thesis must be given.

Please visit <http://shura.shu.ac.uk/19362/> and <http://shura.shu.ac.uk/information.html> for further details about copyright and re-use permissions.

101 441 780 5



SHEFFIELD HALLAM UNIVERSITY LIBRARY
CITY CAMPUS POND STREET
SHEFFIELD S1 1WB

~~7/5/96~~

~~19:11~~

14/5 1803

17/5 - 16.54.

28/5/96 - 16.59.

3.7. 16.59.

5/7 16:59

24.7.96

17.00.

15 OCT 2003

S. Hoپر.

ProQuest Number: 10694243

All rights reserved

INFORMATION TO ALL USERS

The quality of this reproduction is dependent upon the quality of the copy submitted.

In the unlikely event that the author did not send a complete manuscript and there are missing pages, these will be noted. Also, if material had to be removed, a note will indicate the deletion.



ProQuest 10694243

Published by ProQuest LLC (2017). Copyright of the Dissertation is held by the Author.

All rights reserved.

This work is protected against unauthorized copying under Title 17, United States Code
Microform Edition © ProQuest LLC.

ProQuest LLC.
789 East Eisenhower Parkway
P.O. Box 1346
Ann Arbor, MI 48106 – 1346

Study of Surface Modifications for Improved Selected Metal (II-VI) Semiconductor Based Devices.

Christopher James Blomfield BSc

A thesis submitted in partial fulfilment of the requirements of Sheffield Hallam
University for the degree of Doctor of Philosophy.

August 1995

Materials Research Institute, Sheffield Hallam University.

Abstract.

Metal-semiconductor contacts are of fundamental importance to the operation of all semiconductor devices. There are many competing theories of Schottky barrier formation but as yet no quantitative predictive model exists to adequately explain metal-semiconductor interfaces. The II-VI compound semiconductors CdTe, CdS and ZnSe have recently come to the fore with the advent of high efficiency photovoltaic cells and short wavelength light emitters. Major problems still exist however in forming metal contacts to these materials with the desired properties. This work presents results which make a significant contribution to the theory of metal/II-VI interface behaviour in terms of Schottky barriers to n-type CdTe, CdS and ZnSe.

Predominantly aqueous based wet chemical etchants were applied to the surfaces of CdTe, CdS and ZnSe which were subsequently characterised by X-ray photoelectron spectroscopy. The ionic nature of these II-VI compounds meant that they behaved as insoluble salts of strong bases and weak acids. Acid etchants induced a stoichiometric excess of semiconductor anion at the surface which appeared to be predominantly in the elemental or hydrogenated state. Alkaline etchants conversely induced a stoichiometric excess of semiconductor cation at the surface which appeared to be in an oxidised state.

Metal contacts were vacuum-evaporated onto these etched surfaces and characterised by current-voltage and capacitance-voltage techniques. The surface preparation was found to have a clear influence upon the electrical properties of Schottky barriers formed to etched surfaces. Reducing the native surface oxide produced near ideal Schottky diodes. All three materials exhibited the formation of several discrete Schottky barriers; for Au/n-CdTe $\phi_b = 0.64, 0.725, 0.96$ and 1.10 ± 0.02 eV, for Au/n-CdS $\phi_b = 0.86$ and 0.96 ± 0.02 eV. An extended study of Au, Ag and Sb contacts to n-ZnSe/n⁺-GaAs substrates again revealed the formation of several discrete Schottky barriers largely independent of the metal used; for Au/n-ZnSe $\phi_b = 0.90, 1.2, 1.45$ and 1.65 ± 0.04 eV, for Ag/n-ZnSe $\phi_b = 1.2$ and 1.45 ± 0.04 eV and for Sb/n-ZnSe $\phi_b = 1.45, 1.65, 1.8$ and 2.1 ± 0.04 eV.

Deep levels measured within this study and those reported in the literature led to the conclusion that Fermi level pinning by native defects is a dominant mechanism in Schottky barrier formation in these systems.

Acknowledgements.

I would first of all like to acknowledge the help and support of my supervisors, Dr IM Dharmadasa, Dr J Young and Dr J Haigh for their advice and guidance offered throughout the course of this study. I also owe many thanks to the technical staff of the Materials Research Institute, particularly Messrs G. Gregory and K. Blake for help and assistance with all matters regarding the Microlab. I am also in gratitude to Dr C Scott at the University of Hull and Dr R Coratger at the LOE-CNRS Toulouse for help and co-operation with DLTS and BEEM experiments respectively. Prof BC Cavenett and Dr K Prior at Heriot-Watt University kindly supplied a number of the ZnSe samples used within this study.

I would like to acknowledge the financial assistance of the Higher Education Funding Council for funding the research and the British Vacuum Council and the Institute of Materials Carnegie Award for funding my attendance at the ICMM '95 Barcelona.

Last but not least I have to thank my family for their continued support throughout my time in higher education, Sophie for putting up with me while writing up and the boys at 157 for all the good times.

"Any smoothly functioning technology will have the appearance of magic"

Arthur C Clarke

Contents.

Chapter 1. Introduction.

1.1	Introduction to metal-semiconductor interfaces	1
1.1.2	Schottky-Mott theory.	2
1.2	Physical properties and applications of II-VI compound semiconductors	3
1.2.1	Applications of ZnSe.	7
1.2.2	Applications of CdTe and CdS	9
1.3	Aims and objectives.	12
1.4	Approach.	13

Chapter 2 Models and theories of Schottky barriers.

2.1	Introduction.	15
2.2	Models of Schottky barrier formation.	15
2.2.1	The Bardeen model.	16
2.2.2	The linear model	17
2.2.3	The effective work function model	18
2.2.4	Models of Fermi level pinning	19
2.2.5	The pinch-off model	23
2.2.6	Summary of models	24
2.3	Current transport mechanisms	24
2.3.1	Thermionic emission	25
2.4	Capacitance of a Schottky barrier	35
2.4.1	Deviations from the ideal capacitance	36

Chapter 3 Review of literature.

3.1	Introduction	39
3.2	Experimental surface studies of CdTe, CdS and ZnSe.	39
3.2.1	Surface studies of CdTe	39
3.2.2	Surface studies of CdS	49
3.2.3	Surface studies of ZnSe	55
3.3	Properties of metal contacts to II-VI compounds	57
3.3.1	Introduction	57
3.3.2	Metal contacts to CdTe	57
3.3.3	Metal contacts to CdS	64
3.3.4	Metal contacts to ZnSe	66
3.4	Deep levels and defects in II-VI compounds	72
3.4.1	Introduction	72
3.4.2	Deep levels in CdTe	73
3.4.3	Deep levels in CdS	76
3.4.4	Deep levels in ZnSe	77
3.5	Summary of deep levels in CdTe, CdS and ZnSe	80

Chapter 4 Experimental techniques.

4.1	Introduction	81
4.2	Surface analysis	81
4.2.1	X-ray photoelectron spectroscopy	81
4.3	Wet chemical etching and contact fabrication	91
4.3.1	Introduction	91
4.3.2	Semiconductor samples	91
4.3.3	Wet chemical etching	91
4.3.4	Metal contact formation	92
4.4	Electrical characterisation	93

4.4.1	Current-voltage (I-V) characterisation	93
4.4.2	Capacitance-voltage (C-V) characterisation	97
4.5	Deep level transient spectroscopy	99
4.5.1	Theory	99
4.5.2	Instrumentation	102
4.6	Ballistic electron emission microscopy	103
4.6.1	Introduction	103
4.6.2	Theory	103
4.6.3	Instrum*entation	106

Chapter 5 Surface studies of II-VI compounds

5.1	Introduction	108
5.2	X-ray photoelectron spectroscopic surface analysis of CdTe, CdS and ZnSe	108
5.2.1	CdTe	110
5.2.2	CdS	120
5.2.3	ZnSe	128
5.4	Summary of surface etching of CdTe, CdS and ZnSe	135

Chapter 6 Electrical characterisation of contacts to etched surfaces.

6.1	Introduction	141
6.2	Au/n-CdTe	141
6.2.1	Non-ideal contacts	141
6.2.2	Ideal contacts	145
6.2.3	C-V characteristics	149
6.2.4	Ageing of contacts	151
6.2.5	Deep level transient spectroscopy of Au/n-CdTe	155

6.3	Au/n-CdS	156
6.3.1	Non-ideal contacts	156
6.3.2	Ideal contacts	160
6.3.2.1	Summary of ideal contacts	160
6.3.3	C-V characteristics	163
6.3.4	Ageing of Au/n-CdS	165
6.4	Metal contacts to ZnSe	170
6.4.1	Non-ideal contacts	170
6.4.2	Ideal contacts; Au/n-ZnSe	172
6.4.3	Ideal contacts, Ag/n-ZnSe	174
6.4.4	Ideal contacts, Sb/n-ZnSe	177
6.4.5	Summary of electrical measurements of metal/n-ZnSe devices	181
6.4.6	Deep level transient spectroscopy of Au/n-ZnSe	182
6.4.7	Ballistic electron emission microscopy studies of Au/n-ZnSe	184

Chapter 7 Discussion of results

7.1	Introduction	191
7.2	Schottky barrier heights in the context of present theories	192
7.2.1	Schottky model	192
7.2.2	Linear model	194
7.2.3	Effective work function model	195
7.2.4	Models of Fermi level pinning	196
7.3	Thermodynamics of metal-semiconductor interfaces	199
7.3.1	Introduction	199
7.3.2	Heat of reaction	200
7.3.3	Heat of formation	201
7.3.4	Summary	203
7.4	The role of defects in determining the Schottky barrier height	204

7.4.1	CdTe	204
7.4.2	CdS and ZnSe	206
7.4.3	Native defects and the Schottky barrier	208

Chapter 8 Conclusions and recommendations for future work.

8.1	Wet chemical etching	212
8.2	Electrical characterisation	213
8.3	Future work	215
8.4	Contribution to device technology	217

References	219
-------------------	------------

Appendix 1

A1.1	Refereed publications.	229
A1.2	Conferences attended	230

Chapter 1

Introduction.

1.1 Introduction to metal-semiconductor interfaces.

Metal-semiconductor contacts are of fundamental importance to the operation of virtually all semiconductor devices. Decades of research effort have been expended investigating the fundamental physics of such systems but as yet no unifying theory exists to unambiguously explain their behaviour. Often the metal contact is required to provide a gateway for electrons to and from the outside world, such contacts are of low resistance over a large range of electric fields, ideally obeying Ohm's law. Alternatively, the metal-semiconductor contact can form the active region of a specific device. In this instance the contact usually behaves in an asymmetric manner allowing preferential current flow in one direction, the metal-semiconductor system is said to be a rectifier. Many processes of contact formation are often based on empirically derived recipes rather than a thorough understanding of the underlying chemistry and physics. Although device dimensions have decreased by several orders of magnitude over the last three decades there is still uncertainty in producing metal contacts with the desired properties. Such factors now limit the progression to true nanoscale microelectronics. A general lack of understanding of the metal-semiconductor interface for many materials has meant that these materials have as yet not reached their full potential.

Models of metal-semiconductor contact behaviour have evolved in parallel with advances made in analytical methods. Early theories were based upon macroscopic a.c. and d.c. transport measurements. With the development of ultra high vacuum surface analysis came the facility to directly observe the emerging metal contact as sub-monolayers of metal were deposited onto the clean semiconductor surface. Such techniques yielded a wealth of

new experimental evidence which was followed in turn by new theoretical models born out of ever increasing computer power.

1.1.2 The Schottky-Mott theory.

The earliest theoretical attempts to explain the behaviour of metal-semiconductor systems were made almost simultaneously by Mott(1938) and Schottky(1938). Both hypothesised the formation of a potential barrier due to charge transfer at the interface between the metal and the semiconductor. Mott suggested that the difference in work functions of a semiconductor (or salt in his terminology) and a metal, induced a space charge region (which we now refer to as a depletion region) with a linear electrostatic potential. Schottky, on the other hand supposed that the space charge region had a constant density of charged impurities (ionised dopants) and that the electrostatic potential varied quadratically. The Schottky model was largely accepted, the potential barrier at the interface subsequently taking his name. The magnitude of the Schottky barrier ϕ_b , is the parameter responsible for the so called "ohmic" or "rectifying" nature of the metal contact. Figure 1.1 shows how a Schottky barrier may form when a metal and a semiconductor, of work functions ϕ_m and ϕ_s respectively are brought into intimate contact (in this case $\phi_m > \phi_s$, which is the most common case). Thermodynamic considerations dictate that the Fermi levels (E_F) of both materials must coincide, this in turn produces a transfer of electrons from the conduction band (E_c) of the semiconductor to the metal. The result of electron transfer is a build-up of negative charge at the surface of the metal. This charge is contained within a narrow surface region penetrating $< 0.5 \text{ \AA}$ into the metal known as the Thomas-Fermi screening distance, Rhoderick and Williams (1988). An equal but opposite charge must exist within the semiconductor, this charge in an n-type semiconductor consists of uncompensated donors created by receding conduction electrons. The charge in the semiconductor is distributed over a much larger distance due to the lower conductivity, a region then exists depleted of conduction electrons known as

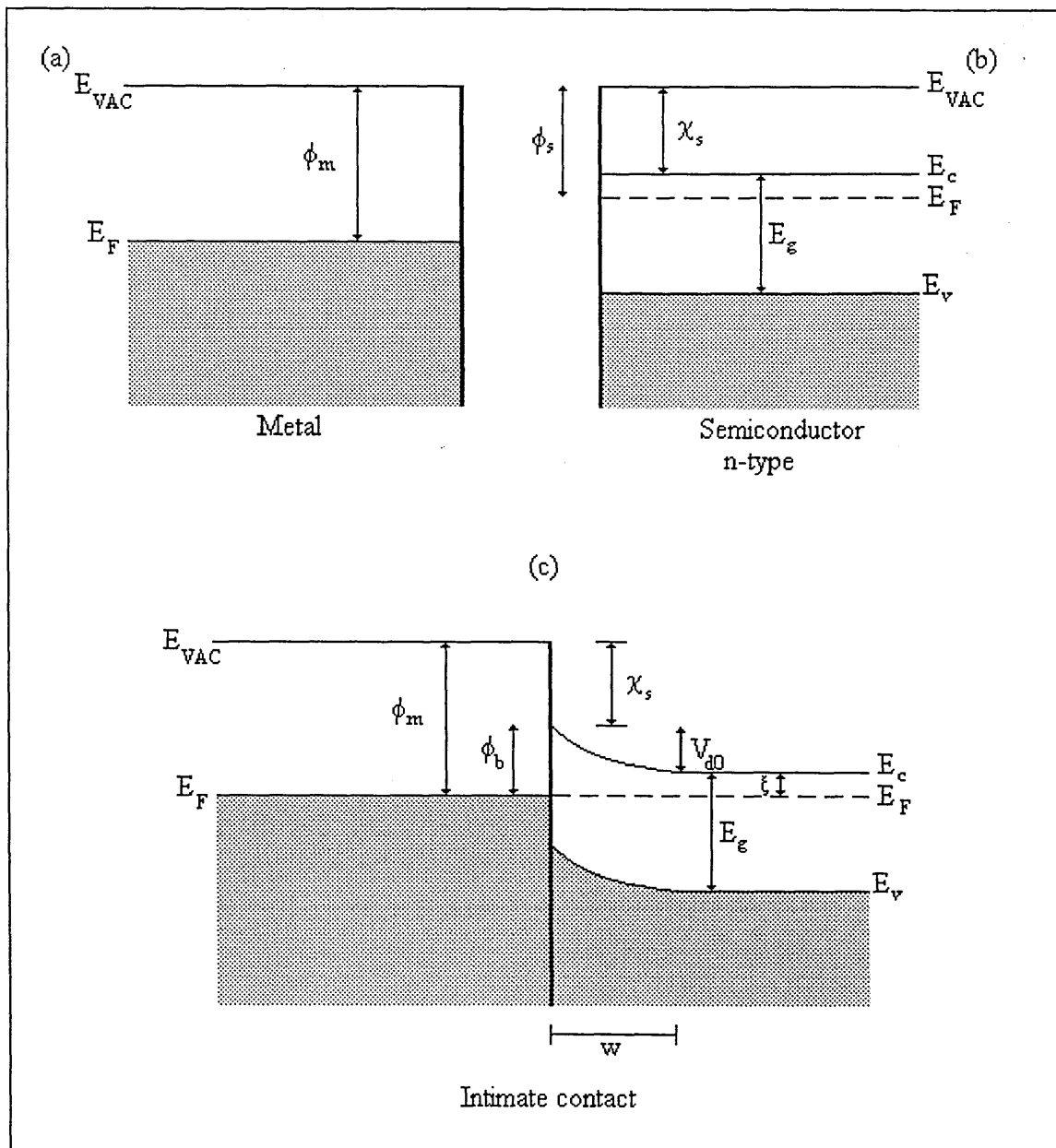


Figure 1.1 A schematic energy band diagram of a metal, (a) of work function ϕ_m and an n-type semiconductor, (b) of work function ϕ_s . A Schottky barrier is formed when the two are brought into intimate contact (c). χ_s is the electron affinity of the semiconductor and ξ is the difference between the bottom of the conduction band and the Fermi level. V_{d0} is the zero bias band bending.

the depletion region, of width w . The rearrangement of the charge carriers induces band bending in the conduction and valance bands of the semiconductor which in turn produces the potential or Schottky barrier. From figure 1.1 it is clear that the Schottky barrier height, ϕ_b , measured from E_F is related to ϕ_m and the semiconductor electron affinity, χ_s , by the following expression;

$$\phi_b = \phi_m - \chi_s \quad (1.1)$$

The Schottky-Mott theories of barrier formation and hence equation (1.1) were based upon the notion of a perfect intimate contact between the metal and the semiconductor, in many cases such a situation is not possible. Many reported barrier heights did not reflect the linear relationship with ϕ_m predicted by equation (1.1). Such observations prompted Bardeen (1947) to suggest a model of Schottky barrier formation where the level of charge distribution and hence band bending and barrier height were dependent upon the occupancy of surface states present at a thin interfacial layer between the metal and semiconductor. These surface states in sufficient quantities were said to possess a charge neutrality level ϕ_0 which acted to pin E_F . The equation for Schottky barrier height could then be modified to the so called Bardeen limit;

$$\phi_b = E_g - \phi_0 \quad (1.2)$$

ϕ_0 is generally measured upwards from the valence band (E_V). The origin of surface states and the exact mechanism of E_F pinning have been the source of much debate within the literature. Heine (1965) first suggested that these states were metal induced gap states (MIGS) due to exponentially decaying wave functions of the metal adatoms. The role of defects created by the metal overlayer was investigated by Spicer *et al* (1979) and

incorporated into the unified defect model (UDM). Disorder at the interface producing disorder induced gap states (DIGS) was a mechanism proposed more recently by Hasegawa and Ohno (1986) to explain observed barrier heights. Other models have received much attention which focus not on the pinning of E_F but on the chemistry of the interface. Freeouf and Woodall (1981) suggested that the work function of the metal ϕ_m , may be modified to an effective work function ϕ_{eff} which would then replace ϕ_m in equation (1.1). Kurtin *et al* (1969) derived a parameter defined as the index of interface behaviour S , being the difference in electronegativity of two constituents of the semiconductor compound. When $S = 1$ the barrier height obeyed the Schottky limit and when $S = 0$ the barrier followed the Bardeen limit. Models of this nature were able to explain the behaviour of many systems but were more qualitative than quantitative.

There have been many attempts to explain the potential barrier between the metal and the semiconductor since Mott and Schottky's original propositions. Many of these theories will be expanded upon in the following chapter and later tested against the results obtained here. In a recent review on the subject of metal-semiconductor interfaces Williams (1991) concluded that a number of processes including chemical reactions, MIGS, defects, interface bonding and crystallography, and interdiffusion may all contribute to the Schottky barrier formation. Similarly, Brillson (1994) suggested that the picture of an abrupt metal-semiconductor interface was far from the true situation of a complex three dimensional system with interrelated chemical, structural and electronic properties.

1.2. Physical properties and applications of II-VI compound semiconductors.

The II-VI compounds have become the focus of much interest recently due to their central role in new devices such as short wavelength solid state lasers and high efficiency photovoltaic solar cells. These two areas of research are driven by the expanding

optoelectronics industry and the requirements of low cost environment-friendly energy. Within the optoelectronics industry there is a need for higher capacity storage systems based upon the replacement of conventional red solid state lasers by shorter wavelength blue lasers, increasing storage capacity many times. Thin film photovoltaic cells are among the most promising contenders to provide cheap, long term renewable energy sources in the future. It is the inherent physical properties of the II-VI compounds such as a wide direct band gap coupled with advances made in thin film processing technology that have made many of these devices a reality. Many problems still remain with this group of materials which must be solved before they can realise their full potential. Not the least of the problems is the non-amphoteric nature of some of the semiconductors within this group, unusual defect structures and difficulty in producing reliable metal contacts.

Compound	E_g^\diamond (eV)	ϵ_s^\diamond	a^\diamond (Å)	m_e/m_o^\diamond	ΔH_{298}^\square (kJmole ⁻¹)	Ionicity* (ΔX)
CdS	2.6	5.4	5.83	0.21	149.4	0.8
CdSe	1.7	10.0	6.05	0.13	144.8	0.45
CdTe	1.5	11.0	6.48	0.14	100.8	0.37
ZnS	3.6	5.2	5.41	0.4	205.2	0.95
ZnSe	2.7	8.4	5.67	0.1	163.2	0.81
ZnTe	2.3	9.0	6.09	0.1	119.2	0.55

Table 1.1. Physical properties of II-VI compounds. \diamond Ruda (1992). \square Kubaschewski *et al* (1993). *following the definition of Kurtin *et al* (1969).

1.2.1 Applications of ZnSe.

The use of ZnSe for optoelectronic applications is evident from table 1.1, with a band gap of 2.7 eV it is an ideal candidate for the production of short wavelength, blue-green light emitting devices and lasers. This property, combined with a close lattice match to GaAs (< 1 %) identifies ZnSe as having excellent potential for incorporation into monolithic blue optoelectronic devices.

Early light emitting devices incorporating ZnSe were produced by Livingstone *et al* (1973). n-type ZnSe doped with Al and Mn^{2+} or Cu^{2+} to provide luminescent centres was incorporated into a metal-insulator-semiconductor (MIS) structure to produce light in the

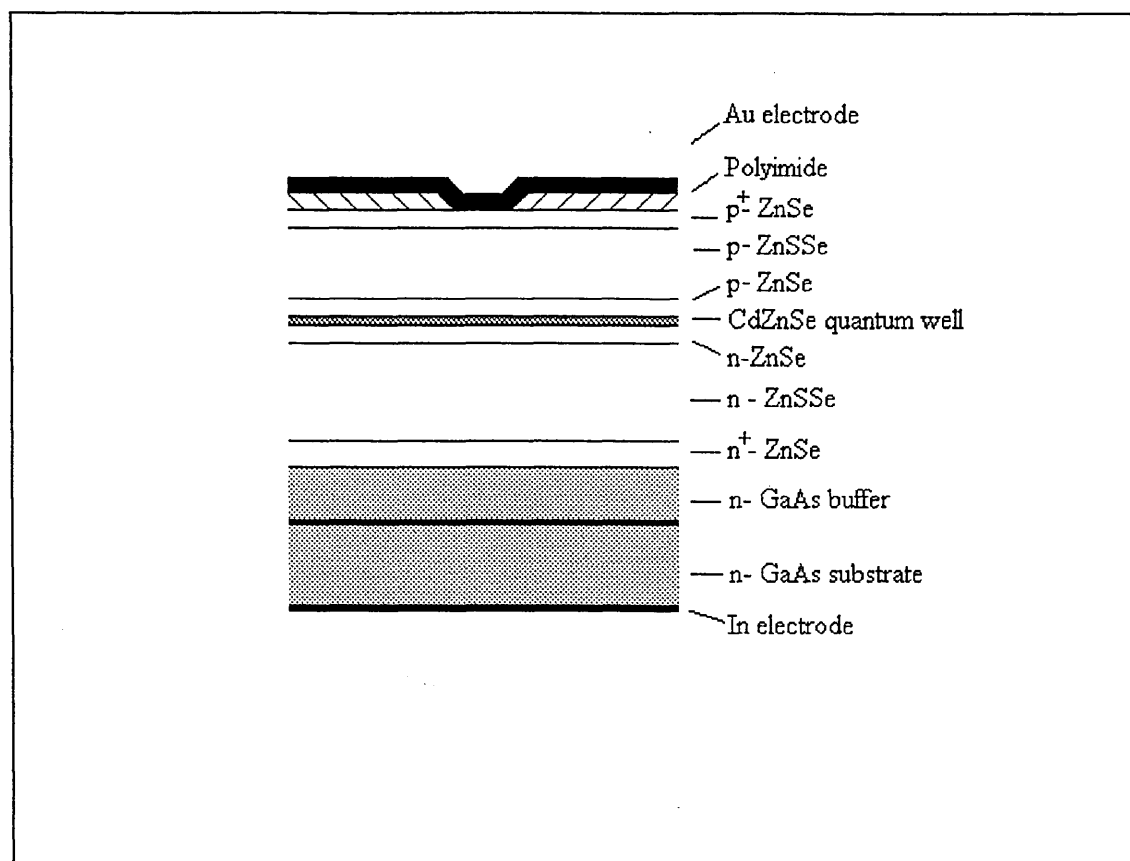


Figure 1.2 ZnSe based blue solid state laser after Haase *et al* (1991).

yellow-orange and blue regions. Gold was used to form a Schottky contact onto a thin layer of ZnO produced by chemical etching of the ZnSe substrate to give electroluminescence in forward bias.

The development of true-blue solid state lasers was severely hindered by the lack of n and p type doping, a problem which was resolved by Park *et al* (1990). By doping ZnSe with nitrogen free radicals generated by a rf plasma source, doping levels of up to $1 \times 10^{18} \text{cm}^{-3}$ were readily attained. Using this same technique researchers at 3M in the USA soon produced the world's first blue solid state laser Haase *et al* (1990) as depicted in figure 1.2.

Under the application of a forward bias, electrons (n-ZnSe) and holes (p-ZnSe) are injected into the quantum well here they may recombine radiatively to emit a photon. The charge carriers are confined by the ZnSe to the $\text{Cd}_x\text{Zn}_{1-x}\text{Se}$ quantum well. The initial photon then interacts with an electron in the conduction band, causing it to recombine with a hole in the valence band stimulating the emission of a second photon. These photons are optically confined by the difference in refractive indices between ZnSe and the ZnSSe cladding region. A Fabry-Perot cavity is produced by cleaving the device at both ends allowing the partial internal reflection required for true laser action. This particular device produced light at the wavelength of 490 nm in the temperature range 77-200K. Since the production of this first device, improvements have been made which allow lasing at room temperature although device lifetimes are still only a matter of a few seconds. The main problems are the high resistance of the metal contact to p-ZnSe. Band gap engineering has been suggested as one possible solution and some progress has been made using graded BeTe/ZnSe and $\text{ZnTe}_x\text{Se}_{1-x}$ structures by Mensz (1994) and Fan *et al* (1993) respectively. A second major problem is the lattice mismatch between ZnSe and the $\text{Cd}_x\text{Zn}_{1-x}\text{Se}$ quantum well structure which, upon heating induces dislocations which

destroy laser action, Guha *et al* (1993). One solution to this problem has been demonstrated by Gaines *et al*(1993) using $Zn_{1-x}Mg_xS_ySe_{1-y}$ as the quantum well structure. A full review of recent advances made in this very active area of research are given by Neumark *et al* (1994) and Prior (1994).

1.2.2 Applications of CdTe and CdS.

A number of parameters make CdTe an ideal candidate for high efficiency low cost photovoltaic solar cells for terrestrial energy conversion. A near ideal band gap of 1.45 eV coincides directly with the maximum power region of the solar spectrum. The short absorption length of photogenerated carriers means that most carriers can be generated within or close to the depletion region, leading to high efficiencies for thin film material. There are many relatively inexpensive methods of producing large area polycrystalline thin films of photovoltaic quality, reviewed by Ullal (1992). CdTe is commonly combined with a wider band gap window material such as CdS which enables the cell to convert a greater proportion of the solar spectrum. Using this configuration high conversion efficiencies approaching a predicted 18% have been achieved, Ullal (1992). Many problems still exist with this technology before it meets the stated goals of the USA Department of Energy of 15% efficiency modules with a 30 year life span, (Annan (1993)). The current state of the art in CdS/CdTe based photovoltaics was reviewed by Chu and Chu (1995) where the reproducibility and instability of metal contacts to these materials was identified as a key area for device improvement.

There are primarily two types of cell in the thin film category. The metal-semiconductor cell in which the active junction is at the interface between the metal and semiconductor and the heterojunction cell in which the active junction is the p-n junction between the two semiconductors. The energy band diagrams of both types of cell are shown in figure 1.3.

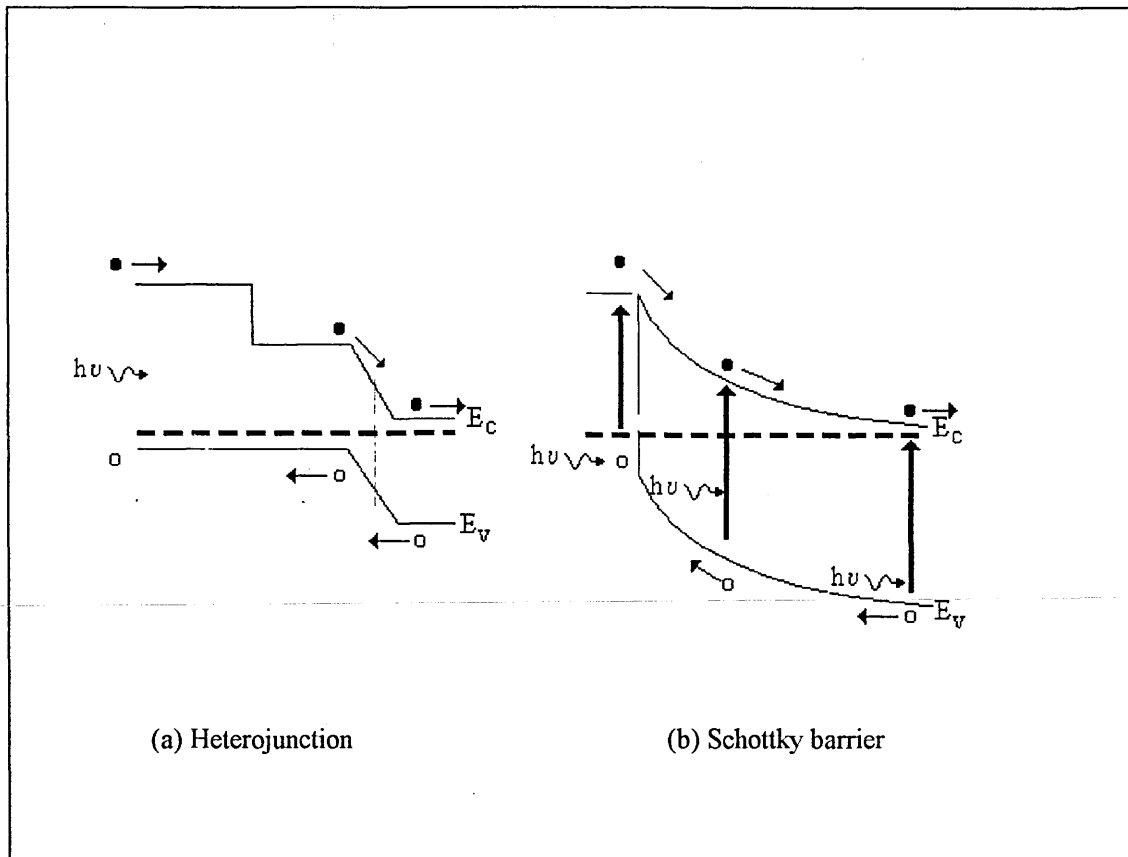


Figure 1.3 (a) Heterojunction photovoltaic solar cell (b) Schottky diode type photovoltaic solar cell.

The Schottky barrier solar cell requires a semi-transparent metal layer onto n-type material as the front contact. Photons then enter the device via this thin metal layer; photons of energy $h\nu > \phi_b$ are absorbed by the metal forcing electrons over the Schottky barrier, photons with $h\nu \geq E_g$ enter the semiconductor and create electron hole pairs in the vicinity of the depletion region, the remaining photons with $h\nu \approx E_g$ can then create electron hole pairs in the neutral region. Efficiencies of this type of cell were reported by Fulop *et al*(1982) of $\approx 8.6\%$. Controlling the magnitude of the Schottky barrier by pre-contact formation treatments such as annealing in air or inert atmosphere can produce a thin oxide layer. This leads to the formation of a MIS structure upon the subsequent formation of metal contacts. Electrons entering the cell tunnel through this insulator and

pass over the barrier as in the metal-semiconductor device. For thicknesses of insulator of only a few monolayers this can actually increase the efficiency due to an increase in the open circuit voltage. In this manner Raychaudhuri(1987) has reported Schottky barrier MIS cells of $\approx 15\%$ efficiency.

A second type of solar cell which has received much attention recently is the heterojunction cell. This normally consists of two materials one of which is doped n-type and the other p-type. The advantage in having a second material is that the larger band gap allows the cell to capture a greater portion of the solar spectrum improving the efficiency of the cell. A schematic of the heterojunction cell together with a band diagram is shown in figure 1.3(a). In this case the window material is formed from n-type CdS which has a band gap of 2.42 eV at room temperature. For the two materials CdTe ($E_g = 1.45$ eV) has the smaller bandgap, CdS therefore forms the window material on the illuminated side of the cell. CdS is then able to absorb photons with greater $h\nu$ and therefore shorter λ , the longer wavelengths then go on to be absorbed by the CdTe layer. This produces a cell with a greater spectral response than the Schottky type device and should therefore have a greater efficiency. Of course the thickness of the window layer is vital as there is a compromise between absorption of light and scattering of photons in the CdS. The ideal situation is for the second semiconductor, in this case CdTe, to have a high collection efficiency. In that way the electron-hole pairs are generated close to the depletion region of the p-n junction and efficiency is high. This type of photovoltaic device now accounts for most of the research effort on CdTe solar cells and is the state of the art in thin film photovoltaics. The highest efficiency reported to date was produced by Britt and Ferekides (1993) who claimed an efficiency of 15.8%.

1.3 Aims and objectives.

Most theories of Schottky barrier formation have evolved through experimental observations of elemental or group III-V semiconductors. One of the broad aims of the project was to objectively test the applicability of these theories to metal II-VI compound interfaces. Although much progress has been made previously the level of II-VI compound related knowledge falls far short of that for elemental and III-V compounds. The very nature of metal-semiconductor interfaces is such that any information on the mechanisms of Schottky barrier formation should ultimately lead to a better understanding of the material itself. As well as providing new experimental evidence on metal/II-VI systems regarding the physical models of Schottky barrier formation, the practical insights gained from these studies should lead to new methodologies of contact formation and processing. Ultimately such advances should yield new contact technologies and devices. The scope of the project therefore fell into three broad categories:

- The study of treatments using modern surface analytical techniques which influence the chemical nature and composition of the semiconductor surface. The aim being to establish repeatable processes which can provide a variety of substrates for subsequent metal contact formation.
- The macroscopic electrical properties of metal junctions formed on these surfaces. Having achieved a method of producing different surfaces, metal contacts formed to these surfaces inevitably exhibit different interface properties. The interfacial properties of different metal-semiconductor contacts then relate to the macroscopic behaviour of the contact as a whole.
- The effects of time on such metal contacts in terms of the stability of the devices. Time effects generally introduce a non-abruptness to the interface, or at the very least allow

a period of time over which chemical reactions can take place between the metal and the semiconductor.

1.4 Approach.

In order to achieve the aims stated above there has from the beginning of the project been a conscious effort to employ methods of semiconductor surface modification which are directly applicable to device manufacture. For many thin film devices and certainly for large area devices such as the photovoltaic cell the only practical method of surface modification is that of wet chemical etching. There have been many previous studies of such techniques which will be reviewed in full in Chapter 3. The wet chemical etching of CdTe has been shown by Dharmadasa *et al* (1989) to influence the Schottky barrier height of Au and Sb contacts on n-CdTe. Surface modifications induced by the chemical treatments were found to influence the deep level defect structure of CdTe, Sobiesierski *et al* (1988) which in turn influenced the barrier height. These results are as yet far from understood but form an excellent point from which to begin the work. Three materials CdTe, CdS and ZnSe were chosen not only for their technological importance but because a pattern of the behaviour of the group of materials as a whole could then be established. In this manner it is then possible to determine patterns of group behaviour which may be easier to interpret compared with isolated data. The program of work has taken the following outline.

- Wet chemical etching procedures were developed from the literature and applied to all three materials. Initially the surface oxidation of the compound was monitored with X-ray photoelectron spectroscopy (XPS). The effects of different alkaline and acidic

etchants on the oxidation state and stoichiometry of the surface was monitored in order to establish suitable etching procedures.

- Metal contacts were then formed onto selected surfaces and characterised by conventional current transport mechanisms. Chemical etchants which gave surfaces of reduced oxide content were especially investigated, the Schottky barrier characteristics of contacts formed to these surfaces were then monitored.
- Electrical characteristics of these aged metal contacts were monitored macroscopically by I-V techniques. In such a way it was possible to relate microscopic interfacial interactions predicted by the thermodynamics of the interface with the macroscopic device characteristics.
- Intrinsic properties of the semiconductor were analysed by DLTS to determine the possible number of deep levels within a specific material and to investigate the relation of these traps with possible Fermi level pinning at the interface.
- Selected contacts were analysed with state of the art ballistic electron emission spectroscopy (BEES) which allows the Schottky barrier height to be investigated with a spatial resolution in the nm range. Ballistic electron emission microscopy (BEEM) allows the structure of the interface to be related to electronic characteristics. Results from both of these microscopic techniques could then be related to the macroscopic I-V characteristics of specific devices.

Chapter 2.

Models and theories of Schottky barriers.

2.1 Introduction.

The Schottky-Mott theory of barrier formation as introduced in chapter 1 is now recognised as a gross over simplification for many metal-semiconductor systems. The mechanism of Schottky barrier formation depends upon a number of parameters including interfacial reactivity, structure, surface/interface states and defects. The main models of Schottky barrier formation described here are all based upon these physical variables.

The function, measurement and physical understanding of the Schottky barrier relies upon the correct interpretation of the current transport and capacitance properties. The main mechanism of current transport, namely thermionic emission over the barrier is discussed collectively with competing processes such as recombination and generation. As it is anticipated that most of the diodes fabricated will have some form of interfacial layer the effects of such layers on current transport and capacitance of the device are also discussed.

2.2 Models of Schottky barrier formation.

Many theories of Schottky barrier formation have emerged, as yet there exists no quantitative predictive theory to explain the magnitude of Schottky barrier height. It is the intention here to provide an overview of the most popular models.

2.2.1. The Bardeen model.

In Bardeen's model of surface states and rectification at the metal-semiconductor interface, (Bardeen (1947)) the first attempt was made to explain the many experimental results which disagreed with the Schottky model. A model was proposed based upon a high density of localised states within the bandgap. It was suggested that if such states were present in sufficient density they would accumulate charge from the semiconductor. An equilibrium level ϕ_0 , (measured from the valance band, E_v) was defined as a level of charge neutrality between filled and empty states at which E_F was pinned. The Fermi energies of the bulk semiconductor and the bulk metal must align upon contact between the metal and the semiconductor. If a high density of surface states exist then most of the charge transferred from semiconductor to the metal (and vice versa) will be accommodated by the surface states. The semiconductor is effectively shielded from the charge transfer and the Schottky barrier becomes independent of the metal. E_F is effectively pinned by the surface state density. If there is a low density of surface states then charge will be accumulated within the semiconductor which will then follow the Schottky model.

Bardeen's model offered an explanation for much anomalous data of the time, (Meyerhof (1947)), but as Bardeen predicted did have a few shortcomings . The main problem was the necessity for an interfacial layer present between the metal and the semiconductor in which to contain the surface states. Heine (1965) was the first to point out that the presence of the metal overlayer modified the surface states and introduced metal-induced gap states within the forbidden band gap.

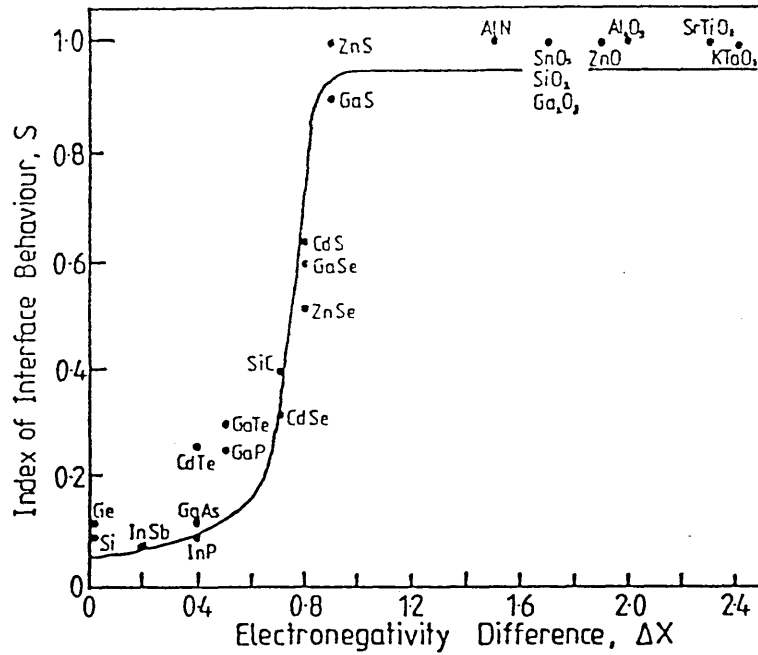


Figure 2.1. The "S" curve of interface behaviour after Kurtin *et al*(1969).

2.2.3. The effective work function model.

The effective work function model of Freeouf and Woodall (1981) assumes that the Schottky model is essentially correct but equation (1.1) should be modified to;

$$\phi_b = \phi_{eff} - \chi_s \quad (2.1)$$

where ϕ_m , the work function of the metal is modified to ϕ_{eff} , an effective work function. The effective work function was assumed to arise as a result of microclusters at the interface, non-stoichiometry, oxide species and metal-semiconductor interaction and is a

interface, non-stoichiometry, oxide species and metal-semiconductor interaction and is a weighted average of the work functions of these different phases. It was assumed that ϕ_{eff} would be due in the main part to contributions from the semiconductor anion of work function ϕ_{anion} through the following reactions;



This type of reaction is often chemically/thermodynamically favourable and so this model has received a lot of attention as it is conceptually very simple. A major problem with quantifying this model is the lack of published data for values of ϕ_{eff} for different metal-semiconductor interfaces.

2.2.4 Models of Fermi level pinning.

Following Bardeen's initial predictions of E_F pinning, several groups have proposed different mechanisms by which surface/interface states may arise.

2.2.4.1. Metal induced gap states (MIGS) model.

Heine(1965) was the first to predict the existence of states induced within the semiconductor by the metal overlayer rather than the surface states predicted by Bardeen. Heine calculated that the exponentially decaying tails of the metal wave functions would penetrate into the surface of the semiconductor thus introducing states due to the metal which could then be responsible for "pinning" E_F . This work was continued by Flores *et al* (1973), the initial motivation being the confirmation of Kurtin's covalent-ionic transition.

They calculated a distribution of states due to Al and Cu overlayers for a range of zincblende (110) semiconductors. Following the work of Cowley and Sze (1965) where the Schottky barrier height was given by;

$$\phi_b = S\phi_m + b \quad (2.2)$$

where S was defined as;

$$S = \frac{1}{1 + D\delta e^2} \quad (2.2 (a))$$

where, D = density of surface states

δ = effective distance between resonance surface states and opposite charge at the metal surface..

In this manner they were able to construct a curve of S v ΔX , not to be confused with the "S" parameter adopted by Kurtin. The model was in good agreement for "covalent" materials but not for "ionic" materials. Tejedor *et al* (1977) went on to develop this model further by introducing a level ϕ_0 at the interface. This neutrality level ϕ_0 , was defined as a level below which all interface charges at the semiconductor surface are cancelled out by the lack of states within the valence band. Again this concept was applied to the Si (111) and the zincblende (110) surfaces. Such a model is not really applicable to strongly ionic crystals such as CdTe, CdS and ZnSe as the electron-electron interaction assumed is by the definition of ionic bonds questionable.

Louis and Flores (1981) applied this model to "real" metal-semiconductor junctions by categorising possible metal-semiconductor interfaces into the following categories;

- non-reactive, no chemical compound is formed between metal and semiconductor
- etched surfaces, in which the semiconductor has been pre-treated to leave a remnant oxide layer.
- reactive interfaces, a new chemical compound is formed between the metal and the semiconductor.

From these three categories they drew the conclusions that for clean "covalent" junctions, the neutral level, ϕ_0 was independent of any surface effects and ϕ_b reached the Bardeen limit. For "ionic" junctions, Bardeen behaviour can become Schottky-like behaviour with physisorbed layers or the presence of relaxation. With etched covalent surfaces the density of states at ϕ_0 and hence the ability to pin E_F decreases with oxide thickness and hence Schottky - like behaviour ensues.

The MIGS model was again modified by Tersoff (1984) and (1985) in which a branch point E_B was introduced, calculated from the semiconductor band structure. A low density of MIGS would draw E_F towards E_B but would be insufficient to completely remove any dependence upon the semiconductor work function

2.2.4.2 The unified defect model.

In the unified defect model first introduced by Spicer *et al* (1979) and (1980), E_F is pinned by electronic states due to defects within the semiconductor. Clean surfaces of several III-V compounds (GaAs, InP and GaSb) were studied as sub-monolayer quantities of either metal adatoms or oxygen were added. E_F stabilisation was observed at different positions in each material independent of the adatoms being metal or oxygen in origin. In the original model it was assumed that two electronic levels were created due to the removal of anions or cations in the surface region of the semiconductor. Later refinements were

made, Spicer *et al*(1986) which proposed that the most likely defects in III-V semiconductors were of the antisite type where a cation site is occupied by an anion and vice versa. The As on Ga (As_{Ga}) antisite defect was identified as being responsible for deep levels at $E_v + 0.74$ and $E_v + 0.5$ eV for GaAs in the advanced unified defect model Spicer *et al* (1988).

One crucial difference between the MIGS model and the defect model is that the MIGS model requires the deposition of several monolayers of metal before the metal can assume a true metallic character and band structure to subsequently produce metal-induced gap states. The defect model requires only sub-monolayers of adatoms to induce specific defects. The main analytical treatments of this model have involved specifically III-V compounds, no treatment of II-VI compounds has yet been published.

2.2.4.3. The disorder induced gap states model.

In the disorder induced gap states model of Hasegawa and Ohno (1986), disorder at the surface of the semiconductor induced by the deposition of either a metal or an insulator was found to be responsible for a continuum of disorder induced gap states (DIGS). The spectrum of states was said to consist of donor and acceptor - like states with a charge neutrality level between the two, at E_{HO} . E_F was then pinned at this level in a similar manner to the MIGS model. For most tetrahedrally bonded semiconductors Hasegawa found the position of E_{HO} to be largely independent of the specific nature of the disorder. It was calculated that E_{HO} would in fact occur about 5 eV below the vacuum level E_{VAC} , the barrier height would then be given by;

$$\phi_b = 5.0 - \chi_s \quad (2.3)$$

Equation 2.3 implies that ϕ_b , should be largely independent of the metal and the surface preparation procedure used. One advantage of this model over other models of E_F pinning is that it allows for pinning in the presence of a thin oxide layer.

2.2.5 The pinch - off model.

Inhomogeneities at the metal semiconductor interface were first proposed by Ohdomari *et al* (1979) and Ohdomari and Tu (1980) to be responsible for many anomalies observed in metal-semiconductor device characterisation by current-voltage (I-V) and capacitance-voltage (C-V) techniques. Freeouf *et al* (1982) incorporated a similar model into their EWF model. Both groups worked on the principle that interfacial inhomogeneities would lead to the formation of a number of diodes under one metal contact. The current transport properties of these devices would then resemble a number of parallel diodes. More recent work by Tung (1991) suggested that previous models of parallel conduction were in serious error when the inhomogeneities of the Schottky barrier height were on a scale less than or comparable to the depletion width. No specific mechanism of Schottky barrier inhomogeneity was implied, the Schottky barrier was said to be a "function of the interface atomic structure". One important consideration that previous models of inhomogeneity had failed to consider was the effect of "pinch-off". The "pinch-off" effect describes the action of a region of high Schottky barrier height on a small "patch" of lower barrier height, in a similar manner to the operation of a field effect transistor. The conduction path of the lower barrier is "pinched - off" by the barrier of greater magnitude. An area can be described as "pinched- off" if majority carriers originating from outside the space charge region have to traverse a barrier higher than the band edge position at the metal-semiconductor interface, in order to reach the interface. Tung (1992) investigated at great length the effects of dimensions and area ratios and together with Sullivan *et al* (1991) explained many anomalies of normal Schottky barrier measurement. The "pinch-

off" model was used to explain such effects as greater than unity ideality factors, temperature dependence of the ideality factor and differences in Schottky barrier height depending upon the measurement technique employed. Tung (1993) has questioned many of the models outlined above particularly models of E_F pinning. Agreement between this model and a large body of experimental data was demonstrated although no comparison with data from II-VI compounds has been made.

2.2.9 Summary of models.

It is apparent that there are many models of Schottky barrier formation. Those outlined above are generally considered in the literature to be significant attempts at explaining the physics of the Schottky barrier. Several empirically based models also exist such as the "two-thirds " model of Mead and Spitzer (1964) which have received little attention in the literature from the last decade or so. It seems plausible that more than one of these physical phenomena may exist at the same time, a possibility which has been proposed by Williams (1991) but which none of the models recognises. Tung's model of Schottky barrier inhomogeneity has been extensively tested against metal contacts to Si and also explains many of the anomalies of normal Schottky barrier theory. No application of this model to II-VI compounds has as yet been made.

2.3 Current transport mechanisms.

The transport of electrons from the semiconductor to the metal and vice versa is the primary function of all metal contacts, understanding the mechanisms of current transport is therefore fundamental to the operation of the Schottky barrier.

2.3.1 Thermionic emission.

The primary current transport mechanism in Schottky barriers is thermionic emission over the barrier. Contacts in which this is the sole mechanism of current transport are described as ideal.

In Bethe's thermionic emission theory as described by Rhoderick and Williams (1988) the main current limiting phenomena is the emission of electrons over the potential barrier. Drift and diffusion of carriers through the depletion region are assumed to be negligible. Figure 2.2 shows the position of the quasi - Fermi level for electrons which remains flat throughout the semiconductor. For an applied forward bias of V , there is an exponential increase in the concentration of electrons at the semiconductor side of the interface given as a function of N_c , the density of states in the conduction band. The total electron concentration n_e , on the semiconductor side of the interface is given by ;

$$n_e = N_c \exp\left(\frac{-q(\phi_b - V)}{kT}\right) \quad (2.4)$$

Kinetic theory gives the electron flux incident upon unit area of the interface as $n_e \bar{v} / 4$, where \bar{v} is equal to the mean thermal velocity of electrons in the semiconductor.

The current density $J_{s \rightarrow m}$, is given by ;

$$J_{s \rightarrow m} = \frac{qN_c \bar{v}}{4} \exp\left(\frac{-q(\phi_b - V)}{kT}\right) \quad (2.5)$$

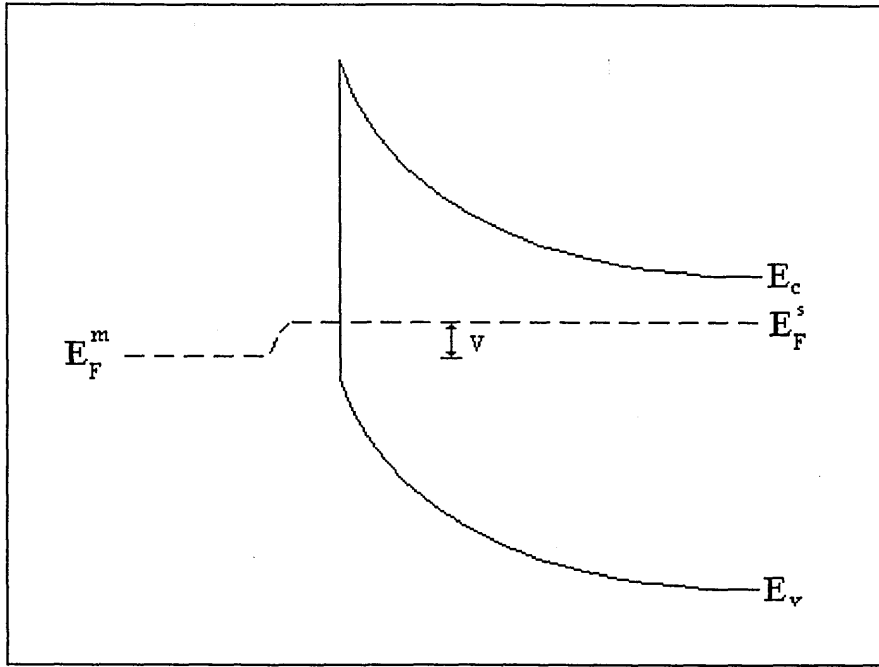


Figure 2.2. The position of the quasi-Fermi level for an applied bias V according to thermionic emission theory after Rhoderick and Williams (1988).

There is a complementary flow of electrons from the metal into the semiconductor, however from the metal side of the interface the application of the bias V has no effect on the barrier. The metal is effectively presented with a zero bias situation *ie* $V = 0$.

The current density from the metal into the semiconductor, $J_{m \rightarrow s}$, is given by;

$$J_{m \rightarrow s} = \frac{qN_c \bar{v}}{4} \exp\left(\frac{-q\phi_b}{kT}\right) \quad (2.6)$$

The total net current is then equal to:

$$J = J_{s \rightarrow m} - J_{m \rightarrow s} \quad (2.7)$$

$$J = \frac{qN_c \bar{v}}{4} \exp\left(\frac{-q\phi_b}{kT}\right) \left\{ \exp\left(\frac{qV}{kT}\right) - 1 \right\} \quad (2.8)$$

For a semiconductor with a Maxwellian distribution of electron velocities, the mean velocity of electrons is equal to, $\bar{v} = (8kT / \pi m^*)^{1/2}$, where m^* is the effective mass of electrons in the semiconductor. The density of states within the conduction band N_c , is given by;

$$N_c = 2 \left(\frac{2\pi m^* kT}{h^2} \right)^{3/2} \quad (2.9)$$

If these substitutions are made into equation (2.8) the total current due to thermionic emission is equal to ;

$$J = A^* T^2 \exp\left(\frac{-q\phi_b}{kT}\right) \left\{ \exp\left(\frac{qV}{kT}\right) - 1 \right\} \quad (2.10)$$

where,

$$A^* = 4\pi m^* q k^2 / h^3 \quad (2.10(a))$$

and is equivalent to the Richardson constant for thermionic emission but the free electron mass m is replaced by the effective electron mass m^* .

Equation (2.10) is often written in the literature as,

$$J = J_o \left\{ \exp\left(\frac{qV}{kT}\right) - 1 \right\} \quad (2.11)$$

where J_o , the saturation current density is,

$$J_o = A^* T^2 \exp\left(\frac{-q\phi_b}{kT}\right) \quad (2.11(a))$$

Equation (2.11) is the equation of ideal thermionic emission in the Schottky barrier, assuming that ϕ_b is independent of applied bias V .

2.3.1.1 Deviations from ideal thermionic emission.

There are many phenomena which cause the current transport to deviate from that described by equation (2.11) above.

2.3.1.2 Image force lowering.

Intimate contacts *ie* devoid of an interfacial layer, display a bias-dependent reduction in the barrier height due to the image force as shown in figure 2.3. This reduction in the barrier height $\Delta\phi_i$, is related to the Schottky barrier height ϕ_b , by the following equation,

$$\phi_e = \phi_b - \Delta\phi_i \quad (2.12)$$

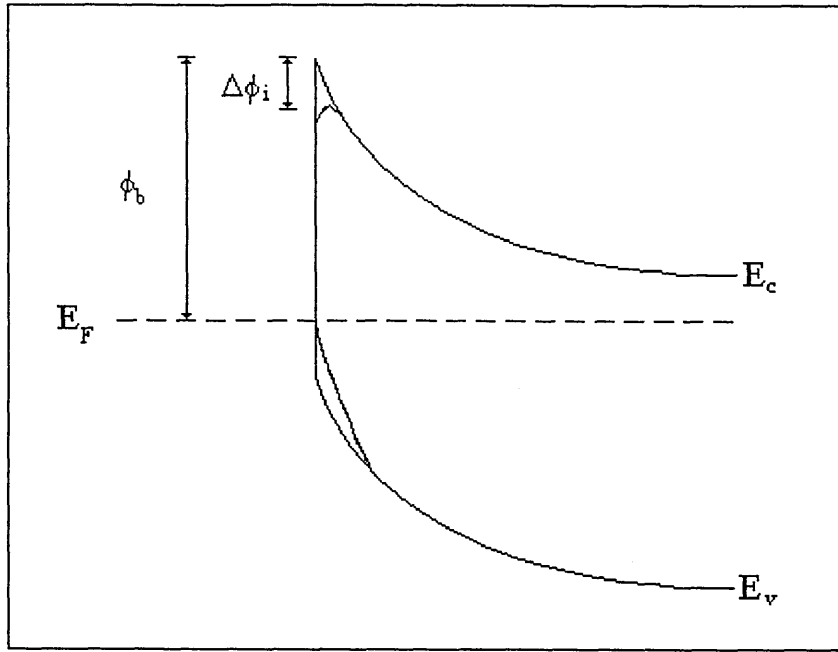


Figure 2.3. The effects of image-force on the conduction and valence bands after Rhoderick and Williams (1988).

If the bias dependence of ϕ_e is linear ($\delta\phi_e/\delta V$ is equal to a constant, β) then the effective barrier height can be re-written as;

$$\phi_e = (\phi_b)_o - (\Delta\phi_i)_o + \beta V \quad (2.13)$$

Applying this bias dependence of the Schottky barrier height to the equation for thermionic emission gives;

$$J = J_o \exp\left(\frac{qV}{nkT}\right) \left\{ 1 - \exp\left(\frac{-qV}{kT}\right) \right\} \quad (2.14)$$

The ideality factor, n , is usually introduced at this stage, the main function of which is to define the quality of the diode. It is in fact a literal expression of the bias dependence of the Schottky barrier height, in this case is written as,

$$\frac{1}{n} = 1 - \beta = 1 - \frac{\delta\phi_s}{\delta V} \quad (2.15)$$

Typical values for II-VI materials doped in this range give $n \approx 1.02$ which can be considered as the theoretical limit of the ideal Schottky barrier. The saturation current J_0 is now modified to be;

$$J_0 = A^* T^2 \exp \left[-q \left\{ \frac{((\phi_b)_o - (\Delta\phi_i)_o)}{kT} \right\} \right] \quad (2.16)$$

2.3.1.3 Recombination and generation.

A common mechanism of current transport is the recombination of electron hole pairs via recombination centres within the band gap. Recombination centres may be intrinsic to the material or extrinsically introduced by surface imperfections or interfacial defects. Those centres which occur close to the centre of the band gap were proposed as the most efficient recombination centres in the model developed by Shockley and Read (1952). The recombination current density at low forward bias is given by,

$$J_r = J_{r0} \exp\left(\frac{qV}{2kT}\right) \left\{ 1 - \exp\left(\frac{-qV}{kT}\right) \right\} \quad (2.17)$$

where

$$J_{r0} = \frac{qn_i w}{2\tau_r} \quad (2.17(a))$$

n_i is the intrinsic electron concentration, w is depletion region thickness and τ_r is the carrier lifetime within the depletion region. Rhoderick and Williams point out that there are several shortcomings to this theory namely;

- the energy levels of the recombination centres coincides with the intrinsic level.
- the capture cross-sections for electrons and holes are equal.
- the recombination centres are distributed uniformly.

Equation 2.17 can therefore be considered as a simplification of the real situation.

The total current density, J_{Tot} , from a combination of the thermionic and recombination currents is given by;

$$J_{Tot} = J_{te} + J_r \quad (2.18)$$

$$J_{Tot} = \left\{ J_{i0} \exp\left(\frac{qV}{kT}\right) + J_{r0} \exp\left(\frac{qV}{2kT}\right) \right\} \left\{ 1 - \exp\left(\frac{-qV}{kT}\right) \right\} \quad (2.18(a))$$

The ratio of the thermionic emission and recombination currents is proportional to,

$$T^2 \tau_r \exp \left\{ q \frac{(E_s + V - 2\phi_b)}{2kT} \right\} \quad (2.19)$$

From the above relation it is evident that recombination current is more prevalent in semiconductors with high Schottky barriers, in material with a low carrier lifetime and at low applied forward bias. The ratio of thermionic emission to recombination also increases with temperature so recombination will therefore be more noticeable at low temperatures for a particular diode.

2.3.1.4 Quantum mechanical tunnelling.

Quantum mechanical tunnelling may occur in two possible modes dependent upon the temperature, T and donor concentration N_d . Field emission occurs most noticeably in heavily doped semiconductors at energies close to E_F . As the temperature increases electrons are given more energy and so can pass through the barrier at a higher energy than E_F , this process is known as thermionic field emission. At even higher temperatures the dominant process is thermionic emission.

Padovani and Stratton (1966) formulated an exact treatment of quantum mechanical tunnelling which was reviewed by Rhoderick and Williams (1988). The parameter E_{∞} was defined such as;

$$E_{\infty} = \frac{\hbar}{2} \left(\frac{N_d}{m^* \epsilon_s} \right)^{1/2} \quad (2.20)$$

and determines the probability of an electron tunnelling. ϵ_s is the semiconductor permittivity ($\epsilon_s \times \epsilon_0$), m^* is the effective mass of electrons in the semiconductor ($m_r \times m_e$). E_{00} for CdTe, CdS and ZnSe, assuming a doping concentration of $\approx 5 \times 10^{22} \text{ m}^{-3}$ ($5 \times 10^{16} \text{ cm}^{-3}$) was calculated to be 3.35, 3.9 and 3.83 meV respectively which is approximately equal to $1/10kT$ at $T = 300\text{K}$ ($= 25.8 \text{ meV}$). This shows that thermionic emission will be the dominant process in contacts to these materials at these donor concentrations.

2.3.1.5 Interfacial layers.

The current transport properties can be influenced a great deal by the presence of thin interfacial layers which are almost inevitable in most practical devices not prepared under UHV conditions. Figure 2.4 shows a schematic idealised energy band diagram of a metal-insulator semiconductor (MIS) Schottky barrier. Typically, interfacial layers are formed from oxide films although they may be too thin to develop the full band structure of an insulator. The analysis of Card and Rhoderick (1971) assumes a thin insulating layer of thickness δ . On the application of a forward bias V , some of the potential is dropped across the interlayer introducing a bias dependence of the Schottky barrier height. The presence of the insulating layer means that thermionic current is reduced by the finite probability of electrons then tunnelling through the layer, the thicker the layer then the less is the current. The modification of the current voltage relationship can be understood by a modification in the diode quality factor, n . A relationship for the diode quality factor was derived by Card and Rhoderick (1971), where;

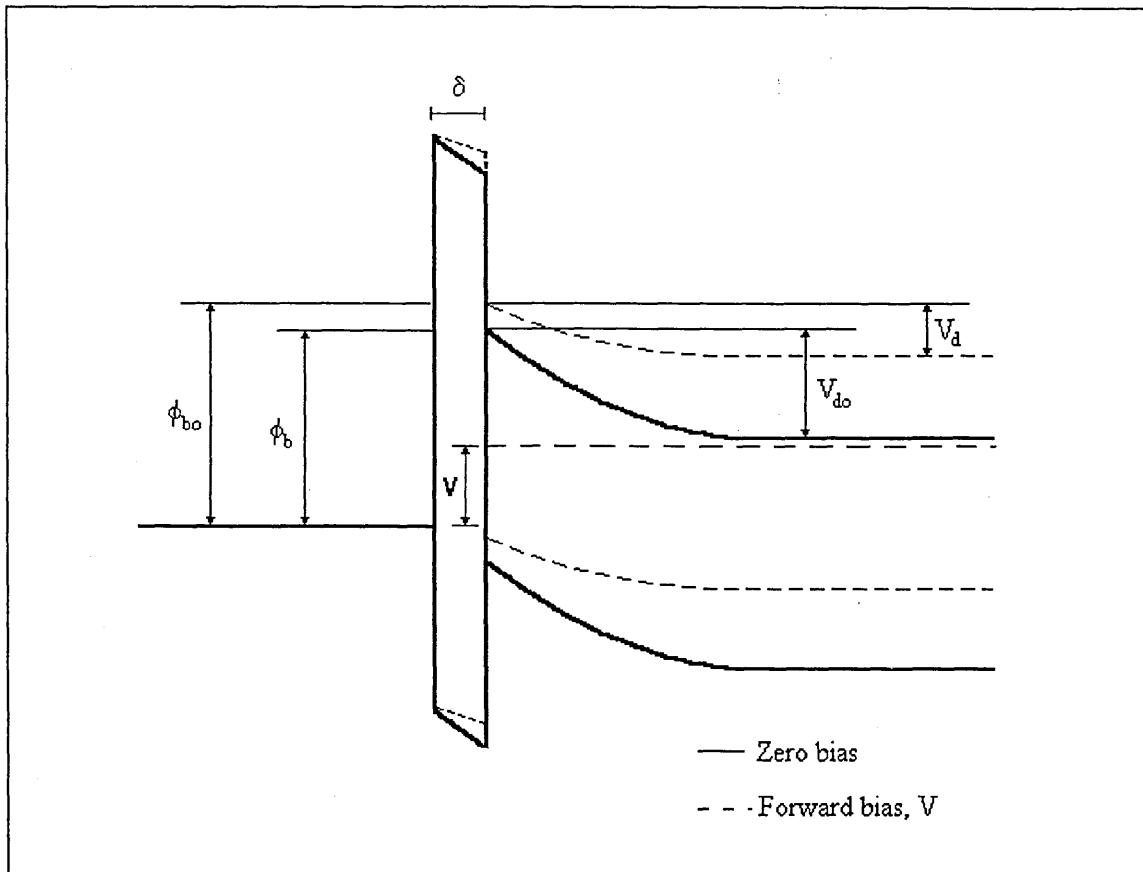


Figure 2.4 A Schottky barrier with an interfacial layer.

$$n = 1 + \frac{(\delta / \epsilon_i) \{ (\epsilon_s / w) + qD_{sb} \}}{1 + (\delta q D_{sa} / \epsilon_i)} \quad (2.21)$$

In this analysis the interface states are divided into two groups of densities D_{sa} and D_{sb} . The first group D_{sa} , can be considered to be in equilibrium with the metal and thus hold ϕ_b constant, the second D_{sb} are in equilibrium with the semiconductor and hold V_d constant, increasing n . Rhoderick and Williams state that a thin film of SiO_2 in which $\delta < 30 \text{ \AA}$ thick would produce $n \approx 1.3-1.5$. These values are however dependent upon ϵ_s and ϵ_i of the particular semiconductor and oxide or interfacial film.

2.4 Capacitance of a Schottky barrier.

The depletion region of the Schottky barrier can in many respects be considered as a voltage dependent capacitor. In the ideal case where minority carriers are negligible, the effect of holes can be neglected providing the barrier height is in excess of $3kT/q$. For an applied reverse voltage V_r , the induced band bending will be equal to the diffusion voltage V_d . Following the exact analysis of an electric field in a Schottky barrier of Rhoderick and Williams, the maximum electric field due to uncompensated donors is given by;

$$E_{\max}^2 = \frac{2qN_d}{\epsilon_s} \left(V_d - \frac{kT}{q} \right) \quad (2.22)$$

Gauss's theorem states that charge due to uncompensated donors is given by the expression;

$$Q_d = \epsilon_s E_{\max} \quad (2.23)$$

$$= (2q\epsilon_s N_d)^{1/2} \left(V_d - \frac{kT}{q} \right)^{1/2} \quad (2.24)$$

The capacitance of unit area is defined as ;

$$C = \frac{\partial Q_d}{\partial V_r} = \frac{\partial Q_d}{\partial V_d} \quad (2.25)$$

differentiating equation 2.24 with respect to V_d gives ;

$$C = \left(\frac{q \epsilon_s N_d}{2} \right)^{1/2} \left(V_d - \frac{kT}{q} \right)^{-1/2} \quad (2.26)$$

The band bending, V_d induced by an applied reverse bias V_r is equal to $V_d = V_r + V_{d0}$, where V_{d0} is the band bending at zero bias and in turn is equal to $V_{d0} = \phi_b - \xi$. ξ is the difference between E_F and the bottom of the conduction band, E_c . If these expressions for V_d are substituted into equation 2.26 the capacitance of the Schottky barrier due to a reverse bias V_r becomes;

$$C = \left(\frac{q \epsilon_s N_d}{2} \right)^{1/2} \left(\phi_b - \xi + V_r - \frac{kT}{q} \right)^{-1/2} \quad (2.27)$$

The capacitance of the Schottky barrier is normally measured using a small a.c. carrier signal superimposed upon a d.c. bias signal as explained in Sec 4.4.2.

2.4.1. Deviations from the ideal capacitance.

As with electron transport over the barrier there are several mechanisms which commonly occur in real devices which have a profound influence on the capacitance of the Schottky barrier. These are namely interfacial layers between the metal and semiconductor and deep traps within the band gap.

2.4.1.1 Interfacial layer effects.

The effects of thin interfacial layers on the capacitance of the Schottky barrier have been discussed in detail by Cowley (1966) and Crowell and Rideout (1969). The band diagram

of such a layer will of course look much the same as that of figure 2.4. If the interfacial layer is sufficiently thin then the occupancy of interface states is governed predominantly by electrons tunnelling from the metal. In Cowley's analysis the plot of C^{-2} versus V_r remains linear with gradient of $2 / q \epsilon_s N_d$ but the intercept on the V_r axis is increased from V_i to V_i' given by;

$$V_i' = V_{d0} - \frac{kT}{q} + \alpha \left(\frac{2qN_d}{\epsilon_s} \right)^{1/2} \left(V_{d0} - \frac{kT}{q} \right)^{1/2} + \frac{qN_d \alpha^2}{2\epsilon_s} \quad (2.27)$$

where;

$$\alpha = \frac{\delta \epsilon_s}{\epsilon_i + q \delta D_s} \quad (2.28)$$

The parameter α accounts for the increase in the intercept and is largely dependent upon the thickness of the interfacial layer, δ , the permittivity of the interfacial layer ϵ_s , and the density of states of the layer D_s .

2.4.1.2. Deep traps.

Deep traps can be considered as localised electron states within the bulk of the semiconductor. The term "deep" implies they are energetically far from either the valence or conduction band and are therefore not ionised at room temperature. The occupation of the trap varies in the depletion region of the Schottky barrier as shown in figure 2.5. Those traps below E_F are occupied by electrons, those above are empty and have a net positive charge. The state of occupation and therefore the state of charge will depend upon the degree of band bending which in turn is dependent upon the bias voltage applied to the device.

The degree of influence of deep traps on the overall charge in the depletion region and hence the capacitance is largely dependent upon the test frequency employed. It is normal to make capacitance measurements with an a.c. bridge operating with a d.c. bias and a sinusoidal a.c. test signal of frequency ω_s . The rate of change of the d.c. signal is much less than the a.c. test signal and so can be ignored. The contribution the traps have to the overall capacitance will depend upon the speed at which the traps open, fill and empty. The influence of the traps is therefore a function of the ratio of ω_s to $\tau_t^{-1} (= 2e_n)^{-1}$ where e_n is the probability of a trap emitting an electron into the conduction band in unit time .

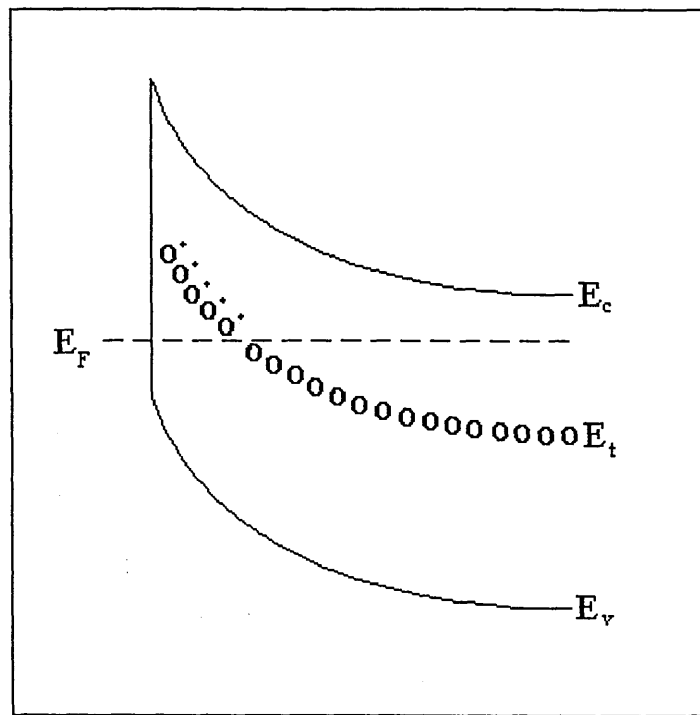


Figure 2.5 Charge state of deep traps under zero bias.

Chapter 3

Review of literature.

3.1 Introduction.

The study of metal - semiconductor contacts can be divided into three broad areas, namely semiconductor surface studies, current transport across the metal - semiconductor interface and deep levels within the semiconductor. A thorough understanding of the physics and chemistry of the metal - semiconductor interface can not be gained without considering these physical properties for the systems under investigation. Presented here is a review of the key works in these three areas for CdTe, CdS and ZnSe. It is apparent from the literature that interest in these various topics is driven by the applications of the materials. For instance, early studies of CdTe surfaces concentrated on wet chemical etching in an attempt to control electrical properties whereas now many papers are concerned with etchants for producing substrates suitable for epitaxial growth of CdTe and lattice matched compounds.

3.2 Experimental surface studies of CdTe, CdS and ZnSe.

The literature contains much information on the surface analysis of CdTe and CdS but very little on ZnSe. The main issues discussed are the characterisation of native oxides and modifications induced by wet or dry etching and annealing.

3.2.1 Surface studies of CdTe.

The surface analysis of CdTe has largely involved the electron spectroscopies of X-ray photoelectron spectroscopy (XPS) and Auger electron spectroscopy (AES). Both of these techniques have been used for well over a decade to provide information on the surface properties of CdTe such as native oxidation, and surface modification.

Ambiguities remain in assigning the correct native oxide chemical composition and etching mechanisms. Problems arise due in part to the various chemical shifts associated with either Te-O bonds or Cd-O bonds. Perhaps the more obvious oxidation state is that of TeO_2 which produces a chemical shift of some ≈ 3.4 eV from the Te $3d_{5/2}$ peak (Briggs and Seah(1990)). The various native oxides of Te all produce noticeable shifts in the Te 3d peaks. The Cd 3d peaks pose a different problem in that any shift they produce is typically much less than 1 eV and is therefore difficult to detect with conventional spectrometers. Cd $3d_{5/2}$ peaks associated with Cd-Te bonds have binding energies of 405.2 eV whereas those of the native oxides such as CdO and CdTeO_3 are 404.2 eV and 405.5 eV respectively (Briggs and Seah (1990)). Further information regarding the chemical state of Cd can be obtained through analysis of the X-ray generated Auger electron features. Al and Mg X-ray sources generate strong Auger spectra associated with transitions in the Cd MNN shell. The Auger features associated with the Cd $M_4N_{45}N_{45}$ and $M_5N_{45}N_{45}$ transitions show energies and shapes which are markedly different if the Cd atoms from which they originate are bonded Cd-Te or Cd-O. In this manner a qualitative analysis of the level of Cd oxidation can be determined. Care must be exercised when employing this type of analysis as, with Mg $K\alpha$ radiation the Cd $M_4N_{45}N_{45}$ peak actually overlaps with the Te $3p_{1/2}$ photoelectron peak. The confusion in correctly assigning the native oxides of CdTe may explain why there seems to be some disagreement within the literature as to the composition of the native oxide. One school of thought suggests that the native oxide can be accounted for purely by the oxidation of Te whereas a second group cites contributions from Cd and Te to the total oxidation of the surface. It should be noted that of the groups proposing Te oxidation, most have not monitored the Cd Auger features for any evidence of Cd oxidation.

A pioneering study of the effects of chemical etching on CdTe surface properties was performed by Patterson and Williams (1978). The (110) CdTe surface was subjected to a number of chemical treatments and subsequently analysed by XPS. A range of oxidation states and, as depicted in figure 3.1, changes in stoichiometry were induced. Cd depletion

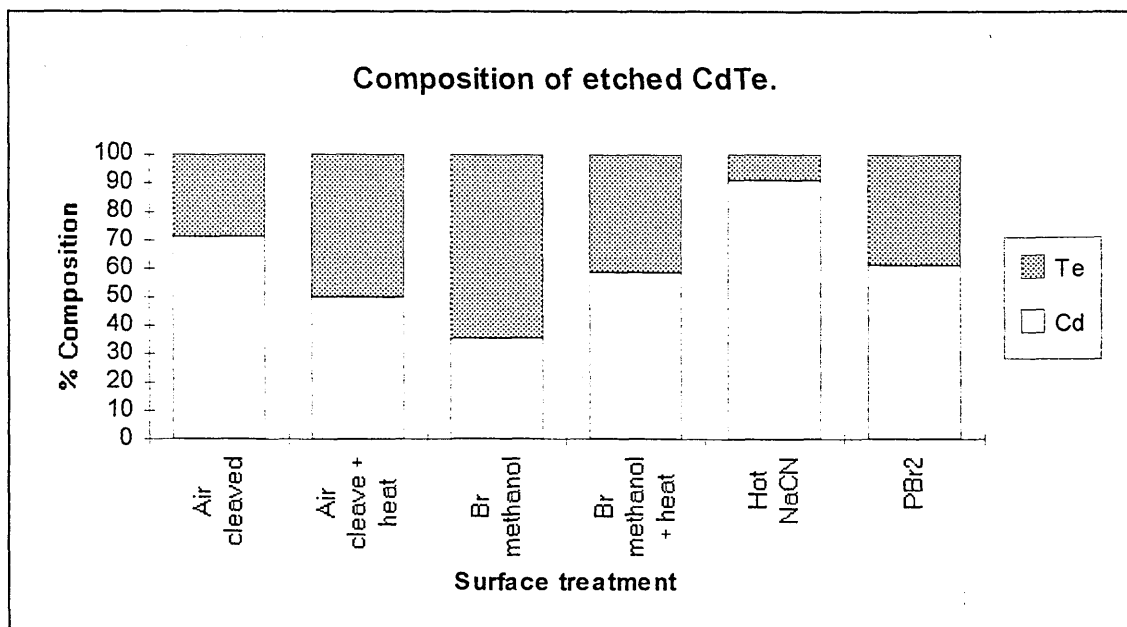


Figure 3.1 The composition of etched CdTe as determined by XPS analysis after Patterson and Williams (1978).

and a high oxide content were observed for acid etched surfaces ($K_2Cr_2O_7/Ag^+$, HNO_3 and ethylene diamine tetra acetic acid (EDTA)). The oxide was attributed to TeO_2 , due to the chemical shift observed for the Te 3d peaks. HNO_3 etched surfaces repeatedly exhibited a third chemically shifted species (possibly TeO_3 or Te_2O_5). Stoichiometric surfaces with a reduced oxide content were produced by boiling NaCN solutions and Br_2 in methanol, which had a tendency to leave a residue of Br. The best surfaces in terms of maintaining surface stoichiometry were those produced by annealing the air exposed, cleaved crystals under vacuum (10^{-6} Torr) for 2 hours at $450\text{ }^\circ\text{C}$ the resultant surface was oxide free and stoichiometric.

Both the structure and composition of the etched (111) CdTe surface were investigated by Solzbach and Richter (1980). All samples were etched in 2% Br_2 in methanol prior to entry into the UHV system. The surfaces were Te rich in agreement with the results of Patterson and Williams. LEED patterns revealed the surface to be amorphous. TeO_2 ,

(identified from the chemical shift of the Te $3d_{5/2}$ peak) was observed for samples exposed to laboratory air for several days. The samples were then ion etched in UHV producing a stoichiometric ordered surface on which thin oxide layers were then grown by exposing the sample to ultra-violet radiation in the presence of ozone. The oxide again produced a chemical shift in the Te 3d doublet. No such chemical shift was observed for the Cd 3d peaks. Changes in the peak energy and shape of the Cd $M_5N_{45}N_{45}$ Auger peak indicated that Cd was involved in the oxidation process. Semiquantitative analysis of the O 1s peak revealed that the level of O was in excess of that which could be accounted for by the exclusive presence of TeO_2 . Computer simulations based upon the free energy of possible oxides indicated that the most likely oxide was $CdTeO_3$. They concluded that the formation of CdO and TeO_2 was only likely for levels of Cd or Te in excess of the stoichiometric levels of $CdTeO_3$.

The (111) surface was again studied by Gaugash and Milnes(1981) using AES to investigate wet chemical etching. Solutions of aqueous NaOH, and aqueous NaOH + Na_2SO_4 produced shiny almost stoichiometric surfaces. An aqueous solution of chromic acid containing 7g $K_2Cr_2O_7$ and 3g H_2SO_4 on the other hand left the surface rich in Te again with a bright polished finish. Te layers, approximately 600 - 800 Å thick were reported for etchants of 70% HCl and 30 % HNO_3 . Surface oxides, as with Solzbach and Richter(1980) were again attributed to $CdTeO_3$ as Cd was found to be uniformly distributed throughout the oxide layers.

Häring *et al*(1983) were the first group to correlate the surface properties of (110) CdTe with the electrical characteristics of metal contacts formed onto such surfaces. The chemical etchants and the results obtained largely followed those of Patterson and Williams. Br_2 methanol etched samples were depleted of Cd, the excess Te appeared to be in the elemental state. Subsequent heat treatment of the sample in H_2 atmosphere returned the surface to a stoichiometric composition. The most likely mechanism for this

was identified as the formation of gaseous H_2Te or the evaporation of Te. Chromic acid etched surfaces were also depleted of Cd and enriched in Te. In this case the Te was more than 50% TeO_2 (identified from the chemical shift of the Te $3d_{5/2}$ peak). Häring's group also investigated the oxidation rates of the (100) surface and found it to be much slower than the (110) surface. The H_2 heat treatment at 450 °C removed all native oxides or excesses of elements by evaporation.

The surface chemistry of n and p-type CdTe photoelectrodes was the subject of the comprehensive study by Ricco *et al* (1984). Oxidised surfaces exhibited E_F pinning which was attributed to the oxidation products of elemental Te which having a large work function would be expected to subsequently produce a high Schottky barrier, essentially pinning E_F . Figure 3.2 demonstrates the range of surface stoichiometric control achieved by this group with oxidising and reducing wet chemical etchants.

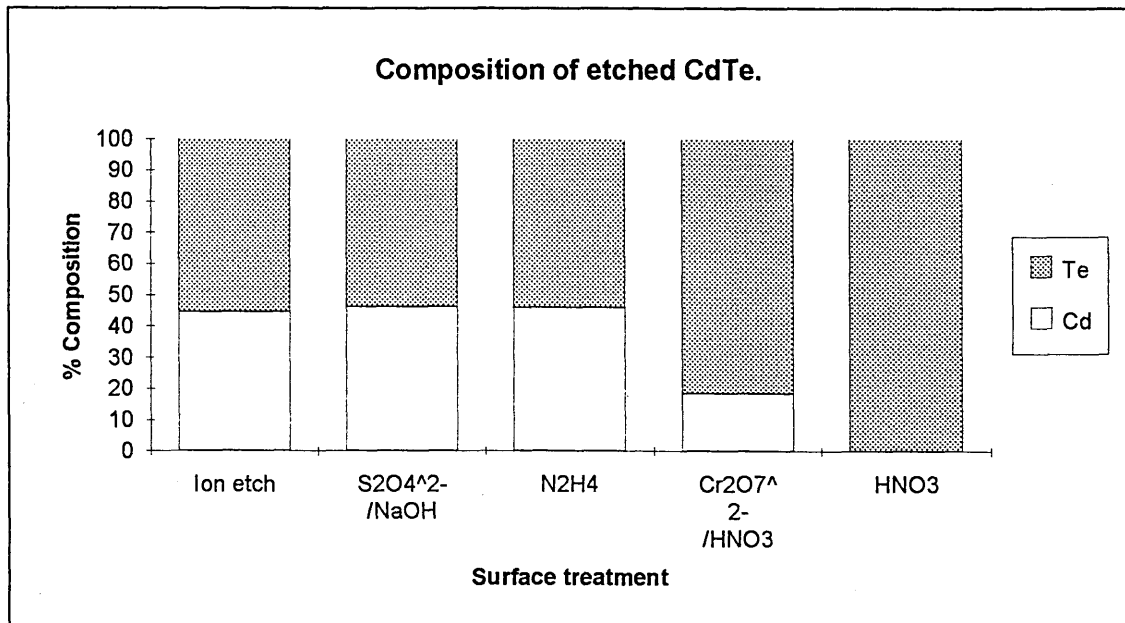
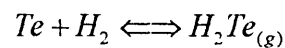
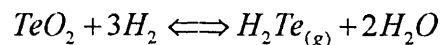


Figure 3.2 Composition of oxidised and reduced CdTe surfaces determined from XPS by Ricco *et al* (1986).

Lu *et al*(1987) again employed AES to investigate the effects of wet chemical etching on the polished (111) surface of CdTe. The results were similar to previous authors but one etchant, dithianite (0.6M Na₂S₂O₄ / 2.5M NaOH) replaced some of the Te with S to form CdS. Gibbs free energies of CdS and CdTe were quoted as -22.0 kcal/mol and -37.4 kcal/mol respectively, suggesting the substitution of S into the CdTe surface is an energetically favourable reaction. H₂ heat treatment produced a stoichiometric surface with a reduced oxide content in agreement with Häring *et al* (1983). The successful removal of excess Te or TeO₂ was attributed to the following reactions :



and



These assumptions were later correlated with further XPS and LEED analysis of similar surfaces (Lu *et al* (1990)). Chemomechanically polished surfaces (1.5% Br in ethylene glycol) had an enriched Te layer, which was identified as being in the elemental (Te⁰), state. Subsequent Ar ion sputtering in UHV removed this layer but produced an amorphous surface layer in terms of structure. Annealing these surfaces at 300 °C for 5 min restored the ordered stoichiometric (111) surface, with no evidence of surface reconstruction.

Air grown native oxides on the (100) surface of CdTe were investigated by Choi and Lucovsky(1988). In a similar manner to Solzbach and Richter samples were subjected to a 1% Br₂ methanol pre-treatment and then treated to either an *in situ* Ar⁺ ion etch or chemical etch to remove the excess Te. Samples were left under normal laboratory conditions for a number of days to produce air grown oxide layers. After analysis this oxide layer was removed by dissolution in deionised water. From the results of their analysis they concluded that the native oxide of CdTe was a combination of Cd-O and

Te-O bonds. Following the thermodynamic calculations of Rhiger and Kvass (1982) CdTeO₃ was assumed to be the dominant native oxide.

Dharmadasa *et al*(1989) investigated the effects of surface preparation on the electrical properties of metal contacts formed to etched surfaces, in a similar manner to Häring *et al*. The surface treatments followed earlier work by the same group (Sobiesierski *et al* (1988)), in which photoluminescence spectroscopy was used to characterise deep levels of chemically etched surfaces. p-type CdTe was cleaved under UHV, XPS revealed this surface to be stoichiometric and oxide free. These surfaces were then etched in treatments similar to Patterson and Williams. 1% Br in methanol produced an enrichment of Te, subsequent treatment of this surface with hydrazine removed the Te layer to produce a layer of enriched Cd composition. Etching samples in a strong oxidising solution of chromic acid (K₂Cr₂O₇ + H₂SO₄) followed by a reducing etch of (Na₂SO₄ + NaOH) lead to a depletion of Te at the surface. Sb and Au contacts were then formed onto these surfaces, Cd rich surfaces systematically produced higher Schottky barriers ($\phi_b = 0.94$ eV) than Te rich surfaces ($\phi_b = 0.72$ eV) these two discrete barrier heights were tentatively ascribed to the deep levels enhanced by wet chemical treatments. The transport properties of devices formed to these surfaces will be discussed below (Sec 3.3.2).

The successful growth of epilayers by molecular beam epitaxy (MBE) on CdTe substrates was investigated by Waag *et al*(1989). All the substrates were chemo-mechanically polished and thoroughly degreased in organic solvents followed by a 90 s etch in 1.5% Br₂ in methanol. Samples prepared in this way were rich in Te. The surface chemistry was then monitored as samples were heated *in situ* from 100 up to 450 °C. At 200 °C the Cd to Te ratio again approached stoichiometry as surface oxides desorbed. Temperatures in excess of 200 °C resulted in the preferential evaporation of Cd leaving a surface consisting of 58% Te. At the elevated temperature of 350 °C the oxygen content of the surface was estimated to be 5% of one monolayer.

Bose *et al*(1989) investigated the effects of surface treatments to polycrystalline CdTe in an attempt to explain the apparent improvement in efficiency of metal/n-CdTe solar cells after a Ru⁺ ion treatment as reported by Mandal *et al*(1987). The samples were firstly etched in a saturated aqueous solution of chromic acid containing H₂SO₄ and K₂Cr₂O₇ followed by a wash in 0.1M Na₂S₂O₃. All samples were then subjected to Ru⁺ ions in an acidic aqueous solution of 0.01M RuCl₃. Unetched surfaces showed a strong contribution from TeO₂. This oxide layer was removed by bombardment with Ar⁺ ions. After etching in the Ru⁺ ion solution the surfaces were quite different from the as-received surfaces having been completely oxidised. The oxide was identified as a Te⁴⁺ state, possibly TeO₂ or CdTeO₃. Ru⁺ ions were shown to play a catalytic role in the oxidation of CdTe, thicker surface oxides produced increased band bending which improved the efficiency of the photoelectrochemical solar cells.

Following the earlier work of Waag *et al* (1989), Wu *et al* (1993) investigated the best surface treatments on (100) CdTe with the aim of producing a substrate surface suitable for the epitaxial growth of CdTe and ternary lattice matched compounds such as CdHgTe and CdMnTe. The pre-treatment consisted of thoroughly degreasing the samples in organic solvents and a 30s etch in 15% HCl with a final wash in deionised water. Substrates prepared in this manner exhibited a strong surface oxidation manifest by a chemical shift of the Te 3d peaks associated with TeO₂, calculated to be at least 17 Å thick in good agreement with Patterson and Williams (1978). MBE growth of epitaxial CdTe proved unsuccessful on such surfaces. The oxide layer was reduced by adjusting the time of the HCl treatment to about 20s. CdTe surfaces produced by such an etch had a reduced oxide layer which was estimated to be 20-30% of one monolayer. Subsequent heating of the sample to between 300 - 340°C reduced this oxide layer to zero, epitaxial growth on such surfaces was then possible.

As well as studies on etched CdTe, several groups have worked with the ternary compounds of CdTe such as $\text{Hg}_{1-x}\text{Cd}_x\text{Te}$, some of these studies can be applied to CdTe. Davis *et al* (1981) etched $\text{Hg}_{1-x}\text{Cd}_x\text{Te}$ ($x = 0.2$) electrochemically using a C cathode in a 0.01 M KOH in ethylene glycol solution. The thickness of the anodic oxides was proportional to the applied voltage. XPS results for these films and standard samples of CdTeO_3 and CdO were used to identify the oxide phase. The X-ray generated Cd $M_4N_{45}N_{45}$ Auger feature indicated that the native oxide phase had a contribution from oxidised Cd. XPS depth profiling showed that oxides prepared in this manner had a uniform composition throughout their depth. Following the work of Robertson *et al*(1978) who constructed a phase diagram for CdO and TeO they concluded the oxide to be a mixture of CdTeO_3 and CdTeO_5 . Rhiger and Kvaas(1982) also studied oxidation of ternary $\text{Hg}_{1-x}\text{Cd}_x\text{Te}$ ($x = 0.3$). Samples were etched in Br_2 containing solutions and then oxidised by either air exposure, anodising in KOH or exposure to O plasma. XPS analysis of the Te 3d and O 1s photoelectron peaks allowed the construction of a TeO stoichiometry plot. In such a plot the monolayer coverage for Te is plotted against O and theoretical lines for the stoichiometric oxides such as, TeO_2 and CdTeO_3 are plotted. In this way the native oxide of samples etched only in Br_2 methanol and air exposed was found to be composed solely of TeO_2 . Samples which had been anodised or plasma etched gave a strong indication of CdTeO_3 being the dominant oxide species.

3.2.1.1 Summary.

It is evident that the surface properties of CdTe are readily influenced by external treatments. XPS analysis of the core level emissions can not unambiguously identify the native oxide phase but monitoring the X-ray generated Cd MNN Auger features shows that Cd is oxidised in most native oxide surfaces. Table 3.1 gives a summary of photoelectron peak binding energies obtained from the literature regarding etched CdTe. It seems the most probable surface oxide is CdTeO_3 although there are several reports of

Surface treatment	Cd 3d _{5/2} , B.E. eV	Te 3d _{5/2} , B.E. eV			Cd Auger (eV) M ₅ N ₄₅ N ₄₅	Reference
		Te ²⁺	Te ¹⁺	Te ⁰		
Polished		572.9			876.6	Solzbach & Richter (1980)
Sputtered		572.0			876.6	
Oxidised			576.1		878.6	
Te (sputter)				573.0	-	
Te(oxidised)			576.2		-	
N, cleaved	405.6	573.0				Häring <i>et al</i> (1983)
Air exposed	405.5	572.5	576.1	-	-	
Sputtered	405.08	572.5	-	-		Ricco <i>et al</i> (1984)
Oxidised			576.2	573.24		
Te (sputter)				573.54		
Te (oxidised)			576.4	573.5		
Unetched	405.4	573.7	576.7	-	880.4	Choi and Luckovsky (1988)
30 days air	405.5	573.6	577.0		879.2	
Sputter	877.8	572.0	-	-	877.8	
Polished	405.4	574.0	577.7			Bose <i>et al</i> (1989)
Sputtered	405.4	574.5	-			
TeO ₂ std			576.1			
CdTeO ₃ std	405.7					
CdO std	403.0					
Oxidised	406.1	573.8	577.1	-	871.9†	Lu <i>et al</i> (1990)
Sputter	409.8		577.2	-	875.8†	

Table 3.1 Binding energies of Te 3d_{5/2}, Cd 3d_{5/2}, and Cd M₅N₄₅N₄₅, Auger feature.

† Modified Auger parameter, $\alpha' = \text{Cd } 3d_{5/2} \text{ (BE)} + \text{Cd } M_4N_{45}N_{45} \text{ (KE)}$.

Br₂ methanol etching producing TeO₂ on surfaces which had a prolonged post-etch air exposure. The best surfaces in terms of stoichiometry and low oxide content are obtained by annealing the samples in H₂ atmosphere; typical conditions are 450 °C for ≈ 2 hours. The required temperature can be reduced by first chemical etching the surface, and then annealing at 300 - 340 °C for 15 min. A number of authors have demonstrated that the surface stoichiometry can be strongly influenced by the etch treatment. The oxidation of the cleaved surface in air is much slower for the (111) surface compared with the (110) surface. This process seems to be self-limiting. Chemically etched surfaces appear to be amorphous when examined by LEED, crystallinity and stoichiometry can be restored by Ar ion etching.

3.2.2. Surface studies of CdS.

Unlike CdTe the surface etching of CdS has not been extensively examined. Surface studies have concentrated on characterising thin films of CdS usually deposited by electrodeposition techniques for example Nair *et al* (1994). Early studies centred upon techniques of chemomechanically polishing wafers cut from single crystal boules of material. Of particular interest was the chemisorbtion of O which was shown to improve many photovoltaic properties of the material, Amalnerkar *et al* (1982). Identification of the native oxide species and correct chemical composition of the surface has many problems analogous to those associated with CdTe. The chemical shift of Cd bonded Cd - S and Cd - O is, as with CdTe less than 1 eV ($\Delta E = 0.9$ eV Briggs and Seah (1990)). S on the other hand does display a larger chemical shift of up to 4.95 eV for the SO₄²⁻ state (Briggs and Seah (1990)). The X-ray generated Auger feature for CdS has not been reported by any authors due to the fact that the energy is 2114.4 eV (for S KL₂₃L₂₃ Briggs and Seah (1990)) and therefore too great for the commonly used Mg and Al K_α lines.

Processes of chemomechanical polishing were discussed by Sullivan and Bracht (1967) by feeding 30% HCl onto a rotating polishing block to produce flat polished surfaces suitable for electronic devices. They reported that epitaxial growth on such surfaces was possible. Pickhardt and Smith (1974) developed a similar technique of producing flat surfaces from wire sawn wafers. The etchant employed by this group consisted of 1% HNO₃, 30% precipitated silica, 0.1% detergent and 10g AlCl₃ per litre of H₂O fed onto a rotating polishing pad. Samples polished in this manner were introduced into a UHV system and heated for 1 min at 450 °C. Subsequent AES analysis, which was in fact the first surface analysis to be performed on CdS, showed there to be less than a monolayer of contamination present after this heat treatment. Pritchard and Wagner (1977) developed polishing techniques to process saw-cut wafers. After initial mechanical polishing the wafers were chemically polished with aqueous HCl/KCl (pH = 2.5) fed onto the rotating polishing pad. Optically flat surfaces were produced within 2-4 hours of polishing. The level of surface damage produced was measured by Ar laser ($\lambda = 457.9$ nm) photoluminescence spectroscopy, sensitive to layers of less than 0.1 μ m. This showed there to be very little damage at the surface, the spectra being identical to that obtained from a cleaved sample. Giving a qualitative indication of the surface damage but no chemical information.

Several groups have applied modern surface analytical techniques to the study of CdS surfaces. Amalnerkar *et al* (1982) studied the effects of oxygen chemisorption on thick films of electrodeposited CdS. The films were heated to 600°C in a N₂ atmosphere containing trace levels of O₂ for varying lengths of time. Subsequent XPS analysis revealed three intense peaks associated with the S 2p photoelectron peaks. The large spread of the peaks (over a 20 eV range) indicated the formation of several chemical species of S. These chemical species were assigned following the analysis of Walton (1980) who demonstrated that the binding energy of S 2p decreased in the fashion SO₂ > SO₄²⁻ > SO₃²⁻ > S²⁻. The films were then heated under vacuum (10⁻⁵ Torr) which lead to

a substantial reduction in the intensity of the two lower binding energy peaks, associated with the desorption of the S species. Further evidence of the formation of SO_x species came from analysis of the O 1s peak which was very broad and chemically shifted to 532.4 eV.

The effects of air annealing on thin films ($\approx 1\mu\text{m}$ thick) of chemical bath deposited β - (cubic) CdS were investigated by Kolhe *et al* (1984) using X-ray diffraction and XPS. Analysis of the Cd 3d peaks revealed that as-grown films had a small content of CdO which was apparent by the appearance of a shoulder to the high binding energy side of the Cd 3d peaks. After air annealing the shoulder dominated the Cd 3d peaks indicating CdO to be the dominant chemical state. Analysis of the O 1s peak revealed the as-grown film to contain several O chemical species associated with chemisorbed oxygen, native oxides of CdS and adsorbed water vapour, the dominant species appeared to be chemisorbed O. The S 2p doublet appeared as a broad peak for the as-grown film again with a chemically shifted species at higher binding energy associated with the S^{2-} and SO_4^{2-} species as reported by Amalnerkar *et al* (1982). Air annealing doubled the intensity of the SO_4^{2-} species while reducing to almost half that of the S^{2-} species. The observations for Cd 3d, O 1s and S 2p peaks indicated that air-annealing induced oxidation of CdS. The composition of the oxide layer was consistent with a layer incorporating CdSO_4 , CdO and CdS.

Roche *et al* (1985) investigated the use of CdS as the photoanode in a photoelectrochemical solar cell. In this type of cell CdS acts as the anode for photon induced currents generated at the interface between CdS and an electrolyte solution. One of the main problems with this type of system is the photocorrosion of the electrode, electrolytes are usually chosen to inhibit this process. Roche and co-workers investigated the different species formed on the surface of CdS after exposure to photocurrents in the

ion probe was uncertain. It was clear that oxygen may bond in two distinctly different configurations on the surface of CdS depending upon the dry etching treatment employed.

The most recent study of CdS surfaces was that of Chen and Munir(1991) who investigated the composition of the polar {0001} surfaces of CdS with AES. The S LMM and Cd MNN peak to peak heights were used to determine the surface stoichiometry of Ar ion etched surfaces. Samples were ion etched with a 25 mA emission current and 2kV beam voltage for 30 min, the beam voltage was then reduced to 0.65 kV for a further 2 hours. The etched surface displayed an initial increase in the intensity of the Cd and S peaks as surface contamination was removed. Further etching lead to the enrichment of S at the surface indicating a preferential sputtering of Cd. Such an

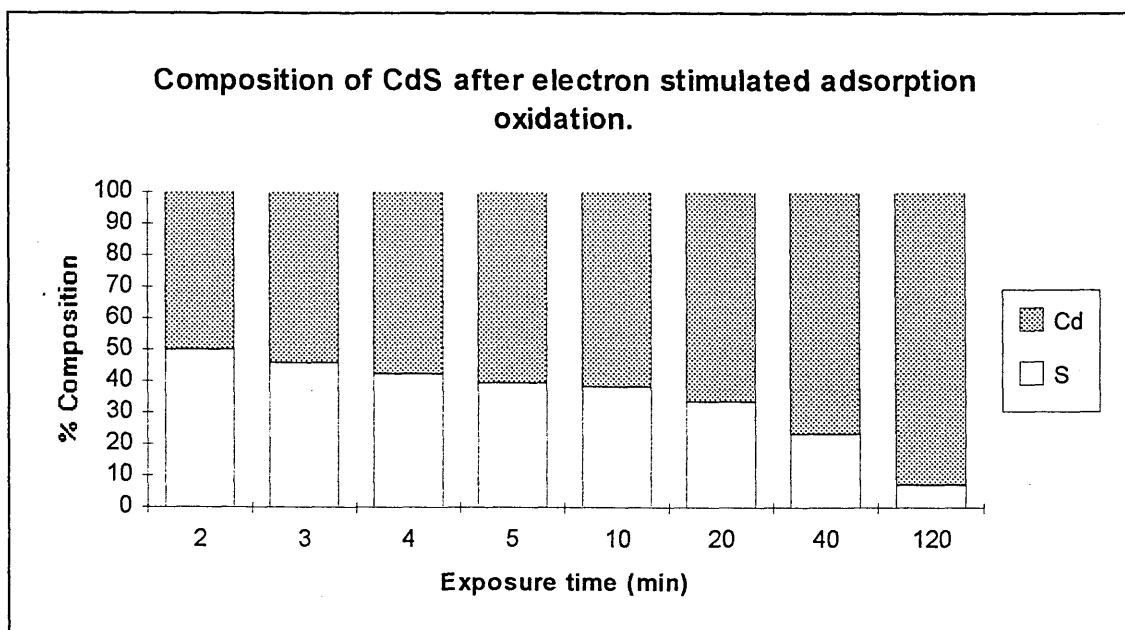


Figure 3.3 The composition of CdS after electron stimulated adsorption oxidation as determined by XPS after Webb and Lichtensteiger (1986)

Compound / treatment	S 2p B.E. (eV)			Cd 3d _{5/2} B.E. (eV)	O 1s B.E. (eV)			Reference
	S ²⁻	SO ₄ ²⁻	SO.		Chemisorb O ₂	CdSO ₄	Adsorb H ₂ O	
Oxidised	162.6	172.8	179.7	-	-	532.4	534.6	Amalnerkar <i>et al</i> (1982)
CdS	160.7	170.5		404.7	530.1	532.4	534	Kolhe <i>et al</i> (1984)
Oxidised	160.6	170.3		406.8	530.0	-	533.6	
CdS	243.4 [†]	-	-	700.1 [†]	-	-	-	Roche <i>et al</i> (1985)
CdSO ₄	236.2 [†]	-	-	700.8 [†]	-	444.9 [†]	-	
CdO	-	-	-	699.4 [†]	444.6 [†]		446.4 [†]	
Cd(OH) ₂	-	-	-	701.7 [†]				
Cd	-	-	-	697.6 [†]	-	-	-	
Oxidised (ESA)	161.5	168.5	-	405.0	528.5	531.2	-	Webb <i>et al</i> (1986)
Oxidised (NCE)	161.6	168.1	-	405.0	-	531.3	-	
CdS	162	-	-	405.4	529.5	532	-	Nair <i>et al</i> (1994)
Cd	-	-	-	405.14	-	-	-	

Table 3.2 A summary of binding energies of S 2p, Cd 3d_{5/2} and O 1s species taken from the literature.

[†] denotes the Auger parameter as defined by Roche *et al* (1984) (see text).

enrichment of S was difficult to explain, normal sputtering mechanisms such as direct energy transfer or thermal sputtering of higher vapour components would lead to enrichment of Cd. One explanation was the so called knock-on effect where forward scattering of the smaller/lighter component below the surface is exposed by further etching, revealing an enrichment of that component on the surface.

3.2.2.1 Summary.

It is evident that CdS is easily oxidised when heated in air. This procedure of course should be avoided as a pre-contact formation procedure. Heating in UHV, as with CdTe seems to desorb much of the surface oxides. A summary of the photoelectron binding energies for typical species reported in the literature is given in table 3.2. No systematic study of the effects of wet chemical etching has been performed on this material so it is difficult to predict suitable etchants.

3.2.3 Surface studies of ZnSe.

Relatively little surface characterisation has been performed on ZnSe, recently interest in successful dry etching techniques for *in situ* processing has driven the need for surface analysis of ZnSe. The practical problems of XPS are similar to those associated with both CdTe and CdS in that Zn core levels like Cd exhibit sub-eV chemical shifts for different chemical species. Se on the other hand has a chemical shift of some 3.6 eV when going from the elemental to oxidised state (for Se 3d level, Briggs and Seah (1990)).

Dry surface etching of ZnSe along with ZnS, CdS and CdTe was investigated by Pearton and Ren (1993). Electron cyclotron resonance generated plasmas of CH₄/H₂/Ar and H₂/Ar gases produced anisotropic smooth surfaces with minimum disruption. Using this technique it was possible to produce micron-deep features. Sotomayor Torres *et al* (1994) used a similar dry etching technique to produce nanometer scale features on MOCVD grown ZnSe on GaAs. Reactive ion etching with an *rf* plasma of 1:2 CH₄:H₂ ratio, produced flat surfaces, etching rates were anisotropic. Surfaces produced in this manner were examined by XPS, the stoichiometry of the surface could be influenced by controlling the ratio of CH₄:H₂. Reducing the ratio increased the amount of Se at the surface. The increase in Se concentration was attributed to a preferential etching of Zn,

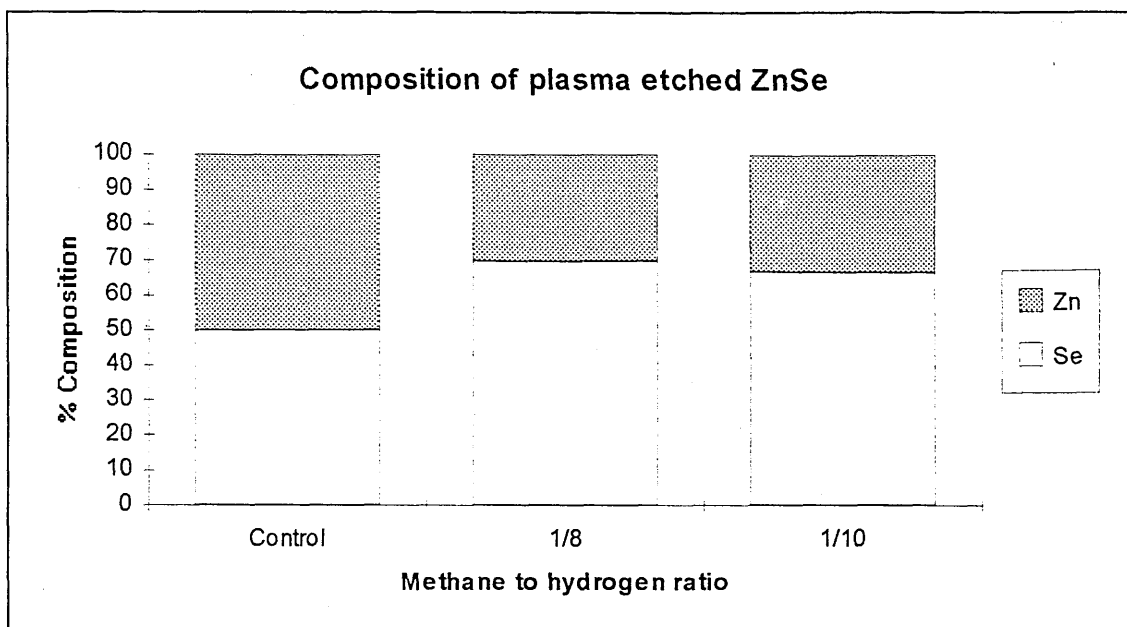


Figure 3.4 Composition of plasma etched ZnSe for varying methane to hydrogen composition after Sottomayor Torres *et al* (1994).

photoluminescence was not able to detect a corresponding increase in Zn vacancies. This was attributed to the larger sampling depth of PL ($\approx 1\mu\text{m}$) as compared with XPS ($\approx 3\text{nm}$).

3.2.3.1 Summary.

Although very little surface analysis of ZnSe has been performed, it seems that it is possible to induce stoichiometric variations at the surface. The chemical shift of the Se core level peaks and the accessibility of both Se and Zn LMM Auger features indicates that surface analysis by XPS in the manner of CdTe and CdS is possible.

3.3. Properties of metal contacts to II-VI compounds.

3.3.1 Introduction.

The properties of metal contacts formed to II-VI compounds have been studied for a number of decades. Early studies concentrated on macroscopic I-V and C-V methods to characterise the electrical properties. Advances in UHV technology lead to many photoemission studies of the evolving metal/semiconductor interface as a function of metal deposition. Metals were generally evaporated onto vacuum cleaved, atomically clean substrates. More recently attention has turned to metal contacts formed to epitaxial layers. Presented here is a review of the key papers dealing with metal contacts to CdTe, CdS and ZnSe.

3.3.2 Metal contacts to CdTe.

Kuech (1981) produced an early analysis of metal contacts to single crystal CdTe. The contacts were fabricated by cleaving crystals of CdTe in a stream of metal vapour and gave Schottky barrier heights, $\phi_b = 0.65$ and 0.45 eV for Au and Cd respectively. Air cleaved samples repeatedly produced ϕ_b 's = 0.71 eV for Au. Au contacts formed with Cd interlayers produced some interesting results: interlayers greater than 2 \AA gave the barrier height of pure Cd i.e. $\phi_b = 0.45$ eV. Those contacts which exhibited some evidence of alloying or intermixing produced a high barrier of $\phi_b = 0.95$ eV. The low barrier could be converted to this high value by annealing the sample at temperatures up to 200°C , temperatures greater than this produced a degradation of the electrical properties as evidenced by an increasing n value. Kuech suggested that the pinning of E_F in this manner was due to defects induced by the alloying process.

Continuing from their earlier work on chemical etching Patterson and Williams (1982) formed metal contacts to vacuum cleaved and air exposed CdTe. All the vacuum cleaved

interfaces were non-abrupt and Cd out diffusion into the metal contact was observed for Al, Cu and Ni. Oxide layers on the surface prior to contact formation produced higher barriers in all cases. They could not explain why this should happen but commented that the complexity of the system was such that much more experimental data was necessary.

Indeed Williams group continued to be very active in the field and produced many key papers. Dharmadasa *et al* (1989) reported the formation of two distinct Schottky barriers for Au and Sb contacts on etched CdTe. Surfaces chemically etched to be Te rich (deficient in Cd) repeatedly gave $\phi_b = 0.72$ eV for both Au and Sb, while surfaces chemically etched to be rich in Cd (Te deficient) gave $\phi_b = 0.93$ eV. The appearance of two barriers not only for Au but for Sb contacts also, raised important issues of metal-semiconductor theory. The two barrier heights could well be explained by the EWF model for Au alone as for Te/n-CdTe, $\phi_b = 0.72$ eV and for Au/n-CdTe, $\phi_b = 0.92$ eV. However as the same Schottky barriers were observed for Sb, the barrier height must be independent of the metal work function, ϕ_m . The only other model proposed to explain these results was the UDM model. The barrier heights were related to deep levels due to Te vacancies at $E_c - (1.0 - 0.9$ eV) and $E_c - 0.7$ for Cd vacancies as reported by Zanio (1978) for defects in CdTe. This point was later reinforced by Williams *et al* (1989) in a comprehensive summary of the measurements made of metal layers on CdTe. Schottky barriers formed onto chemically etched CdTe generally exhibited a stronger pinning of E_F , this pinning was attributed to the formation of defects due to changes in surface stoichiometry enhancing defect states. Fowell *et al*(1990) characterised similar Au contacts on CdTe using the technique of ballistic electron emission microscopy (BEEM) introduced by Kaiser and Bell (1988). The BEEM technique allows the barrier height to be measured with high lateral resolution of approximately 10Å. Figure 3.5 shows the distribution of barrier heights they achieved over an area 200 X 400 Å square. It is interesting to note that although there are only fifteen sample points, the barrier heights appear to be split into discrete levels around those values determined by the macroscopic

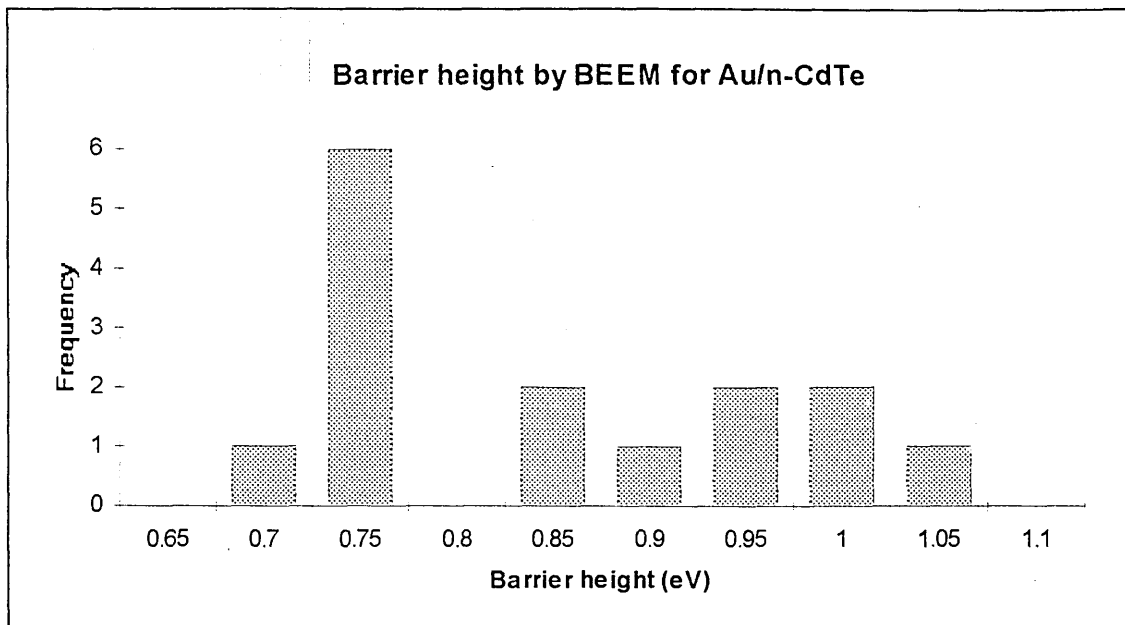


Figure 3.5 The variation of Schottky barrier height as determined by BEEM for Au contacts to chemically etched CdTe after Fowell *et al* (1990).

I-V measurements of Dharmadasa *et al* (1989).

Vitomirov *et al* (1991) realised an etching/surface treatment procedure to give clean CdTe surfaces. CdTe (111) surfaces were etched in 0.05% bromine methanol solution, rinsed in methanol and dried in an inert atmosphere. The samples were then annealed at temperatures $< 350^{\circ}\text{C}$ which lead to the desorption of excess Te to produce surfaces with a decreasing Te content. Deposition of Au overlayers lead to the disruption of the interface leading to the segregation of Te to the surface and the intermixing of Cd in the Au overlayer. E_F was pinned to a position 0.55 eV above the valence band maximum (VBM) leading to $\phi_b = 0.9$ eV, in good agreement with $\phi_b = 0.93$ eV observed for Te deficient surfaces by Dharmadasa *et al* (1989). One explanation of this behaviour was given to be the formation of mid-gap levels due to the non-stoichiometric surface induced by the post etch anneal .

Van Meirhaeghe *et al* (1991) took (111) n-CdTe single crystals and etched them in 2% Br₂ in methanol solution, samples were then annealed in an Ar atmosphere at temperatures (T_a) between 160 to 350 °C. XPS analysis revealed the unetched surface to be heavily oxidised, chemical etching removed most of the oxide to leave a Te rich surface. Monitoring the surface composition for increasing T_a revealed that Te preferentially desorbed, a stoichiometric surface was achieved at around 240°C and further heating depleted the surface of Te still further. Au contacts formed by vacuum evaporation onto the annealed surfaces showed barrier heights dependent upon the annealing temperature and hence surface composition. A maximum barrier of $\phi_b = 0.92$ eV was reported for stoichiometric surfaces ($200\text{ °C} < T_a < 240\text{ °C}$), Cd rich surfaces ($T_a > 240\text{ °C}$) produced $\phi_b \approx 0.82$ eV. The high barrier for stoichiometric surfaces was explained in terms of the EWF model. The stoichiometric surface was supposed to be unreactive leading to ϕ_b dependent upon the metal work function alone while Cd rich surfaces having a lower barrier height were more dependent upon interfacial reaction leading to barrier lowering. Incidentally the low barrier for Cd rich surfaces was in contradiction of Dharmadasa *et al* who reported the higher barrier of $\phi_b = 0.93$ eV for Cd rich surfaces.

3.3.2.1 Metal - CdTe interface studies.

Au, Ag and Al were evaporated onto the clean cleaved and oxidised surfaces of CdTe by Humphreys *et al* (1980), the evolving interface being studied by photoemission while thick layers were characterised by C-V techniques. They found that the metal-CdTe interface was unstable with strong evidence for intermixing. Au films formed onto vacuum cleaved surfaces produced $\phi_b = 0.96$ eV whereas air exposed oxidised surfaces had $\phi_b = 1.1$ eV when measured by the C-V technique. The suggestion was made that

defects created at the interface influenced the Schottky barrier height but no clear conclusions could be made.

Dharmadasa *et al* (1987) formed metal overlayers to chemically etched (110) CdTe, using eighteen different metals. Surfaces were prepared by etching in a solution of 1% Br in methanol followed by a wash in KOH in methanol. I-V and C-V analysis gave Schottky barriers ranging from ohmic in nature to an upper threshold of 0.73 eV. Ni, Co, Sb, Fe, and Pb yielded barriers between 0.69-0.77 eV, with excellent agreement between I-V and C-V results. Au, Ag and Hg contacts gave barrier heights of 0.72 eV when characterised by the I-V technique but yielded consistently higher values when measured by C-V methods. Cd, Zn, Sn, Pb, Ga and Al all produced inconsistent values when measured by both C-V and I-V techniques to give $\phi_b \leq 0.62$ eV. Cr, Mn and V produced ohmic like contacts. Soft x-ray photo-emission spectroscopy (SXPS) was used to study the effects of depositing thin overlayers of Ag and Mn as representative of the two common barrier cases. Mn deposited on to chemically etched CdTe formed oxides of Mn whereas Mn deposited onto cleaved CdTe crystals formed compounds such as Mn telluride's. Ag deposited onto CdTe showed a segregation of Te to the surface of the metal suggesting alloying/bonding of Ag with Cd to release Te.

Metal overlayers on cleaved (110) CdTe surfaces were investigated by Friedman *et al* (1988) none of the observed interfaces were abrupt. Ag, Cu and Au all showed some evidence of Te segregation to the surface of the metal layer. It was concluded that this Te was reacted with the metal forming the relevant tellurite. Cu and Au overlayers both had dissociated Cd segregated within the metal overlayer. All metals induced E_F pinning at $E_V + (0.8 - 1.0)$ eV, leading to barrier heights of 0.65 - 0.45 eV. Shaw *et al* (1988) also formed thin metal layers (< 10nm) on cleaved (110) CdTe, the evolving interface was studied with both photoemission and photoluminescence spectroscopy. Interfaces were heated *in situ* and laser annealed. Photoluminescence revealed the formation of a

deep level; at $E_v + 1.1$ eV, laser annealing produced another level at $E_v + 0.75$ eV. Both of these levels were observed on samples obtained from different sources and were therefore assumed to be native to CdTe. The progressive out-diffusion of Te into the metal overlayer was observed and these two levels were linked with a Te vacancy or Te vacancy-impurity complex. Photoemission showed that for Au/n-CdTe the initial E_F position was $E_v + 0.55$ eV ($\phi_b = 0.95$ eV) in agreement with EWF model for Au/n-CdTe. Annealing tended to pin E_F at $E_v + 0.9$ eV ($\phi_b = 0.55$ eV) which was very close to the first deep level, further laser annealing lead to pinning of E_F at $E_v + 1.0$ eV ($\phi_b = 0.45$ eV) in reasonable agreement with the second of the deep levels observed by photoluminescence spectroscopy.

Trafas *et al* (1990) observed the chemical and surface reactions as metal layers were formed on the cleaved (110) surface of CdTe. The seven metals used were divided into three groups :

- non disruptive and non reactive (Ag and In)
- disruptive but weakly reactive (Pd and Au)
- highly reactive (Al, Ti and Ce).

Of the reactive metals, all released Te which appeared at the metal surface. Au and Pd caused the release of both Cd and Te. Thin Ti interlayers (0.4 nm) were introduced prior to Au formation, there was a negligible interaction between Au and the CdTe substrate, Cd was still segregated to the metal surface but to a lesser degree than without the interlayer. It should be noted that the relative inactivity of Ag, In and Au is in marked contrast with the results of Dharmadasa *et al* (1987) who reported some degree of reactivity for these metals on chemically etched surfaces.

3.3.2.2 Summary.

Metal contacts formed on CdTe exhibit behaviour contradictory to the Schottky model, a number of barrier heights have been observed for Au/n-CdTe as can be seen from figure 3.6. Two of these barriers at 0.72 and 0.93 eV were also observed for Sb, Dharmadasa *et al* (1989). There appear to be at least three distinct barrier heights, independent of the measurement technique or the group. Such results indicate that pinning of E_F plays an important role in the formation of the Schottky barrier height. Shaw *et al* (1988) and Dharmadasa *et al* (1989) have both highlighted the importance of deep levels due to defects. BEEM experiments have demonstrated that such contacts can be highly inhomogeneous on the sub-nanometer scale. Interfaces have been shown to be highly reactive with both Cd and Te segregating to the surface for most metals including Au.

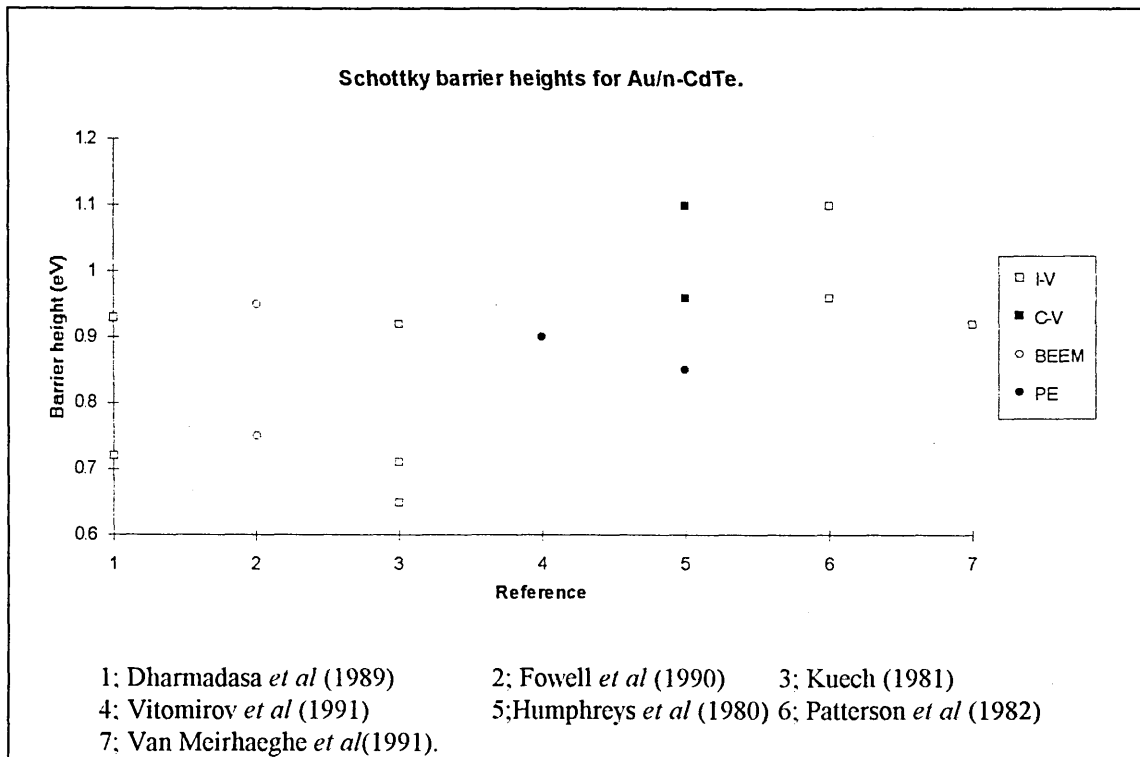


Figure 3.6 Summary of Schottky barrier heights observed for Au/n-CdTe.

3.3.3 Metal contacts to CdS.

One of the earliest studies of metal contacts to CdS was performed by Spitzer and Mead (1963). Au, Cu, Al, Ag, Ni and Pt contacts were formed to vacuum cleaved CdS surfaces. These results were compared to contacts formed to chemically etched surfaces. Pt again produced the highest barriers with Au consistently giving Schottky barriers of 1.0 eV. Al consistently produced ohmic devices.

Goodman (1964) also studied a number of metals, vacuum evaporated onto the different faces of CdS. Samples were etched in HCl acid, crystals were then thoroughly washed in deionised water prior to contact formation on the $(10\bar{1}0)$, $(11\bar{2}0)$ and the polar (0001) and $(000\bar{1})$ surfaces. Barrier heights for Al, Ag, Cu, Pd, Au, and Pt were calculated by C-V, I-V and photoresponse techniques to yield a range of values from $\phi_b = 0.8$ eV to ohmic in nature. No dependence upon surface orientation was established. The chemically etched surface of CdS was investigated by Lepley and Ravelet (1976) who etched the CdS single crystals in a variety of etchants prior to contact evaporation. Schottky barrier heights were found to vary from 0.61-0.80 eV for Au/n-CdS characterised by I-V measurements, with C-V results always producing slightly higher values.

An extensive study of metal contacts formed on UHV cleaved II-VI and III-V semiconductors including CdS was performed by Brillson and co-workers. The results were published in a number of papers (Brillson (1978(a)), Brillson (1978(b)), Brillson (1979), Brillson *et al* (1980), Brucker and Brillson (1981(a)) and Brucker and Brillson (1981(b))). Through this work a model was developed in which, for a particular semiconductor, the magnitude of the Schottky barrier was dependent upon the reactivity, the heat of reaction (ΔH_R) of the metal overlayer. Non-reactive metals were said to produce high barriers and reactive metals produced low barriers or ohmic contacts. Plots

of ΔH_R versus ϕ_b had the classic "S" shape as reported by Kurtin *et al* (1969) (Sec 2.2.2.) with the transition between reactive and unreactive metals occurring at $\Delta H_R \approx 0.5$ eVatom⁻¹ for metal/CdS systems. Schottky barriers were measured for UHV cleaved CdS for Au, Cu, Al and In using photoemission studies. Au and Cu produced $\phi_b = 0.8$ eV and $\phi_b = 0.4$ eV respectively while Al and In produced ohmic contacts.

Sobiesierski *et al* (1990) used the technique of photoemission to study the evolving interfaces of several metals deposited onto the vacuum cleaved (10 $\bar{1}$ 0) CdS surface. The metal overlayers produced a wide range of movement of E_F which indicated a wide range of subsequent Schottky barriers. Al produced only a small shift whereas Au produced the largest shift leading to $\phi_b = 1.04$ eV. This group also studied interfacial reactions for some of these metals. Al was found to form a thin layer of aluminium sulphide which formed a diffusion barrier preventing further reaction with the bulk film. Sn formed a mixed phase containing metallic Sn and Sn-S bonds on the surface. The formation of large Schottky barriers for Pd which was observed to form Pd-S bonds with heating was contrary to the theory of Brillson which suggested that only non-reactive metals, formed high barriers.

3.3.3.1 Summary .

Figure 3.7 shows Schottky barrier heights for Au/n-CdS as measured by a number of different groups. It seems that like CdTe there appears to be more than one Schottky barrier height for this system. This observation is irrespective of the characterisation technique employed as Sobiesierski *et al* (1990) and Lepley and Ravelet (1976) have both reported $\phi_b \approx 1.05$ eV by photoemission and C-V techniques respectively. A second barrier of $\phi_b \approx 0.8$ eV has been reported by Lepley and Ravelet (1976), Spitzer and Mead

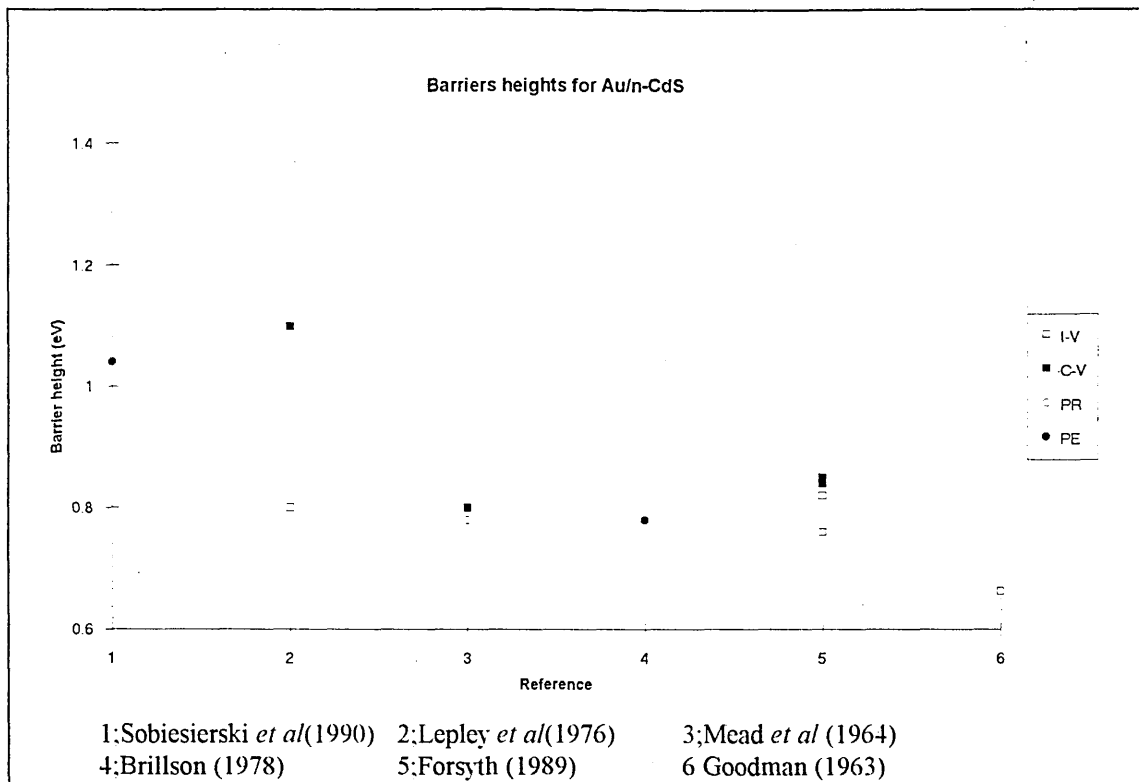


Figure 3.7 Schottky barrier heights reported for Au/n-CdS system.

(1963) and Brillson (1978) by I-V, C-V and photoresponse and photoemission respectively.

3.3.4 Metal contacts to ZnSe.

One of the first studies of metal/ZnSe systems was conducted by Swank *et al* (1969). Contacts were formed by *in situ* vacuum evaporation onto UHV cleaved (110) ZnSe surfaces and compared with contacts formed onto chemically etched (1 min in (40% conc H₂SO₄ + 60% K₂Cr₂O₇) followed by 25% NaOH) (110) surfaces. Of the ten metals investigated all but the most reactive (Mg, Ca and Ba) produced barriers in accordance with Schottky's model. Barrier heights determined by the I-V technique, for Au and Al gave $\phi_b = 1.5$ and 0.6 eV respectively with ideality factors close to unity. Contacts

formed on chemically etched surfaces initially had ideality factors close to unity but with time these contacts displayed a slow departure from ideality accompanied by an increase in the barrier height.

The relationship between the surface of ZnSe and metal contacts formed onto it was investigated by Tyagi and Arora (1975). Chemical etching was again employed to produce a ZnSe surface suitable for contact fabrication. Single crystal n-ZnSe samples were etched in a solution of 1% bromine in methanol for 5 min, followed by 0.5 min rinse in hot NaOH. Metal contacts were then formed by through-mask vacuum evaporation. All contacts were characterised by the I-V and C-V techniques and gave very ideal characteristics. Omission of the NaOH wash resulted in non-ideal, irregular characteristics. This non-ideality was attributed to the formation of a thin interlayer after the Br₂ etch which was removed by the NaOH solution. Schottky barrier heights for Au and Al of $\phi_b = 1.37$ and 0.68 eV, respectively, with ideality factors close to unity were reported. Nedeoglo *et al* (1977) used similar chemical treatments, reducing only the concentration of Br₂ and NaOH in the solutions. The Schottky barrier heights of metal contacts formed by vacuum evaporation were again determined by I-V and C-V methods. Barrier heights determined by the C-V method were always in excess of those measured by I-V by approximately 0.1 eV. A linear relationship between the Schottky barrier height ϕ_b , and the metal work function ϕ_m , was determined and given by :

$$\phi_b = 0.42 \phi_m - 0.63 \quad (3.1)$$

The temperature dependence of barrier height was investigated in the range 70 to 300K, a relationship describing the potential barrier height in relation to temperature was given as :

$$\phi_b(T) = \phi_b(0) - \alpha T \quad (3.2)$$

where α varies for different metals (4.0×10^{-4} eV/K for Au) and is of the same order of magnitude as the temperature coefficient of the ZnSe band gap.

Tarricone (1980) studied Au/n-ZnSe interfaces in an attempt to understand the role of interfacial layers in electroluminescent devices. The (111) surface of single crystal ZnSe samples was etched in a 10% bromine methanol solution for 3 min. The surface was heated slightly prior to the evaporation of 300-500 Å of Au. I-V characterisation of these devices produced non-ideal characteristics with $n > 1.5$, making the barrier height unobtainable by this technique. Photoelectric measurements of these devices yielded barrier heights of 1.65 eV whereas C-V characteristics yielded a value of 1.9 eV. The electroluminescence of the diode in forward bias was characterised at 180 K, photoemission was observed at a forward bias of 1.8V. Metal contacts to several semiconductors including ZnSe were investigated by Tam and Chot (1986) as part of a study of the Richardson constant. ZnSe surfaces were etched in a solution of 1% Br₂ in methanol prior to contact formation. Au and Ag/n-ZnSe gave $\phi_b = 2.0$ and 1.6 eV respectively.

The group of Cammack have thoroughly investigated metal contacts formed on MBE ZnSe layers on highly doped GaAs substrates. The model of the metal/n-ZnSe/n⁺GaAs system was initially developed through the work of Colak *et al* (1989) and was based upon the concept of a Schottky barrier at the metal-semiconductor interface, ϕ_b and a heterojunction barrier, ϕ_{HJ} at the ZnSe/GaAs interface. Previous XPS studies of the ZnSe/GaAs heterojunction indicated that there was a valence band offset, $\Delta E_v = 0.96$ -1.10 eV (Kowalczyk *et al* (1982)) leading to a conduction band offset, $\Delta E_c = 0.15$ -0.30 eV. The -0.27% lattice mismatch between ZnSe and GaAs was thought to be responsible for a high density of interface states at the heterojunction ($\approx 10^{12}$ cm⁻²), in some instances these states were thought to pin the heterojunction barrier ϕ_{HJ} and thus introduce a bias dependence to ϕ_{HJ} . Marshall *et al* (1989) extended this work to account

for observations of photocurrents in similar samples and Ayyar *et al* (1990) introduced the three dimensional concept of "current spreading". Heuken *et al* (1993) reported similar results for MOVPE grown ZnSe on GaAs, again the system was modelled by two back to back Schottky barriers.

3.3.4.1 Metal-ZnSe interface studies.

Asano *et al* (1984) studied the effect of intermediate adsorbed layers of oxygen on the surface of ZnSe using photoemission spectroscopy. They concluded that both Se-O and Zn-O bonds were formed by the photoenhanced oxidation process. Subsequent deposition of Au films onto the oxidised surface resulted in the desorption of SeO₂ and breaking of the Zn-O bonds after only a monolayer of Au deposition.

The formation of Schottky barriers onto the (100) surface of ZnSe was studied by the group of Weaver. Ultraviolet photoemission was used to monitor band bending and hence Schottky barrier formation and the degree of interfacial reaction taking place at the evolving interface. Xu *et al* (1988) initially studied the evolution of the Au (100) ZnSe interface. No interfacial reaction was observed between Au and the substrate. Band bending was observed as the Au adatoms formed a metallic layer indicating Schottky barrier formation in accordance with the Schottky model. Monitoring the final position of the valence band maximum (VBM) which occurred after $\approx 15\text{\AA}$ of Au deposition led to $\phi_b = 1.45\text{ eV}$. Vos *et al* (1988) continued this work by investigating the influence of metal interlayers on Schottky barrier formation for both Al and Au, again on (100) ZnSe. E_F pinning positions at 2.17 and 1.25 eV above the VBM ($\equiv \phi_b = 0.55$ and 1.47 eV) were observed for Al and Au. The same contacts characterised by the I-V technique yielded $\phi_b = 0.76$ and 1.36 eV respectively. The possibility of controlling the barrier height was investigated by introducing thin interlayers of Al prior to the evaporation of Au producing $\phi_b = 1.35$, 1.15 and 0.95 eV for 0.5, 1.5 and 10 \AA of Al respectively. Anderson *et al* (1989) investigated the possibility of forming epitaxial metal contacts to (100) ZnSe using fcc Au (1.8% lattice mismatch) and bcc Co (0.5 % lattice mismatch).

Au formed an abrupt interface and grew uniformly. Co, on the other hand disrupted the substrate, dissociating Zn into the metal layer while Se segregated to the surface. The E_F position was found to be 1.29 and 1.72 eV above the VBM ($\equiv \phi_b = 1.43$ and 1.0 eV) for Au and Co respectively. Co interlayers lowered the Schottky barrier height observed for Au in a similar fashion to Al, Co deposited onto Au/n-ZnSe led to the inter diffusion of Co into the metal layer which liberated Zn into the metal overlayer segregating Se to the surface. Vos *et al* (1989) extended their previous studies to the wider group of metals Ti, Co, Cu, Pd, Ag, Au, Ce and Al. They reported that the interface chemistry was divided into three groups namely:

- non-disruptive (Au and Ag)
- disruptive (Co, Cu, Pd and possibly Al)
- disruptive and reactive (Ti and Ce)

E_F pinning above the VBM had a large spread leading to a range of Schottky barrier heights. In explaining these results both the MIGS and UDM models were discounted there being a general agreement with the Schottky model. A departure from Schottky-like behaviour was however demonstrated by both Ag and Pd. Vos *et al* (1990) attempted to explain these results by introducing deliberate defects into the ZnSe surface. Using atomic, neutral and ionic Ag they were able to investigate different mechanisms of metal film formation. Atomic deposition produced abrupt interfaces with almost no disruption, ionic deposition induced a shoulder on the Zn 3d peak indicative of intermixing of Zn and Ag. Both modes of deposition pinned E_F to identical positions producing $\phi_b = 1.05$ eV. Such barrier heights were explained in terms of the EWF rather than the UDM model.

More recently Chen *et al* (1994) have studied the metal/ZnSe interface and attempted to control the barrier height with interlayers. Au and Al layers were formed onto (100)

epitaxial n- and p-ZnSe, after thermal decapping of a protective Se overlayer. Photoemission showed that Au formed abrupt interfaces whereas Al reacted with the substrate releasing Zn into the metal overlayer. The formation of Al_2Se_3 was seen as a favourable reaction as the heat of formation ($\Delta H_f = -540 \text{ kJ mol}^{-1}$) was much less than that of ZnSe ($\Delta H_f = -159.1 \text{ kJ mol}^{-1}$). Al and Au gave Schottky barrier heights of 0.55 and 1.55 eV respectively, p-type material produced barriers of 2.15 eV for Al and 1.15 eV for Au. A Se interlayer was introduced on p-type material by not entirely decapping the sample, Au evaporated on to this layer produced a modified barrier height of 0.89 eV.

3.3.4.2 Summary.

Many authors have reported the behaviour of metal contacts to ZnSe to follow the Schottky model. Figure 3.8 shows that for Au/n-ZnSe the barrier height varies from 1.36 to 2.0 eV giving $\Delta\phi_b = 0.64 \text{ eV}$. From this data it is difficult to say whether the barrier heights fall into discrete levels as was observed for CdTe and CdS. The interfacial chemistry like that of CdTe has been extensively studied and appears to be no less complicated, abrupt interfaces appear to be formed with both Au and Ag. Although most other metals cause disorder and intermixing with strong evidence of selenite formation. Chemical etching was shown to influence the quality of Schottky barriers as well as leading to interlayers which in turn influence the properties of the interface. The electrical properties of epilayers grown on GaAs substrates seem to be influenced by a barrier at the heterojunction although this was found to be strongly sample dependent.

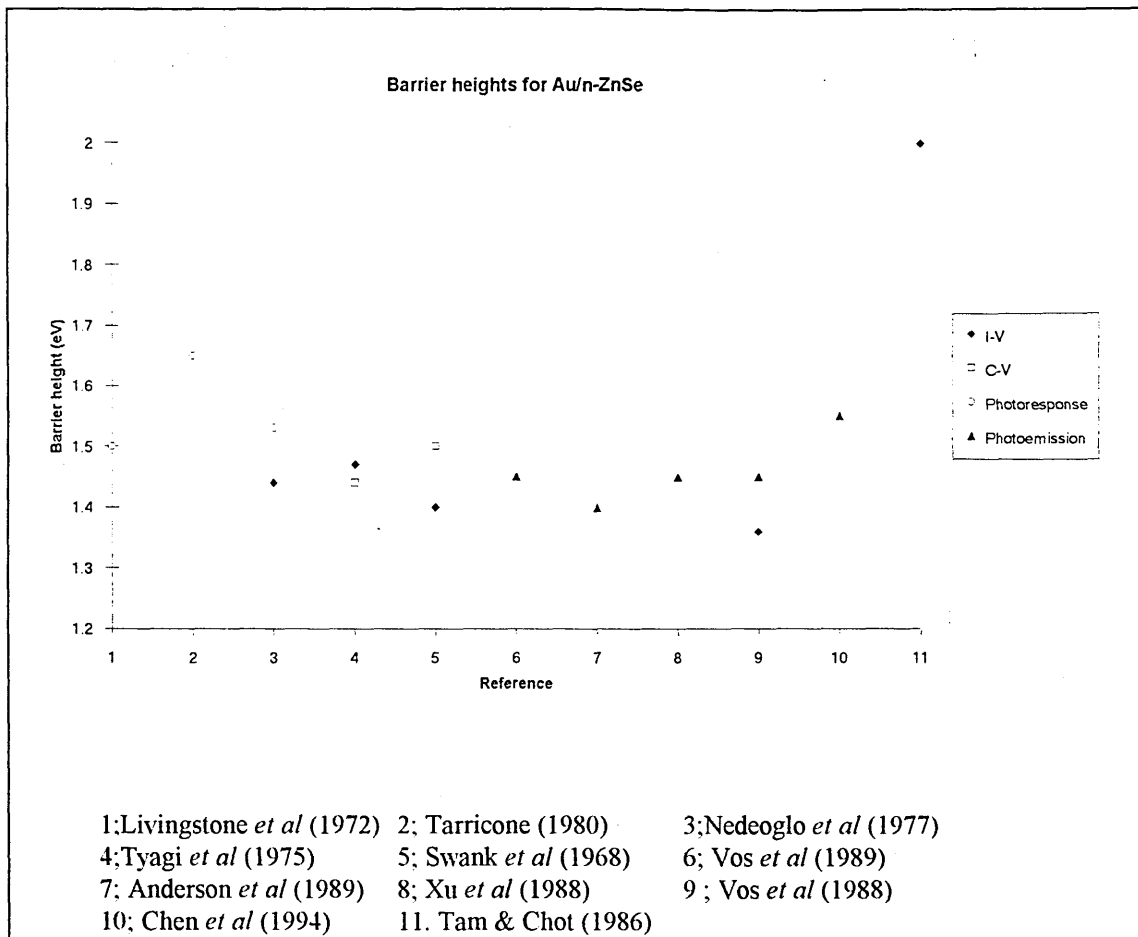


Figure 3.8 Summary of Schottky barrier heights for Au/ZnSe contacts.

3.4 Deep levels and defects in II-VI compounds.

3.4.1 Introduction.

Deep levels can play an important role in determining the electrical properties of metal-semiconductor interfaces and relating deep levels to particular physical phenomena has been an active area of research for several decades. Various mechanisms including native defects and impurities are believed to contribute to deep level formation. Vacancies of A (V_A) or B (V_B) for a compound semiconductor AB or antisite structures where B occupies the site of A (B_A) or vice versa (A_B) are examples of simple native defect

structures. Van Vechten (1975) has calculated the enthalpy of formation for different antistructure pairs, $B_A A_B$ for a number of III-V and II-VI compound semiconductors. Typical values for GaAs and InSb of 0.70 and 0.54 eV compared with 1.87, 3.34 and 2.51 eV for CdTe, CdS and ZnSe respectively demonstrate that such defect structures are energetically more favourable in III-V's than II-VI's. Such calculations predict the dominant defects to be vacancies and interstitials in II-VI compounds.

Of the many methods which exist for the investigation of deep levels, deep level transient spectroscopy (DLTS) is one of the most attractive as it utilises the transient capacitance of a biased Schottky or p-n junction diode to detect deep levels. Quantitative information on activation energies, capture cross-sections and trap concentrations can be obtained.

3.4.2 Deep levels in CdTe.

Much work has been done on the assignment of many of the deep levels found in CdTe. Zanio (1978) in his review of CdTe has collected together a number of common native defects and levels due to impurities; at that time many of these levels were not fully understood or even correctly assigned. Levels close to the centre of the band gap at $E_c - 0.55$ to 0.85 eV were assigned to Cd vacancies.

Takebe *et al* (1982) annealed samples of Al doped bulk grown single crystal CdTe under various partial pressures of Cd (p_{Cd}). Essentially two levels were assigned to $E_c - 0.68$ eV at high p_{Cd} and $E_c - 0.74$ eV at low p_{Cd} . These two deep defects were therefore related to Cd concentrations. In investigating the role of defect levels and minority carrier lifetimes in photovoltaic devices, Sitter *et al* (1982) characterised a number of deep levels in thin epitaxial films of CdTe. Two levels associated with vacancies of Te and Cd were identified at mid-gap points, $E_c - 0.46$ and 0.64 eV respectively. Collins *et al* (1982)

identified a number of levels present in several different bulk grown samples at $E_c - 0.34$ eV. The presence of this level in every sample indicated that it was associated with a native defect of the material. Other levels at mid gap were associated with In dopants. Similar levels were observed by Verity *et al* (1982) for samples of CdTe from different sources, levels at $E_c - 0.22, 0.28, 0.34, 0.45, 0.78$ and 0.89 eV were reported. Isett and Raychaudhuri (1984) identified similar levels as Collins, working with bulk samples of CdTe. A dominant level which occurred in all their tested samples occurred at $E_c - 0.85$ eV and was associated with native defects. Gelsdorf and Schröter (1984) deformed bulk crystals of CdTe and observed deformation induced changes to DLTS spectra. Deformation inevitably led to structural defects, the main level occurring at $E_c - 0.72$ eV, although this level was not assigned to Cd or Te vacancies. Tomitori *et al* (1985) studied Au contacts on cleaved, Te rich and Cd rich CdTe surfaces. Several traps of activation energies $E_c - 0.22, 0.28, 0.33$ and 0.38 eV were reported. The level at $E_c - 0.33$ was studied in some detail and appeared to be related to either Te vacancies or Cd interstitials. The concentration of this particular trap decreased with time at the surface of the cleaved Au/n-CdTe sample but increased at the Cd rich Au/n-CdTe interface. Lee *et al* (1988) conducted a thorough study of defects in n and p CdTe by the DLTS technique; four deep levels $E_c - 0.36, 0.65, 0.74$ and 1.15 eV were detected consistently. The level at $E_c - 0.74$ eV was identified as a double negatively charged Cd vacancy. The presence of this level in the work of other groups can be seen from figure 3.9 and is attributed to the high vapour pressure of Cd. The level at $E_c - 1.15$ eV was attributed to Te vacancies and that at $E_c - 0.65$ eV to Cd interstitials. This assignment is in contradiction to that of Sitter who attributed the level to Cd vacancies.

Clearly CdTe has many experimentally observed deep levels and concentrations of these levels are readily influenced by annealing in inert and atmospheric conditions as well as partial pressures of Cd and Te. Many of the above authors have also reported a relationship between carrier and deep level concentrations. Other techniques of spectral analysis have been used to yield spectral information on deep levels. Sobiesierski *et al*

(1988) have correlated photoluminescence measurements with the chemical composition of the CdTe surface. The surface stoichiometry was influenced by etching with various chemical etchants (Sec 3.2.1), this in turn led to the enhancement of certain deep levels. Levels at $E_c - 0.875$, 0.92 , 1.125 , 1.4 and 1.475 eV and two edge transitions at $E_c - 1.54$ and 1.59 eV were detected at 4K. The levels at 0.875 and 0.92 eV were most intense for Te rich surfaces (Cd deficient), whereas levels at 1.125 and 1.4 eV were most intense for surfaces rich in Cd (Te deficient). Once corrected for the temperature dependence of the band structure of CdTe, levels for Cd deficient surfaces were found to be $E_c - 0.725$ and 0.77 eV in good agreement with defects reported by Lee and Takebe for Cd vacancies. The levels for Te deficient surfaces were found to be $E_c - 0.975$ and 1.25 eV and Lee has reported a deep level associated with a Te vacancy at 1.15 eV. Garcia-Garcia *et al* (1990) have related the surface composition to deep levels again using photoluminescence. Levels associated with mechanical polishing could be removed by Br_2 methanol etches but produced Cd depletion which in turn lead to deep levels associated with Cd vacancies. Br_2 methanol followed by KOH produced high quality surfaces comparable to cleaved crystals. The photoluminescence concentrated mainly on valence band edge transitions but the dependence of deep level concentration on surface treatment was demonstrated.

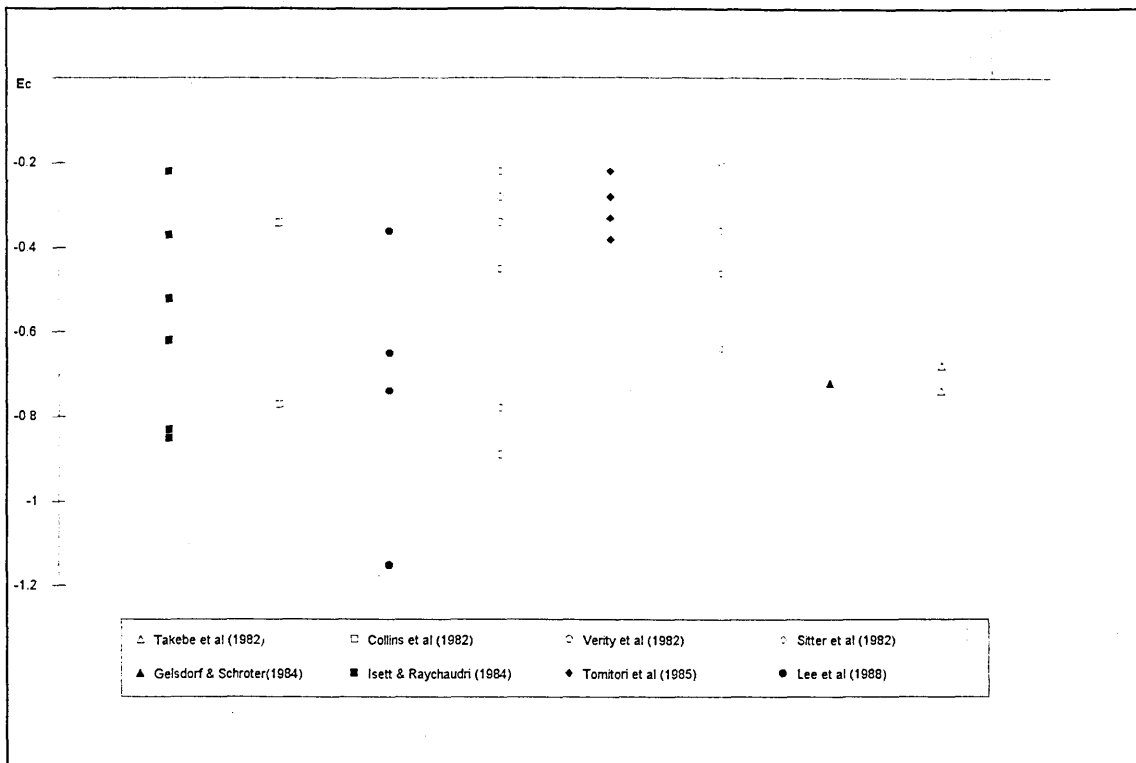


Figure 3.9 Summary of reported deep levels for CdTe.

3.4.3 Deep levels in CdS.

An early study of deep levels in bulk-grown, low resistivity CdS was carried out by Grill *et al* (1979). Au Schottky contacts were formed by *in situ* vacuum evaporation onto the cleaved surface. DLTS was used to characterise a number of electron traps at $E_c - 0.21$, 0.27, 0.33, 0.42, 0.47, 0.625 and 0.735 eV, no assignment was given as to the nature of these levels. Levels with activation energies much greater than 1 eV could not be investigated as temperatures greater than 435 K induced irreversible effects on the metal contact. Bessomi and Wessels (1980(a)) investigated deep levels in polycrystalline CdS, Cu Schottky contacts were formed by sputtering Cu through a mask. A large number of electron traps were reported the relative concentration of which was dependent upon the surface preparation and the degree of reactivity between Cu and CdS. Traps with activation energies at $E_c - 0.16$, 0.31, 0.32, 0.38, 0.42, 0.53, 0.69 and 0.96 eV were

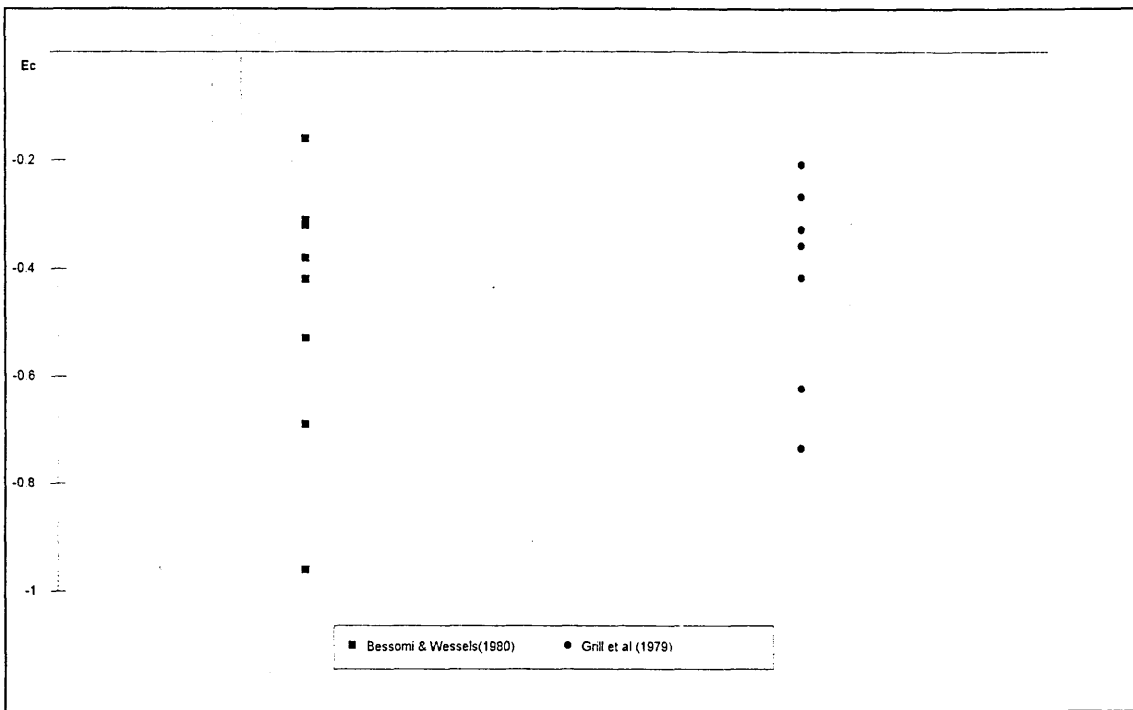


Figure 3.10 Summary of deep levels reported for CdS.

reported, again no assignment was given for the origin of the levels. At present these are the only two authors to report deep levels in CdS and their results are summarised in figure 3.10. It should be noted that the limit on temperature induced by the reactivity of the contacts means that more than half of the band gap can not be investigated for CdS.

3.4.4 Deep levels in ZnSe

Bessomi and Wessels (1980(b)) studied deep levels on epitaxial (100) n-ZnSe on (100) GaAs substrates with DLTS using Schottky contacts formed from Au. Five electron traps were identified at $E_c - 0.33$, 0.35 , 0.42 , 0.71 and 0.86 eV. The traps at $E_c - 0.33$ eV and $E_c - 0.35$ eV were tentatively assigned to donor impurities such as Cl, Al and In. A possible Se vacancy or Se vacancy complex was identified as being responsible for the level at $E_c - 0.86$ eV. DLTS of epitaxial n-ZnSe on p-GaAs diodes was used by Shirakawa and Kukimoto (1980), to define three electron traps at $E_c - 0.30$ eV assigned

to a Zn vacancy-interstitial-Ga complex, $E_c - 0.33$ eV assigned to a Se vacancy and $E_c - 0.48$ eV assigned to a Cu impurity. The activation energies, although not the assignments were in excellent agreement with Bessomi and Wessels. A fourth level at $E_c - 1.1$ eV was also observed at high temperatures (400-500K). This level was not studied in detail because as reported by Grill *et al* (1979) for CdS the high temperatures degraded the diodes beyond which measurements could not be performed. A level at $E_c - 0.34$ eV was again observed by Verity *et al* (1982). Aware that this level had been observed previously by other workers, the initial assignment was given to be a native defect such as a Se vacancy or Zn interstitial. The concentration of this level did not however increase when samples were irradiated with electron beams of sufficient energy to produce Se vacancies or Zn interstitials, leading to the conclusion that this level was due to an impurity complex. Ga doped n-ZnSe/n⁺GaAs with Al Schottky contacts was used by Venkatesan *et al* (1989), who identified two electron traps. A prominent level at $E_c - 0.26$ eV was observed in all Ga doped samples, nominally undoped samples had a very low concentration of this level which was assigned to Ga atoms on Zn sites. Again $E_c - 0.34$ eV was observed but was assigned to a Se vacancy. A set of samples produced in one of the four MBE systems used to provide samples consistently had a deep level at $E_c - 0.8$ eV which was not observed in samples grown on other systems. The high temperatures required to observe this level (390 - 410K) meant that it was not extensively investigated. Mayajima *et al* (1990) doped samples with Ga in a similar experiment. Again they observed a level at $E_c - 0.26$ eV and ascribed it to a complex of a Zn vacancy and Ga dopants. A second level at $E_c - (0.40-57)$ eV was ascribed to a complex of interstitial Se and the Ga dopant. High resistivity ZnSe/GaAs heterostructures were investigated by Han *et al* (1992) using the technique of transverse acoustoelectric voltage spectroscopy. This technique has the advantage that deep levels can be studied without excessively heating the sample and without the need for a rectifying metal contact. Deep levels at $E_c - 1.949$ eV and $E_c - (1.5-1.82)$ eV were verified by low temperature photoluminescence which detected peaks at 1.9 eV, and a broad peak at 1.6 to 1.8 eV. These levels were associated with As impurities which had

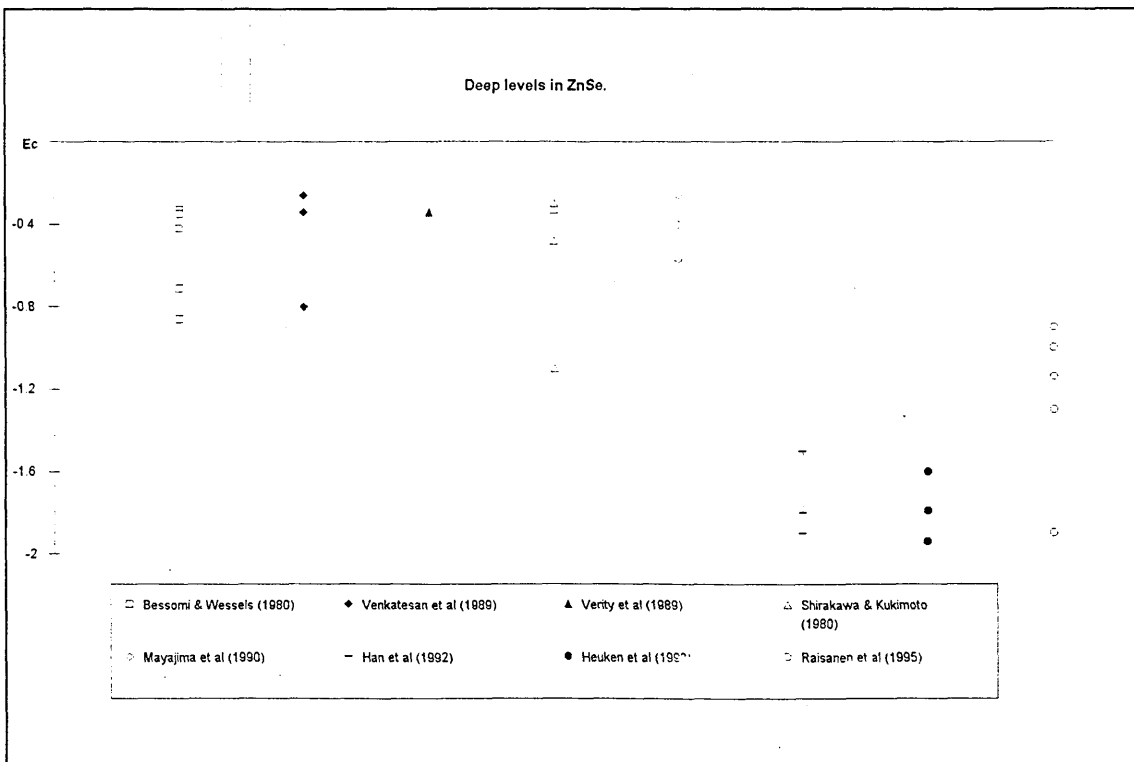


Figure 3.11 Deep levels in ZnSe.

diffused from the GaAs substrate after the formation of an interfacial layer of Ga_2Se_3 . Heuken *et al* (1993) reported several deep levels in MOVPE grown ZnSe on GaAs substrates which were in good agreement with some of the measurements reported by Han *et al* (1992). Photocapacitance measurements indicated the presence of several traps localised at the ZnSe/GaAs interface with activation energies of $E_c - 1.94$ (donor), 1.60 and 1.79 (acceptors) eV. The most recent study of deep levels in ZnSe was performed by both photoluminescence and cathodoluminescence analysis of MBE ZnSe/GaAs epilayers (Raisanen *et al* (1995)). Several levels were reported at $E_c - 0.9$, 1.0, 1.14, 1.3, 1.9 and 2.6 eV. Samples grown at different beam pressure ratios (BPRs) of Se to Zn were either Se or Zn rich (Zn or Se deficient), the intensity but not the activation energy of the deep levels was a function of the BPRs. Deep levels at $E_c - 0.9$, 1.0 and 1.14 eV were dominant in Zn rich (Se deficient) samples whereas Se rich samples exhibited a dominance of the $E_c - 1.9$ eV level. All the measurements were performed at 90K but it

was not clear if the appropriate temperature corrections were made to the deep level energies.

3.5 Summary of deep levels in CdTe, CdS and ZnSe.

It is evident from the above information that the defect structures of the II-VI materials have many common features. The majority of reported defects have been assigned to vacancies of cation or anion or vacancy/dopant impurity complexes as predicted by Van Vechten (1975). Several groups have observed stoichiometry dependent deep levels, indeed for CdTe and ZnSe deep levels have been related to surface preparation techniques or partial beam pressures respectively. These features offer the prospect of controlling simple vacancy type defects by merely influencing the stoichiometry of the material. Relatively little is known about the defect structures of the wider gap materials CdS and ZnSe due in part to the instability of metal contacts to these materials. Some progress has been made with ZnSe by employing low temperature techniques such as photoluminescence and cathodoluminescence.

Chapter 4.

Experimental techniques.

4.1 Introduction.

The experimental techniques involved in this study can be divided into those employed for surface characterisation of the semiconductor, metal contact fabrication and the electrical characterisation of metal-semiconductor contacts. The microscopic surface analysis combined with macroscopic electrical characterisation provides a wealth of information on the behaviour of the interface. These two orders of analysis meet in the ballistic electron emission microscopy experiments performed on a limited selection of samples. The primary surface analysis technique employed was X-ray photoelectron spectroscopy, (XPS). The main purpose of the surface analysis was characterisation of the etched semiconductor surface in terms of chemical composition. The electrical properties of metal-semiconductor devices were analysed in the first place with an automated current-voltage (I-V) system, other electrical techniques used were capacitance-voltage (C-V) and deep level transient spectroscopy (DLTS).

4.2 Surface analysis.

4.2.1 X-ray photoelectron spectroscopy.

4.2.1.1 Theory.

The basic principle of XPS is the interaction of an X-ray photon with a sample to induce the ejection of a photoelectron as shown schematically in figure 4.1. In this figure the direct core level ionisation of the K level by an incident photon having energy $h\nu$, is depicted. The resulting K shell vacancy is filled by means of an atomic

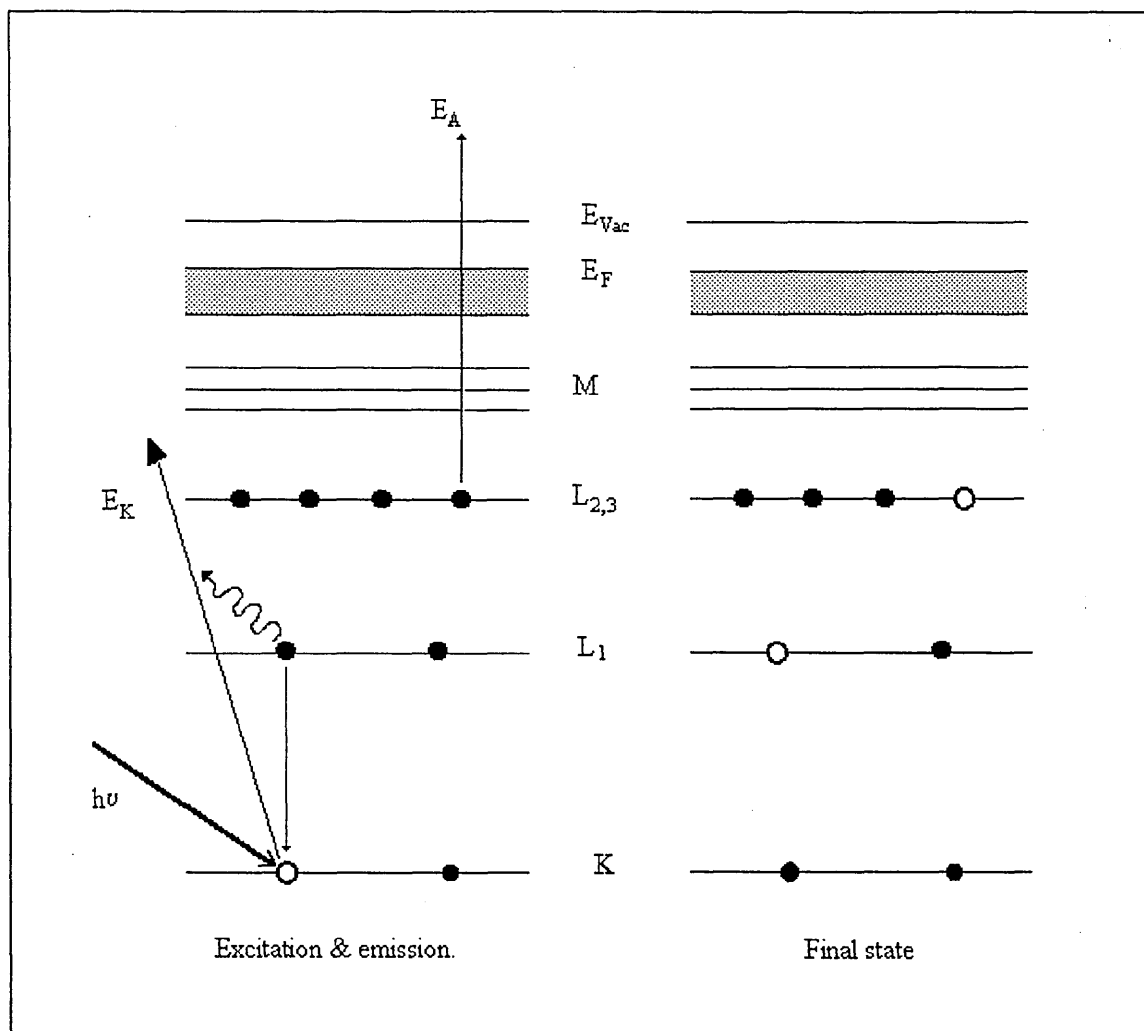


Figure 4.1. Schematic representation of the photoelectron and Auger emission processes.

relaxation process in this case from the L_1 level. The difference in energy of the two levels ($E_K - E_{L1}$) can then result in the emission of an X-ray photon (X-ray fluorescence (XRF)) or an electron through the non-radiative Auger process. Auger emission is favoured over XRF for relatively low K level binding energies ($BE < 2$ keV). The kinetic energy of the ejected photoelectron, E_K and its determination are the cornerstones of XPS. E_K is given by the expression:

$$E_K = h\nu - E_B - E_R - \phi - \delta E \quad (4.1)$$

where;

E_B = the binding energy of the photoelectron.

E_R = the recoil energy, should be included as most electron emissions are not elastic but suffer some energy loss due to matrix effects, it is usually ignored as of the order (0.1 - 0.01eV) and small compared with uncertainties in other parameters.

ϕ = the spectrometer work function, can vary from instrument to instrument.

δE = the electrostatic charging of the specimen, usually ≈ 0 eV for conductors but can be up to several eV for insulators and semiconductors.

Auger emission is of equal importance to the photoelectron process and is commonly observed in the photoelectron spectra. The process depicted in figure 4.1 is named the KL_1L_{23} transition after the origin of the Auger electron, the kinetic energy of this electron is given by;

$$E_{KL_1L_{23}} = E_K - E_{L_1} - E_{L_{23}}^* \quad (4.2)$$

where

E_K = binding energy of K level electron.

E_{L_1} = binding energy L_1 level electron.

$E_{L_{23}}^*$ = binding energy of the L_{23} electron in the presence of a vacancy in the L_1 level.

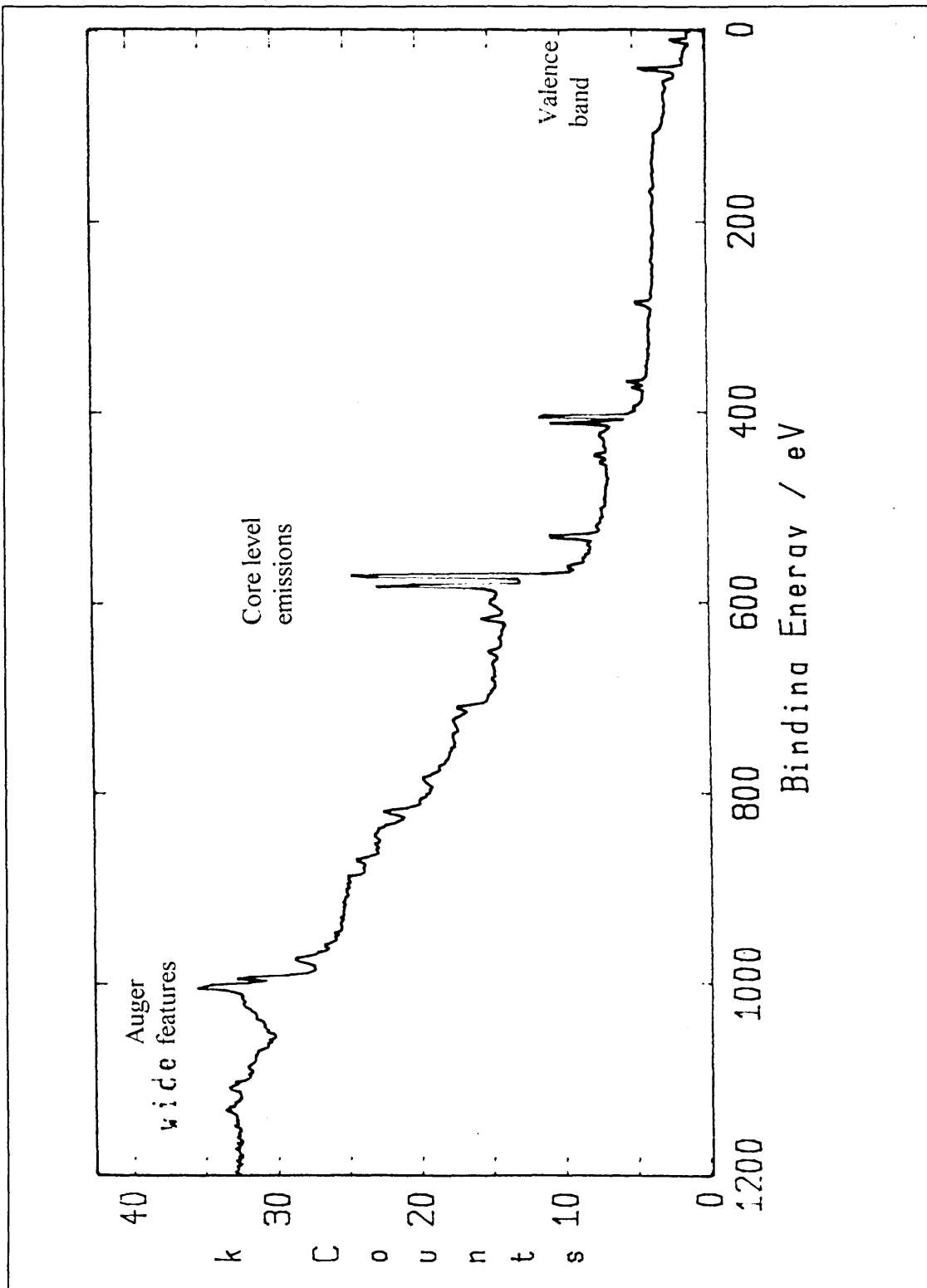


Figure 4.2 A wide scan photoelectron spectrum of Ar etched CdTe taken at 100 eV pass energy with Al K_{α} radiation.

4.2.1.2 Spectral interpretation.

A typical photoelectron spectra is shown in figure 4.2, several features are exhibited by this spectra that are characteristic of all XPS spectra. Typically a spectra will consist of core level emission peaks superimposed on a rising background of inelastically scattered electrons with X-ray induced Auger features and at low energies the valence band spectra.

Core level emissions as the name suggests originate from the tightly bound core electrons. Core level structure provides a direct reflection of the electronic structure of the atom in question. Core level peaks may have variable intensities and widths and may occur as doublets for non-S levels. Doublets arise through spin-orbit coupling. Doublet separation may be as much as several eV in some instances and increases with atomic number for a given sub-shell. The intensity of a particular core level emission is primarily governed by the concentration of the element within the sample and the atomic photoemission cross section σ and is given by :

$$I = nf\sigma y \lambda AT \theta \quad (4.3)$$

where

n = atomic concentration of the element.

f = X-ray flux

σ = photoemission cross section

y = photoelectric efficiency factor

A = sampling area

T = detection efficiency

λ = inelastic mean free path

θ = angular efficiency factor for instrument.

These terms are practically collected together in a term defined as the sensitivity factor, S . Tables of published sensitivity factors determined on a range of instruments exist (Briggs & Seah (1990) and Wagner *et al* (1979)). For an element with an intensity I_x and sensitivity factor S_x the concentration C_x is given by :

$$C_x = \frac{I_x / S_x}{\sum_i I_i / S_i} \quad (4.4)$$

This is the most common analytical method for the quantification of XPS data and is accurate to $\approx 5\%$ which can often be improved by establishing sensitivity factors on the machine on which the data is to be acquired. The line widths of core level photoelectron peaks are usually expressed in terms of the full width at half maximum (FWHM). Assuming all the influential terms to be Gaussian distributions the line width ΔE_c can be expressed as :

$$\Delta E_c = (\Delta E_n^2 + \Delta E_p^2 + \Delta E_a^2)^{1/2} \quad (4.5)$$

where

ΔE_n = intrinsic core level width

ΔE_p = natural line width of exciting radiation

ΔE_a = analyser resolution (a constant for CAE mode)

Practically the dominant term in this expression is the line width of the X-ray source. The actual binding energy of the photoelectron is an intrinsic property of the material, showing slight variations for a particular element and energy level dependent upon the chemical environment of the atom, molecule or ion. This variation is known as the chemical shift and is a very important feature of XPS as it makes possible the quantitative identification of different chemical species of an element.

Usually the second most prominent feature on the photoelectron spectra are the X-ray generated Auger features as described above. These features are observed in most XPS spectra, occasionally interacting with core level photoelectron peaks. One advantage of multi-source spectrometers is the ability to change the excitation source, typically from Mg to Al. Such a change of excitation source and hence energy causes a change in the kinetic energy of the photoelectron peaks (equation 4.1) but not the Auger peaks, as their kinetic energy is independent of the excitation radiation (equation 4.2). If the spectrum is displayed in the counts versus binding energy (Figure 4.2) manner then the photoelectron peaks are seen to move to a higher energy by 233 eV when the excitation source is changed from Mg to Al. The opposite effect is observed when the spectra is displayed in counts versus kinetic energy scale where the Auger features move 233eV. Other common features usually observed as satellites to the main photoelectron peaks are due to interactions of the emitted electron as it departs from the atom. Shake-up satellites are due to the interaction of the emitted electron with the valence electrons causing the promotion of a valence electron to a higher energy. The emitted electron then suffers a loss of a quantum of energy which is manifest as a peak to the slightly higher binding energy side of the main peak. Shake - off is due to the total emission of a valence electron. Plasmon loss peaks result from oscillations in the conduction band due to the emitted electron suffering discrete energy losses. These losses are consequently observed as a series of peaks again to the higher binding energy side of the main feature.

The low binding energy region of the spectra is usually dominated by the valence band spectra, for unmonochromated Al and Mg sources these are usually closely spaced and not well resolved peaks. For this reason such spectra are usually studied in detail at least with monochromatic sources or more commonly with ultra violet photon sources or synchrotron radiation which has a tuneable wavelength.

4.2.1.3 Instrumentation.

4.2.1.3.1 Vacuum system.

All XPS experiments are performed in the UHV environment (10^{-10} mbar), this is often the cause of most of the expense of the instrument but is necessary to reduce surface contamination and improve the signal to noise ratio due to reduced collisions of electrons with residual gases. Systems are generally constructed from stainless steel and Mu metal, all vacuum seals are formed with Cu or Au gaskets. The system usually has to be baked up to temperatures of 150°C primarily to desorb water vapour and adsorbed gases. Baking is absolutely necessary if the vacuum has been broken or degraded by a particularly volatile sample.

4.2.1.3.2 X-ray source.

The VG Microlab instrument at Sheffield Hallam University as with most commercial instruments has two X-ray sources of Al and Mg. The source consists of a thin film of either Mg or Al anode material on a Cu substrate. A high energy electron beam incident on the anode causes the emission of core level electrons. Relaxation produces an X-ray of characteristic energy dependent upon the energy level transition. Each material then produces a unique set of discrete X-rays.

X-ray line	Energy (eV)	Width (eV)
Mg K_{α}	1253.6	0.7
Al K_{α}	1486.6	0.85

Table 4.1 X-ray energies and line widths for Al and Mg K_{α} lines as used on the VG Microlab.(Briggs and Seah (1990))

4.2.1.3.3 Electron analyser.

The concentric hemispherical analyser (CHA) is most commonly used in XPS. The maximum energy resolution is achieved by running the analyser at a constant energy or constant analyser energy (CAE) sometimes referred to as fixed analyser transmission (FAT) mode. Electrons emitted by the sample are focused via the transmission lens to the retarding plate where they are electrostatically retarded to a fixed pass energy. Only electrons of energy equal to the pass energy are then allowed to enter the analyser where a fixed potential and hence fixed field exists between the concentric plates. The decelerating voltage is then swept to cover the desired photoelectron energy range. Ultimately the energy resolution of the analyser is a function of the hemispherical radius (which is fixed of course), the width of the entrance and exit slits and the pass energy of the lens. The actual choice of slit width and pass energy is dependent largely on the application and is usually a compromise between resolution and signal to noise ratio.

4.2.1.3.4 Electron detector.

Once photoelectrons of a particular energy have been transmitted through the analyser they are then detected by the electron detector which in the VG Microlab consists of five channeltrons. The electron enters the channeltron which is usually formed from a lined glass tube, this electron induces further electron emissions which multiply as the electrons pass along the spiral channeltron until they are detected as a current. Typical gain of a channeltron is as high as 10^6 to 10^8 .

4.2.1.4 Experimental details.

As with any form of materials analysis the method is usually specific to the sample of interest. In this case some common methods of surface analysis were adapted to suit the analysis of II-VI compounds.

4.2.1.4.1 Samples.

Prior to entry into the vacuum system all samples were thoroughly washed in acetone; this serves to reduce contamination and preserves the vacuum. All samples were mounted upon stainless steel sample stubs with air-drying, Ag conducting paste. Immediately after mounting samples were placed in the load lock for at least thirty minutes to out-gas. Some electrostatic charging was observed for low conductivity polycrystalline samples of ZnSe; this was referenced to the adventitious C 1s peak at 285 eV. The only other samples where charging was a problem were non-conducting oxide powder standards used to identify native oxide species. These samples were mounted either by pressing into Pb sheet or by double sided adhesive tape, again the adventitious C 1s peak was used for charge referencing.

4.2.1.4.2 Experimental set-up.

For each sample analysed the common practice was adopted of obtaining a wide survey scan at pass energy 100 eV step size 1 eV together with narrow scans at pass energy 20 eV and step size 0.05 eV. The C and O 1s features were monitored for all samples. Both of these elements serving as excellent indicators of surface contamination, C was also used for charge referencing. The main Auger transitions were monitored for each sample, these are vital when identifying the different chemical species as the chemical shift of the photoelectron peak alone may sometimes prove ambiguous (Sec 3.2.1).

4.3 Wet chemical etching and contact fabrication.

4.3.1 Introduction.

Wet chemical etching was investigated in order to establish suitable processing procedures prior to contact formation. The effects of the chemical etchants were characterised by XPS surface analysis. Chemical etching procedures were established which were then used to prepare a suitable semiconductor surface prior to the formation of electrical contacts by vacuum evaporation.

4.3.2 Semiconductor samples.

Single crystals of CdTe and CdS were used for surface etching and electrical measurements. Both of these materials were doped in the $5 \times 10^{16} \text{cm}^{-3}$ range. The (100) CdTe surface was used for etching and contact formation whereas the CdS was cleaved to reveal the (10 $\bar{1}$ 0) surface. Polycrystalline ZnSe nominally undoped and therefore highly resistive was used for surface etching experiments. Comparison was made with (100) n-ZnSe $\approx 3 \mu\text{m}$ thick epilayers doped with I in the range $\approx 10^{16} \text{cm}^{-3}$. The samples were grown by molecular beam epitaxy (MBE) on (100) n⁺-GaAs ($\approx 10^{18} \text{cm}^{-3}$) substrates after Simpson *et al* (1992) at Heriot-Watt University. All electrical measurements were made on samples prepared in this manner.

4.3.3. Wet chemical etching.

A range of wet chemical etchants were adapted from the literature, many of these solutions had been used with some success in the wet chemical etching of II-VI and III-V compounds previously. In the first place samples of CdTe, CdS and polycrystalline ZnSe were etched and then analysed by XPS to determine the surface stoichiometry and the level of surface oxidation. Samples were initially washed in hot

Etchant	Etchant composition
1	1% Br in 200 ml CH ₃ OH
2	0.2g K ₂ Cr ₂ O ₇ , 20 ml H ₂ SO ₄ , 30ml H ₂ O
3	Air cleaved or as received.
4	Ar ion sputter in UHV (5 kV 100μA)
5	Etch 2 followed by etch 7
6	Etch 1 followed by 0.8g NaOH, 30ml H ₂ O at 90°C
7	0.6g NaOH, 1.0g Na ₂ S ₂ O ₃ , 75ml H ₂ O at 90°C
8	0.4g NaOH, 40ml H ₂ O, 1ml H ₂ O ₂

Table 4.2. Etchant numbers and compositions.

acetone in an ultrasonic bath to remove any surface contamination. They were then thoroughly washed in pure water and then etched in one of the etchants depicted in table 4.2. After etching samples were rinsed in pure water or methanol depending upon whether the etchant was in aqueous or organic solvent. Finally samples were rinsed in methanol and dried in N₂. From this point the sample was either mounted on a stub for surface analysis or placed in the metalliser for contact formation. The effect of varying the etch time was investigated as will be shown in Chapters 5 and 6.

4.3.4 Metal contact formation.

After etching samples were transferred to an Edwards metalliser equipped with rotary and diffusion pumps, quartz crystal oscillator thickness monitor and d.c. evaporation source. Samples were mounted onto a shadow mask with holes of either 0.5 or 1.0 mm in diameter. The samples and mask arrangement were placed in the vacuum chamber immediately after the etching procedure leading to exposure of the sample surface to the atmosphere for \approx 5 min. The Au, Ag and Sb contacts were evaporated from twisted W wire baskets from either wire or granular 99.999% (5N) pure sources.

Evaporation of the metal was performed at a vacuum of $\approx 10^{-6}$ mbar, usually contacts were ≈ 5000 Å thick except for those prepared specifically for BEEM experiments where the thickness did not exceed 200 Å as measured by the quartz thickness monitor.

Often one semiconductor crystal was used several times for contact fabrication, the existing contacts were then removed by gentle mechanical polishing with 0.05µm alumina paste in an aqueous suspension. This technique was quite successful over several contact fabrication cycles but the surfaces became damaged and unsuitable for contact formation quite easily. Removal of contacts by etching proved to be a better method. Au contacts were removed using a KI solution producing shiny flat surfaces, this method was also suitable for the ZnSe/GaAs epilayers where mechanical polishing was impossible.

4.4 Electrical characterisation.

4.4.1 Current voltage (I-V) characteristics.

4.4.1.1. Theory

As discussed in Section 2.3 the current traversing the Schottky barrier in the ideal case can be described by the thermionic emission equation. Equation 2.10 below can be modified to equation 4.1 for values of forward bias greater than $3kT/q$ (0.08 V at 300K) and below the point where there is a strong dependence upon the series resistance.

$$J = J_0 \exp\left(\frac{qV}{nkT}\right) \left\{ 1 - \exp\left(\frac{-qV}{kT}\right) \right\} \quad (2.10)$$

$$J = J_0 \exp\left(\frac{qV}{nkT}\right) \quad (4.6)$$

It is more common to measure current I , directly rather than current density J . Equation (4.7) shows that a plot of $\ln I$ should yield a straight line within the boundary conditions. n can be determined from the gradient.

$$\ln I = \ln I_0 + \frac{qV}{nkT} \quad (4.7)$$

and

$$\ln I_0 = \ln SA^{**}T^2 + \left(\frac{-q\phi_b}{kT}\right) \quad (4.7(a))$$

where A^{**} is the Richardson constant modified to take into account the effective mass of electrons within the semiconductor (known as the effective Richardson constant), S is the area of the contact which must be measured accurately and ϕ_b is in the true sense an effective barrier height as the lowering due to the image force is neglected.

A semilog plot of this type is the standard format for diode characterisation. In fact the Log of the current is plotted against the modulus of the voltage; in this manner both forward and reverse currents are displayed in the same quadrant and the magnitude of the current can be easily identified, as shown schematically in figure 4.4.

4.4.1.2 Instrumentation and measurement.

All I-V characteristics must be taken in the dark to minimise photocurrents. These problems may be intensified in II-VI materials as they are particularly sensitive to

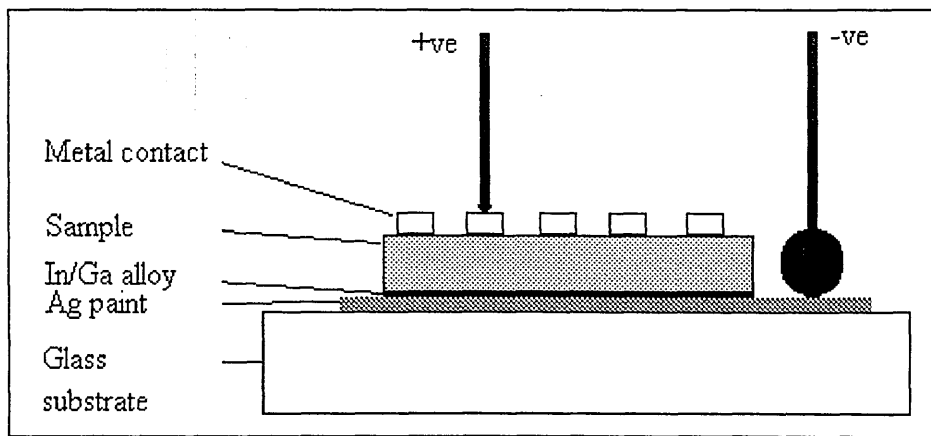


Figure 4.3 Sample mounting and measurement arrangement.

light. Typical contacts were 0.5 mm in diameter; manipulators with contact pins were used to make electrical contacts to each individual device. A fully automated acquisition and analysis system was developed based upon a Keithley 230 voltage source and a Keithley 619 multimeter under P.C. control via a GPIB interface. All samples were mounted on glass slides as shown in figure 4.3 with conductive silver paint. Ohmic contacts were formed with In/Ga alloy on the back of each sample.

Many laboratories have developed such automated acquisition systems. It is normal to incorporate a subroutine within the software to allow the extraction of parameters such as the diode quality factor n , and the Schottky barrier height, ϕ_b . Ohdomari *et al* (1979) and later McClean *et al* (1986) have published routines for extracting the effects of recombination and generation from the forward I-V characteristic to yield true values of both parameters. In this case the operator chooses by eye an upper and a lower limit within which a linear least squares fit provides the gradient and the intercept of the line. In turn these parameters yield the barrier height and quality factor. There are numerous deviations from ideal thermionic emission (Sec 2.3.1); usually a characteristic is described as ideal if $n < 1.1$. The closer this figure to the theoretical minimum of $n = 1.02$ (image force lowering) then the more ideal. Figure 4.4 shows schematically how the various current transport mechanisms and interfacial layers may

affect the I-V characteristics. A true I-V characteristic realised on a real contact is usually a convolution of all of the mechanisms involved in current transport. Extreme care must be exercised when interpreting such characteristics.

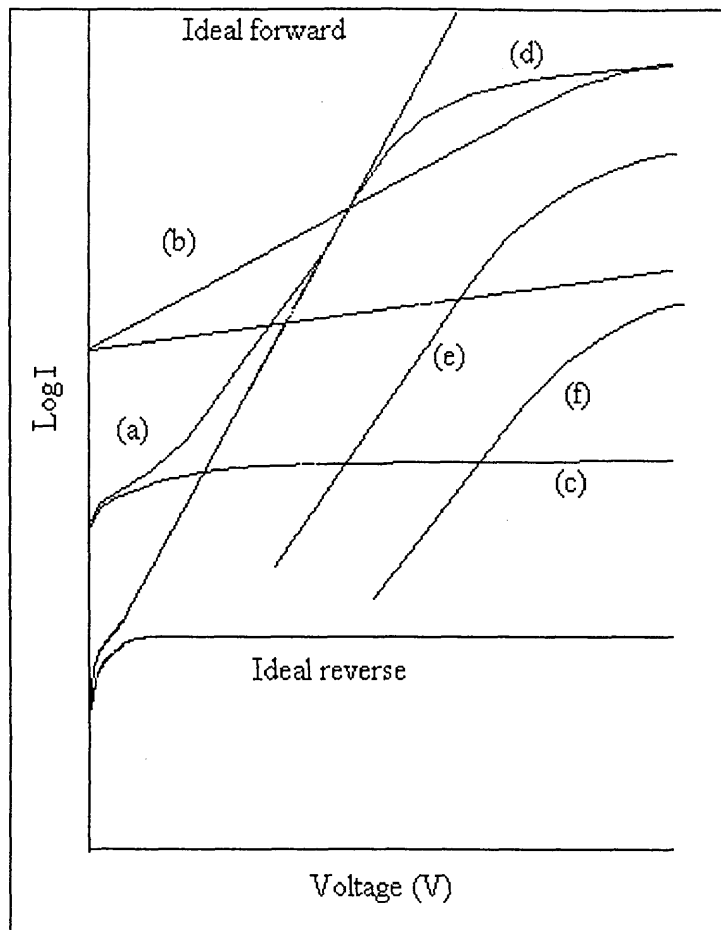


Figure 4.4 Schematic representation of ideal and non-ideal characteristics.

- (a) recombination and generation current
- (b) quantum mechanical tunnelling
- (c) reverse leakage current
- (d) series resistance
- (e) interfacial layer of thickness δ_1
- (f) interfacial layer of thickness $\delta_2 > \delta_1$

4.4.2 Capacitance -voltage (C-V) characterisation.

4.4.2.1 Theory.

The capacitance of the Schottky barrier of unit area was discussed earlier (Sec 2.4), equation (2.27) can be rearranged into the form below where S represents the area of the device.:

$$\frac{1}{C^2} = \frac{2(V_r + \phi_b - \xi - \frac{kT}{q})}{q\epsilon_s N_d S^2} \quad (4.8)$$

Plotting $1/C^2$ versus V_r will yield a straight line graph with gradient $2/q\epsilon_s N_d S^2$ and intercept on the V_r axis of $-\phi_b + \xi + kT/q$. The Schottky barrier can then be determined from such a plot as ξ is the difference between the bottom of the conduction band, E_c and the Fermi level E_F , given by;

$$\xi = \left(\frac{kT}{q} \right) \ln \left(\frac{N_c}{N_d} \right) \quad (4.9)$$

Where N_c is the density of states in the conduction band and N_d is the donor density, obtained from the gradient of the line.

4.4.2.2. Instrumentation and measurement.

Samples were mounted in exactly the same way as for I-V measurements and the same probe station arrangement was employed. All measurements were performed with a Wayne Kerr 6425 component analyser, a four terminal bridge capacitance meter. The maximum operating frequency available was 300kHz, a bias voltage V_r was provided externally, measurements were taken in the parallel resistor-capacitor configuration and

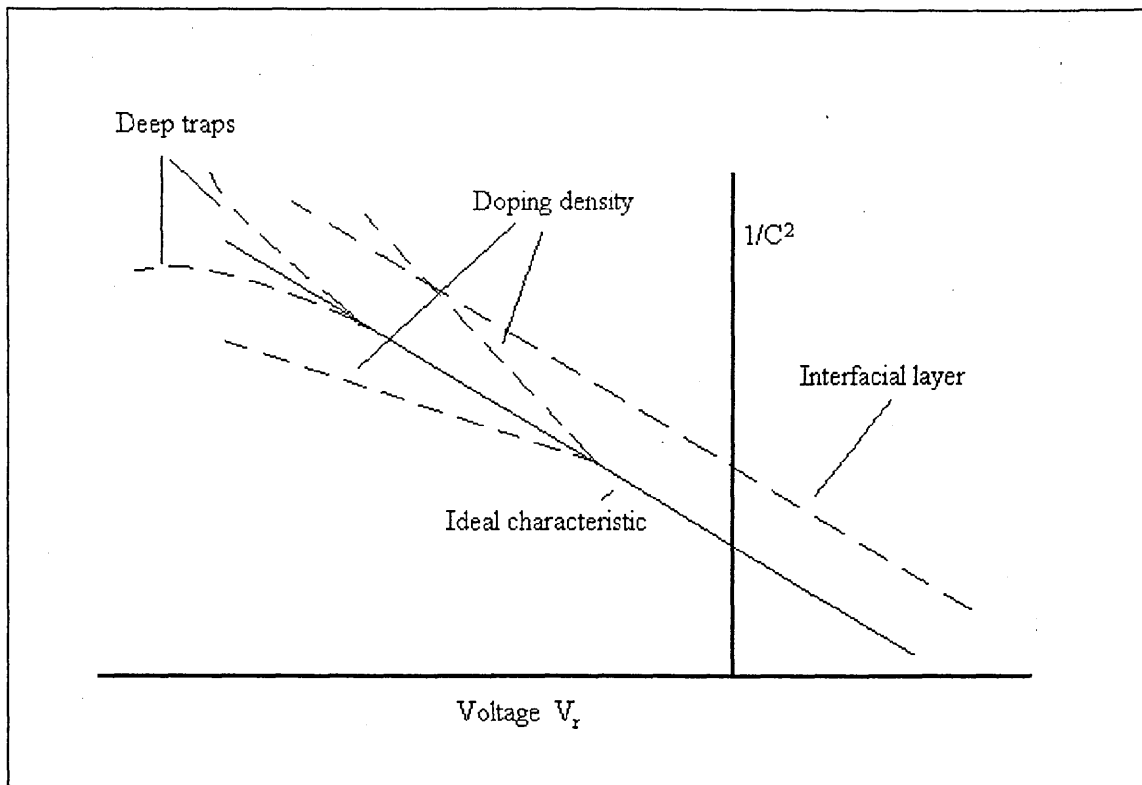


Figure 4.5. Deviations from the ideal capacitance.

an a.c. test signal of 30 mV was employed. Accurate measurements could only be performed if the leads were trimmed correctly both in open and short circuit.

As discussed in Sec 2.4.1 there are several mechanisms which cause deviation from ideal capacitance which are manifest in the $1/C^2$ versus V_r plot as shown in figure 4.5. The limit of the test frequency to a maximum value of 300KHz was potentially a problem in capacitance measurements as most capacitance measurements reported in the literature are performed in the MHz range (*e.g.* Cowley (1966)) minimising the effect of traps on the capacitance characteristics.

4.5. Deep level transient spectroscopy.

4.5.1 Theory.

The technique of deep level transient spectroscopy (DLTS) was first introduced by Lang (1974). The technique is a high frequency scanning thermal capacitance-transient method which has found many applications in the observation of a wide variety of both electron and hole traps. It is possible with this technique to measure the activation energy, capture cross-section and concentration of carrier traps. With the system employed in this work only the activation energy was quantitatively determined.

Deep levels resulting from vacancies, dopants or other imperfections can capture or trap electrons (or holes). Once trapped the electron (hole) may either recombine with a hole (electron) or be re-emitted into the conduction (valence) band. The basic principle of DLTS is the observation of capacitance transients due to the emptying of these traps in the depletion region of a Schottky barrier or a p-n junction. Electrons or holes remain trapped until they acquire sufficient energy to be re-emitted into the conduction process. The emission rate of the trap determines the probability of this process occurring. If the emission rate for electrons, e_n is greater than that for holes, e_p then the trap is likely to be empty of electrons and capable of electron capture. Such a trap in n-type material is described as a majority carrier trap.

For the case of a Schottky barrier on n-type material, the device is held at a negative bias $-V_r$ and has capacitance C_r . If this bias is momentarily reduced to $-V_r'$ where $-V_r < -V_r'$ (known as a majority carrier pulse) there is a corresponding increase in the capacitance to C_r' at the end of the pulse, the capacitance then has a transient response

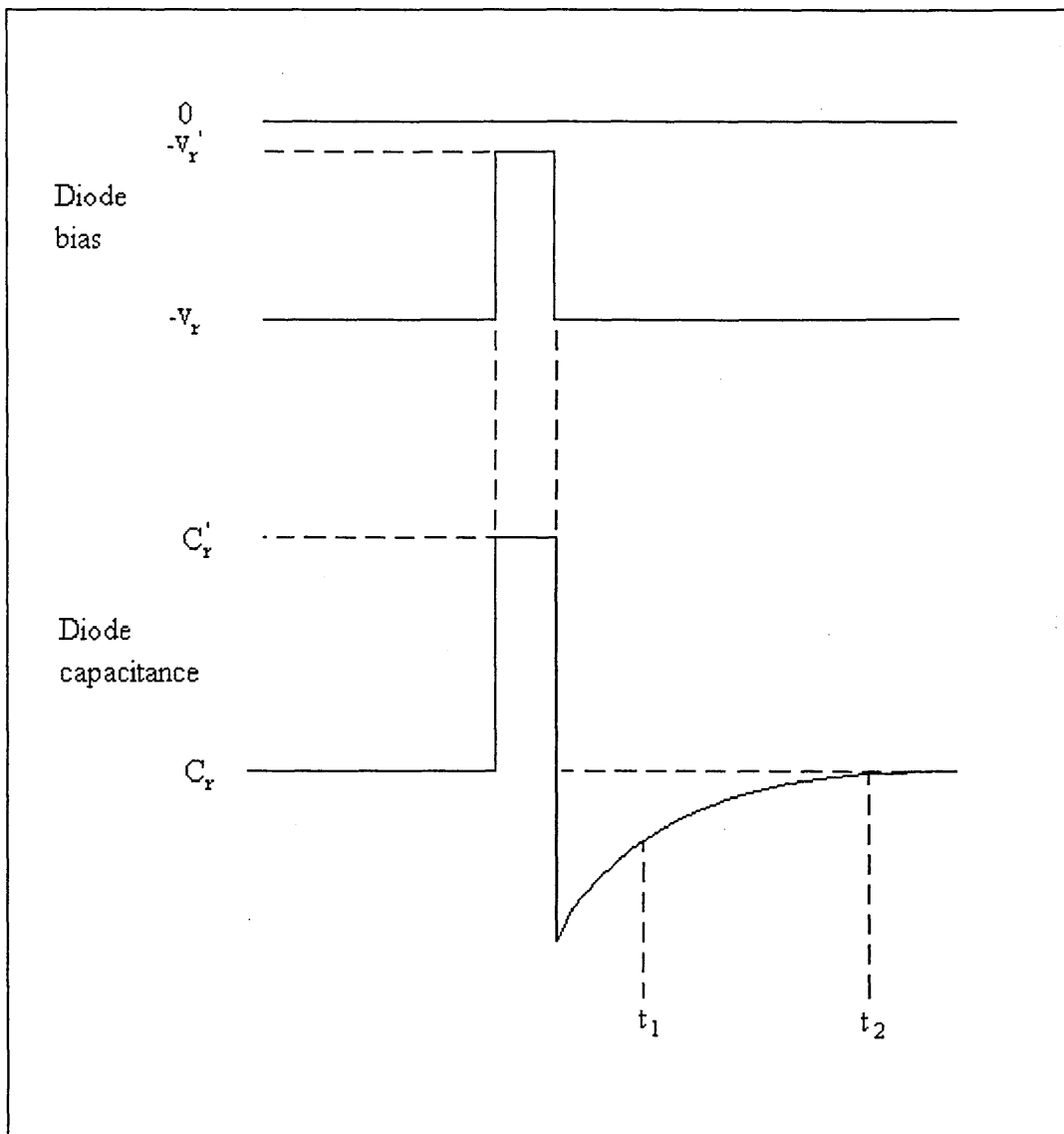


Figure 4.6 Schematic representation of the time dependence of capacitance after a voltage pulse V_r' after Lang (1974).

as it returns to C_r as depicted in figure 4.6. The emission rates of traps are temperature dependent, and it is this essential feature which makes DLTS possible. The capacitance transient is sampled at a rate window defined by the limits t_1 and t_2 . The capacitance at time t_2 , $C(t_2)$ is then subtracted from the capacitance at time t_1 , $C(t_1)$ to give the DLTS signal, $S(T) = C(t_1) - C(t_2)$. The temperature dependence of the emission rates means

that $S(T)$ will vary with temperature and so a full peak may be achieved by performing a full thermal scan and plotting $S(T)$ versus T .

Following the analysis of Lang (1974) the emission rate for majority carrier traps in n-type material is given by :-

$$e_n = \left(\frac{\sigma_n \langle v_n \rangle N_D}{g_n} \right) \exp \left(\frac{-\Delta E}{kT} \right) \quad (4.10)$$

where

σ_n = electron capture cross-section

v_n = mean thermal velocity of electrons

N_D = the effective carrier concentration.

g_n = the degeneracy of the trap level

ΔE = the activation energy of the trap level (energy between trap and E_c for electron trap and E_v for hole trap).

For the case of minority carriers all the subscripts can simply be changed to p. To calculate the value of ΔE the maximum value of the emission rate e_n is determined from the maximum value of $S(T)$. This maximum, τ_{\max} occurs at a specific temperature, T on the thermal scan. The relationship between τ_{\max} and the gate time constants t_1 and t_2 is given below: -

$$\tau_{\max} = (t_1 - t_2) \left[\ln \left(\frac{t_1}{t_2} \right) \right]^{-1} \quad (4.11)$$

From equation 4.11 one value can be obtained for the emission rate with a corresponding temperature, T . By simply varying the time constants t_1 and t_2 and performing a number of scans a graph of $\ln(e_n)$ (or (τ_n)) versus $1000/T$ can be plotted. From this activation plot ΔE may be accurately determined and the capture cross-section, σ_n will be a function of the intercept on the y-axis from a rearrangement of 4.10.

4.5.2 Instrumentation.

All DLTS measurements were performed at the University of Hull. The system was much the same as the original experimental set-up of Lang (1974) and has been described by Verity *et al* (1982). The main requirements are for a fast response time to monitor rapid changes in the occupancy of traps, accurate measurement of small capacitances against a relatively large steady state reverse bias junction capacitance and conversion of the transient signal into a suitable output form. A Boonton 72B capacitance meter capable of measuring capacitance of 3000pF was used. As with Lang's experiment a dual input signal averager (or boxcar) was used. The Boonton meter applies a steady reverse bias; a filling pulse with adjustable amplitude and width is then applied. A sampling pulse is then fed into the boxcar, the width of the pulse determining the time constants t_1 and t_2 . The rising edge of the sampling pulse triggers channel (a) of the boxcar and channel (b) is triggered by the falling edge. After averaging the resultant difference signal is coupled to the Y-input of an X-Y recorder. The X-input is coupled to a calibrated thermocouple to provide the temperature axis. Samples were mounted onto a cold finger in a liquid nitrogen cryostat with a back contact made with Ag paint and the front contact with a Au wire.

4.6 Ballistic electron emission microscopy.

4.6.1 Introduction.

Ballistic electron emission microscopy (BEEM) is the newest technique available for the study of the metal-semiconductor interfaces. The Schottky barrier height can be determined at a very high spatial resolution (< 2 nm) for metal contacts of 10-20nm in thickness, (thick when compared with the sub-monolayers analysed in photoemission spectroscopy).

4.6.2 Theory.

The technique of ballistic electron emission microscopy was developed from the scanning tunnelling microscope first demonstrated by Binnig *et al* (1982). The STM relies upon the tunnelling of an electron from the end of a point probe terminated by a

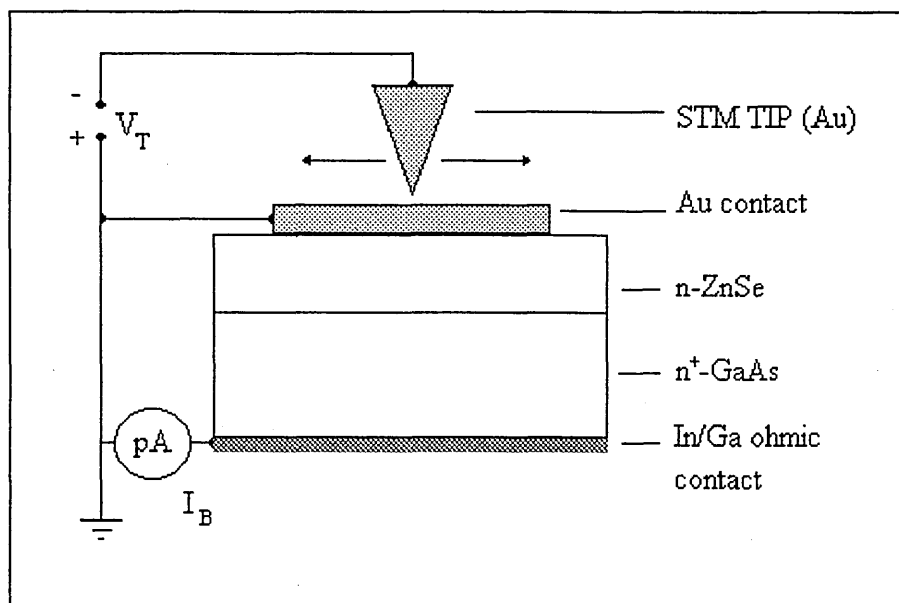


Figure 4.7. Schematic diagram of the STM tip-Au/n-ZnSe/n⁺-GaAs device arrangement employed for BEEM experiments.

single atom into the surface of the sample to be analysed. At a specific tip potential a current exists between the tip and the sample known as the tunnelling current. This current varies with the distance of the tip from the sample surface. If this current is then maintained through a feedback system, the tip-sample distance also remains constant and the tip then follows the contours of the sample surface. A topographic map is obtained by converting the z-axis movement into a grey scale on an x-y axis plot producing a two dimensional representation of the three dimensional surface relief. In the BEEM experiment (shown schematically in figure 4.7 and energetically in figure 4.8(b)) the STM tip acts as an electron emitter injecting electrons into the metal contact which acts as the base. When the tip bias (V_T) exceeds the Schottky barrier height (ϕ_b) electrons can enter the semiconductor which acts as the collector in the three terminal BEEM arrangement first employed by Kaiser and Bell (1988) and Bell and Kaiser (1988). In order to maximise the BEEM current the thickness of the metal overlayer must not exceed the mean free path of electrons in the metal, which is practically less than 100nm for most metals, Crowell and Sze (1967). The spatial resolution of the technique is limited by the fact that only a narrow cone of electrons can contribute to the collector current. Carriers with a large momentum component parallel to the interface are reflected back into the metal layer and hence the resolution at the metal-semiconductor interface is $\approx 2\text{nm}$. The detailed understanding of the electron transport between tip and semiconductor is still limited. Several transport mechanisms have been suggested by Bauer *et al* (1993(a)) and Bauer *et al* (1993(b)) which may contribute to the overall ballistic current; these are depicted schematically in figure 4.8(a). BEEM spectra are usually obtained by sweeping the tip bias while holding the tunnelling current I_T constant, and measuring I_B as function of tip bias. The usual spectra obtained from a ballistically emissive area has a take-off point which yields the Schottky barrier height. The current I_B as a function of tip bias voltage

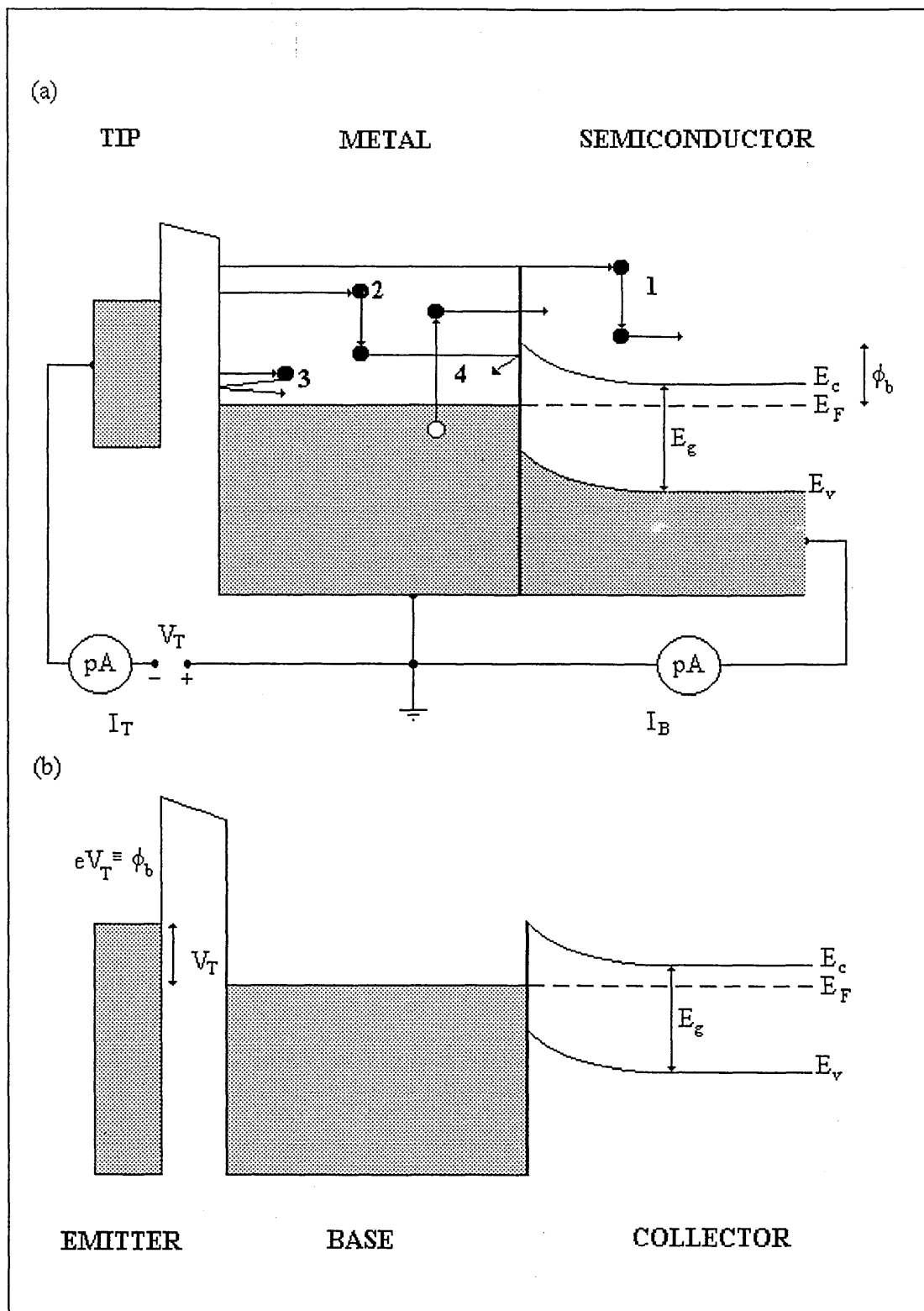


Figure 4.8. Schematic representation of the BEEM experiment, (a) transport processes; 1. ballistic electron transport, 2. inelastic scattering, primary electron excites a secondary electron, 3. quasi-electron electron-phonon scattering (energy losses

negligible), 4. reflection at the interface Bauer *et al* (1993). (b) energy band diagram of emitter (tip), base (metal) and collector (semiconductor), Kaiser and Bell (1988).

V_T was given by Kaiser and Bell (1988) as :-

$$I_B(V) = RI_T \int dE \left[f(E) - f(E - eV) \right] \times \theta(E - (E_F - eV + eV_T)) \quad (4.12)$$

The constant R is bias independent and measures the attenuation due to scattering in the metal layer (in eV^{-1}), $f(E)$, the Fermi function is defined as :-

$$f(E) = \left\{ 1 + \exp \left[\frac{(E - E_F)}{kT} \right] \right\}^{-1} \quad (4.13)$$

Equation 4.12 has been adopted as the standard model for ballistic current crossing over the barrier and is generally referred to as the BK model.

4.6.3 Instrumentation.

All BEEM and BEES experiments were performed at the laboratories of CEMES-LOE/CNRS, Toulouse France. The STM employed was a home built instrument the operation of which was described in detail by Coratger *et al* (1991). Essentially the STM sits on a series of dampers on an independent concrete plinth, such precautions are necessary in order to reduce vibrations. The sample is mounted with Ag conductive paint, the tip scans across the sample horizontally. The flat mirror finish of most semiconductor samples meant that tips were simply constructed by snipping Au wire

under tension to produce the single atom termination necessary. The tip approached the sample via an electromagnetic servo arrangement or louse as described by Coratger *et al* (1991). When sufficiently close to the sample surface (several nm) a tunnelling current could be established between tip and sample. The BEEM images and spectra were obtained in the dark under normal atmospheric conditions using the experimental arrangement depicted in figure 4.7. A Cu wire was connected to the metal contact with Ag conducting paint, the remainder of the contact was then investigated with the STM. Both topographic and BEEM images were obtained simultaneously via PC control. For BEEM imaging the tip bias V_T was set so that eV_T was in excess of the Schottky barrier height, ϕ_b (eV). The tip was then scanned across the surface, topographic and BEEM images were obtained simultaneously. For BEEM spectroscopy the tip was kept in a constant position as the tip bias V_T was swept up to 3 V, a number of scans were averaged (usually 20) to improve signal to noise ratio. The data was then fitted to the BK model to yield Schottky barrier height and the scattering parameter R.

Chapter 5

Surface studies of II-VI compounds.

5.1 Introduction.

Surface analysis techniques have been used to characterise the effect wet chemical etching has on surface properties such as the composition and the oxidation of CdTe, CdS and ZnSe. Care has been taken to ensure that the analysed surfaces are as close to the surface which eventually forms the metal-semiconductor interface as possible. For instance, samples were air exposed after the chemical etching for approximately five minutes. This exposure simulates the period of air exposure during contact fabrication as samples are placed into the evaporator from the etching bath prior to contact formation. Such air exposure ultimately leads to partial oxidation of the surface and contamination from adventitious carbon and oxygen from air-borne hydrocarbons and water vapour. In some instances these contaminants can prove useful. C acts as a reference point for charge referencing, O provides a standard for qualitative oxidation analysis.

5.2 X-ray photoelectron spectroscopic surface analysis of CdTe, CdS and ZnSe.

Analysis was performed on chemically etched, air exposed and Ar sputtered CdTe, CdS and ZnSe. An atomically clean reference surface can only realistically be obtained by cleaving a sample under UHV conditions which was not possible in this case. All spectra were therefore referenced relative to the ionically sputter-cleaned surface of each particular material. Monitoring the peak position of the C 1s photoelectron emission provided a reference point from which sample charging could be monitored. Semiquantitative analysis of the surface was achieved by utilising empirically derived

atomic sensitivity factors combined with equation (4.4) after Wagner *et al* (1979). This technique allows the semiquantitative analysis of heterogeneous samples (Sec 4.2.1.3). Sensitivity factors taken from the literature for elemental standards as well as those derived from sputter cleaned II-VI compounds on the VG Microlab at SHU (referred to as CJB dataset) are given in table 5.1. It should be noted that sensitivity factors which appear in the literature are generally derived from pure elemental standards; they are inaccurate should matrix effects play an important role in determining the photoelectron spectra of the binary alloy. Sensitivity factors are also a function of the electron analyser transmission characteristics and on the mode in which the analyser operates. The data of Briggs and Seah (1990) were determined in constant pass energy mode and are normalised to $F_{1s} = 1.00$. The data of Wagner *et al* (1979) are based upon a double-pass cylindrical mirror electron analyser for photoelectrons generated by a Mg X-ray source, again they are normalised to $F_{1s} = 1.00$. The CJB dataset is based upon analysis of the sputter cleaned semiconductor compounds the composition of which was stoichiometric. All data were acquired in the constant pass energy mode with a similar electron analyser to that of Briggs and Seah using Al X-rays as the excitation radiation. It was not practical to determine the sensitivity factor of F so the data are not normalised to this point.

S	Zn		Se		Cd		Te	Reference
	3p	2p _{3/2}	3d	3p	3d _{5/2}	4d	3d _{5/2}	
0.54	0.75	4.8	0.67	1.05	3.5	-	5.4	Briggs & Seah(1990)
0.35	-	5.3	0.48	-	2.55	-	4.0	Wagner <i>et al</i> (1979)
1.35	3.17	-	-	2.26	3.50	2.03	7.14	CJB dataset*

Table 5.1 Atomic sensitivity factors for elements of II-VI compounds.

* derived from sputter cleaned semiconductor compounds.

Surface contamination in the form of overlayers of carbon and oxygen was ignored for purposes of quantification; the surface was assumed to consist only of the two elements forming the binary compound. With this assumption in mind peak areas for two peaks of similar binding energy must be used for quantification. Higher binding energy peaks are diminished more by the surface contamination due to their smaller escape depths.

5.2.1 CdTe.

p-type (110) CdTe samples were used for the etching experiments (Sec 4.3.3). Initially the air exposed, oxidised surface was analysed, the only surface preparation being a wash in acetone. This sample was then sputter cleaned *in situ* with Ar ions at 5kV and 100 μ A to provide an atomically clean surface. The effect of ion sputtering was monitored by taking successive scans as sputtering proceeded. Sputter etching for 120 min produced a surface which was contaminant free and stoichiometric in agreement with Solzbach and Richter (1980). This surface then formed the reference surface for quantitative analysis. The core level photoelectron peaks of both Cd and Te were monitored at the maximum resolution of the system together with C and O 1s peaks, no other elements were detected on the surface. The MNN X-ray initiated Auger features of both Te and Cd were also monitored in order to determine further information on the chemical state of the surface.

Surface composition in terms of the concentrations of Te and Cd was determined using the 3d_{5/2} peak which is the most intense core level emission for both Te and Cd. The 3d doublet for both elements is shown in figure 5.1 for a variety of surface preparations. The most obvious feature of the Te 3d peaks is the chemically shifted species at ≈ 3.4 eV higher binding energy than the main peak. This chemical species was associated with TeO₂ by Patterson and Williams(1978). The Cd 3d peaks show no such chemical shift as expected. The peak binding energies, intensities and full width at half maximum are shown

Etchant	Te 3d _{5/2}			Te3d _{5/2} 2nd species			Cd 3d _{5/2}		
	See p92 B.E. eV	Int kceV/s	FWHM	B.E. eV	Int kceV/s	FWHM	B.E. eV	Int kceV/s	FWHM
1	572.6	66.00	1.73	-	0	0	404.9	12.06	2.1
2	572.4	49.87	1.81	-	0	0	405.0	22.84	1.8
3	572.8	31.3	1.47	576.2	2.95	1.49	405.3	14.18	1.8
4	572.6	71.36	1.56	-	-	-	405.2	35.00	2.1
5	572.7	36.73	1.62	576.3	3.88	2.25	405.0	19.72	1.8
6	572.4	26.03	1.64	576.3	1.32	1.81	404.8	10.82	2.1
7	572.3	28.74	1.70	576.3	3.14	2.04	405.0	17.06	2.1
8	572.4	18.04	1.32	576.5	3.31	2.16	405.1	30.93	2.1

Table 5.2 Binding energies, intensities and full width at half maximum values for the Te 3d_{5/2} and Cd 3d_{5/2} peaks for a range of chemically treated CdTe surfaces and the as-received surface.

in Table 5.2 for the different surface treatments.

The composition of CdTe varied in much the same way as expected. The as-received sample appeared rich in Te but sputter cleaning restored the surface to stoichiometry as was reported by Lu *et al* (1990) for sputtered CdTe (111) surfaces. The semiquantitative compositional analysis of the etched surfaces is shown in table 5.3. A comparison of the composition calculated with the sensitivity factors of Briggs and Seah(1990) and Wagner *et al* (1979) is made with that calculated with the CJB dataset sensitivity factors. The published sensitivity factors appear to give an over-estimate of the Te concentration in CdTe, the CJB dataset values give a more sensible result suggesting that the surface

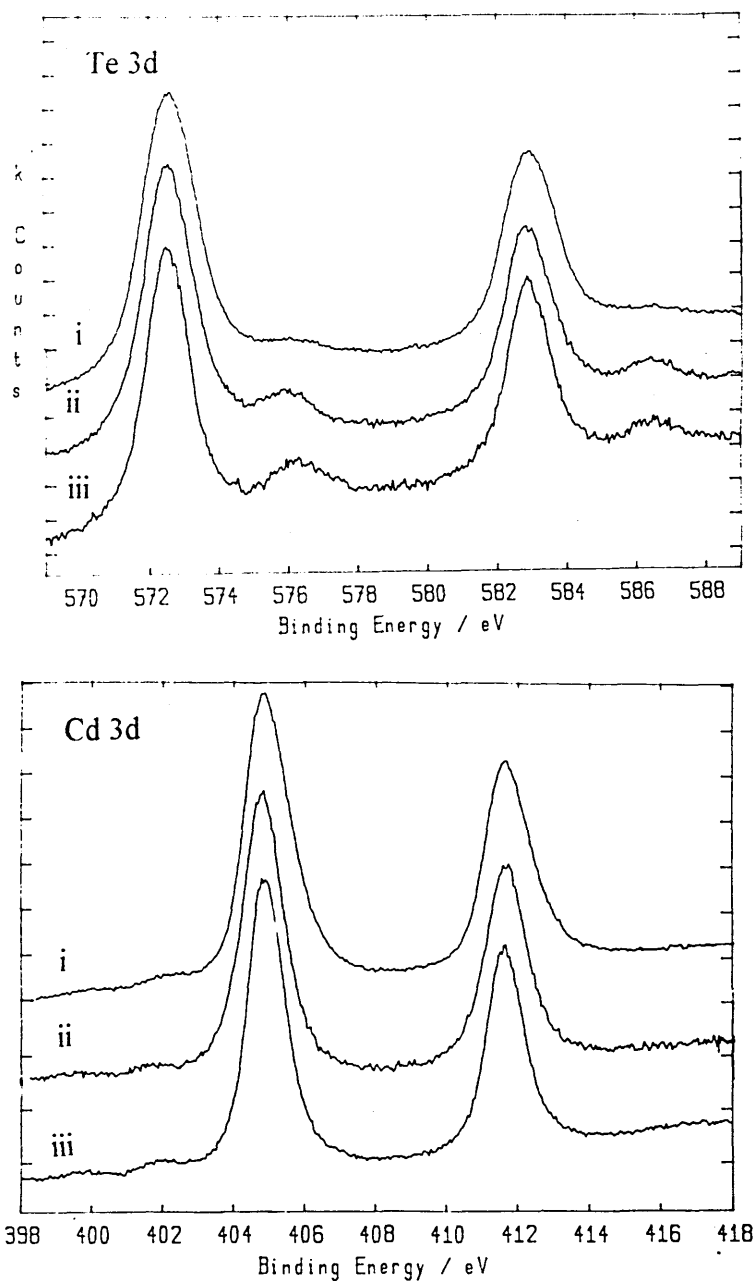


Figure 5.1 (a)Te 3d and (b)Cd 3d photoelectron peaks for i) Te rich surface etch 2 (chromic acid), ii) the as-received surface etch 1 and iii) a Cd rich surface etch 8 (hydrogen peroxide solution). The chemically shifted species at higher binding energy for Te 3d peaks is associated with native oxides, no such peak is evident for Cd 3d.

Etchant	Briggs & Seah		Wagner <i>et al</i>		CJB dataset	
	At %	At %	At %	At %	At %	At %
	Te	Cd	Te	Cd	Te	Cd
1	71.2	28.8	70.75	29.25	65.1	34.9
2	78.4	21.6	66.0	34.0	59.9	40.1
3	68.3	31.7	60.6	39.4	54.2	45.8
4	66.8	33.2	56.5	43.5	50.0	50.0
5	65.1	34.9	56.8	43.2	50.3	49.7
6	70.9	29.1	61.7	38.3	55.35	44.65
7	59.5	40.5	50.8	49.2	44.2	55.4
8	39.0	61.0	30.6	69.5	25.3	74.7

Table 5.3 Composition of etched CdTe surfaces, as determined by sensitivity factor analysis.

composition can be varied from Te rich to Cd rich (figure 5.2) in agreement with Patterson and Williams (1978) and Dharmadasa *et al* (1989). Lu *et al* (1990) reported that chemo-mechanical polishing with a bromine methanol solution produced a CdTe (111) surface with a composition of 33.5% Cd and 66.4% Te which is in reasonable agreement with that of table 5.3.

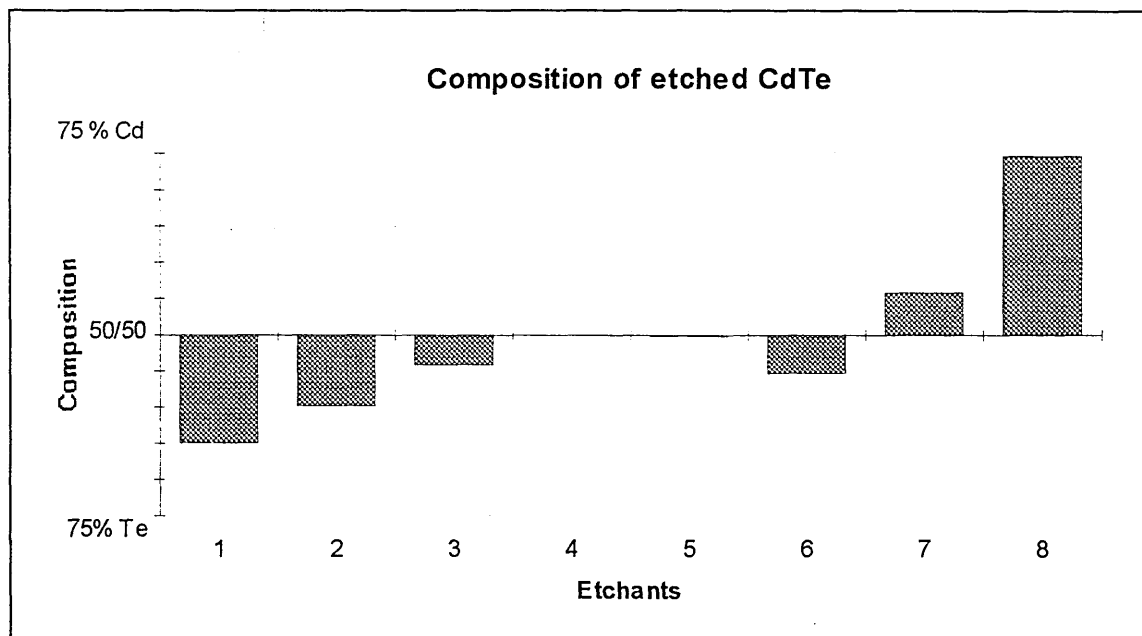


Figure 5.2 Composition of etched CdTe surfaces as determined by empirically derived sensitivity factors.

5.2.1.1 Oxidation of CdTe surfaces.

There is a considerable debate as to the nature of the native oxide of CdTe as was discussed in Chapter 3. In order to investigate the properties and composition of the oxide both the photoelectron peaks of Cd 3d, Te 3d and O 1s were monitored together with the X-ray induced Auger electron Cd and Te MNN series. The analysis is further complicated by the fact that when using Mg K α radiation as reported in the literature (e.g. Solzbach and Richter (1980) and Choi and Luckovsky (1988)), there is an overlap between the Cd M₄N₄₅N₄₅ Auger feature and the Te 3p_{1/2} photoelectron peak which confuses interpretation of the Auger feature. This overlap is avoided here by using Al K α radiation, as there is a 233 eV difference between the Al and Mg K α lines (Sec 4.2).

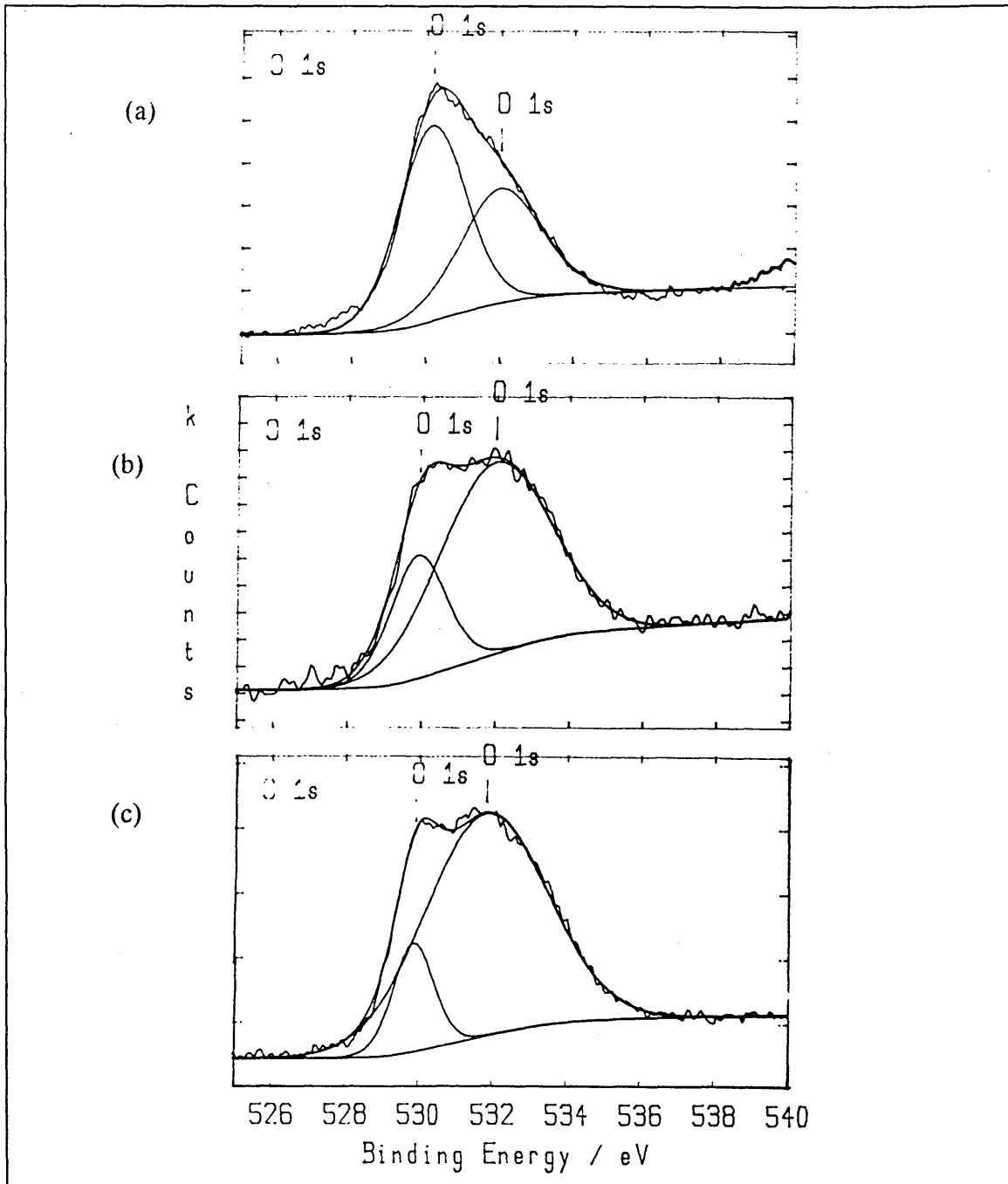


Figure 5.3 The O 1s photoelectron peak for (a) etch 2, (b) etch 3 (as-received) and (c) etch 7. The first species at ≈ 530.2 eV is associated with physisorbed O, the second at 532.2 eV is associated with native oxides of CdTe. The ratio of the first to the second indicates the qualitative oxidation of the surface.

As can be seen from figure 5.3 the oxygen 1s peak consists of more than one chemical species, Table 5.4 shows that the first species is centred at $530.2 \pm 0.15\text{eV}$ which has been associated with physisorbed oxygen by Bose *et al* (1989). The second species occurs at $532.2 \pm 0.20\text{ eV}$ which has been observed by Waag *et al* (1989) to be the chemically shifted O 1s species for oxygen bonded to the native oxides of CdTe. The ratio of the two peak areas provides a qualitative indication of the level of native oxide on the surface. The physisorbed oxygen peak serves as a useful normalisation to account for differences in sample size and atmospheric exposure times. Figure 5.4 shows that the level of native oxide is influenced by the surface treatment.

Etchant	O 1s First species			O 1s Second species		
	B.E. eV	Int kceV/S	FWHM eV	B.E. eV	Int kceV/S	FWHM eV
1	530.1	9.57	2.35	532.4	11.23	3.05
2	530.1	9.68	2.01	531.9	9.61	2.62
3	530.3	3.02	1.80	532.4	5.77	2.50
4	-	-	-	-	-	-
5	530.4	19.75	2.44	532.2	0.90	1.16
6	530.0	4.07	1.61	532.1	11.60	3.85
7	530.1	4.4	1.58	532.3	11.90	3.25
8	530.4	11.47	2.02	532.7	14.01	3.62
TeO ₂ std.	530.4	5.39	4.59	531.4	13.15	1.82

Table 5.4 The results of deconvoluting the O 1s doublet reveal two peaks associated with two different sources of O 1s photoelectrons.

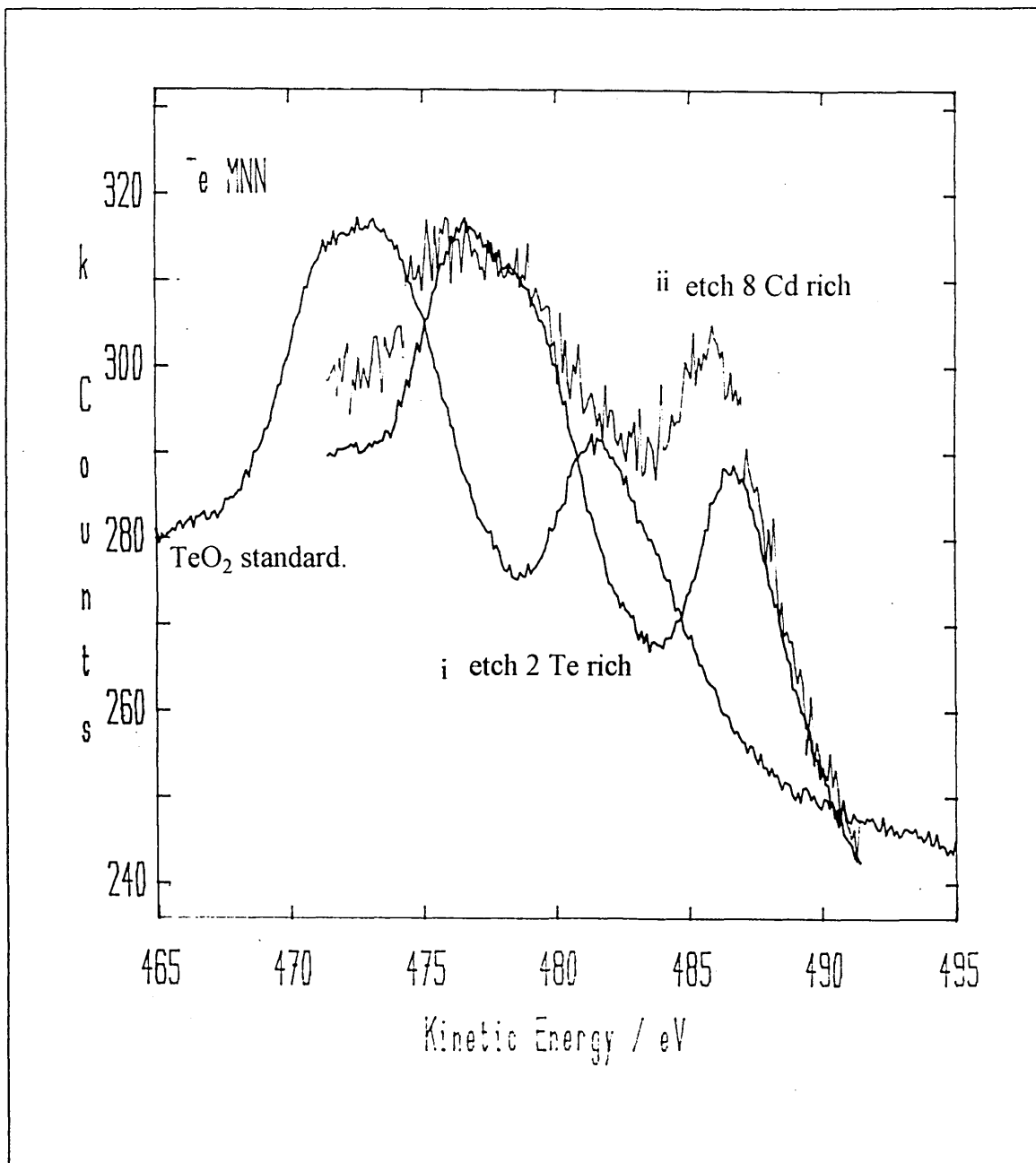


Figure 5.5(a) The Te MNN Auger features for a variety of surface treatments. All Te MNN features for Te rich or stoichiometric surfaces are identical to (i) whereas all Cd rich surfaces display features similar to (ii) which appears to be a convolution of (i) and (iii) (TeO₂).

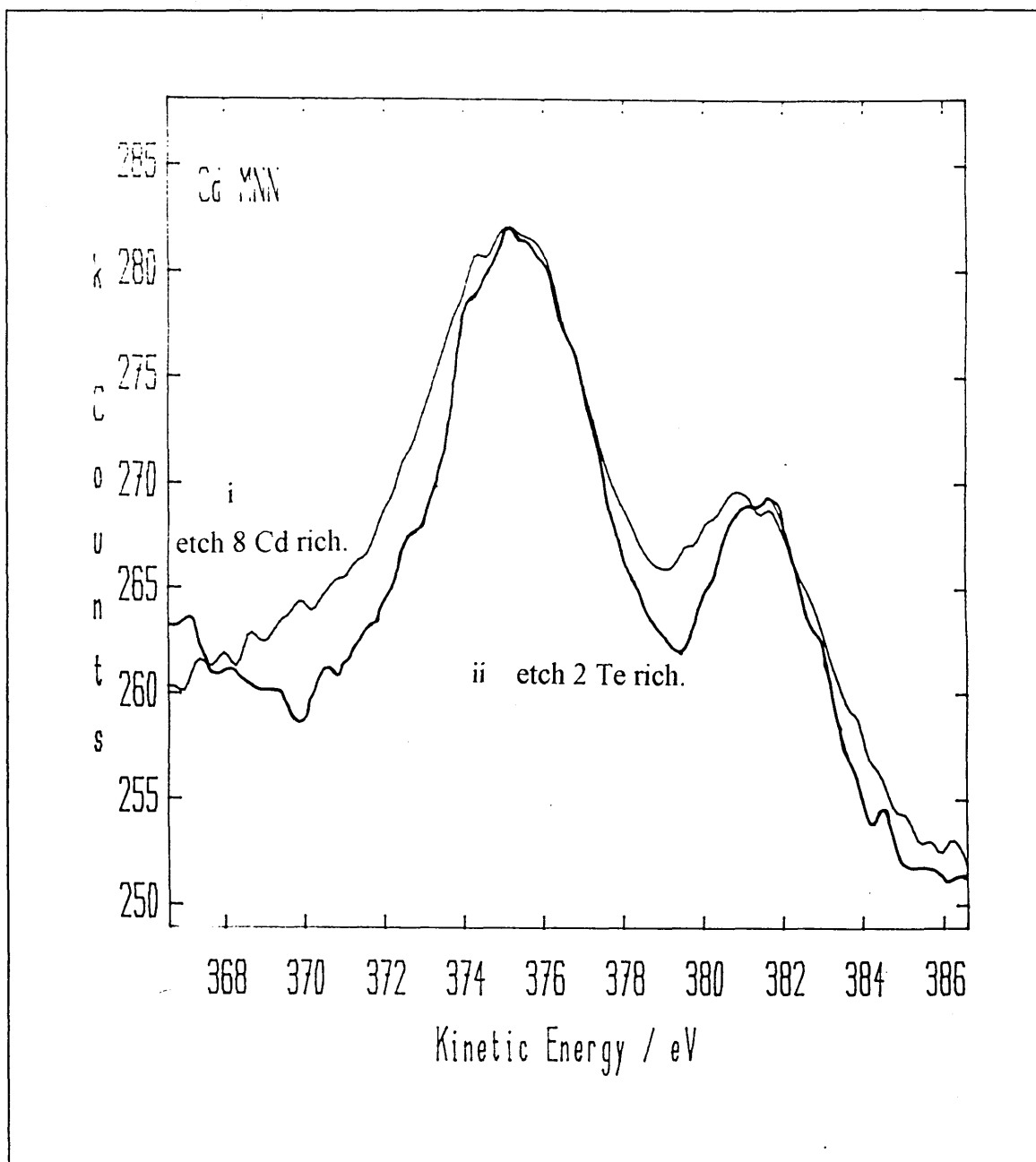


Figure 5.5(b) The Cd MNN Auger feature for a variety of surfaces. All Cd MNN features for Cd rich surfaces were identical to (i) and those for Te rich surfaces were identical to (ii).

stoichiometric surfaces display identical Te MNN Auger features indicates that the bonding of Te changes very little from stoichiometric to Te rich surfaces. This is

consistent with the formation of Te-Te bonds rather than Cd-Te bonds. Figure 5.5 (b) shows the Cd MNN Auger feature for Cd rich (etch 8) and Te rich (etch 2) surfaces. This feature is identical for Te rich and stoichiometric surfaces but broadened for Cd rich surfaces, indicating the transition of Cd bonding from Cd-Te to another species. The high oxide content of these surfaces observed by XPS indicates this species to be CdO.

5.2.2 CdS

n-type CdS samples of low resistivity were analysed in a similar systematic manner as CdTe. Samples were first cleaved from a wafer revealing the $(10\bar{1}0)$ surface, this cleavage often resulting in samples with several facets due to step edges. Only the flattest of which were used for surface analysis experiments. Initially the air exposed surface was monitored and then sputter cleaned *in situ* with Ar ions at 5kV and 100 μ A. The sample was sputtered for 45 min, to remove the surface oxide layer and contaminants. Chieh and Munir (1991) have reported that sputtering the surface for much longer periods of up to 120 min produces a slight S enrichment on the (0001) surface. The surface composition was monitored after etching for 5 and 45 min and found to be constant within experimental error and was therefore assumed to be stoichiometric. As with CdTe the core level emissions of Cd and S together with the C and O 1s peaks were monitored at maximum resolution, no other elements were detected at the surface. The Cd MNN Auger feature was also monitored but the Auger transition of S occurs at 2114eV which is beyond the excitation of Al K α radiation so little information could be obtained from these features.

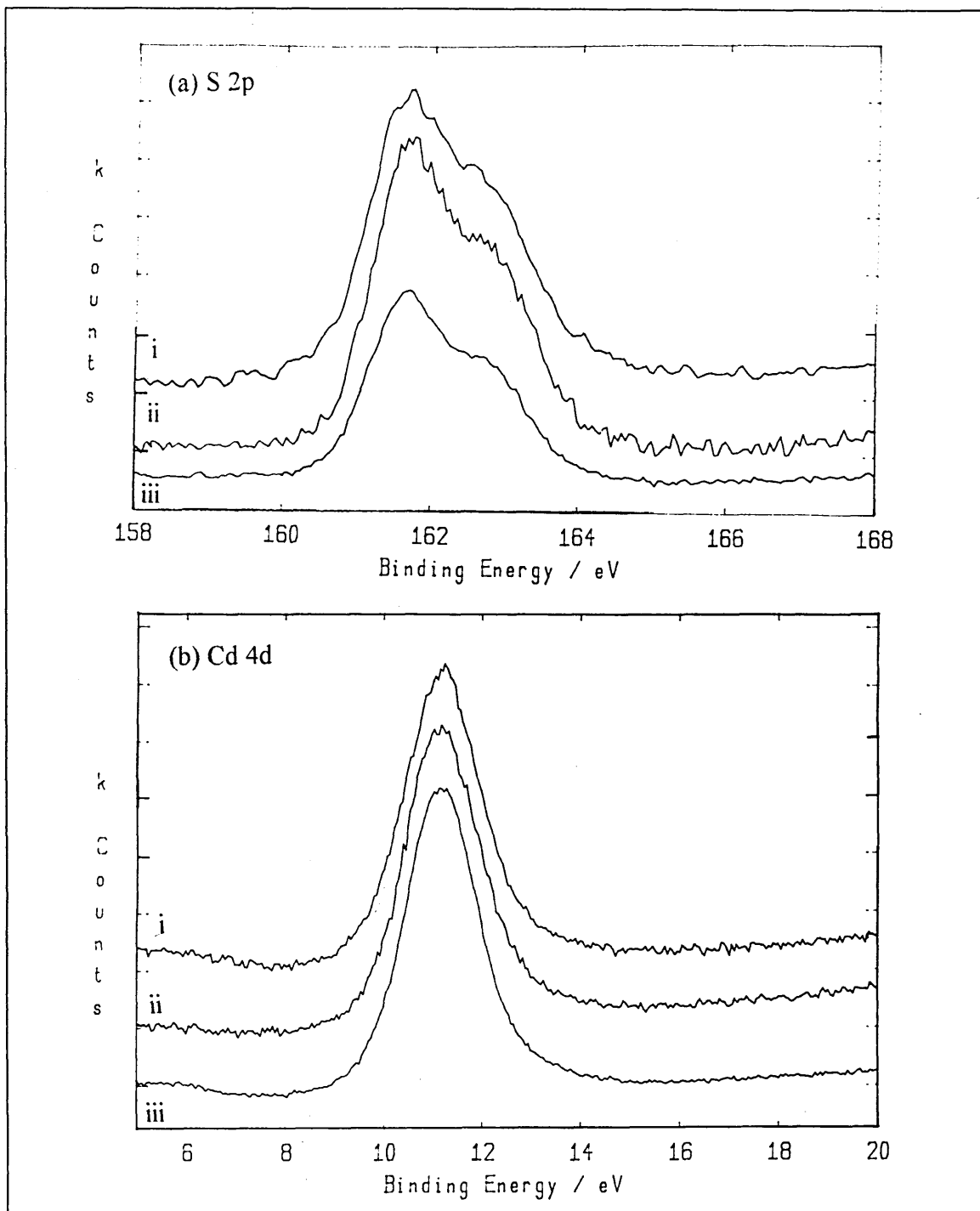


Figure 5.6 The (a) S 2p and (b) Cd 4d core photoelectron features for (i) S rich etch 1 (Br methanol), (ii) as received etch 3 and (iii) Cd rich etch 7 (NaOH and $\text{Na}_2\text{S}_2\text{O}_3$ solution). Neither the S 2p or Cd 4d peaks reveal a chemically shifted species.

The surface composition in terms of Cd to S ratios was determined using the Cd 4d and S 2p peaks which are separated by ≈ 150 eV, consequently both of these peaks are influenced by adventitious surface layers to a similar extent. The Cd 4d peak is a symmetrical single peak whereas the S 2p peak can be resolved into two components associated with S 2p_{1/2} and S 2p_{3/2} as can be seen from figure 5.6. For purposes of quantification the intensity of the S 2p peak as a whole was used. None of the chemically shifted S 2p species reported by Kolhe *et al* (1983) or Webb and Lichtensteiger (1986) (Sec 3.2.2.) were observed. The peak positions, intensities and full width at half maxima are shown in table 5.5 for air exposed, sputter cleaned and chemically etched CdS surfaces.

Etchant	S 2p _{3/2}			S 2p _{1/2}			Cd 4d		
	B.E. eV	Int kceV/s	FWHM	B.E. eV	Int kceV/s	FWHM	B.E. eV	Int kceV/s	FWHM
1	161.9	3.69	1.35	162.8	3.02	2.11	11.5	9.32	1.77
2	161.4	3.80	1.11	162.3	8.07	2.04	11.1	16.77	1.84
3	161.6	3.49	1.05	162.8	3.64	1.04	11.3	11.46	1.79
4	161.1	7.18	1.22	162.2	6.36	1.73	10.9	20.33	1.89
5	162.0	2.91	1.14	163.2	2.19	1.59	11.7	8.34	1.79
6	162.0	1.56	1.08	163.1	1.22	1.62	11.7	7.79	1.99
7	161.6	13.91	1.13	162.8	11.85	1.43	11.2	42.71	1.76
8	161.9	3.06	1.37	163.1	2.41	1.47	11.6	8.58	1.84

Table 5.5 Binding energies, intensities and full width at half maximum values for S 2p and Cd 4d peaks for a range of chemically etched CdS surfaces and the as received surface.

The unetched air-exposed sample was found to be slightly rich in Cd, as reported by Chieh and Munir (1991) for the AES analysis of (0001) CdS surface. Sputtering with Ar ions produced a stoichiometric, contaminant free surface which formed the reference for quantification. There are no published atomic sensitivity factors for the Cd 4d peak so comparison with the CJB dataset was impossible. The semiquantitative compositional analysis is shown in table 5.6 for the air exposed, sputter cleaned and chemically etched surfaces of CdS. This compositional variation is shown graphically in figure 5.7, comparison of this with figure 5.3 shows that CdS is etched in much the same manner as CdTe.

Etchant	CJB dataset	
	At % S	At % Cd
1	52.0	48.0
2	51.5	48.5
3	48.3	51.7
4	50.0	50.0
5	47.9	52.1
6	34.9	65.1
7	47.5	52.5
8	48.9	51.1

Table 5.6 Composition of unetched, sputter cleaned and chemically etched CdS calculated with CJB dataset sensitivity factors.

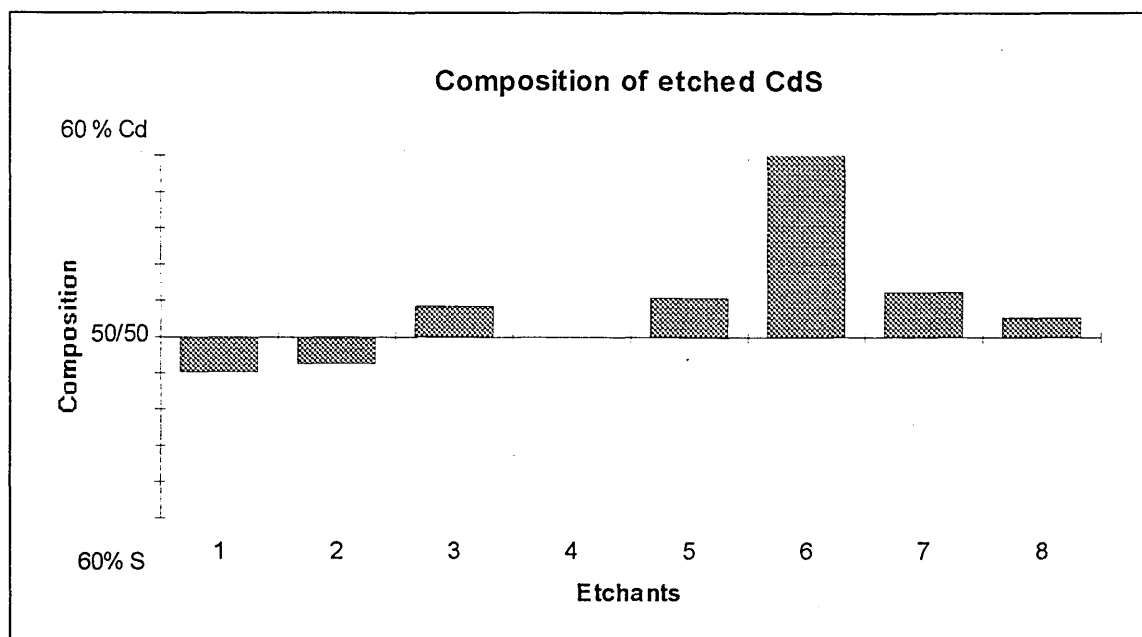


Figure 5.7 Stoichiometric variation of chemically etched CdS

5.2.2.1 Oxidation of CdS

The O 1s photoelectron feature was a broad peak which was deconvoluted into two constituents much the same as that of CdTe. All samples were air exposed prior to placing into the vacuum chamber so that there was a certain amount of physisorbed O present on the surface. Kolhe *et al* (1983) suggested that O bonded to Cd in the form Cd-O to form CdO and O bonded to Cd and S to form CdSO₄ would have peaks at 531.28 and 532.4 eV respectively (Table 3.2 Sec 3.2.2). This value for CdSO₄ was in good agreement with that obtained from the analysis of a standard crystalline CdSO₄ sample supplied by Johnson Matthey. In this case the O 1s peak occurred at 532.9 eV. Table 5.7 shows that several chemical species of O could well be present at the surface. The first species has an average peak value of 529.8 eV, very close to that associated with physisorbed O from water vapour. Cadmium hydroxide did not form at the surface apart for the unetched

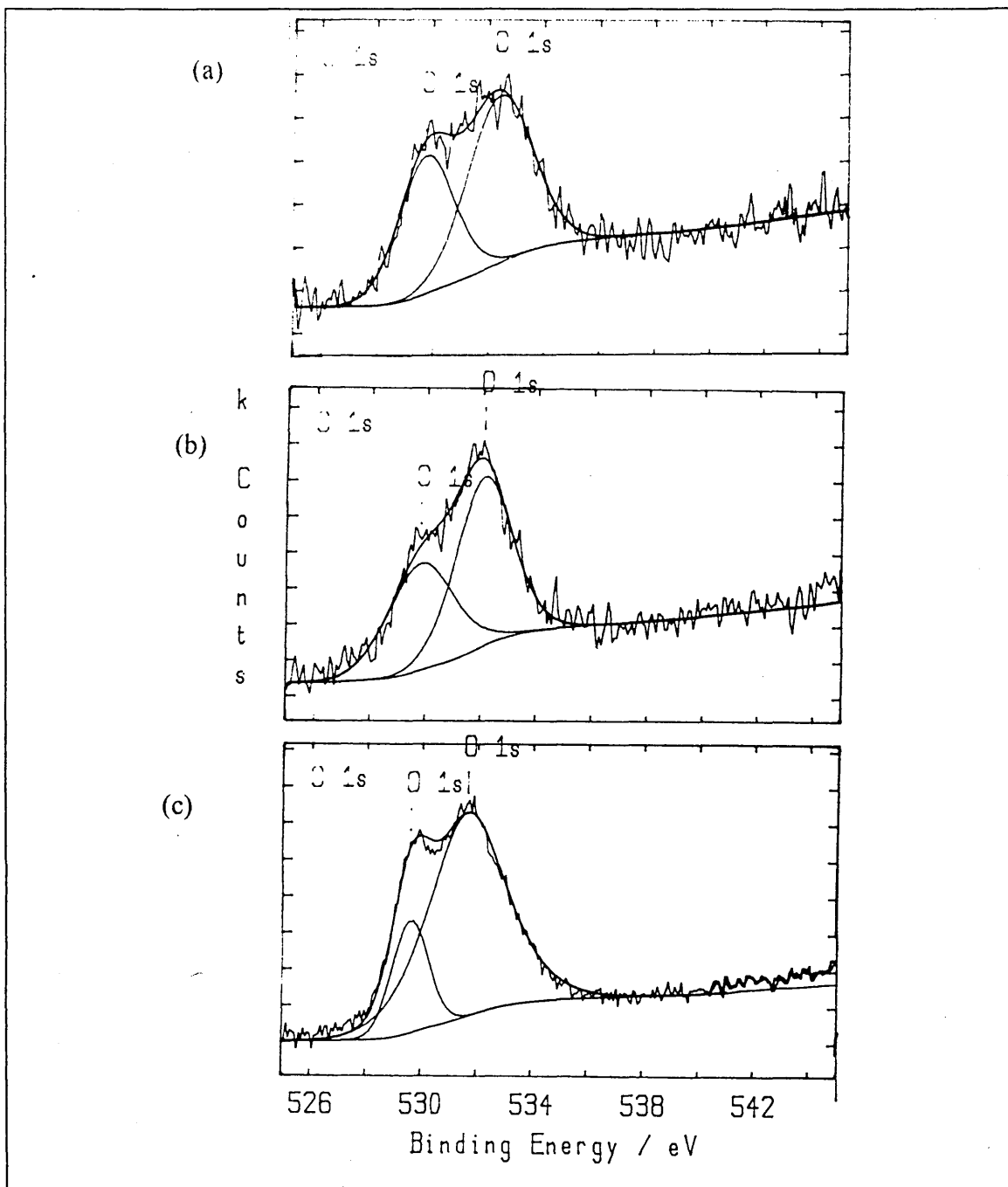


Figure 5.8 The O 1s feature for (a) etch 2 (S-rich), (b) etch 3 (air cleaved) and (c) etch 8 (Cd-rich). First species at ≈ 531.3 eV associated with physisorbed O, second species at ≈ 532.4 eV associated with native oxide of CdS. The ratio of the two species indicates the oxidation of CdS, reduced for etch 2 and increased for etch 8 compared with air cleaved.

sample which had a broad peak, the result of a possible overlap between Cd(OH)₂ and physisorbed O 1s peaks. The second phase was generally much broader than the first which in itself suggested the possibility of two forms of O bonding associated with CdO and CdSO₄ phases. The lack of any significant S 2p peaks associated with the SO₄²⁻ phase suggests that only very small amounts of this phase were present. The O 1s peak was more sensitive to a sulphate phase as there are four O atoms for every S atom forming this phase. Three O 1s spectra are shown in figure 5.8, the spectra were chosen to highlight the changing ratio of the first species to the second species of the O 1s peak for different

Etchant	O 1s First species			O 1s Second species		
	B.E. eV	Int kceV/S	FWHM eV	B.E. eV	Int kceV/S	FWHM eV
1	529.9	3.76	1.35	532.1	5.20	4.3
2	529.6	4.19	1.23	532.0	5.78	3.38
3	529.9	4.15	2.85	532.2	6.49	3.97
4	-	-	-	-	-	-
5	529.9	0.84	1.2	532.3	4.76	3.46
6	-	-	-	531.3	10.84	3.21
7	529.6	7.69	1.18	531.6	56.36	3.87
8	530.0	1.75	1.86	531.9	9.98	2.99
CdSO ₄ Std	-	-	-	532.9	24.58	2.44

Table 5.7. Peak binding energies, intensities and FWHM for two O species of etched CdS.

treatments. The FWHM of the Cd peak offered another indication as to the level of oxide formation but as can be seen from Table 5.7 there is little variation in this parameter apart from that for etch 6 which was almost 2 eV as compared with the average value of 1.8 eV. Combining this with the second phase peak position of 531.3 eV suggests that in this case the native oxide consisted solely of CdO. The second phase can in any event be regarded as originating from the native oxide of CdS whereas the first phase was most likely to originate from a physisorbed O species, the ratio of second phase to first therefore yielded a good indication of the level of oxidation on the surface as shown in figure 5.9.

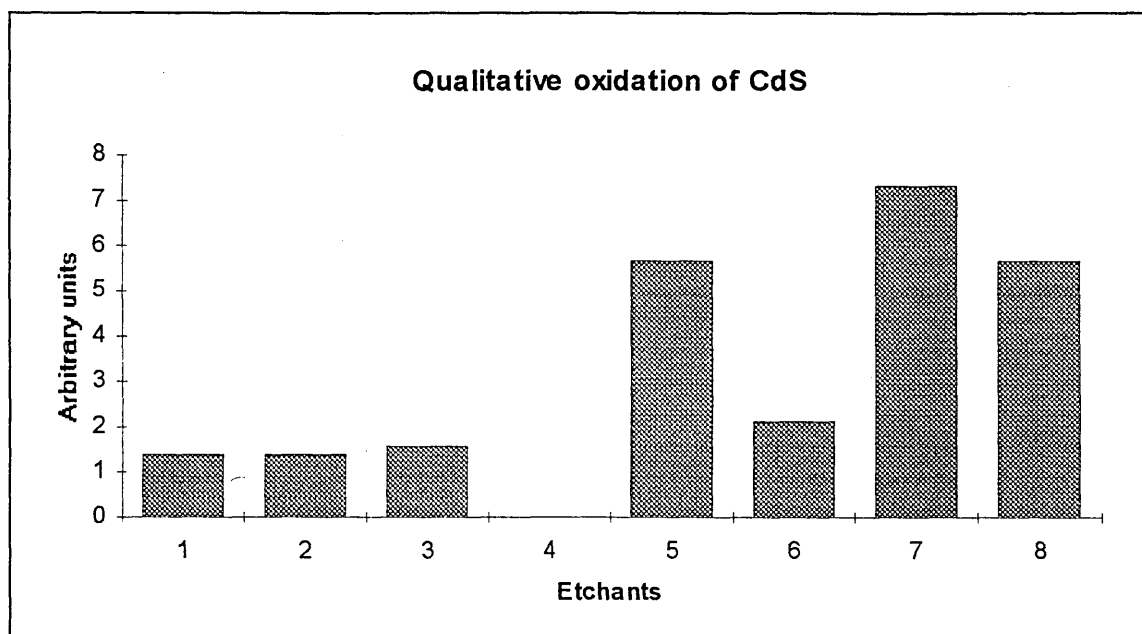


Figure 5.9 The ratio of physisorbed O 1s peak to native oxide peak height provides a qualitative analysis of the level of native oxide on the surface of CdS.

5.2.3 ZnSe

Polycrystalline, high resistivity samples of ZnSe were used primarily for surface analysis experiments, a comparison was made with (100)n-ZnSe/n⁺-GaAs samples. One major problem with the polycrystalline samples was their low conductivity which led to a large degree of static charging, shifting the spectra up to 14 eV in some instances. All spectra were normalised prior to data analysis to the adventitious C 1s peak at 284.5 eV (Briggs and Seah (1990)). Initially analysis was performed on the air exposed material which was subsequently ion etched to reveal a contaminant free stoichiometric surface. The composition remained almost constant as ion etching proceeded indicating no preferential sputtering. The surface produced after 5 min Ar etching was used as the surface from which semiquantitative analysis was based, 5 min being the minimum time required to remove all O and C contamination. The main core level emissions of Zn, Se, O and C were all monitored at maximum resolution as well as the intense Se and Zn LMM Auger features.

The surface composition in terms of the concentrations of Se and Zn was determined using the Se 3d and Zn 3p peaks. As can be seen from figure 5.10 which shows both Se 3d and Zn 3p peaks for a variety of ZnSe surfaces, the Se peak occurs as a broad single peak. SeO₂, which normally has a peak energy of 58.8 eV (Briggs and Seah (1990)) was not observed apart from the unetched surface (figure 5.10 (b)). The Zn 3p peak can be resolved into two peaks associated with Zn 3p_{1/2} and Zn 3p_{3/2}. For purposes of quantification this peak was taken as one; this avoids deconvolution errors as for the case of S 2p peaks in CdS. No chemically shifted phase is observed for the 3d peak or the more intense 2p doublet. The peak energies, widths and intensities are all given in Table 5.8. The peak energy values have been corrected for static charging, the non-consistency of

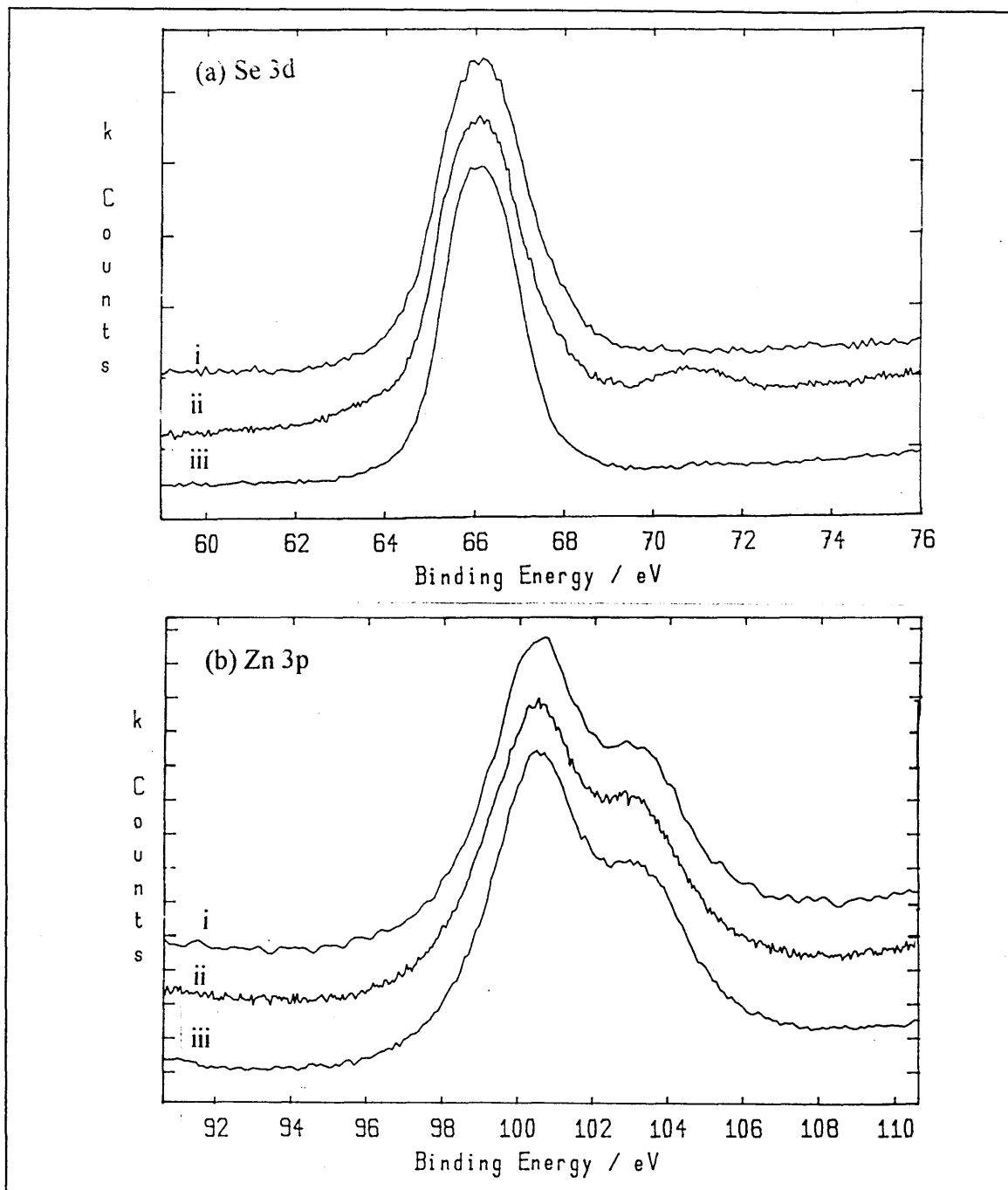


Figure 5.10 (a) Se 3d and (b) Zn 3p peaks for three surfaces of ZnSe (i) Se rich etch 2 (Chromic acid), (ii) as-received etch 3 and (iii) Zn rich etch 7 (NaOH and $\text{Na}_2\text{S}_2\text{O}_3$ solution). Note chemically shifted species associated with native oxide of Se a(ii) reduced for etched surfaces a(i) and a(iii). No such shift was observed for Zn 3p peaks.

many of the values reflects the pitfalls of this technique. The composition in terms of Zn and Se concentrations was determined using the Zn 3p and Se 3d peaks, both have similar binding energy values and are indeed only separated by ≈ 36 eV indicating very similar escape depths.

Etchant	Se 3d			Zn 3p _{3/2}			Zn 3p _{5/2}		
	B.E. eV	Int kceV/s	FWHM	B.E. eV	Int kceV/s	F WHM	B.E. eV	Int kceV/s	FWHM
1	54.6	67.89	2.44	88.3	23.64	2.89	91.2	16.43	3.09
2	54.0	73.02	2.35	88.0	46.96	2.92	90.8	34.00	3.76
3	54.8	13.61	2.16	89.0	16.18	2.85	92.0	9.23	3.16
4	53.9	22.56	2.07	88.2	20.28	2.87	91.2	11.41	3.16
5	53.8	18.15	2.01	88.1	19.93	2.86	91.2	9.66	3.25
6	53.7	52.75	1.99	87.9	53.50	2.8	90.9	34.20	3.27
7	54.0	20.71	2.08	88.2	19.40	2.84	91.2	9.99	3.45
8	54.2	76.35	1.95	88.3	72.98	2.8	91.1	59.7	3.78

Table 5.8 Binding energies, intensities and full width at half maximum values for Se 3d and Zn 3p peaks for a range of chemically treated ZnSe surfaces and the as received surface.

The as-received sample was rich in Zn but sputter cleaning restored stoichiometry by removal of excess Zn. The semiquantitative analysis of the surfaces is shown in Table 5.9

where a comparison is made between composition calculated using the sensitivity factors of Briggs and Seah (1990) and the CJB dataset values (Table 5.1). As with CdTe the Briggs and Seah values gave a constant over-estimate of the atomic percentage of Se in ZnSe. Chen *et al* (1994) have shown that annealing ZnSe leads to a reduction in the Se content whereas Torres *et al* (1994) have shown that plasma etching produces a depletion in Zn at the surface. The CJB dataset sensitivity factors predict that the surface composition can be influenced from Zn rich to Se rich by appropriate etching as shown in figure 5.11.

Etchant	Briggs & Seah		CJB dataset	
	At %	At %	At %	At %
	Se	Zn	Se	Zn
1	54.75	45.25	70.4	29.6
2	39.2	60.8	55.9	44.1
3	29.0	71.0	46.2	53.8
4	33.7	66.3	50.0	50.0
5	32.0	68.0	48.0	52.0
6	30.05	69.95	45.8	54.2
7	33.5	66.5	49.7	50.3
8	29.1	70.9	44.7	55.3

Table 5.9 Composition of as-received, sputter cleaned and etched ZnSe for the sensitivity factors of Briggs and Seah and the CJB dataset (Table 5.1)

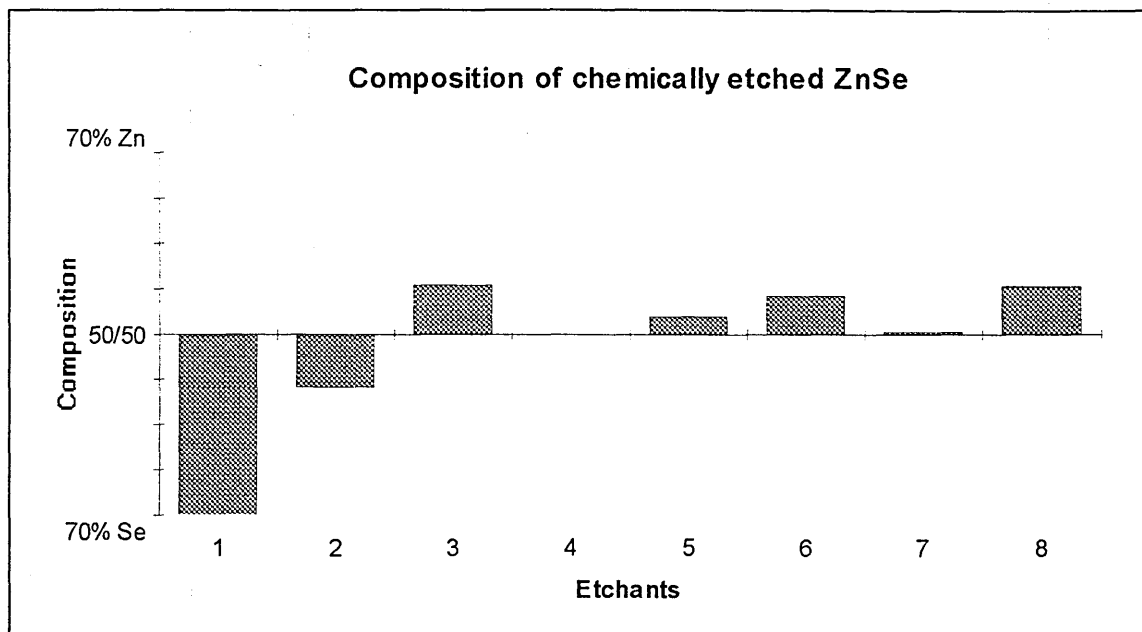


Figure 5.11 Composition of ZnSe after various chemical etchants.

The Se rich surfaces of Table 5.9 have significantly greater Se 3d peak widths (FWHM = 2.40 eV) than those for stoichiometric or Zn rich surfaces (FWHM = 2.0 eV). This indicates that there is more than one chemical species included within the Se 3d peak for Se rich surfaces, which is most likely to be elemental Se, as no chemical shifted species associated with native oxides of Se was observed.

5.2.3.1 Oxidation of ZnSe

Upon first inspection the etched ZnSe surface appears completely oxide free. A careful analysis of the O 1s peak reveals that it does in fact consist of two species as shown in figure 5.12. Figure 5.13 shows that most of the native oxide occurs for those surfaces rich in Zn. Comparison of the "oxide" species binding energy with that of the standard SeO_2 sample showed that even allowing for charge correction errors (which in general would

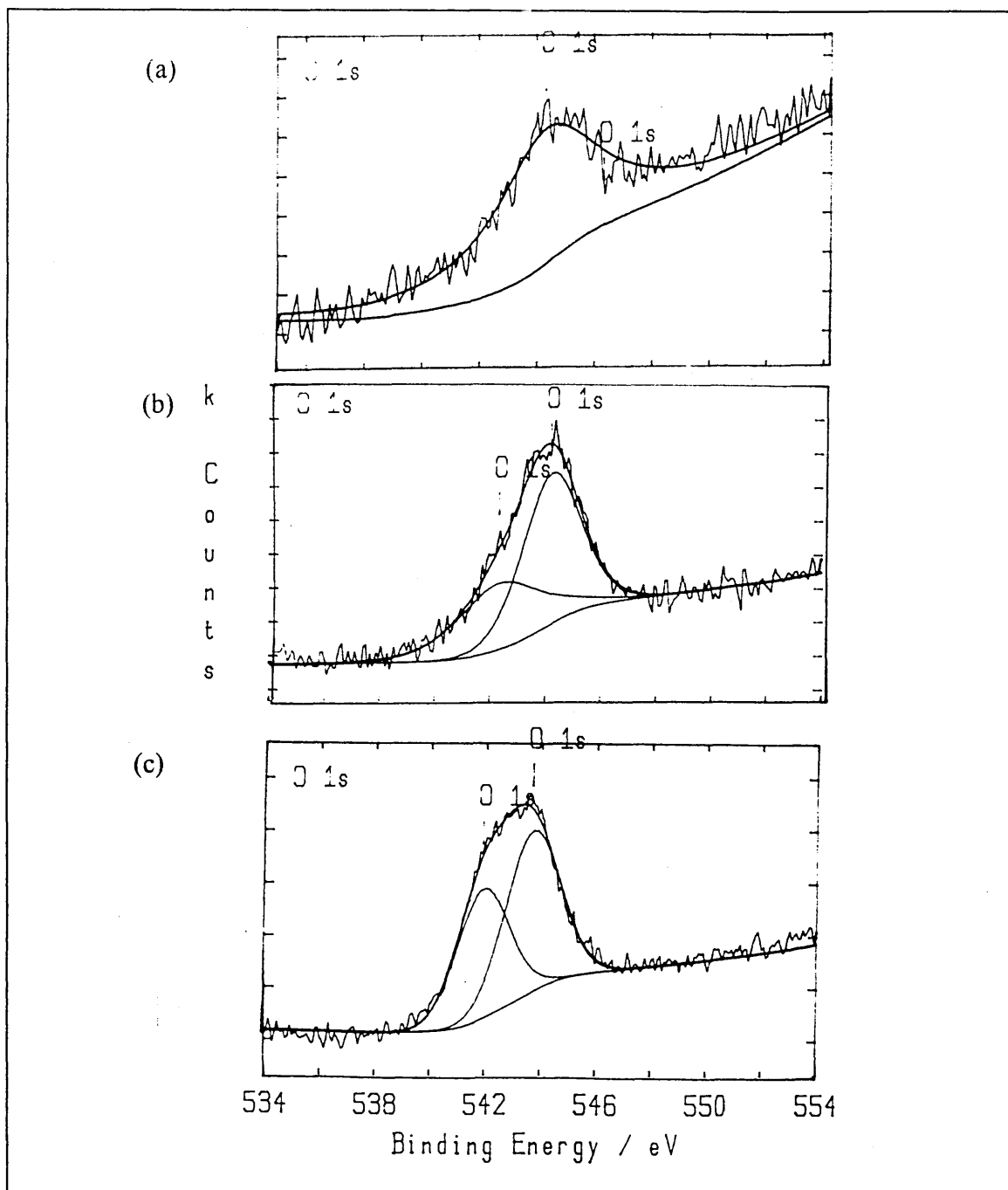


Figure 5.12 O1s feature for (a) etch 1, (b) etch 3 (as-received) and (c) etch 8. First species at ≈ 530.8 eV is associated with physisorbed O, the second at ≈ 532.1 eV is associated with the native oxide of ZnSe. Acid etched surface has no evidence of native oxide, alkali etched surface has reduced oxidation compared with as-received surface.

Etchant	O 1s First species			O 1s Second species		
	B.E.	Int	FWHM	B.E.	Int	FWHM
	eV	kceV/S	eV	eV	kceV/S	eV
1	532.3	12.42	2.76	-	0	
2	531.2	7.17	3.32	532.8	7.17	2.39
3	529.8	3.41	2.04	532.1	33.74	3.19
4	-	-	-	-	-	-
5	531.5	11.96	3.09	-	0	-
6	529.6	1.66	1.57	531.3	24.45	2.56
7	531.5	0.77	1.38	532.1	3.51	2.8
8	529.9	15.03	2.07	531.6	30.51	2.5
SeO ₂ std	-	-	-	532.9	24.58	2.44

Table 5.10 Binding energy, intensity and FWHM for native and physisorbed oxygen on etched ZnSe.

binding energy) the "oxide" species peak energy was too low to be SeO₂. Further information as to the chemical composition of the surfaces was obtained from analysis of the Se L₃M₄₅M₄₅ and Zn L₃M₄₅M₄₅ X-ray generated Auger features. The Se L₃M₄₅M₄₅ feature is shown in figure 5.14 (a) for standard SeO₂, Se rich and Zn rich surfaces. The feature was identical for Zn rich or stoichiometric surfaces, Se rich surfaces induced a slight broadening. XPS data indicated a lack of SeO₂, the broadening was therefore assigned to elemental or hydrated Se. Similar results were observed for dry etched,

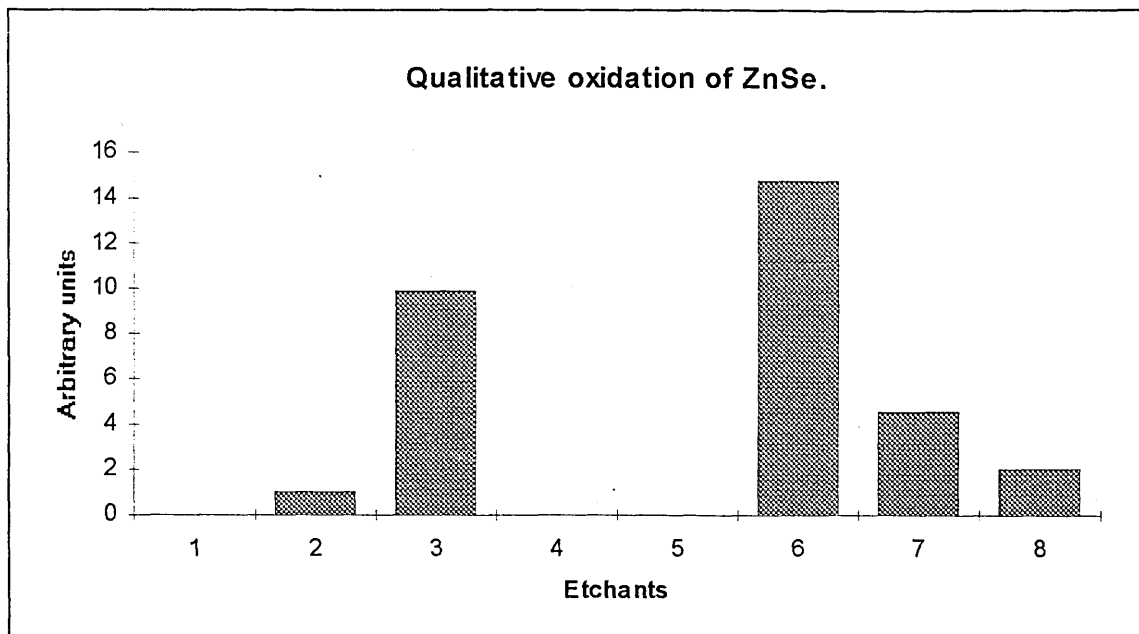


Figure 5.13 Ratio of native oxide to physisorbed oxygen.

Se rich surfaces by Chen *et al* (1994) who found Se rich surfaces to consist of dimerised Se. The Zn $L_3M_{45}M_{45}$ feature, figure 5.14 (b), was identical for Se rich or stoichiometric surfaces and broadened for Zn rich surfaces. The high oxide content of such surfaces indicates that Zn undergoes a bonding transition from Zn-Se to Zn-O for Zn rich surfaces.

5.4 Summary of surface etching of CdTe, CdS and ZnSe.

It is immediately obvious from an analysis of the etching behaviour of CdTe, CdS and ZnSe that all three materials display similar characteristics. Acid etching of the surface induces a depletion of the semiconductor cation to leave a surface rich in the semiconductor anion. The chemical state of this remaining anion appears to be predominantly elemental. Analysis of the oxidation of these surfaces reveals a minimum of

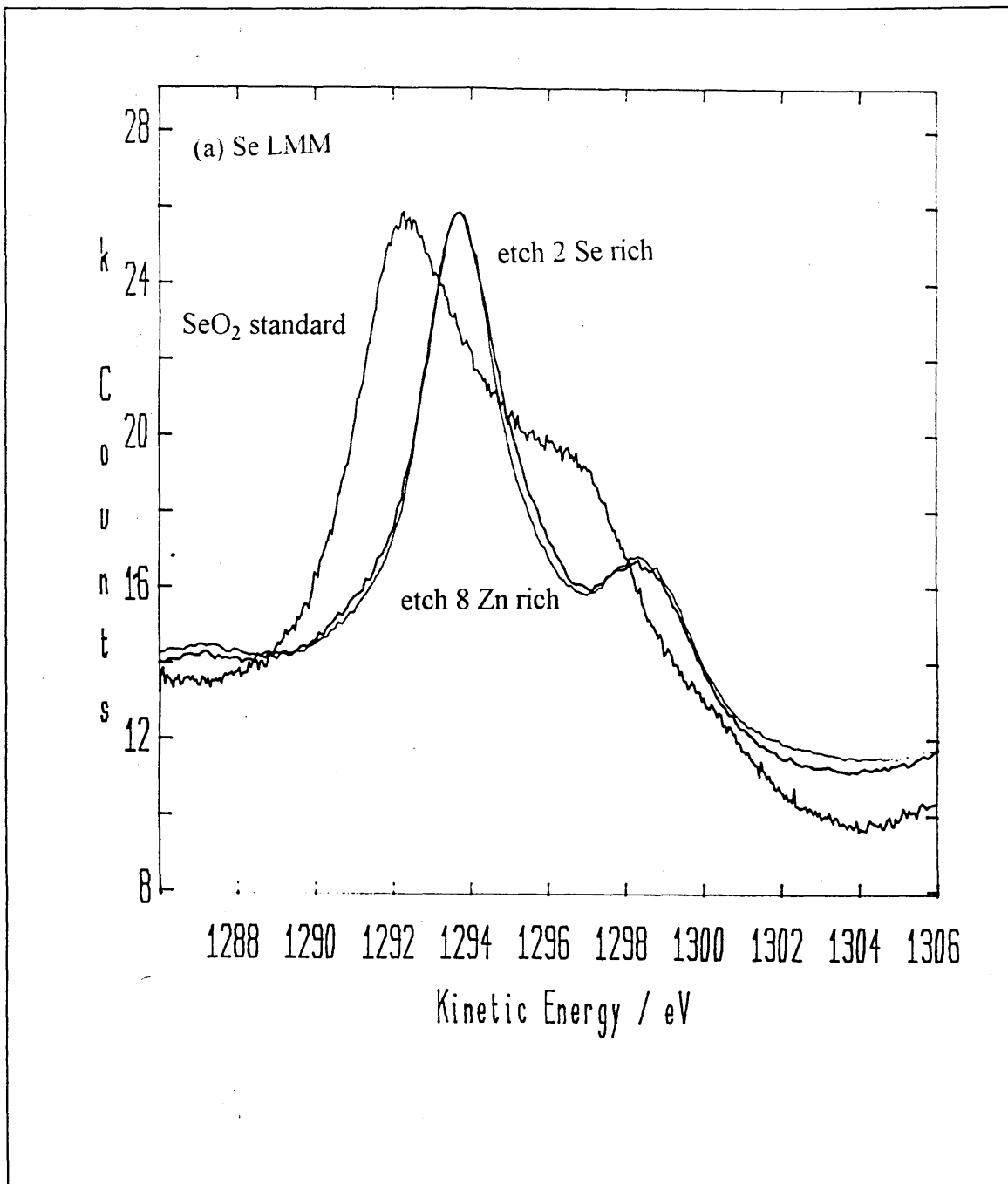


Figure 5.14(a) Se LMM Auger features for etched surfaces of ZnSe. The Se LMM feature is slightly broadened for Se rich surfaces but bears no relation to the feature associated with SeO₂.

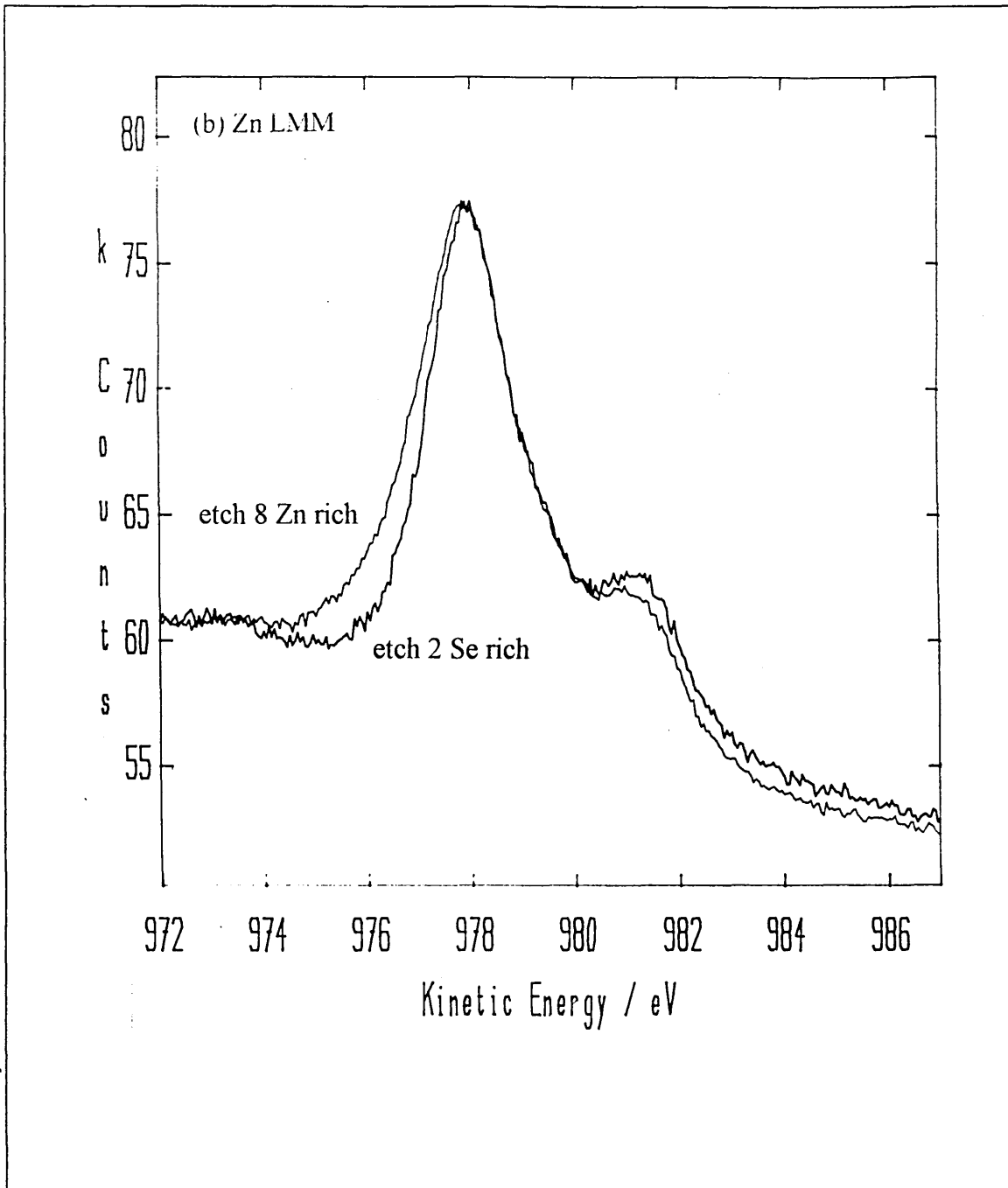


Figure 5.14 Zn LMM Auger features for etched surfaces of ZnSe. The Zn LMM feature is broadened for Zn rich surfaces the high oxide content of these surfaces suggests the formation of ZnO.

surface oxide as evidenced from figures 5.5 (CdTe), 5.11 (CdS) and 5.16 (ZnSe). No chemically shifted species were detected from Te, Se or S associated with oxidation of these acid etched surfaces but the O 1s peak did have a very small shoulder indicating a minimum of oxidation. It is reasonable to conclude that the surface is rich in the semiconductor anion which is either in an elemental or hydrogenated state. Surfaces etched in alkaline solutions show the opposite trend, in that there is a depletion of the semiconductor anion to leave a surface rich in the semiconductor cation. The remaining surface is more oxidised than the acid etched surface and determination of the chemical state is slightly more complex. All CdTe surfaces etched in alkaline solutions display a chemically shifted species of the Te $3d_{5/2}$ peak at 576.3 ± 0.2 eV which is usually associated with TeO_2 , no such species is observed for Se or S. Analysis of the core emissions of the semiconductor cation shows no such chemical shift. Shifts due to the oxidation of Cd and Zn are typically < 0.2 eV and beyond the limit of detection of our system. The Auger features of these elements do however reveal a qualitative indication that the semiconductor cation is involved in bonding with O.

A simple chemical picture of the etching process can be formulated by considering the II-VI compounds as ionic materials as first suggested by Kurtin *et al* (1969). This ionic character means that they behave in respect to aqueous reagents as insoluble salts formed from strong bases such as ZnO and weak acids such as H_2Se (for ZnSe). Etching the surface with a strong acid would form H_2Se liberating the metal ion to Zn^{2+} in solution. The H_2Se could well remain adsorbed on the surface: it would be insoluble in a strong acid due to the high concentration of H^+ inhibiting ionisation to Se^{2-} and HSe^- . Surface analysis would then reveal a stoichiometric excess of Se (semiconductor anion) and differentiation from elemental Se or H_2Se would be undetectable by XPS. The low oxide content can be explained by the fact that O could only be bonded to Zn but again the high H^+ content

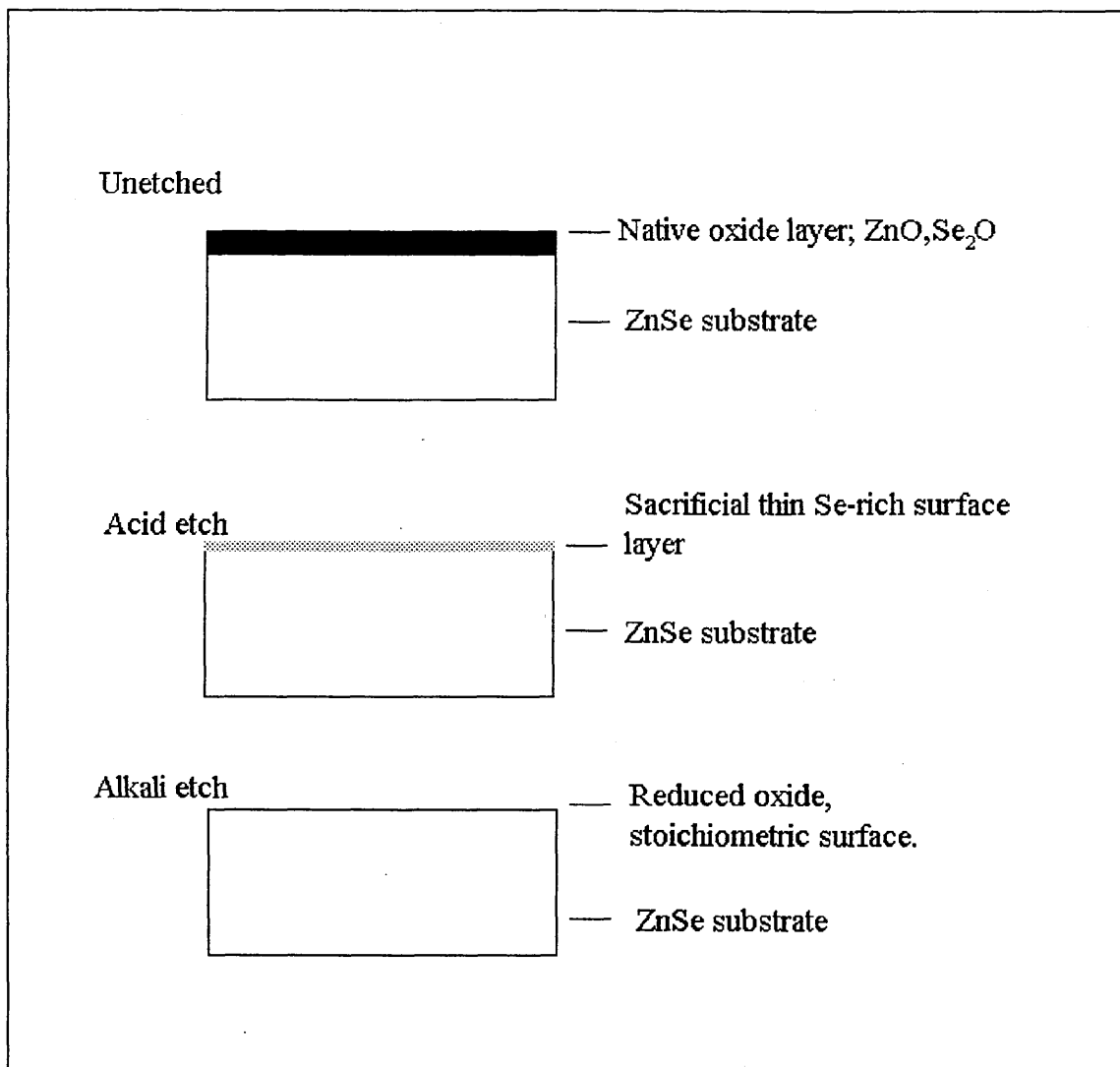


Figure 5.15. A schematic representation of the two stage etching (etch 5 and 6) of II-VI compounds. ZnSe is used in this case as an example but a similar model could be invoked for both CdTe and CdS.

means that ZnO would be removed as Zn^{2+} ions. At high pH Se would dissolve due to the high concentration of OH^- . The semiconductor cation, in this case Zn^{2+} , on the other hand

will be hydrolysed or hydrated to insoluble ZnO or Zn(OH)₂. Surface analysis will reveal a stoichiometric excess of Zn with a high O content and very little Se.

Following this model it is possible to explain the working of etchants 5 and 6, both of which consist of an initial acid etch followed by an alkaline etch. The acid etch creates a sacrificial surface rich in the semiconductor anion (Se for example). Immersion of this surface into an alkaline environment effectively removes the excess anion, (Se, by full ionisation to Se²⁻). The timing of the second stage and concentration of the etchant are crucial factors in obtaining the desired stoichiometry and low oxidation. Over-etching will induce the oxidation of the cation, (to form ZnO for example) and under-etching will incompletely remove the anion leaving a stoichiometric excess of the anion over the cation, (a Se rich surface). Evidence of this behaviour in the case of CdTe is shown in figure 5.3 where etchant 6 has left an excess of Te indicating that the second stage of the etch was not long enough. Figure 5.9 shows a large excess of Cd on the etched surface of CdS indicating an over-etch of the second stage of etch 6. On the whole etchant 5 is the more controllable etchant. Stoichiometric, relatively oxide free surfaces can be produced by typically etching with the acid for 30s and varying the alkaline stage for 6 min for CdS, 4 min for ZnSe and 3 min for CdTe.

The general tendency to etch of the II-VI compounds is CdTe>ZnSe>CdS. This trend agrees with an early observation of II-VI compounds by Warekois *et al* (1962) who predicted that they should etch according to the greater difference in electronegativity, which in this case is CdTe>ZnSe>CdS.

Chapter 6

Electrical characterisation of metal contacts to etched surfaces.

6.1 Introduction

Electrical characterisation of metal-semiconductor devices yields many interesting device parameters as well as information on the interfacial properties. Careful analysis of current-voltage (I-V) characteristics provides directly an indication of diode quality and the magnitude of the Schottky barrier. Other complementary methods of analysis such as capacitance-voltage (C-V) can be adapted to yield information on deep levels as in deep level transient spectroscopy (DLTS). Ballistic electron emission microscopy utilises the ultimate atomic scale resolution of the STM to obtain essentially what amounts to an I-V characteristic on the nm scale. A combination of these techniques is presented here to analyse Schottky barriers formed to CdTe, CdS and ZnSe.

6.2. Au/n-CdTe.

Au/n-CdTe contacts have been thoroughly electrically characterised. I-V measurements were initially used to establish an etching procedure with the maximum chance of producing ideal Schottky barriers. Such ideal barriers were then characterised by both I-V and C-V techniques. The stability of both ideal and non ideal devices was monitored over several months.

6.2.1. Non-ideal contacts.

Surface analysis has shown that the air exposed CdTe surface consists of a thin oxide layer [Sec 5.3]. This layer must be removed to obtain ideal Schottky barriers. Wet chemical

etching has a profound influence on the surface chemistry and can be used to reduce the oxide layer. Over-etching can result in the concentration at the surface of either the constituent elements such as excess Te or oxide species. Both of these phenomena have a profound influence on the electrical characteristics of metal contacts formed onto the etched surface. Figure 6.1 shows the I-V characteristic of a Au/n-CdTe contact formed on CdTe after etching in etch 1 (1% Br methanol) for 2 min. The ideality factor, n and Schottky barrier height, ϕ_b for this device were $n = 2.1$ and $\phi_b = 0.80$ eV respectively. Such high n values are normally associated with recombination of electrons rather than thermionic emission over the barrier. Prolonged etching with etch 1 has been shown to preferentially remove Cd to leave elemental Te at the CdTe surface [Sec 5.1] which in turn may produce recombination centres at the Au/n-CdTe interface leading to a degradation in the ideality of the diode.

Incomplete removal of surface oxides leads to the formation of interfacial layers which in turn result in I-V characteristics of the type shown in figure 6.2. In this case CdTe samples were under-etched in etch 1 (weak 0.5% Br in methanol) for 15, 20 and 60 s respectively. The effect was to partially reduce the surface oxide, leaving an intermediate layer of decreasing thickness the longer the etching time. Subsequent formation of metal contacts to these surfaces lead to the formation of metal-insulator-semiconductor (MIS) structures. Essentially the thinner the interfacial layer the higher the forward current which was shown in figure 6.2. Similar results were obtained by Card and Rhoderick (1971) for SiO_2 interlayers grown under UHV conditions on Si prior to Al contact formation. The final I-V characteristics were much the same as those obtained here. Such control of surface oxide thickness is normally achieved only under vacuum conditions but wet chemical etching can produce similar effects.

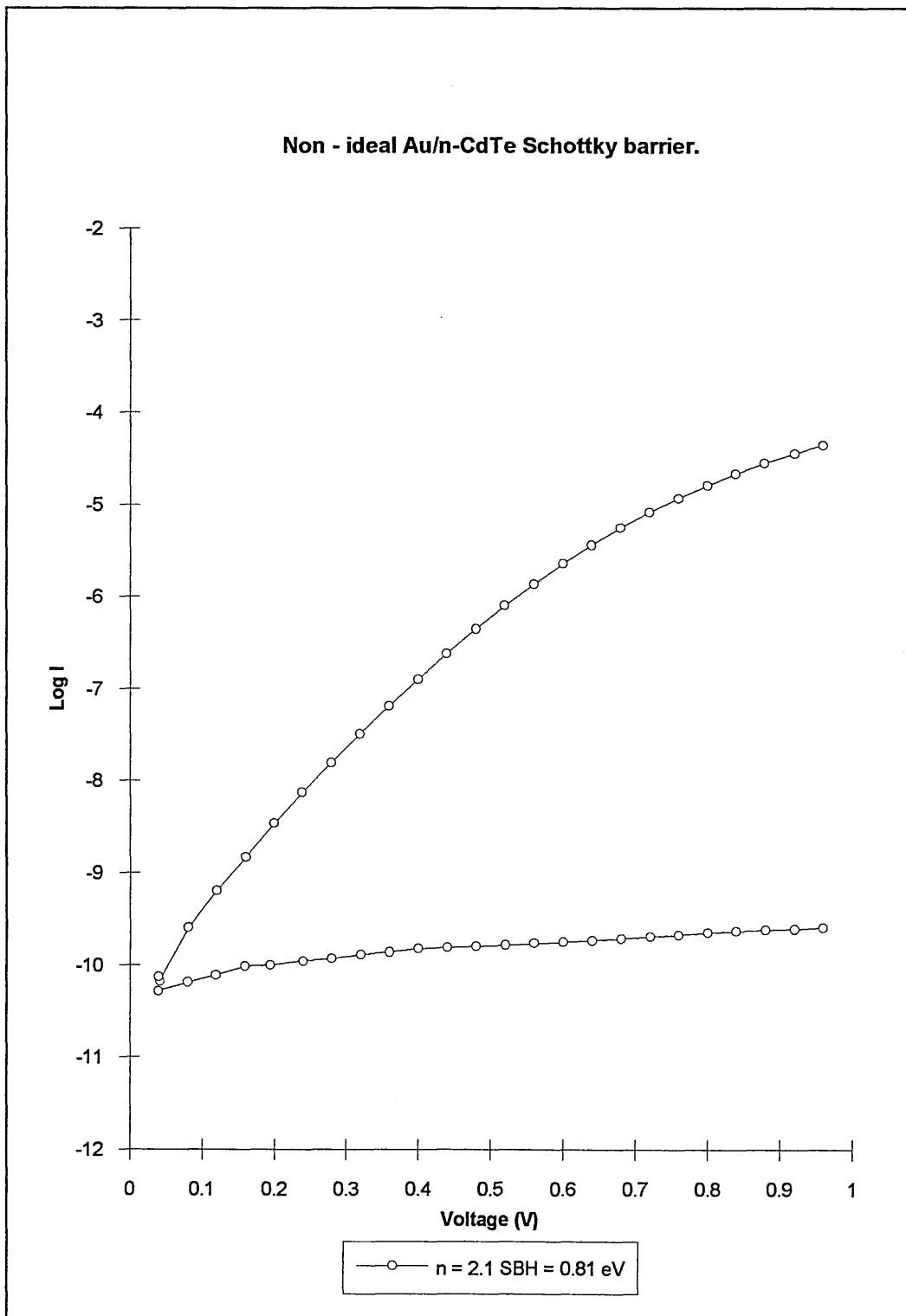


Figure 6.1. I-V characteristic for non-ideal Au/n-CdTe device, prepared by etching CdTe in etch 1 for 2 min.

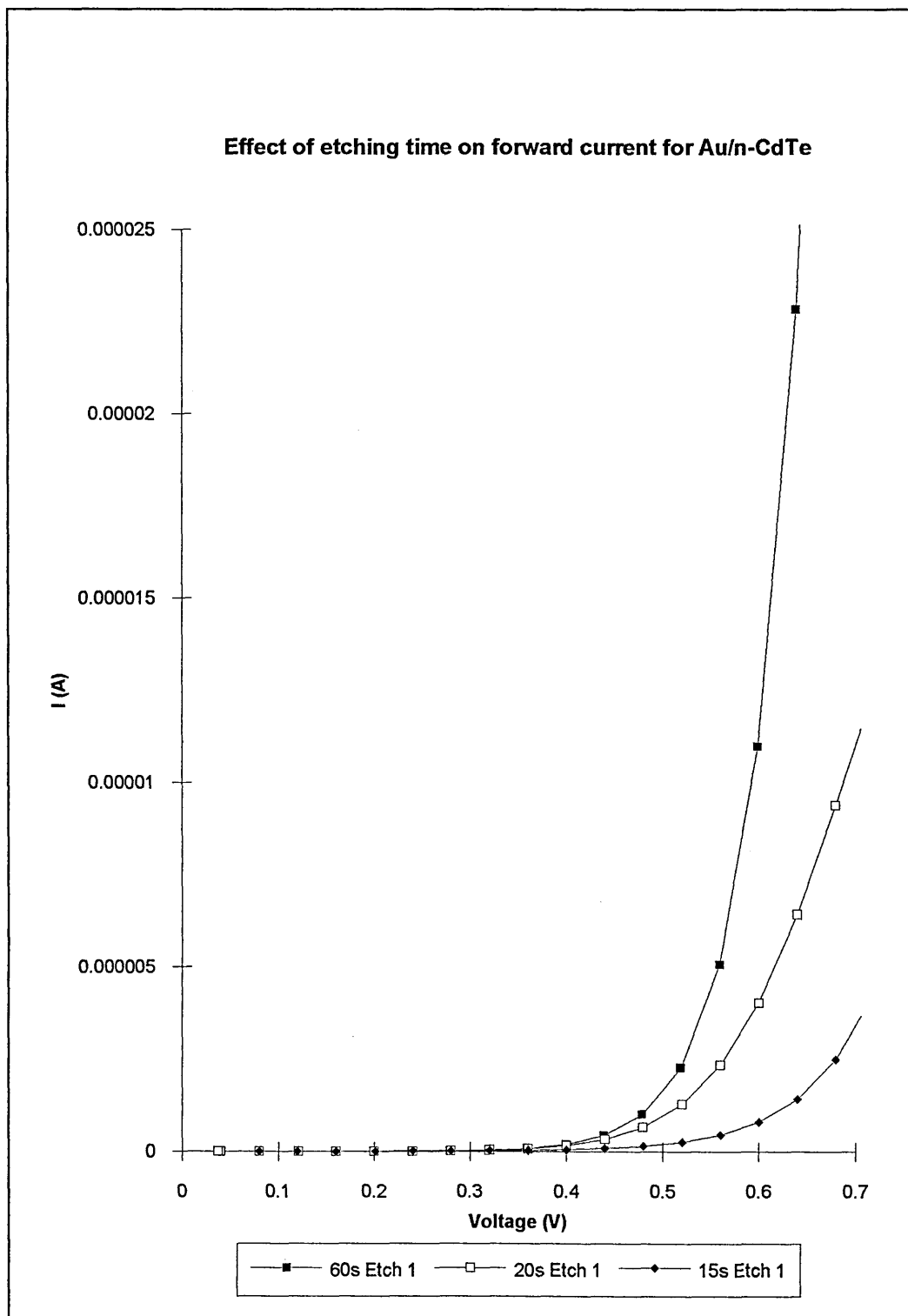


Figure 6.2 Linear I-V characteristics demonstrating the presence of an interfacial layer after etching with etch 1 (0.5 % Br methanol) for 15s, 20s and 60s respectively.

Both of these situations highlight the problem of forming ideal and repeatable Schottky barriers to CdTe. Although XPS has been used to characterise the effects of different chemical treatments on the surface a great deal of fine tuning of the exact etchant concentration and etching time was required in order to establish a regime that would maximise the chances of producing an ideal Schottky barrier.

6.2.2 Ideal contacts.

Figure 6.3 shows the I-V characteristics of four Schottky barriers which were repeatedly observed on etched CdTe. For ideal diodes (*i.e.* where $n < 1.1$) the electrical characteristics followed one of the four shown in figure 6.3, indicating the formation of a number of discrete Schottky barriers. The reverse current of the highest two barriers, $\phi_b = 0.96$ and 1.10 eV were of the same order as the electrical background noise in the system and so are not included in figure 6.3.

The four characteristics were obtained from surfaces prepared via the following routes:

- (a) $\phi_b = 0.64 \pm 0.02$ eV, etch 5 (etch 2, 30s, etch 7, 4 min)
- (b) $\phi_b = 0.725 \pm 0.02$ eV, etch 5 (etch 2, 30s, etch 7, 4 min)
- (c) $\phi_b = 0.96 \pm 0.02$ eV, etch 1, 45s
- (d) $\phi_b = 1.10 \pm 0.02$ eV etch 7, 120s

The effect of these various etchants on the surface stoichiometry has been well characterised [Sec 5.1]. It would perhaps be very tempting to relate a particular surface treatment to a particular Schottky barrier height. For example Te rich surfaces produced by etch 1 generally produced $\phi_b = 0.96 \pm 0.02$ eV. The relationship is however not so straightforward as on occasion a number of ideal Schottky barriers were observed for

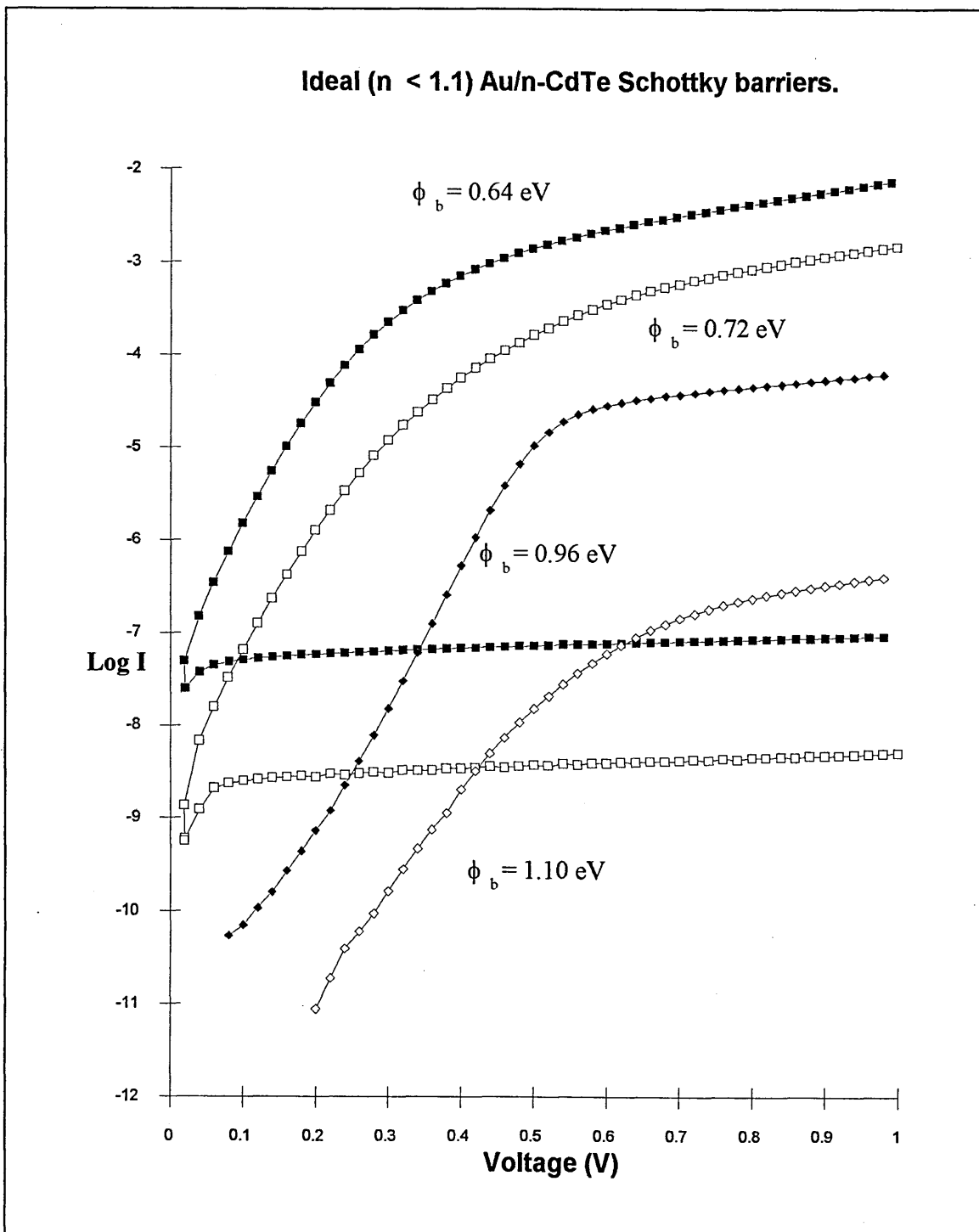


Figure 6.3. Ideal ($n < 1.1$) I-V characteristics for Au/n-CdTe devices formed on chemically etched CdTe. The characteristic of $\phi_b = 1.10 \pm 0.02 \text{ eV}$ is an underestimate as the n value was slightly high in this case $n = 1.13$.

contacts on the same sample. One sample in particular had $\phi_b = 0.64, 0.72$ and 0.95 ± 0.02 eV for adjacent contacts after etch 5.

The ideal nature of these devices can be demonstrated by re-plotting the I-V data in the linearised fashion introduced by Missous and Rhoderick (1986). In this case a plot of $\text{Log} [I/\{1-\exp(-qV/kT)\}]$ should be linear for both forward and reverse biases for ideal diodes. Figure 6.4 shows such a plot for the two diodes of $\phi_b = 0.64$ and 0.725 ± 0.02 eV of figure 6.3. The lack of an observable reverse current for the two higher barriers of $\phi_b = 0.96$ and 1.10 eV meant that this type of plot has little advantage over the conventional interpretation. Analysis by this technique gave $n = 1.03$, $\phi_b = 0.65 \pm 0.01$ eV and $n = 1.03$, $\phi_b = 0.725 \pm 0.01$ eV. These values are in excellent agreement with those obtained by the more conventional analysis and reinforce the highly ideal nature of these devices.

6.2.2.1 Summary of ideal contacts.

The four discrete Schottky barriers have been observed for Au/n-CdTe systems previously by separate groups. Kuech (1981) and Friedman *et al* (1988) have both reported a Schottky barrier height of, $\phi_b = 0.65$ eV for vacuum cleaved surfaces only. Kuech (1981) also observed a barrier of $\phi_b = 0.72$ eV on air cleaved CdTe while Dharmadasa *et al* (1989) observed the same value for chemically etched (Te rich) surfaces. The third barrier of $\phi_b = 0.95$ eV is perhaps the most widely reported Schottky barrier for the Au/n-CdTe system and has been observed on a number of surfaces. For instance, with Cd interlayers (Kuech (1981)), Cd rich surfaces (Dharmadasa *et al* (1989), Vitomirov *et al* (1991) and Van Meirhaeghe *et al* (1991)). The final barrier observed here $\phi_b = 1.1$ eV is the highest Schottky barrier so far reported for the Au/n-CdTe system and has been observed by Patterson and Williams (1982) for air cleaved CdTe (100) surfaces only.

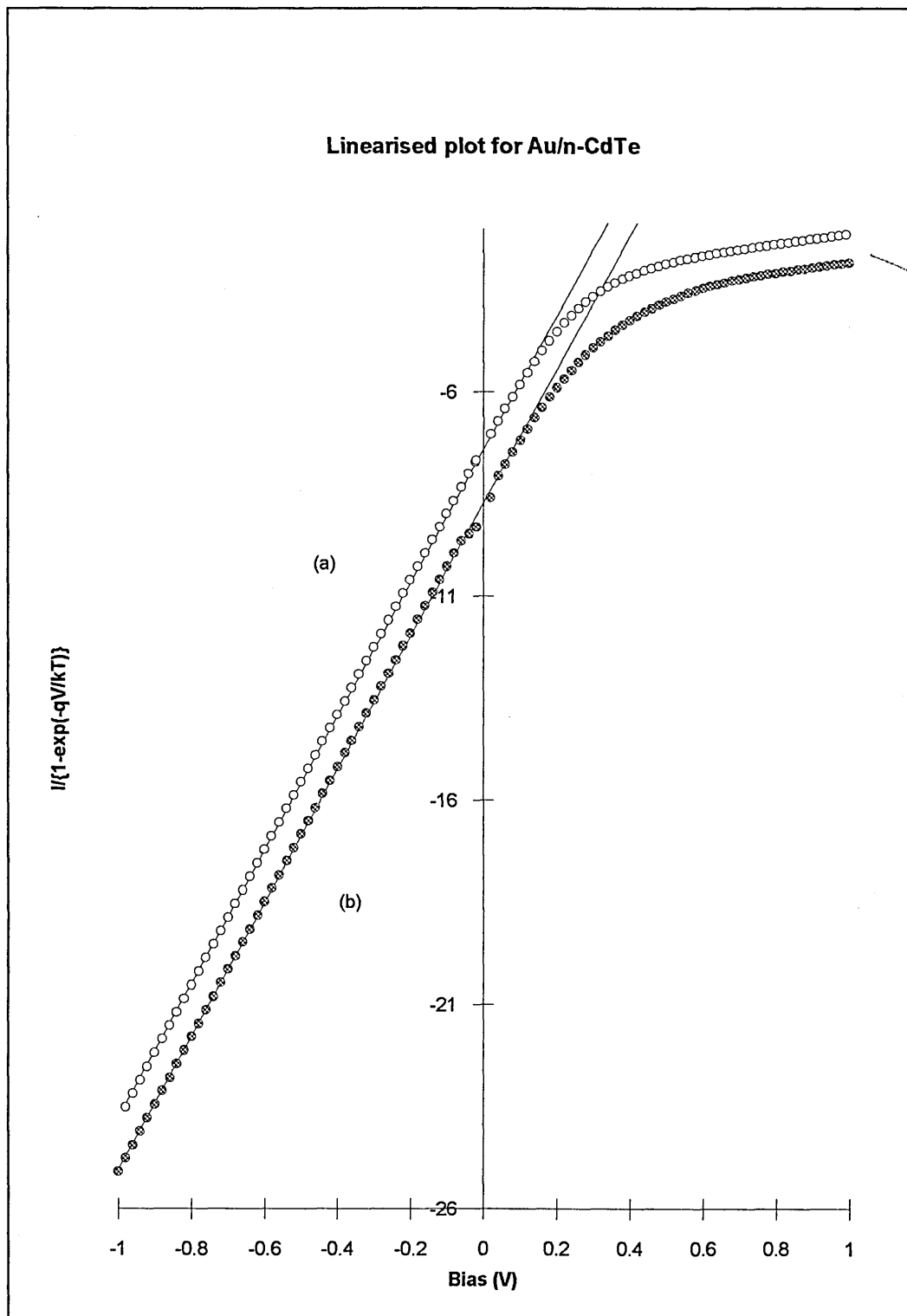


Figure 6.4. Linearised I-V relationship after Missous and Rhoderick for Au/n-CdTe, (a) $n = 1.03$, $\phi_b = 0.65 \pm 0.01$ eV and (b) $n = 1.03$, $\phi_b = 0.725 \pm 0.01$ eV.

A second interesting feature of these contacts is their extremely ideal nature, all but one of the barrier heights exhibited a diode quality factor, $n < 1.1$. In fact when analysed using the technique introduced by Missous and Rhoderick (1986) the quality factor approached the theoretical maximum (1.02, image force). Diodes with the highest barriers ($\phi_b = 1.1$ eV) always had a slightly larger n value of $1.13 < n < 1.2$. The high n value may be accounted for by the fact that this particular barrier was observed only for Cd rich surfaces prepared with etch 7 for 120s. XPS analysis of such surfaces revealed them to have a higher oxide content than Te rich or stoichiometric surfaces.

6.2.3. C-V characteristics.

Several typical C-V plots obtained for Au/n-CdTe are shown in figures 6.5 and 6.6, these plots are typical of those obtained for contacts, which by I-V analysis were characterised as "non-ideal" (figure 6.5) or "ideal" (figure 6.6).

Both figure 6.5 and 6.6 display good linearity indicating a uniform doping distribution in the CdTe samples. Table 6.1 gives the main parameters determined from C-V analysis, namely carrier concentration, N_d and the Schottky barrier height, $\phi_{b(C-V)}$. Schottky barrier heights determined by the C-V technique were for all diodes far in excess of those determined by I-V. In all cases $\phi_{b(C-V)}$ was in fact in excess of the band gap ($E_g = 1.45$ eV) of CdTe. Carrier concentrations determined from the gradient of the plot were in reasonable agreement with the suppliers specification for the wafer ($5 \times 10^{16} \text{ cm}^{-3}$). The indication given by these results is that the gradient of the graph yields the expected value of carrier concentration but the barrier height is in excess of that determined by I-V measurements. Dharmadasa *et al* (1987) have also reported $\phi_{b(C-V)}$ to be in excess of $\phi_{b(I-V)}$ for metal/n-CdTe contacts formed to etched surfaces. The discrepancy between the two methods was much less pronounced than with these results. Such effects were observed by

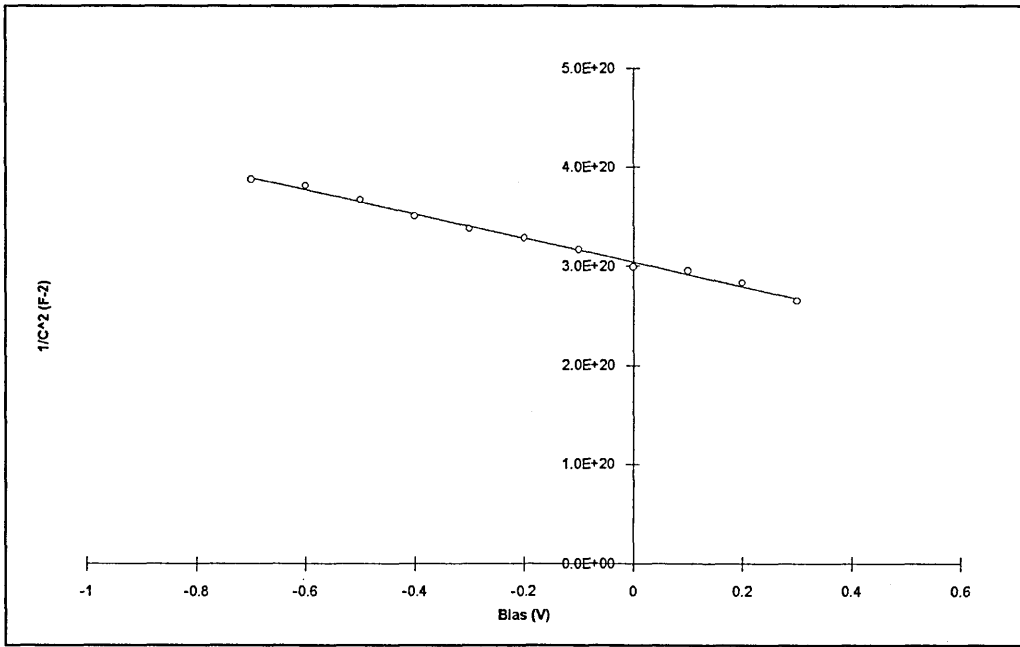


Figure 6.5. $1/C^2$ characteristic for a non-ideal Au/n-CdTe contact ($n = 1.9$, $\phi_{b(I-V)} = 0.76$ eV).

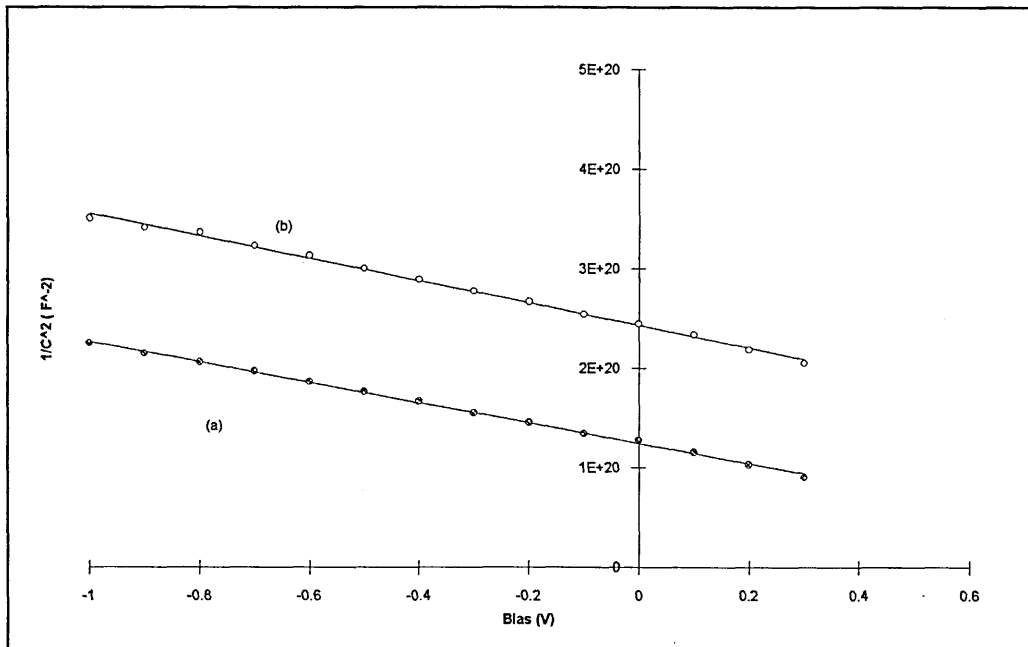


Figure 6.6. $1/C^2$ characteristics for "ideal" Au/n-CdTe contacts, (I-V characteristics gave (a) $n = 1.03$, $\phi_{b(I-V)} = 0.65 \pm 0.02$ eV and (b) $n = 1.03$, $\phi_{b(I-V)} = 0.725 \pm 0.02$ eV).

Figure	Carrier conc	$\phi_{b(C-V)}$	Ideality factor	$\phi_{b(I-V)} \pm$ 0.02
	$N_d \text{ cm}^{-3}$	eV	n (I-V)	eV
6.5	2.8×10^{16}	2.99	1.9	0.76
6.6 (a)	3.3×10^{16}	1.72	1.03	0.64
6.6 (b)	2.9×10^{16}	2.67	1.04	0.95

Table 6.1. A comparison of Schottky barrier heights determined by both I-V and C-V techniques for "ideal" and "non-ideal" Au/n-CdTe contacts.

Cowley (1966) for Au/n-GaP devices where devices prepared in a poor vacuum exhibited $\phi_{b(C-V)}$ in excess of $\phi_{b(I-V)}$ and ϕ_b determined from photovoltaic measurements. A model was developed which described the metal-semiconductor interface as having a uniform distribution of surface states accompanied by a thin interfacial layer. Devices of this nature were then shown to have a $C^{-2} \propto V$ characteristic not dissimilar to that shown by these Au/n-CdTe devices. The gradient yielded the correct value for N_d but the intercept on the ordinate gave over-estimates of the barrier height. What is interesting to note is the apparent sensitivity of C-V measurements to such layers over I-V measurements which showed these same contacts to be ideal (*i.e.* $n \approx 1$). However it should be pointed out that in all cases C-V measurements were carried out perhaps one day or more after I-V measurements of the same devices were performed. Given the instability of the Au/n-CdTe interface (see below) it is possible that an interfacial layer was formed in this time leading to a scenario similar to that predicted by Cowley (1966).

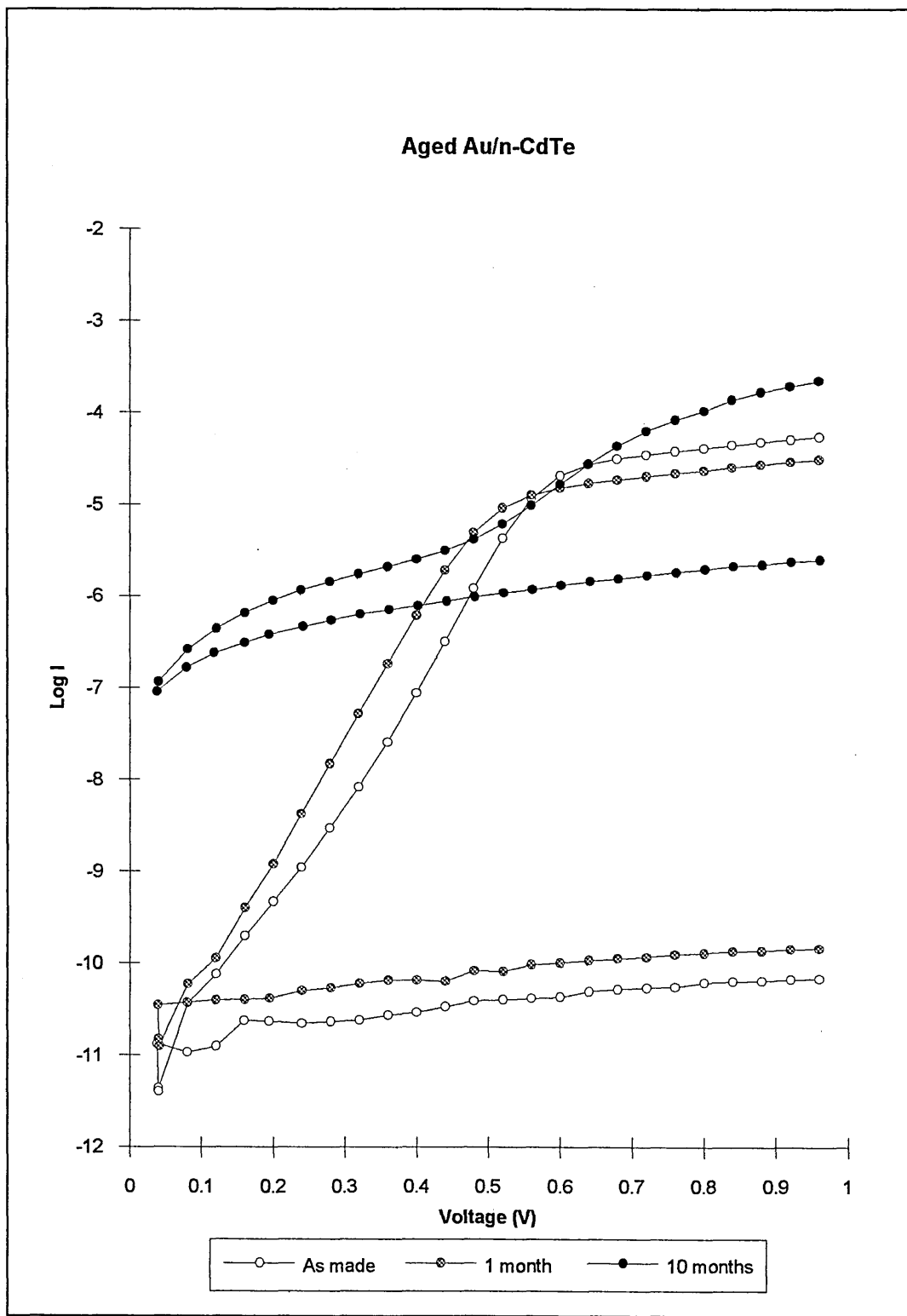


Figure 6.7 Aged Au/n-CdTe, initially ideal, after several months device is becoming ohmic.

6.2.4. Ageing of contacts.

A number of ideal and non-ideal devices were monitored over a period of months in order to investigate the ageing properties. Samples were stored under normal laboratory conditions and monitored every few weeks. For ideal contacts the ageing followed that of the contact shown in figure 6.7. Initially ideal, ($n = 1.08$, $\phi_b = 0.95 \pm 0.02$ eV) the characteristics show an increasing reverse current (I_{rev}), accompanied by an increase in the forward current (I_{for}) at low forward bias (<0.5). After 10 months I_{rev} has increased by four orders of magnitude from its original value and I_{for} shows a strong contribution from non-thermionic emission processes. At a bias of 1V only two orders of rectification are achieved compared with an original value of six orders of magnitude.

A quite different situation arises when the diode is far from ideal. Figure 6.8 shows the ageing of a typical non-ideal diode. The characteristic, although far from ideal (originally $n = 2.2$, $\phi_b = 0.75 \pm 0.02$ eV) actually improves with time. In this case after one month $n = 1.83$, $\phi_b = 0.79 \pm 0.02$ eV and after 10 months $n = 1.68$, $\phi_b = 0.795 \pm 0.02$ eV. These changes are accompanied by a general decrease in the reverse current and an increase in the rectification factor.

There is a marked contrast between these two types of contact. It seems that the presence of the interfacial layer, or disorder at the interface actually improves the stability and lifetime of the devices.

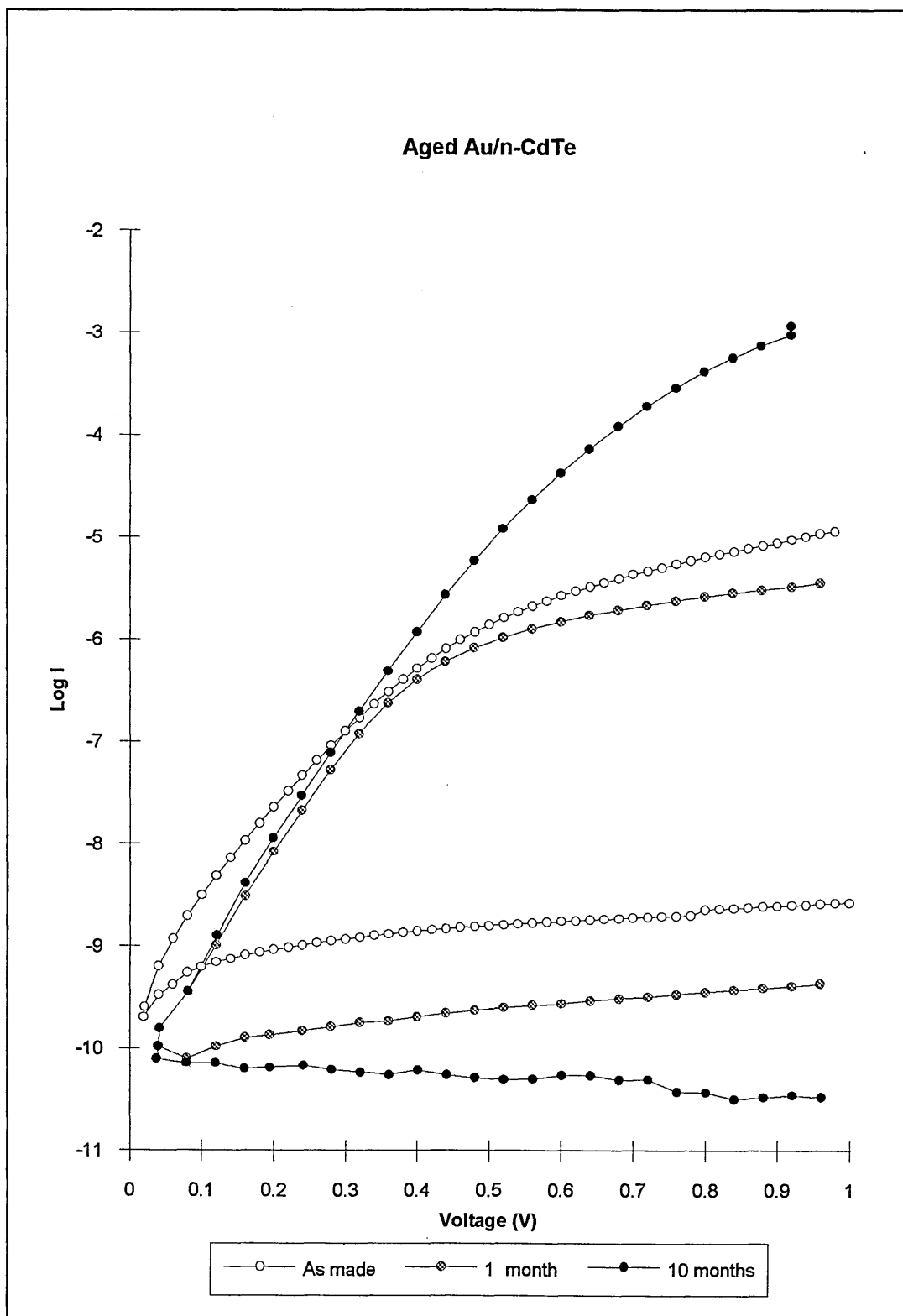


Figure 6.8. Aged Au/n-CdTe, initially with high n value indicative of an interfacial layer.

6.2.5 Deep level transient spectroscopy of Au/n-CdTe.

DLTS was performed on several Au/n-CdTe devices. All contacts tested were on the same sample etched by etch 1 for 1 min, which uniformly gave $n = 2.1$, $\phi_b = 0.75 \pm 0.02$ eV by conventional I-V characterisation. The sample was reverse biased at -1.5 V and a forward pulse of 1 V for 5×10^{-3} s was applied. The ratio of the two gate times t_1 and t_2 was maintained at 3 (e.g. run 1 $t_1 = 5$ ms, $t_2 = 15$ ms, run 2 $t_1 = 6$ ms $t_2 = 18$ ms). Thermal scans were performed from 100K to 350K. Three electron traps consistently appeared in the spectra as shown in the activation energy plot of figure 6.9, at $E_c - 0.75$ eV, $E_c - 0.62$ eV and $E_c - 0.33$ eV. The capture cross-sections and trap concentrations were not determined. A qualitative indication of the concentration could be determined from the area under each S(T) versus T plot following Lang (1974). The most intense level was at $E_c - 0.75$ eV with $E_c - 0.62$ and $- 0.33$ eV having much lower concentrations. Deep levels corresponding to these values have been observed previously by other groups. For instance Lee *et al* (1988) reported levels at $E_c - 0.36$, 0.65 0.74 and 1.15 eV similarly Verity *et al* (1983) reported levels at $E_c - 0.34$ and 0.78 eV among others. A full summary was given earlier (Sec 3.4.2). What seems apparent is that these levels are native to CdTe crystals as they have been observed by a number of other workers. One point to note is that no levels deeper than $E_c - 0.755$ eV were observed; this may in fact be related to the temperature limit imposed due to the noted instability of Au/n-CdTe interfaces. Such temperature restrictions may in fact limit the ionisation of deep levels.

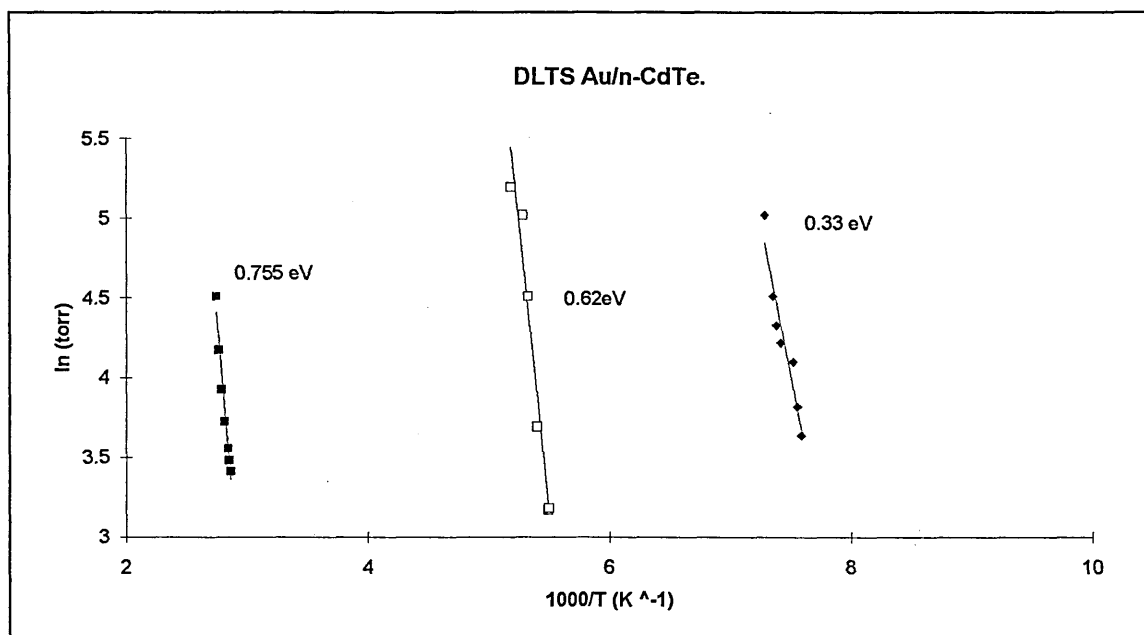


Figure 6.9. DLTS activation energy plots for Au/n-CdTe up to 350K.

6.3 Au/n-CdS.

Au/n-CdS contacts have been thoroughly characterised. As with CdTe, I-V measurements were used to establish etching procedures. Contacts were then characterised with both I-V and C-V techniques and the stability monitored over several months.

6.3.1 Non-ideal contacts.

As with CdTe, CdS has been shown to have a thin oxide layer at the surface and this must be removed in order to obtain an ideal metal-semiconductor junction. As the wet chemical etching of CdS is very similar to that of CdTe the same problems of non-ideality of contacts are encountered. Figure 6.10 shows a typical I-V characteristic of a non-ideal contact for Au/n-CdS. In this case the CdS surface was etched for 30s in etch 2 (chromic acid). The resultant characteristics showed strong contributions from recombination

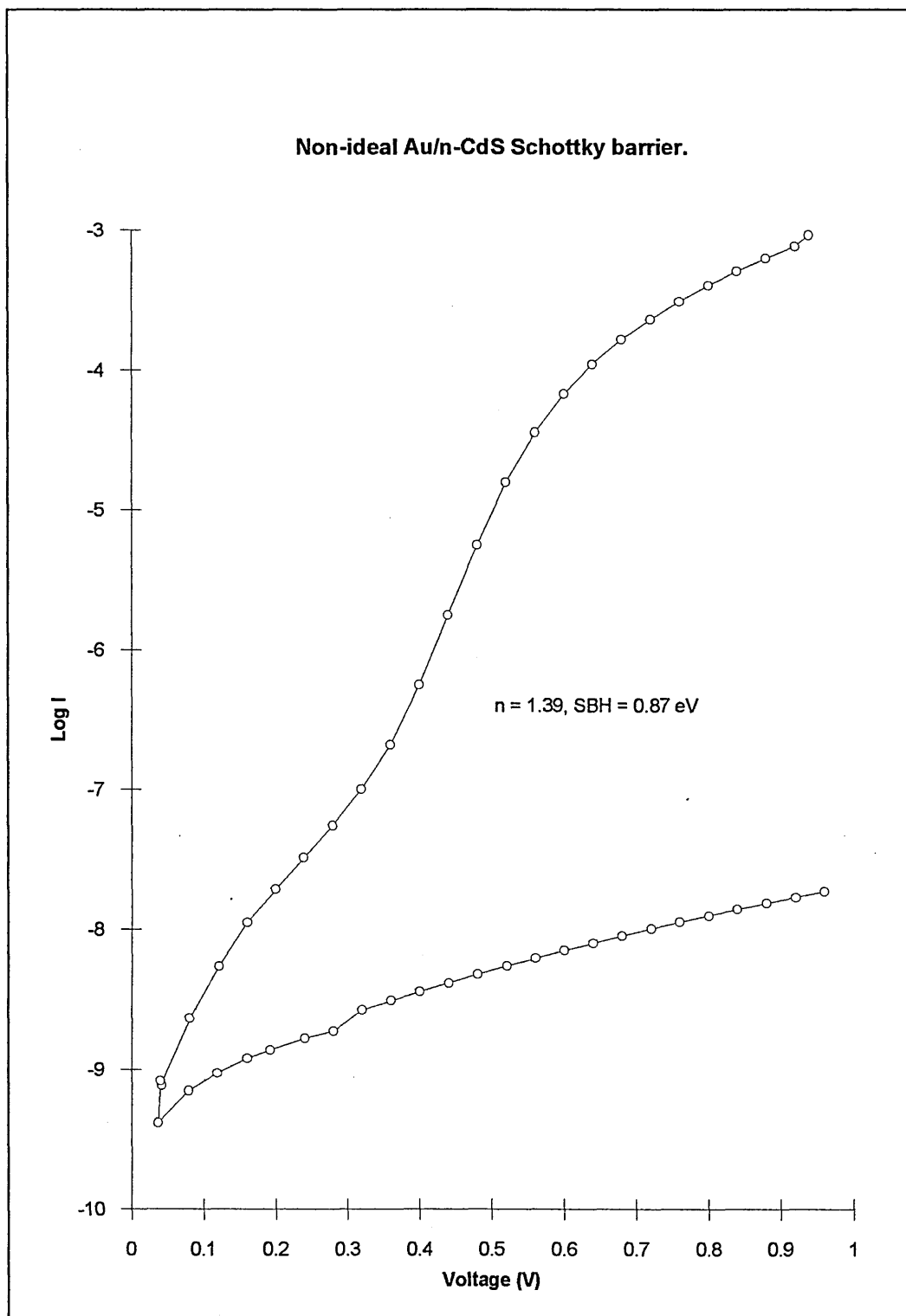


Figure 6.10. A typical I-V characteristic of a non-ideal Au/n-CdS diode formed after etch 2 for 30 s. $n = 1.39, \phi_b = 0.87 \pm 0.02 \text{ eV}$.

current at low forward bias [Sec 2.3.1.2]. As with CdTe such characteristics were commonly observed for contacts in which the correct etching procedure had not been established. In figure 6.10 the small linear portion of forward current (*i.e.* $V > 0.4$ V) yielded $n = 1.39$ and $\phi_b = 0.87 \pm 0.02$ eV.

The effects of etching CdS for different times in etch 2 (chromic acid) prior to contact formation are shown in figure 6.11. Here three samples were etched for 120, 90 and 30s, prior to Au contact evaporation. Table 6.2 shows that as the etching time was decreased the resultant I-V characteristics of the Au/n-CdS contacts became more ideal. Such behaviour is consistent with that associated with an MIS structure where the insulating layer is decreasing in thickness. XPS analysis [Sec 5.2] showed that continued etching with etch 2 resulted in an excess of S. The I-V results can be interpreted as an over etching of the CdS surface which produced a S rich layer on the surface. Subsequent metal contact evaporation would then lead to the formation of a S rich interlayer.

Etch 2	n	ϕ_b
(s)		(eV)
120	2.2	0.81
90	1.82	0.84
30	1.39	0.87

Table 6.2 Effect on diode quality factor, n and Schottky barrier height, ϕ_b of etch time on Au/n-CdS treated with etch 2 prior to contact formation.

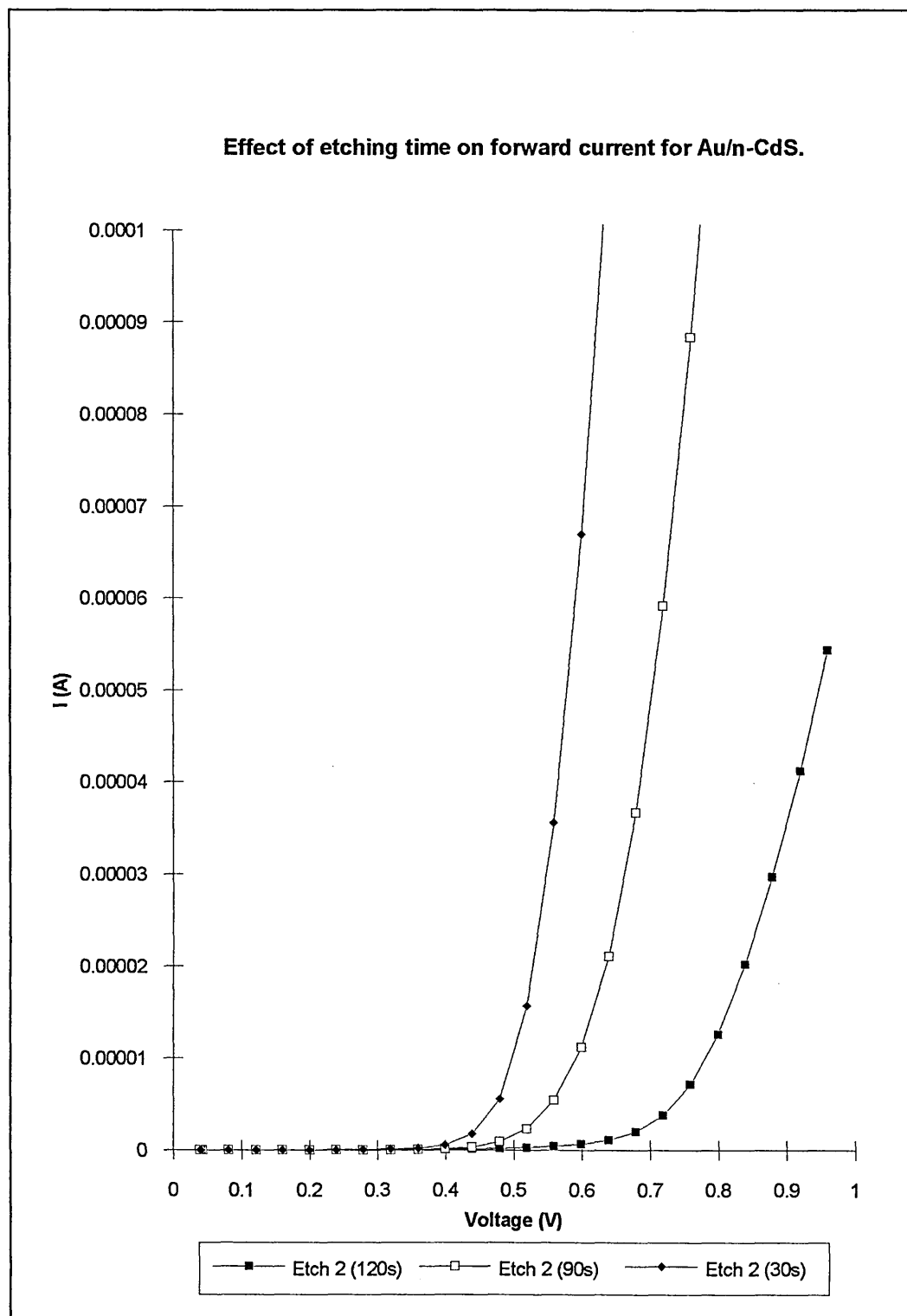


Figure 6.11 The effect of etching time for etch 2 (chromic acid) on the forward current of Au/n-CdS.

6.3.2 Ideal contacts.

Once correct etching procedures had been established, ideal ($n < 1.05$) Au/n-CdS Schottky barriers could be routinely produced. The most effective method of etching was found to be etch 5 (etch 2, 30 s followed by etch 7, 2 - 4 min) which was been shown to produce stoichiometric surfaces with a reduced oxide content (Sec 5.2). Two Schottky barriers were repeatedly observed for the Au/n-CdS system of, $\phi_b = 0.86 \pm 0.02$ eV and $\phi_b = 0.96 \pm 0.02$ eV. Although these two barrier heights are of very similar magnitude they are quite independent as shown in figure 6.12. The reverse current of characteristic (b) was of the same order as the background noise in the system and so was not included within this plot. These two Schottky barrier heights were regularly observed on surfaces prepared with etch 5, contacts prepared in this manner were generally very ideal ($n < 1.1$) as demonstrated in figure 6.13. The Missous and Rhoderick plot shows a re-plot of the data of figure 6.12 (a) which is linear from -1V to 0.0.4V for this particular device. Generally contacts formed by this method were uniform and of good quality, the timing of the second stage of the etch could in fact be varied between 2 and 4 min with little effect on device quality.

6.3.2.1 Summary of ideal contacts.

The lower barrier of $\phi_b = 0.86 \pm 0.02$ eV is in good agreement with values from the literature. Lepley and Ravelet (1976) and Spitzer and Mead(1963) among others have reported Au/n-CdS barriers of $\phi_b \approx 0.80$ eV. No other workers have to date reported the formation of several discrete Schottky barriers. There are many similarities between the results for CdS and those for CdTe particularly the formation of discrete barriers. As with CdTe adjacent contacts on the same sample could produce one of these two barriers.

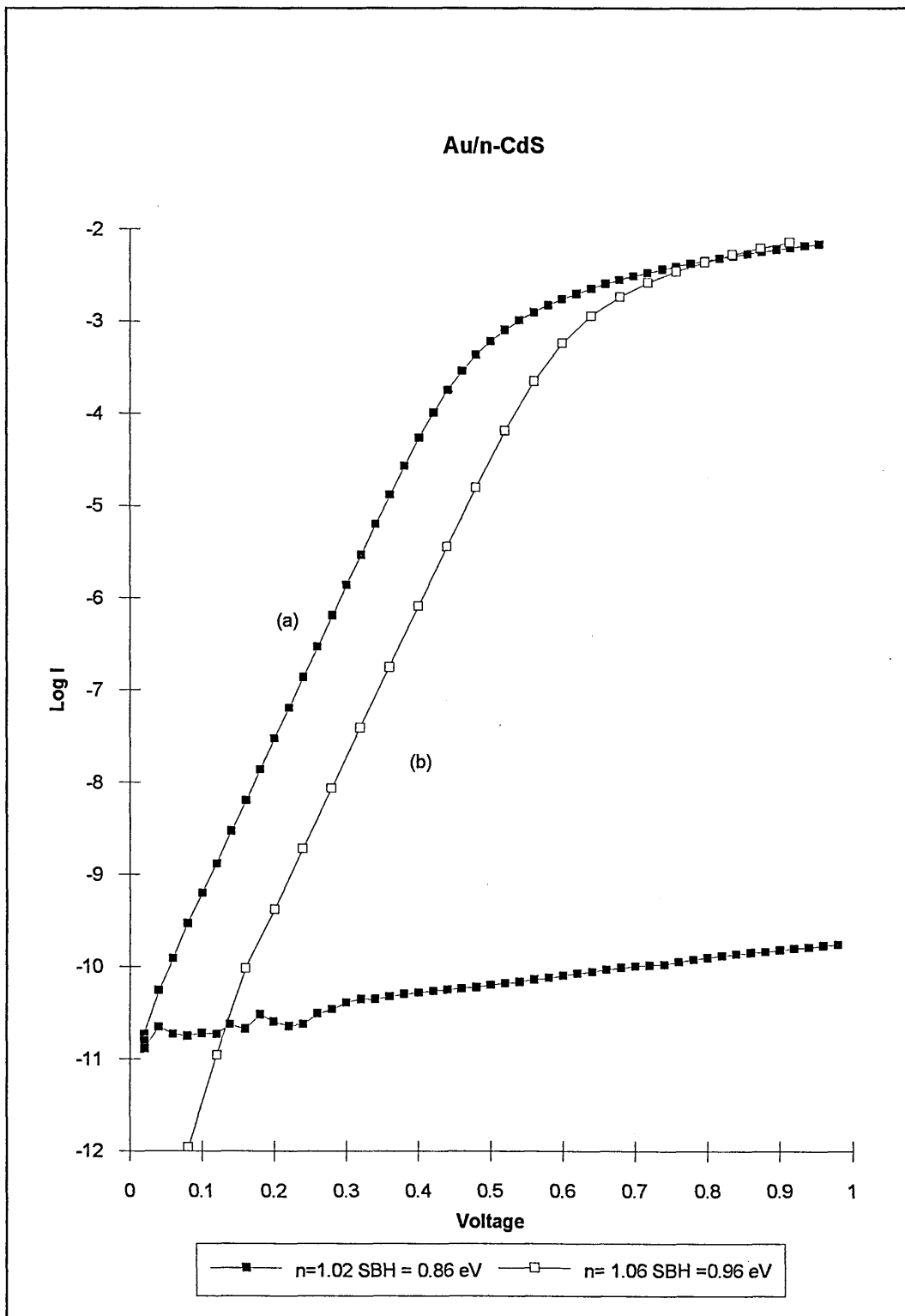


Figure 6.12 Ideal Au/n-CdS devices formed on CdS surfaces etched in etch 5 (etch 2, 30 followed by etch 7, 4 min).

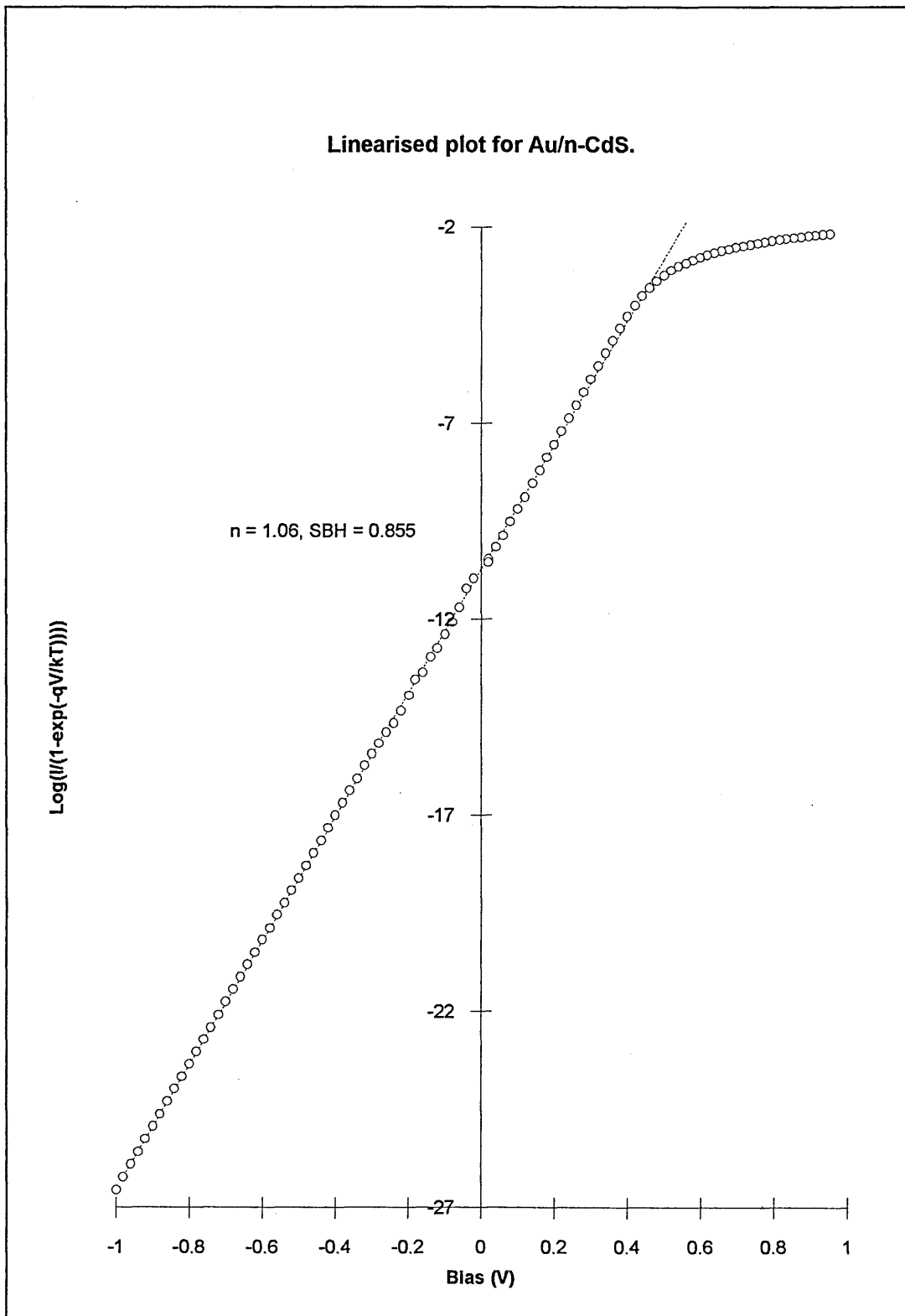


Figure 6.13 Missous and Rhoderick plot for diode (a) of figure 6.12, Au/n-CdS.

6.3.3 C-V characteristics.

Typical C-V plots for contacts defined as "non-ideal" figure 6.14 and "ideal" figure 6.15 are shown below. Figure 6.14 is in fact typical of characteristics realised for contacts which by the I-V technique were classified as non-ideal. The capacitance was generally unstable as the reverse bias was reduced; in fact no stable measurements could be made at forward biases. Ideal contacts displayed linear C-V characteristics as shown in table 6.2. There was generally good agreement between $\phi_{b(I-V)}$ and $\phi_{b(C-V)}$ although as observed for Au/n-CdTe contacts, $\phi_{b(C-V)}$ was always in excess of $\phi_{b(I-V)}$. Similar observations were made by Goodman (1964) for metal contacts evaporated onto CdS. The carrier concentrations determined for both ideal and non-ideal contacts were in reasonable agreement with the specification of the material ($\approx N_d = 5 \times 10^{16} \text{ cm}^{-3}$). These results indicate that there is a uniform doping density within the CdS wafer employed in these studies. All C-V characteristics are probably influenced by interfacial layers but there is less discrepancy between results from I-V and C-V measurements for CdS than CdTe.

Figure	Carrier conc	$\phi_{b(C-V)}$	Quality factor	$\phi_{b(I-V)}$
	$N_d \text{ cm}^{-3}$	(eV)	n (I-V)	(eV)
6.14	4.6×10^{16}	1.70	1.99	0.77
6.15(a)	3.6×10^{16}	1.07	1.02	0.85
6.15(b)	2.8×10^{16}	1.15	1.03	0.95

Table 6.2 A comparison of Schottky barrier heights determined by both I-V and C-V techniques for "ideal" and "non-ideal" Au/n-CdS contacts.

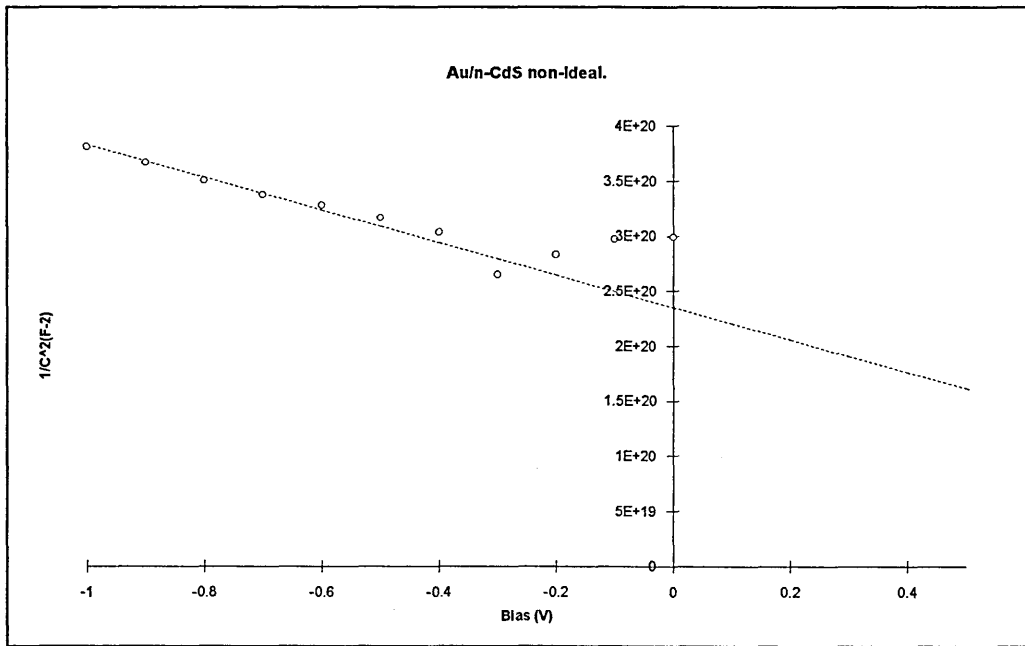


Figure 6.14. Typical $1/C^2$ v V plot for "non-ideal" Au/n-CdS contacts. (I-V gave $n = 1.99$
 $\phi_b = 0.76$ eV)

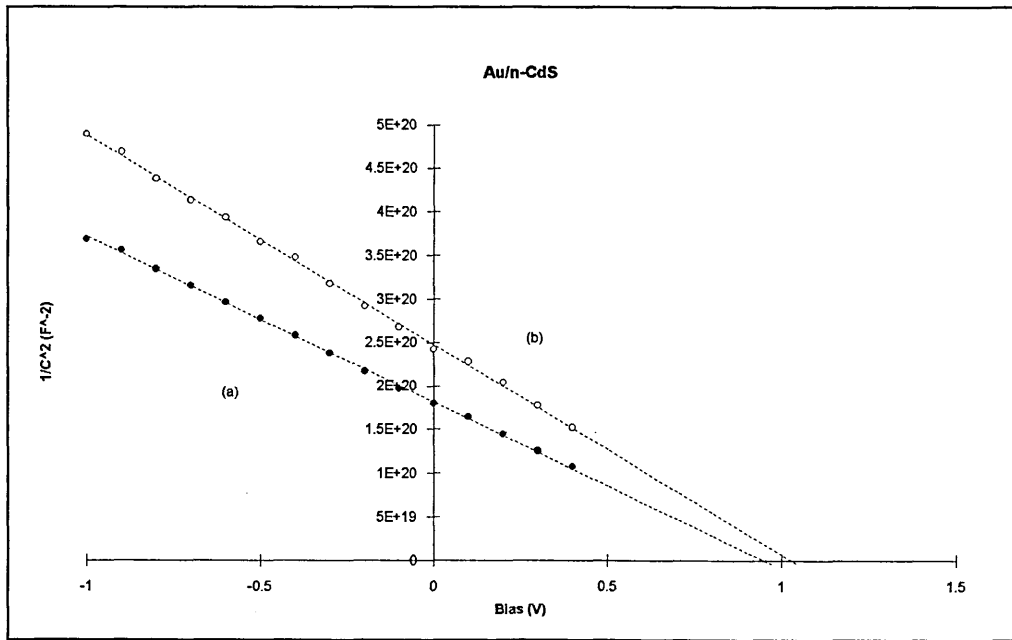


Figure 6.15. $1/C^2$ v V plot for "ideal" Au/n-CdS contacts. (I-V gave (a) $n = 1.02$, $\phi_b = 0.85 \pm 0.02$ eV, (b) $n = 1.03$, $\phi_b = 0.95 \pm 0.02$ eV).

6.3.4 Ageing of Au/n-CdS.

Several Au/n-CdS devices were selected for ageing experiments, which, as with CdTe consisted of monitoring the I-V characteristic over several months. All samples were stored in ambient laboratory conditions in the dark. Characteristics were monitored initially every few days and then over several weekly intervals for approximately one year. Figure 6.16 shows a typical characteristic of a non-ideal Au/n-CdS contact. After several months the current had increased, leading to an increase in n and a decrease in the measured barrier height, as shown in table 6.3. Figure 6.17 shows an I-V characteristic typical of devices exhibiting the lower barrier height of $\phi_b = 0.85 \pm 0.02$ eV. As shown in table 6.3 the initial characteristic was ideal, with $n = 1.03$. After a short period the barrier height "jumped" to $\phi_b = 0.93 \pm 0.02$ eV, which is identical to the higher barrier observed for these surfaces. Repeated monitoring of this sample indicated that the increase in barrier height was a sudden increase and not a slow gradual increase. This is highlighted by the maintenance of the near ideal n value of this device. Similar behaviour was monitored for the higher barrier observed for these surfaces as shown in figure 6.18. A sample was selected which initially had $n = 1.05$, $\phi_b = 0.95 \pm 0.02$ eV. This contact exhibited a similar "jump" in the barrier height to $\phi_b = 1.01 \pm 0.02$ eV but there was a slight degradation in the quality factor ($n = 1.21$). This type of ageing can be termed stage (1) ageing. After several months all the ideal contacts degraded in much the same way. There was an overall increase in the current resulting in an increase in n and a decrease in the barrier height. This type of ageing is clearly distinct from the stage (1) ageing and is termed stage (2) ageing. Stage (2) ageing appears to be common to both ideal and non-ideal contacts and consists of a gradual increase in I_{rev} accompanied by a reduction in the rectification of the device. Such ageing may possibly account for the slightly higher quality factor observed in figure 6.18.

Figure	Quality factor, n	Barrier height	Days
6.16	1.32	0.80	1
"	2.09	0.59	10 months
6.17	1.03	0.85	1
"	1.07	0.93	14 to 21
"	1.21	0.61	>4 months
6.18	1.05	0.95	1
"	1.19	1.01	14 to 21
"	1.20	0.62	> 4 months

Table 6.3. Ageing of Au/n-CdS, results of I-V characterisation of ideal and non - ideal contacts over several months.

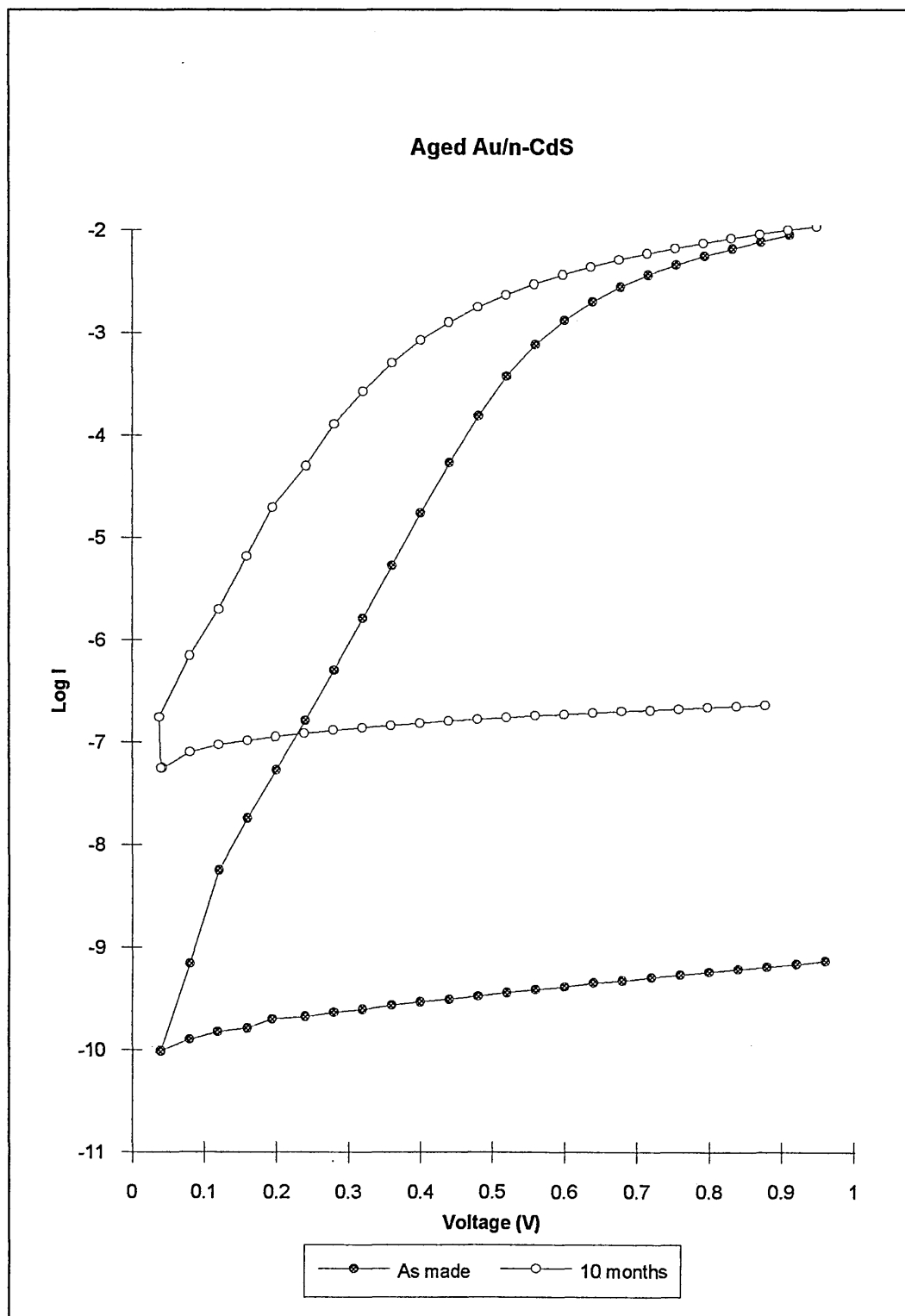


Figure 6.16 The ageing of a non-ideal Au/n-CdS contact, originally $n = 1.32$ $\phi_b = 0.8 \pm 0.02$ eV, after 10 months $n = 2.09$ and $\phi_b = 0.59 \pm 0.02$ eV

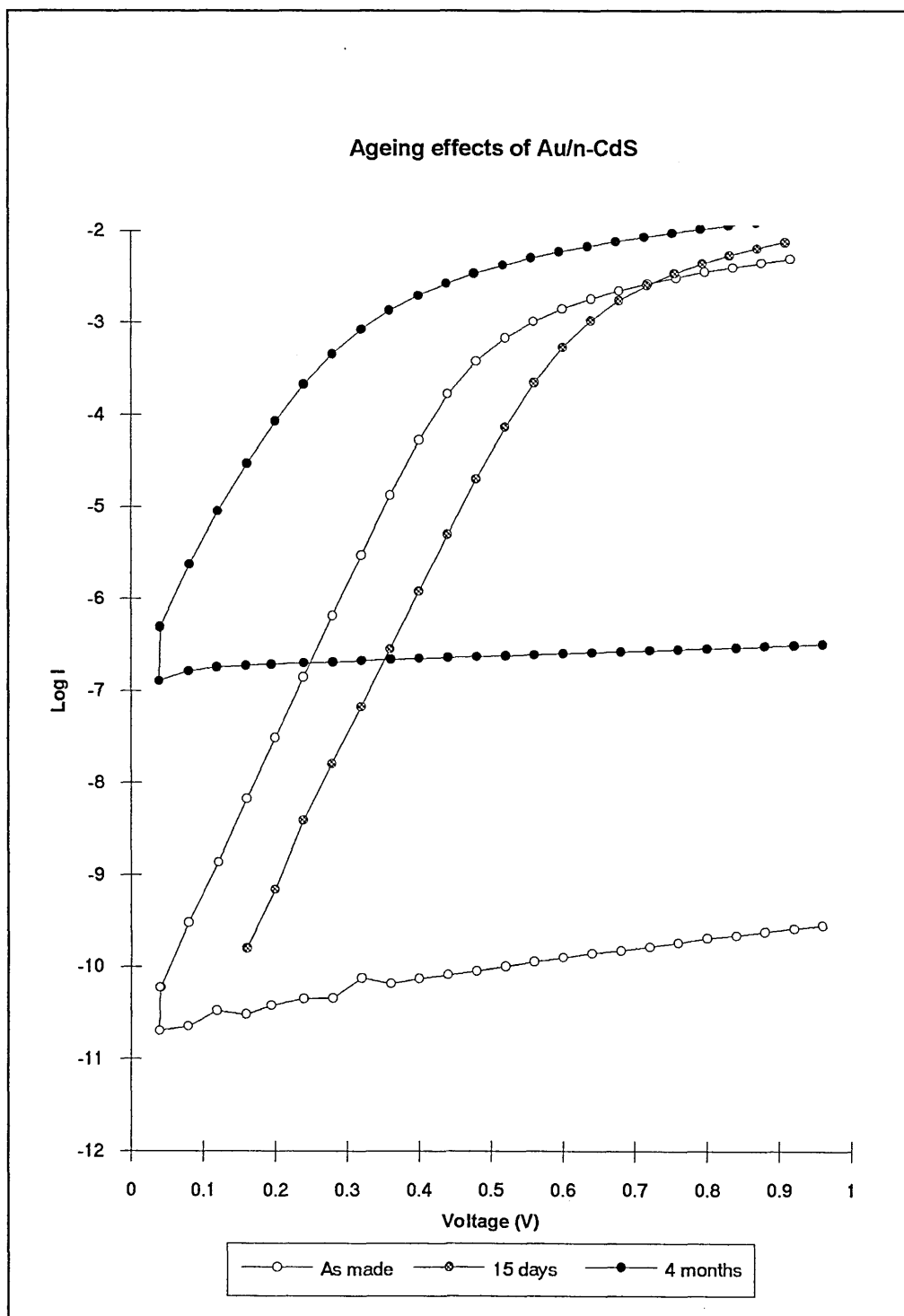


Figure 6.17. Ageing effects of an ideal Au/n-CdS diode, originally $n = 1.03$ $\phi_b = 0.85 \pm 0.02$ eV, after several days $n = 1.07$ $\phi_b = 0.93 \pm 0.02$ eV and after several months $n = 1.21$ $\phi_b = 0.61 \pm 0.02$ eV.

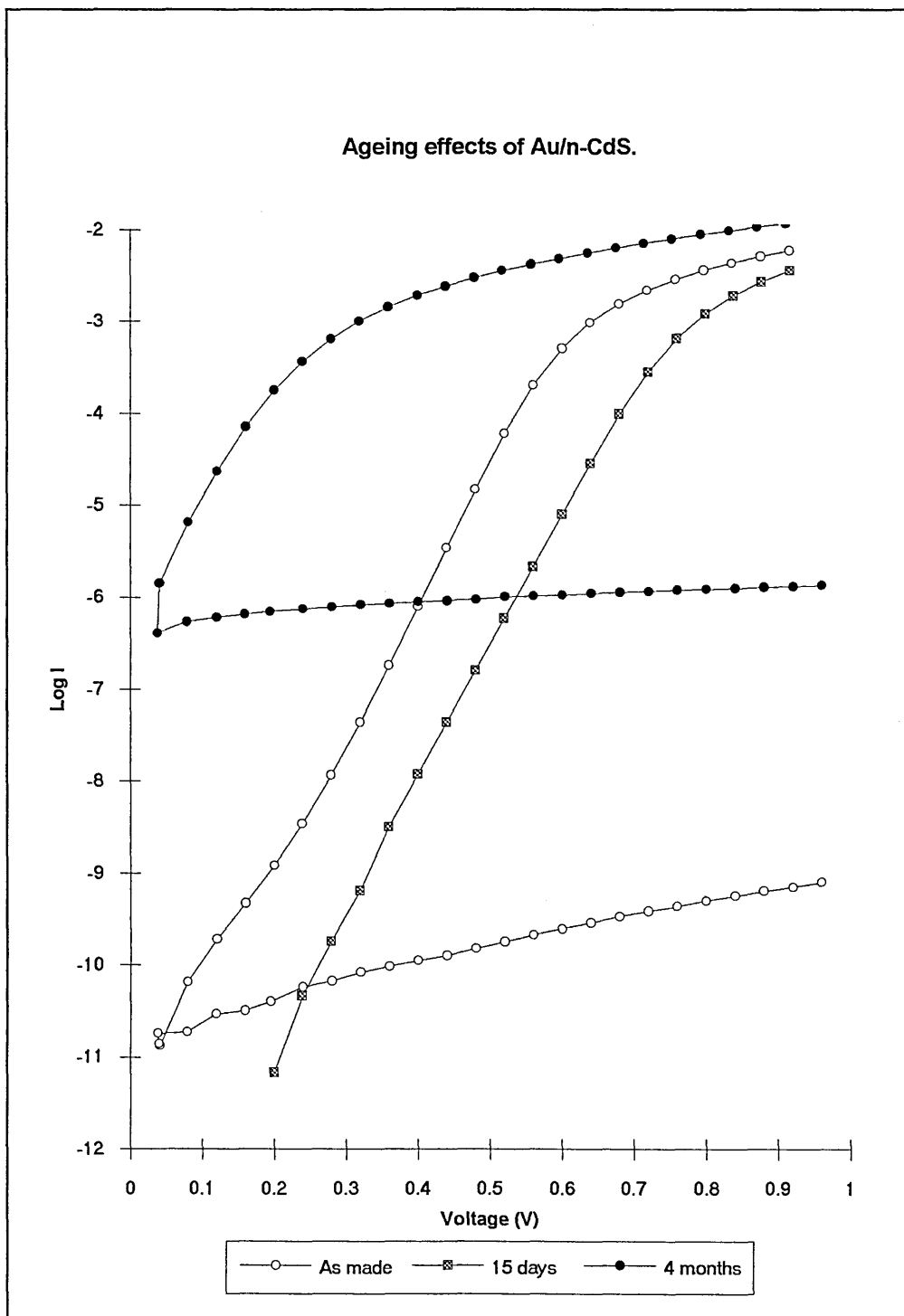


Figure 6.18 A second contact shows similar ageing in this case $n = 1.05$, $\phi_b = 0.95 \pm 0.02$ eV. After several days $n = 1.19$, $\phi_b = 1.01 \pm 0.02$ eV and after several months $n = 1.20$, $\phi_b = 0.62 \pm 0.02$ eV.

6.4. Metal contacts to ZnSe.

XPS characterisation of poly-ZnSe has shown that if a suitable etching time was used etch 7 produced a stoichiometric surface with a reduced oxide content. This etch was used predominantly to etch MBE prepared n-ZnSe on n⁺-GaAs substrates. The characteristics of three metals Au, Ag and Sb were investigated initially by the I-V technique. The very low currents in the devices as a whole meant that only the high forward currents of many of the contacts could be monitored. Similarly metal/n-ZnSe devices exhibited very small capacitances which meant conventional C-V plots were unobtainable. Several devices were selected for both DLTS and BEEM characterisation.

6.4.1. Non-ideal contacts.

Au contacts vacuum-evaporated onto the chemically etched (etch 7) (100) surface repeatedly gave quite ideal characteristics (usually $n \ll 2$) unlike both CdTe and CdS. This may have been the result of using directly etch 7 which produced surfaces ideal for contact formation. The nature of the I-V characteristics was such that it was not possible to obtain the reverse characteristics for any device on ZnSe which of course reduced the information obtainable for any specific device.

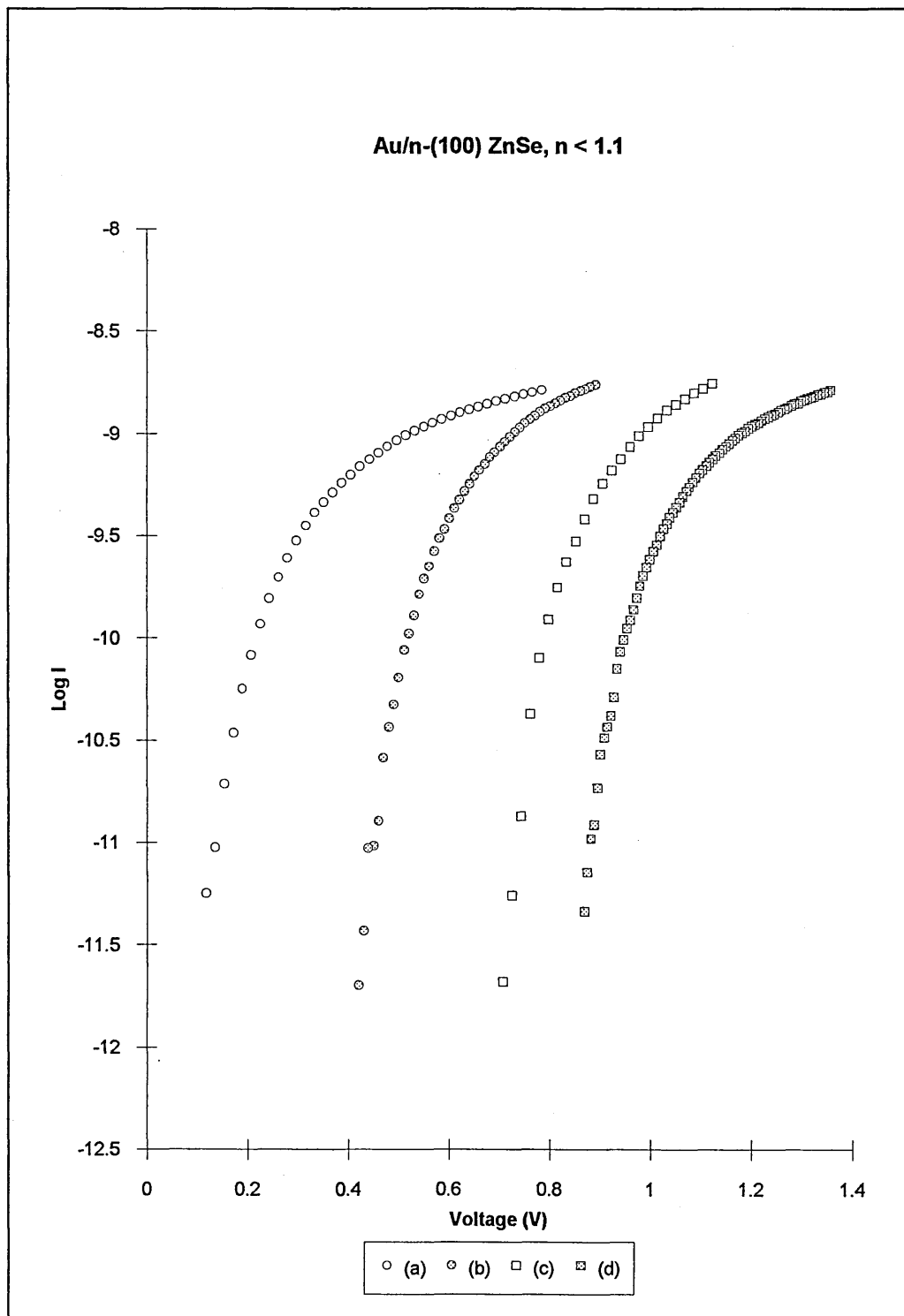


Figure 6.19 Ideal characteristics ($n < 1.1$) for Au/n-(100)ZnSe devices. (a) $\phi_b = 0.9 \pm 0.04$ eV, (b) $\phi_b = 1.2 \pm 0.04$ eV, (c) $\phi_b = 1.45 \pm 0.04$ eV and (d) $\phi_b = 1.65 \pm 0.04$ eV.

6.4.2. Ideal contacts, Au/n-ZnSe.

As mentioned above the majority of devices produced by first etching the surface in etch 7 (2-4 mins) were reasonably ideal with many contacts being very ideal ($n < 1.1$). As with CdTe and CdS several discrete Schottky barriers were repeatedly observed for the as-made contacts. Typical I-V characteristics of the four barriers are shown in figure 6.19 for the Au/n-ZnSe system. Analysis of such characteristics gave barrier heights, $\phi_b = 0.9, 1.2, 1.45$ and 1.65 ± 0.04 eV. In some instances two or three different barriers were observed on the same sample with, for example, one device having $\phi_b = 0.9 \pm 0.04$ eV and an adjacent device having $\phi_b = 1.2 \pm 0.04$ eV.

The highest barrier observed here for Au/n-ZnSe of $\phi_b = 1.65 \pm 0.04$ eV was reported previously by Tarricone for Br methanol etched surfaces. Vos *et al* (1988) among others have reported $\phi_b = 1.47$ eV for Au/n-ZnSe formed under UHV conditions. This value is in excellent agreement with the second highest barrier reported here. Vos *et al* (1988) also reported $\phi_b = 0.95$ and 1.15 eV for Au/n-ZnSe with Al interlayers of 10 and 1.5 \AA respectively which are in reasonable agreement with the lower two barriers. The barrier heights observed here have to some extent all been independently observed albeit for different surface preparation techniques. One interesting point to note is that unlike CdTe where there appeared to be some relationship between Schottky barrier height and the etchant employed, here all surfaces were prepared with the same etchant. Often one sample would have several different barriers on adjacent devices.

6.4.2.1 Ageing of Au/n-ZnSe.

The stability was monitored over a period of several months. Several different ageing mechanisms were apparent from the I-V characteristics. Typical characteristics monitored

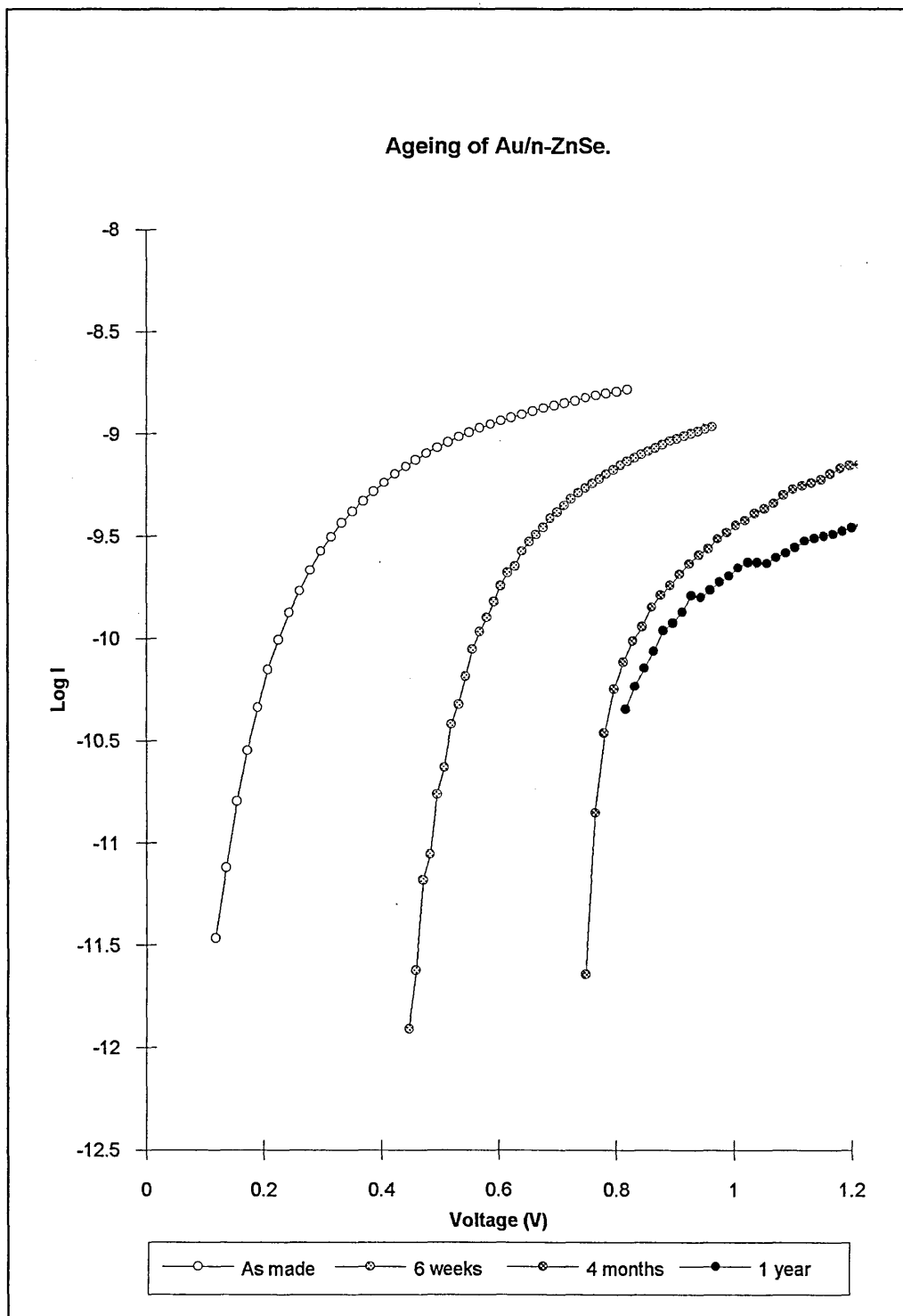


Figure 6.20 The ageing of a typical ideal Au/n-ZnSe diode. Initially this device had $\phi_b = 0.9$ eV. With time this barrier height "jumped" to $\phi_b = 1.2 \pm 0.04$ eV and $\phi_b = 1.45 \pm 0.04$ eV, finally the device started to age in the more conventional sense.

over several months are depicted in figure 6.20. This particular device is shown because it initially had $\phi_b = 0.9$ eV, the lowest barrier height measured. Monitoring several devices showed that some ideal Au/n-ZnSe contacts displayed similar ageing properties as observed for Au/n-CdS devices. In figure 6.20 the barrier height "jumped" through all four Schottky barrier heights so far observed for Au/n-ZnSe, namely $\phi_b = 0.9$ then 1.2 and then finally 1.45 ± 0.04 eV while maintaining the quality factor, $n \leq 1.1$. Similar ageing was observed for other devices. A device with $\phi_b = 1.2 \pm 0.04$ eV would perhaps "jump" to $\phi_b = 1.45 \pm 0.04$ eV for example. The relationship between sample preparation and contact ageing was obviously complicated as devices on the same sample were observed to age differently. Other devices would remain at the same barrier height over a period of months before the forward current started to decrease resulting in an increase in n and a subsequent reduction in ϕ_b , as in fact eventually happened in figure 6.20 after 1 year.

6.4.3 Ideal contacts Ag/n-ZnSe.

Again etch 7 was employed to etch the ZnSe surface and Ag contacts were evaporated and characterised by the I-V technique. As with Au/n-ZnSe more than one discrete Schottky barrier height was observed. Figure 6.21 shows two typical ideal characteristics for Ag/n-ZnSe devices, $n < 1.1$ for both characteristics and $\phi_b = 1.2$ and 1.45 ± 0.04 eV respectively. No relationship between barrier height and surface preparation could be established as only one etchant was employed (etch 7). As with Au, adjacent contacts on the same sample displayed different barrier heights.

Both Nedeoglo *et al* (1977) and Tyagi and Arora (1976) have reported $\phi_b = 1.2$ eV for Ag/n-ZnSe contacts formed to ZnSe surfaces etched in 1% Br methanol solution followed by a wash in hot aqueous NaOH solution. XPS analysis showed that this type of etch

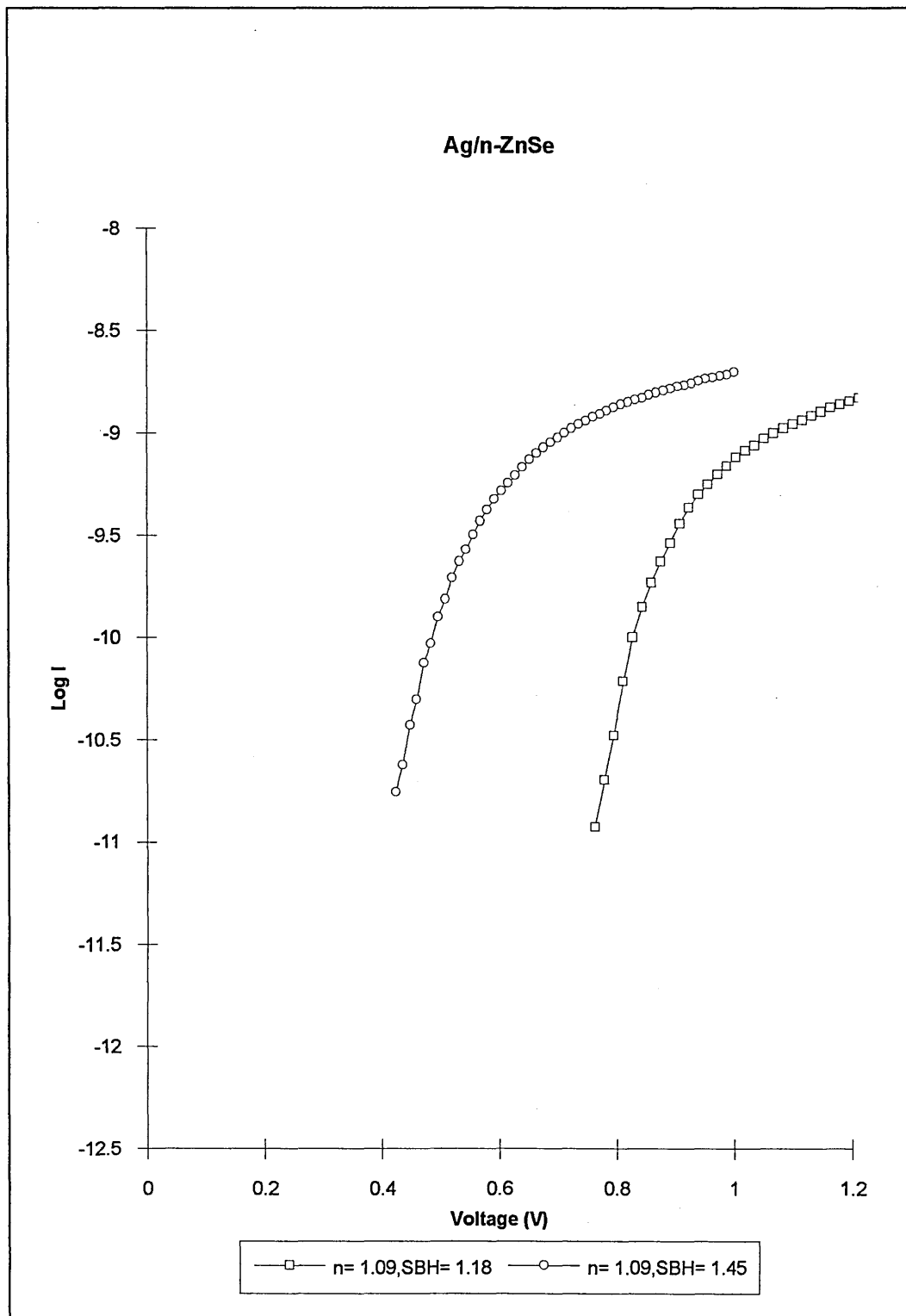


Figure 6.21 Typical characteristics of Ag/n-ZnSe devices prepared by etching ZnSe in Etch 7 for 4 min prior to contact formation.

would produce a very similar surface as etch 7. No group has reported the second barrier of $\phi_b = 1.45 \pm 0.04$ eV.

6.4.3.1 Ageing of Ag/n-ZnSe.

Several devices were selected and monitored over several months for up to one year. A common ageing mechanism was observed for all devices independent of whether they were originally ideal ($n < 1.1$) or non-ideal ($1.4 < n < 2.0$). The forward current was in all cases seen to decrease, consistent with the formation of a more resistive layer at the interface. Such a typical characteristic is shown in figure 6.22 for a Ag/n-ZnSe diode over a period of one year. The three stages of ageing of the device are depicted by the characteristics observed after one month and one year. Unlike Au/n-ZnSe the ageing process was one of slow progress from the as-made case to that after one year.

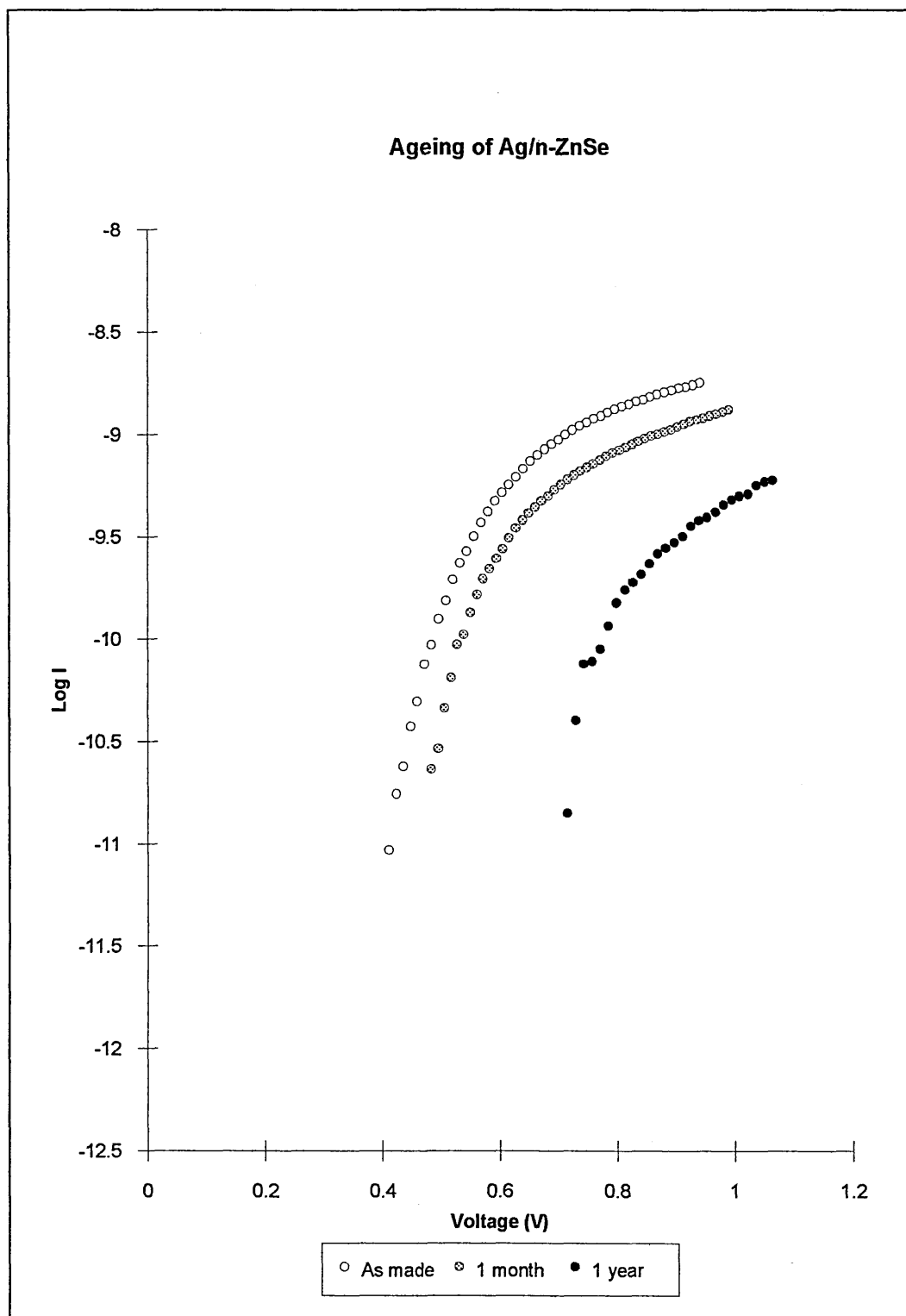


Figure 6.22 Ageing effects for Ag/n-ZnSe showing a gradual ageing of the contact becoming more resistive over one year.

6.4.4 Ideal contacts, Sb/n-ZnSe.

Ideal Schottky barriers were formed with Sb on ZnSe again etched with etch 7. As with Au and Ag a number of discrete barriers were observed. Figure 6.23 summarises the electrical characteristics produced by representative discrete Schottky barriers; all contacts have $n < 1.1$. The barrier heights observed were found to be, $\phi_b = 1.45, 1.65, 1.80$ and 2.10 ± 0.04 eV. These values encompass the highest Schottky barrier yet reported for ZnSe of 2.1 ± 0.04 eV. As with Au and Ag adjacent contacts on the same sample displayed quite different electrical behaviour; often a number of different barrier heights were observed. It is difficult to draw any relationship between surface preparation and Schottky barrier height as all devices were prepared with the same surface treatment (etch 7). Only Tyagi and Arora (1975) have previously reported results for Sb/n-ZnSe contacts. They found $\phi_b = 1.36$ eV for Sb contacts formed to chemically etched (Br methanol followed by NaOH solution) ZnSe.

6.4.4.1 Ageing of Sb/n-ZnSe.

The effect of time on the electrical properties of Sb/n-ZnSe contacts was monitored over a period of several months. Samples were stored under ambient laboratory conditions in the dark. The I-V characteristic of a typical sample monitored over 1 year is shown in figure 6.24. It is evident from this plot that the ageing of the contact follows that of Ag/n-ZnSe devices. The forward current is characterised by a gradual increase in series resistance of the device as a whole and a subsequent reduction in the forward current.

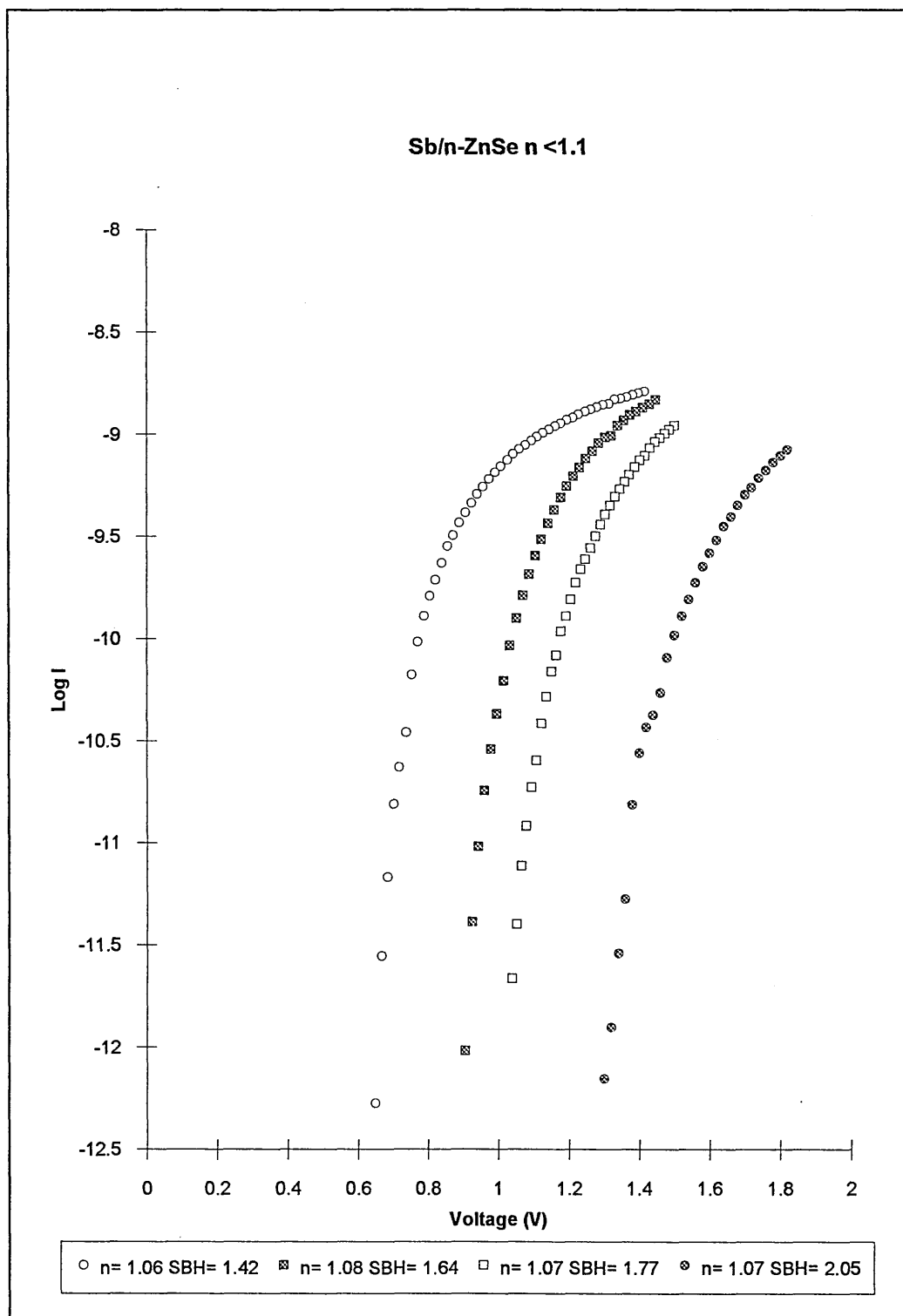


Figure 6.23 Ideal Sb/n-ZnSe devices which show the formation of discrete Schottky barriers for this system.

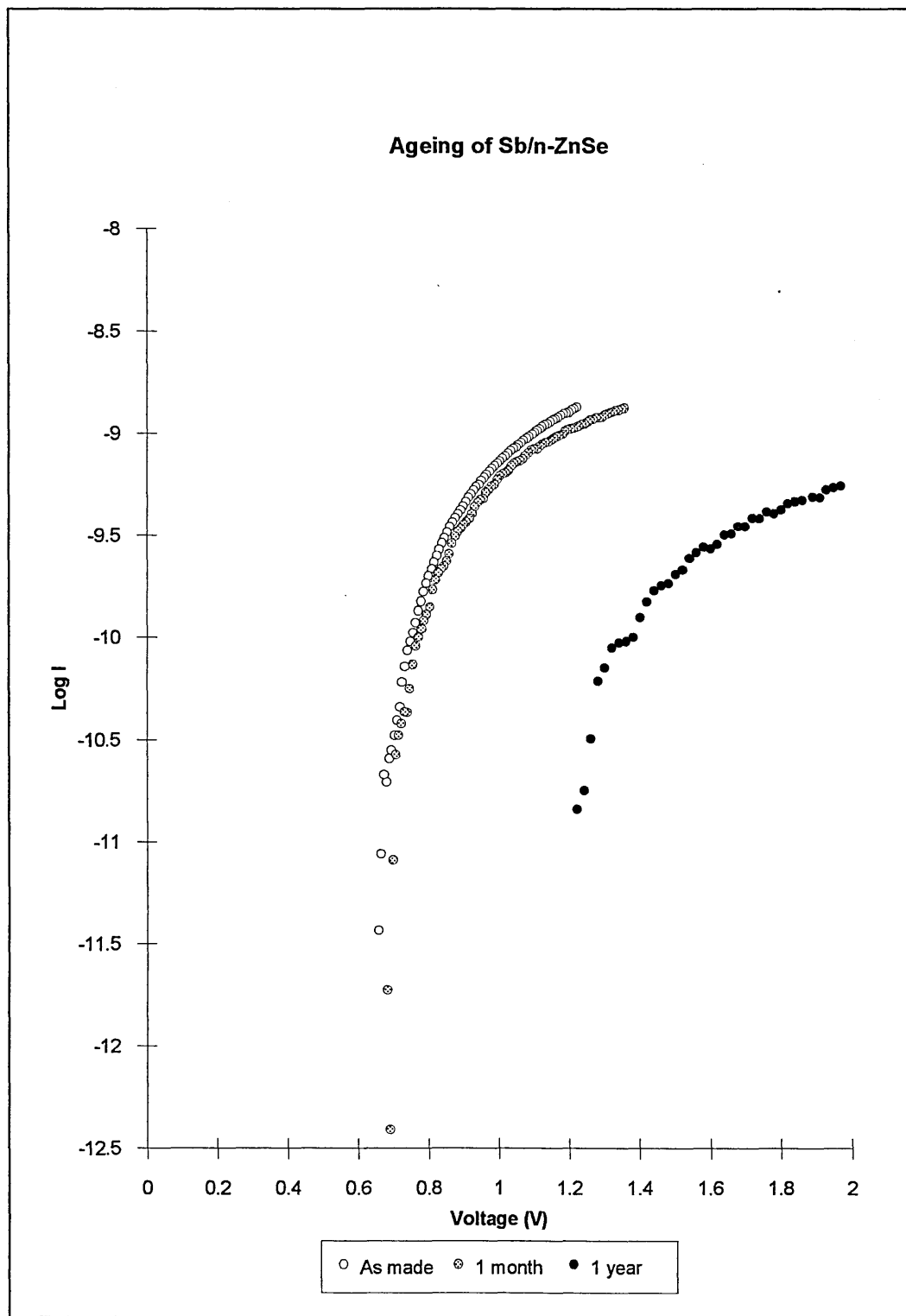


Figure 6.24 Typical ageing effects of Sb/n-ZnSe devices.

6.4.5 Summary of electrical measurements on metal/n-ZnSe.

The most prominent feature displayed by all the I-V characteristics, independent of the metal used is the forward current saturation in nA range. This saturation is a fundamental point in understanding the I-V characteristics and can be explained by considering the whole metal/n-ZnSe/n⁺GaAs device structure. As discussed earlier [Sec 3.3.4] Colak *et al* (1989), Marshall *et al* (1989) and Ayyar *et al* (1990) have considered this device structure by incorporating the Schottky barrier, ϕ_b at the metal semiconductor interface and the heterojunction barrier, ϕ_{HJ} at the ZnSe/GaAs interface as two back to back diodes. The energy band diagram calculated by Colak *et al* (1989) is shown in figure 6.25. Under negative bias, ϕ_b will be reverse biased and ϕ_{HJ} forward biased therefore the reverse current of the Schottky barrier will be very small. Under forward bias the number of electrons entering the metal-semiconductor region will be limited by the reverse current of ϕ_{HJ} . In the model of Colak *et al* (1989), under forward bias the depletion width of the

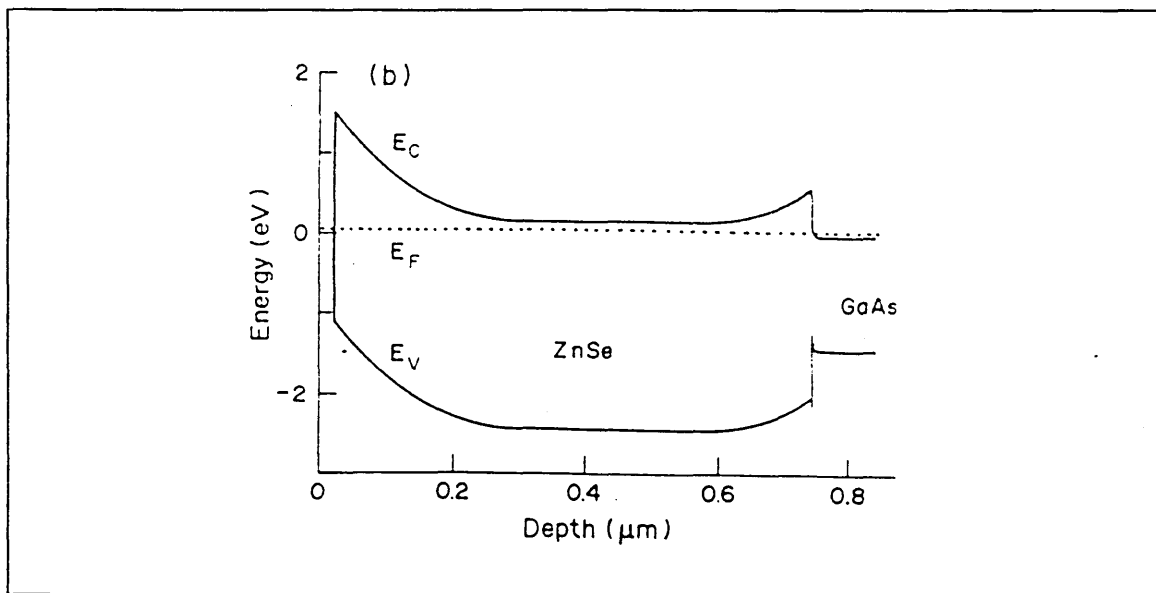


Figure 6.25. Energy band diagram for Au/n-ZnSe/n⁺GaAs, after Colak *et al* (1989).

Schottky barrier W_{SB} decreases as the depletion width of the heterojunction, W_{HJ} increases. At some applied forward bias, V_{min} , $W_{SB} \approx W_{HJ}$ and therefore $\phi_{HJ} = \phi_b - V_{min}$. The actual value of V_{min} was determined from C-V plots, V_{min} being equal to the point of peak capacitance in the forward biased device. Colak *et al* (1989) determined $\phi_{HJ} \approx 0.5$ eV and the resultant forward current saturated at $\approx 10^{-5}$ A. More recently Heuken *et al* (1993) reported $\phi_{HJ} \approx 0.1 - 0.59$ eV and the current saturating at $\approx 10^{-3}$ A. Wang *et al* (1995) have reported similar results for $ZnS_{0.07}Se_{0.93}$ grown on n^+GaAs , in this case $\phi_{HJ} \approx 0.35$ eV on average and the forward current was limited to 10^{-6} A. What is evident is that the magnitude of ϕ_{HJ} seems to vary from sample to sample; in fact this was implicitly stated by Colak *et al* (1989). The heterojunction barrier in this case seems to be of sufficient magnitude to reduce the forward current to the nA range observed. Unfortunately the nA range of the forward current meant it was impossible to quantify this barrier as the capacitance of the devices was below the range of the meter.

6.4.6 Deep level transient spectroscopy of Au/n-ZnSe.

One Au/n-ZnSe device was selected for DLTS. This particular device had been previously characterised by I-V to reveal $n = 1.05$ and $\phi_b = 0.88$ eV. A similar experimental technique was followed as for Au/n-CdTe devices [Sec 6.2.5]. The lower barrier device was in fact the only device which produced a significant capacitance signal on the Boonton meter allowing DLTS to take place. An applied bias of -2V was necessary to achieve a good signal to noise ratio. The filling pulse was 1.25V for 5×10^{-3} s. Figure 6.26 shows the activation energy plot of the device; two electron traps of activation energy $\Delta E = 0.35$ and 0.83 eV were observed. As with Au/n-CdTe devices neither the electron capture cross-

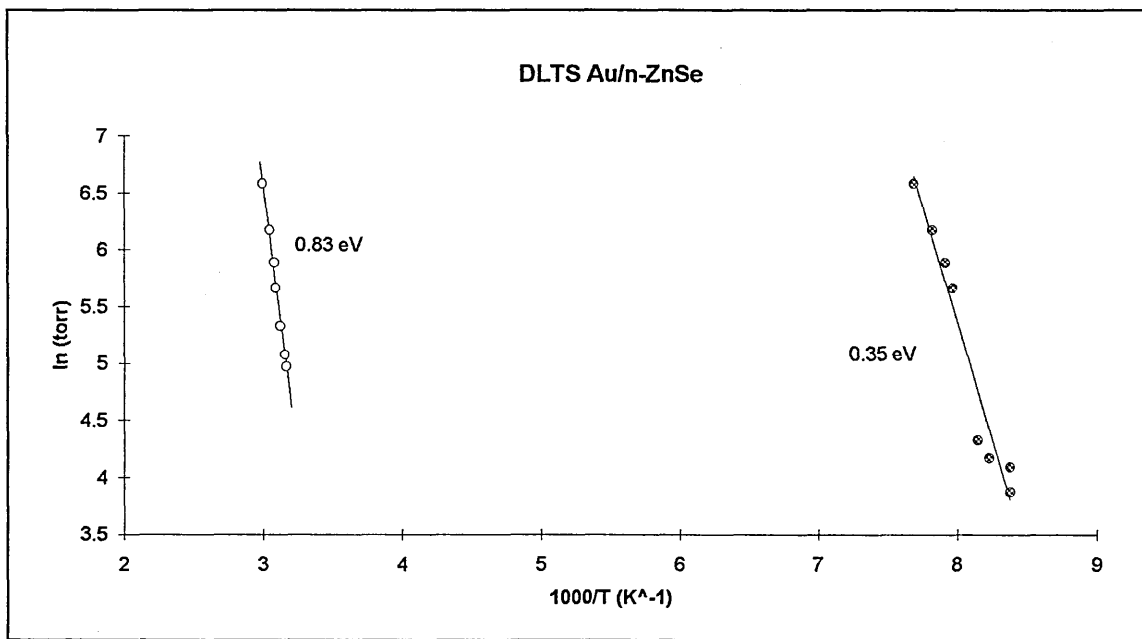


Figure 6.26. Activation energy plot Au/n-ZnSe contact which had $n = 1.05$ and $\phi = 0.88$ eV. Temperature range 100K to 360K.

section nor the trap concentrations of this device were quantified. The trap at $E_c - 0.83$ eV had a higher concentration than the trap at $E_c - 0.35$ eV in that the area under the $S(T)$ versus T plot was much greater, Lang (1974). As was summarised earlier [Sec 3.4.4], a number of deep levels have previously been reported for ZnSe. A number of groups have reported a level with an activation energy close to $\Delta E = 0.35$ eV, (Bessomi and Wessels (1980(b)) $\Delta E = 0.35$ eV, Shirakawa and Kukimoto (1980) $\Delta E = 0.33$ eV, Verity *et al* (1982) $\Delta E = 0.34$ eV and Venkatsen *et al* (1989) $\Delta E = 0.34$ eV). The second deep level observed here is less commonly reported; however Bessomi and Wessels (1980(b)) have reported an electron trap with an activation energy of $\Delta E = 0.86$ eV.

6.4.7 Ballistic electron emission microscopy studies of Au/n-ZnSe.

Au/n-ZnSe devices were investigated by ballistic electron emission microscopy (BEEM). Samples were fabricated in the same way as all the other ideal Au/n-ZnSe devices reported but the thickness of the Au overlayer was kept to a maximum of 15 nm. One contact on the sample was investigated by I-V to check the quality of the devices and yielded $n = 1.05$, $\phi_b = 1.67$ eV. Initially BEEM spectra were monitored, the sample as a whole displaying very low ballistic current. A tunnelling current (I_T) of 20 nA was necessary to improve the signal to noise ratio. Some areas of the same contact produced no measurable ballistic current. Moving the tip to a different position would then produce a measurable characteristic. Typical BEEM spectra from these regions of ballistic emission are shown in figures 6.27 and 6.28. These two spectra are representative of those obtained over the sample; the Schottky barrier height was determined by fitting the data to the Bell and Kaiser model (Bell and Kaiser (1988)). Figure 6.27 gives $\phi_b = 1.78$, R (attenuation factor due to scattering) = 0.0009 eV⁻¹ and figure 6.28 gives $\phi_b = 2.1$ eV, $R = 0.00078$ eV⁻¹. Both spectra show the saturation of the ballistic current at high voltages. The patchy nature of the ballistic current meant that an analysis of the spatial dependence of the Schottky barrier height as determined by Fowell *et al* (1990) [Sec 3.3.2] was not possible. A large number of BEEM spectra were however taken over the sample and are summarised in figure 6.29. BEEM images were taken by scanning the tip of the STM over the sample. Figure 6.30 shows a typical image obtained over an area 40 x 40 nm². On the left of figure 6.30 is a topographic image of the surface; the grey scale indicates the roughness of the Au layer (15nm from white to black). On the right of the figure is the BEEM image; the grey scale indicates the contrast in ballistic current across this region (25 pA from white to black). The region of high ballistic current clearly corresponds to one of the Au grains in the topographic image. Such regions were typical of the Au/n-ZnSe surface. Within each

region the Schottky barrier height was found to be constant, only the scattering parameter R was found to vary.

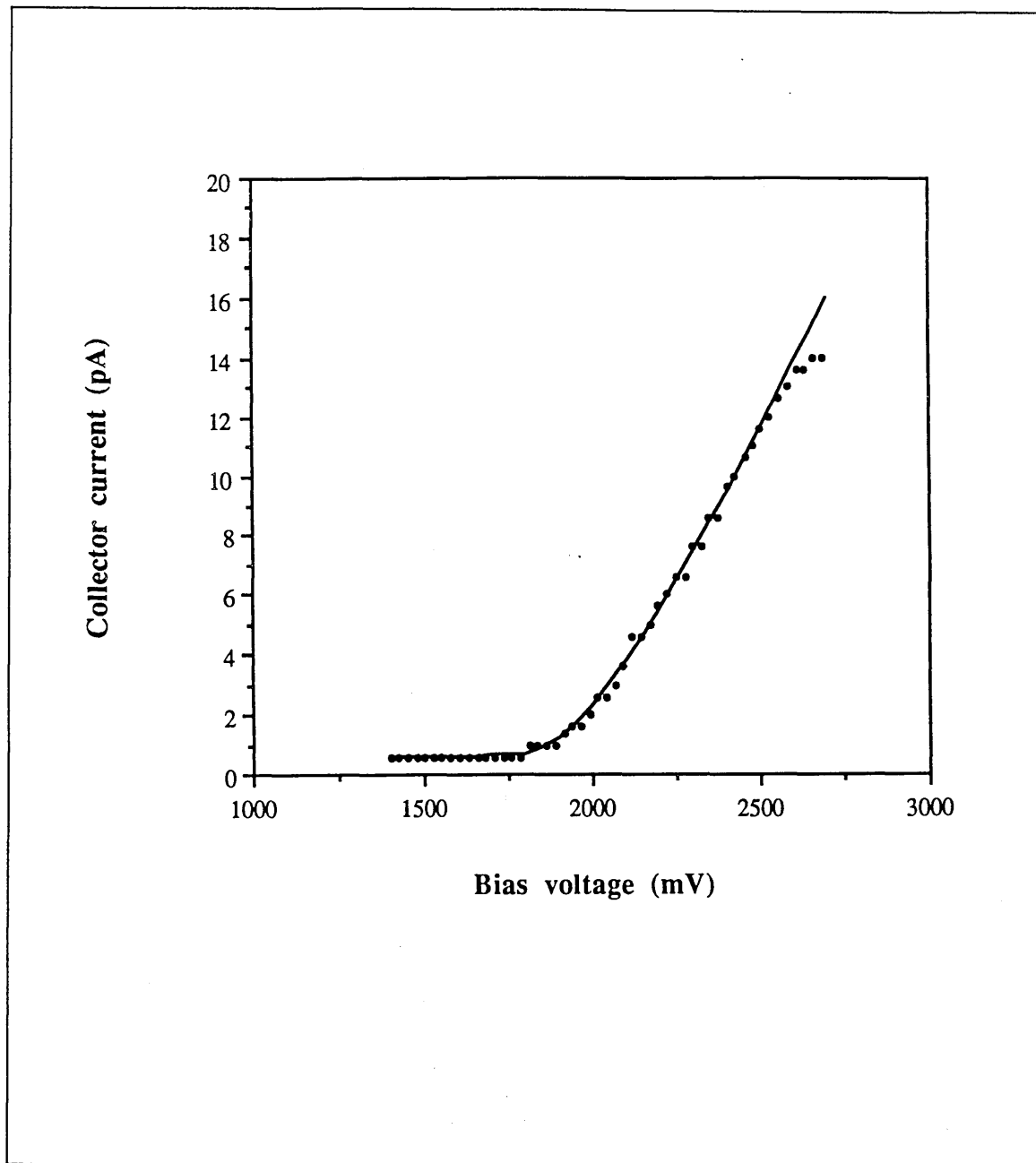


Figure 6.27. BEEM spectra of Au/n-ZnSe device, $\phi_b = 1.78$ eV, $R = 0.0009$ eV⁻¹, note onset of saturation at bias > 2.5V.

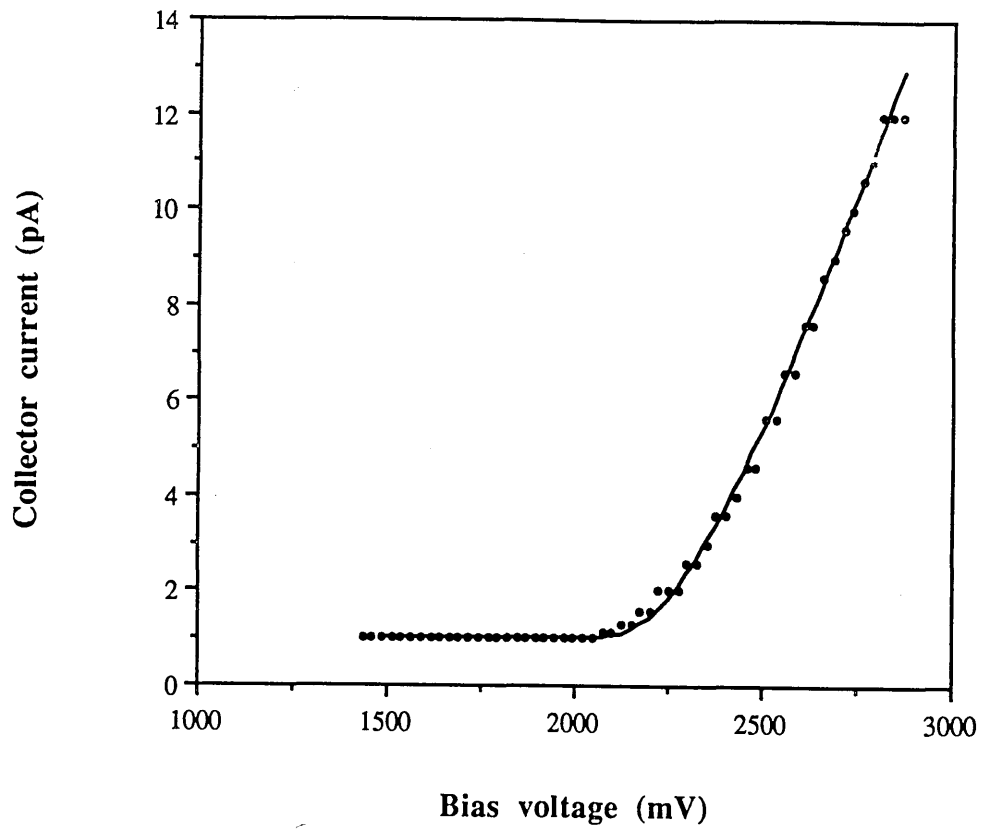


Figure 6.28. BEEM spectra for Au/n-ZnSe device, $\phi_b = 2.1$ eV, $R = 0.00078\text{eV}^{-1}$, note onset of saturation at bias $> 2.5\text{V}$

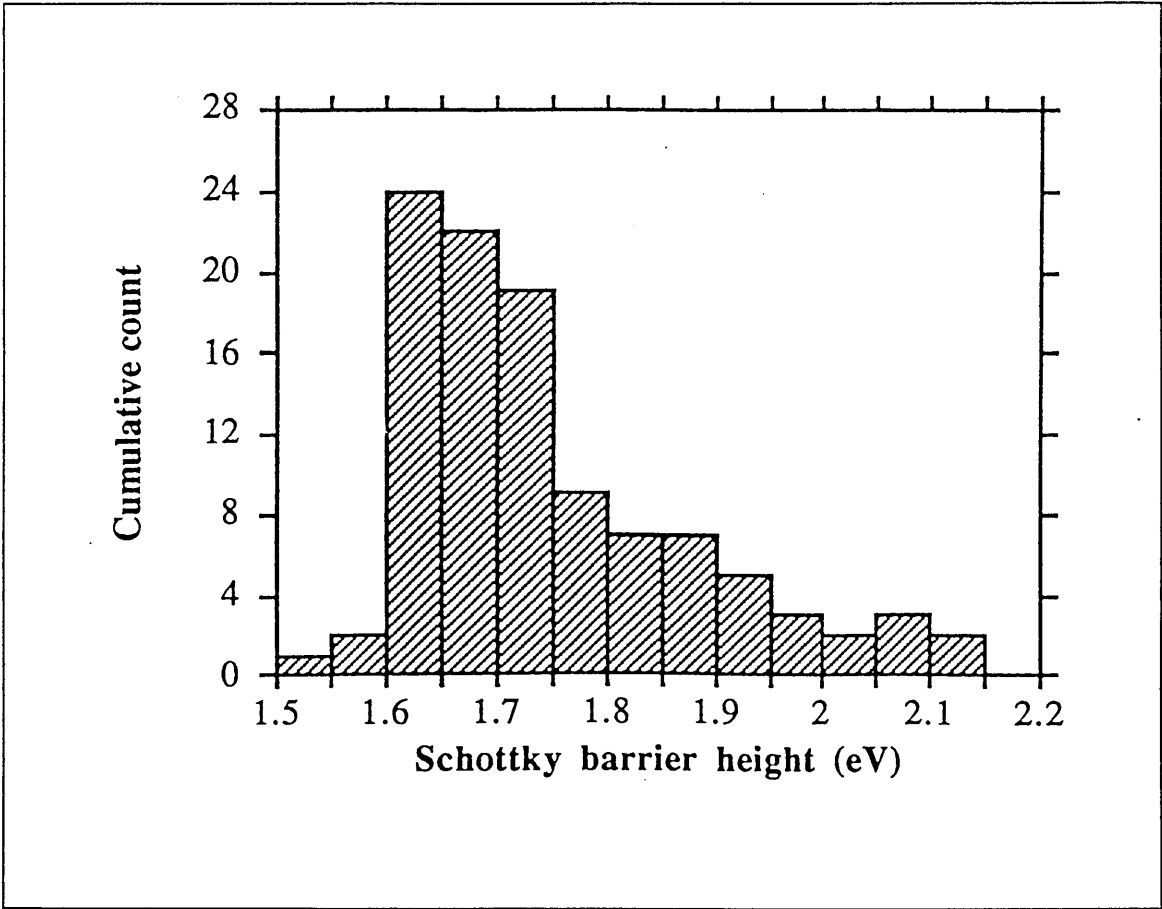


Figure 6.29 Histogram of Schottky barrier heights deduced from more than one hundred BEEM spectra taken on several Au/n-ZnSe contacts.

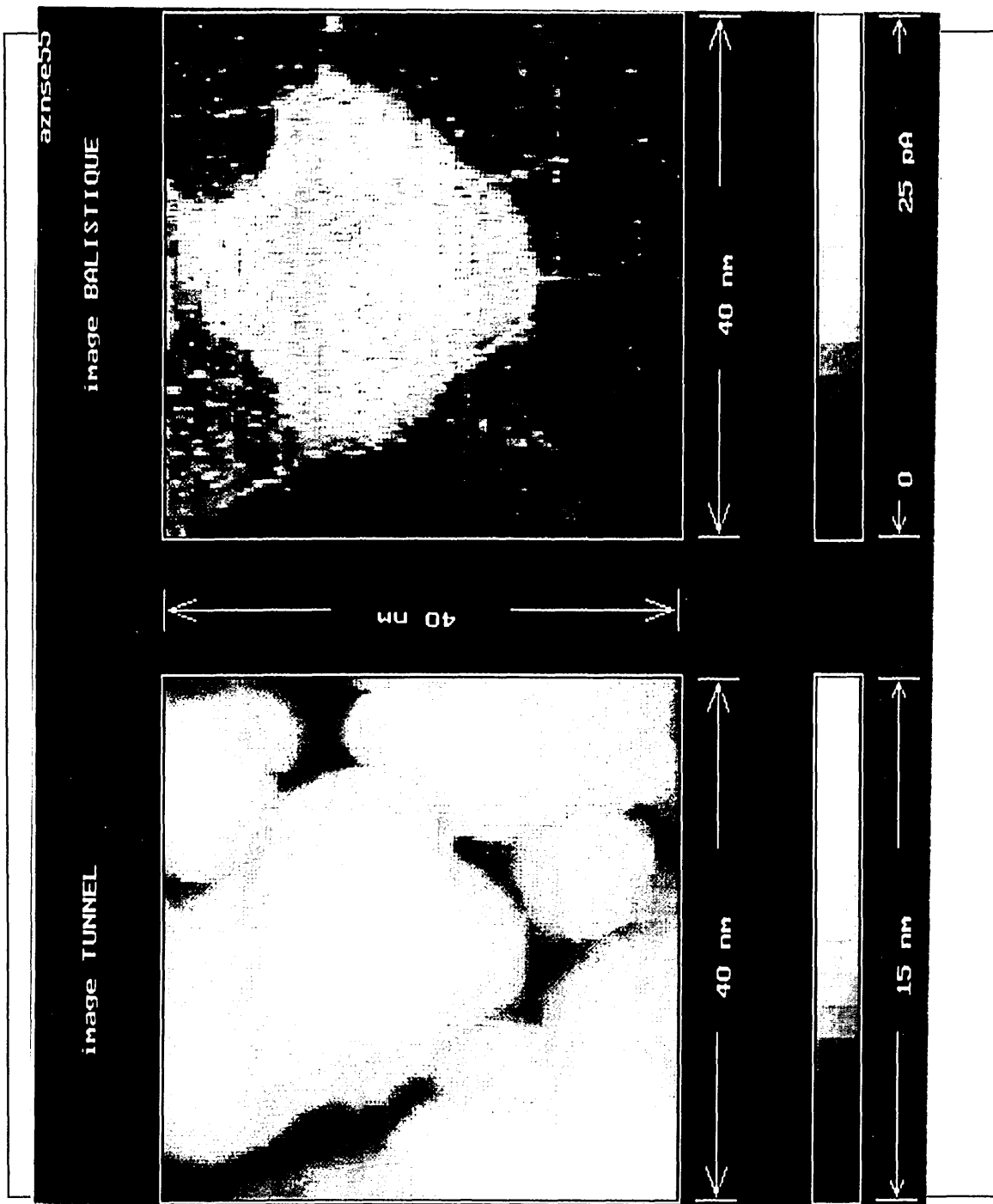


Figure 6.30. BEEM image of Au/n-ZnSe contact, taken with $V_T = 2.4$ V and $I_T = 20$ nA. On the left is the topographic image, black to white indicates 0 to 15 nm in z - direction. On the right is the ballistic image, black to white indicates 0 to 25 pA. Bright patches of

high ballistic current were commonly observed within one contact, the Schottky barrier height within each patch was constant but the scattering parameter R_s varied.

6.4.7.1 Summary of BEEM measurements.

The large number of BEEM spectra taken across the sample and summarised in figure 6.29 (over 100) show a maximum in the distribution at $\approx \phi_b = 1.65$ eV. This value of Schottky barrier height was in excellent agreement with that determined for one of the contacts by I-V ($n = 1.05$, $\phi_b = 1.67$ eV). Careful analysis of figure 6.29 reveals two other maxima centred at $\approx \phi_b = 1.85$ eV and $\approx \phi_b = 2.05$ eV which are in reasonable agreement with I-V measurements of Sb/n-ZnSe which gave $\phi_b = 1.8$ and 2.1 ± 0.04 eV. The level of inhomogeneity on an individual contact was almost impossible to assess at this stage; the very patchy nature of the ballistic current meant the lateral variation could not be fully investigated. It should also be noted that the very high spatial resolution of the STM means that only a very small area of a contact can be investigated at one time. On the scale of figure 6.30 it would in fact be possible to make 10^8 images without repeating the area in one 0.5 mm diameter contact.

A second point of interest in the BEEM images is the contrast observed between regions of high and low ballistic current. Similar results were reported for Pt/Si interfaces prepared by chemical and plasma etching of Si prior to Pt sputtering; these samples were then air exposed before the BEEM experiment was performed, Niedermann *et al* (1993). Talin *et al* (1994) on the other hand reported little contrast in BEEM images of Pt/Si contacts formed under UHV. The patchy regions of ballistic current were therefore related to surface preparation and possible oxidation/physisorbtion of oxygen by Au and Pt surface grains respectively. It may also be possible to invoke such an explanation when understanding BEEM images such as that presented in figure 6.30. Figure 6.31

summarises possible mechanisms which may attenuate the ballistic current, such as oxide precipitates at the ZnSe surface, grain boundary effects and grain orientation. These may all influence the various electron transport mechanisms. As discussed earlier [Sec 4.6], this is an area of still emerging theory.

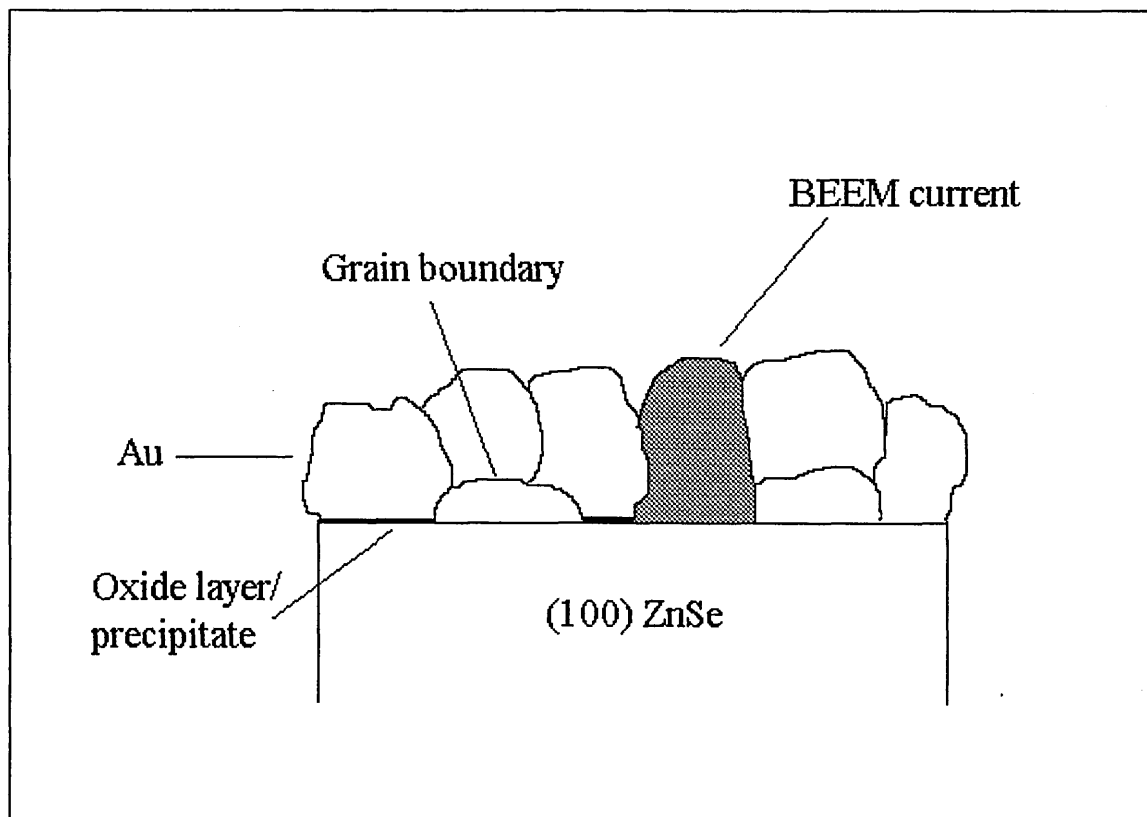


Figure 6.31. Schematic representation of the physical phenomena influencing the observed contrast in BEEM images. The shaded grain emits a measurable ballistic current.

Chapter 7.

Discussion of results.

7.1 Introduction.

The preceding two chapters have outlined many similar properties of CdTe, CdS and ZnSe. The ionic nature of these three compounds means that they behave as weak acids and strong bases when subjected to alkaline or acidic etchants. The resultant surfaces can be modified to an excess of cation over anion or anion over cation with reduced surface oxidation. Metal contacts formed onto such surfaces form discrete Schottky barriers and the extended study on ZnSe showed these barriers to be independent of the metal used. The ageing effects of these devices follow one of two routes, a relatively fast degradation of the contact or dramatic changes in the Schottky barrier height while maintaining the overall quality of the diode. Such results point to a strong contribution from native defects to the Schottky barrier formation mechanism in a manner similar to that first suggested by Spicer *et al* (1979). The data presented here forms an important trial for many of the models outlined in Chapters 1 and 2 and their ability to describe Schottky barrier formation at metal/II-VI interfaces.

Some explanation is offered below of many of these observations, the majority of which are previously unreported. Of particular importance is the concept of discrete Schottky barrier formation. Such effects have been noted only for Sb and Au/n-CdTe by Dharmadasa *et al* (1989). This group however only reported a variation in the Schottky barrier height from sample to sample. In this work multiple Schottky barrier heights across one sample have been observed for CdTe, CdS and ZnSe. While many of these results present a challenge to many theories of Schottky barrier formation it does now seem that a

better understanding of metal/II-VI interfaces would enable realistic control of the Schottky barrier height.

The applicability of the accepted models of Schottky barrier formation is assessed in the context of these new results. The ageing of the metal-semiconductor interfaces is discussed in terms of the bulk thermodynamic properties. Finally the role played by deep levels and native defects is discussed.

7.2 Schottky barrier heights in the context of present theories.

CdTe, CdS and ZnSe have all displayed discrete Schottky barrier formation with Au and ZnSe largely independent of the metal (Au, Ag or Sb) used. The significance of these results in terms of the models presented in Chapter 2 is discussed.

7.2.1 Schottky model.

The Schottky model (Schottky (1938)) implies a linear relationship between the metal work function ϕ_m , and the semiconductor electron affinity χ_s , as given by equation 1.1. The predicted Schottky barrier height for Au/n-CdTe is $\phi_b = 0.92$ eV. This agrees very well with one of the observed barrier heights but does not account for the other three. For Au/n-CdS, the Schottky model predicts $\phi_b = 1.1$ eV. Figure 7.1 shows the barrier heights predicted by the Schottky and EWF models, plotted together with the measured values for Au, Ag and Sb/n-ZnSe contacts. Table 7.1 shows that these barrier heights are very repeatable and determined on a large number of samples. The predicted values are $\phi_b = 1.59, 0.75$ and 1.04 eV for Au, Ag and Sb respectively ($\chi_{\text{ZnSe}(100)} = 3.51$ eV Vos *et al*(1989)). These

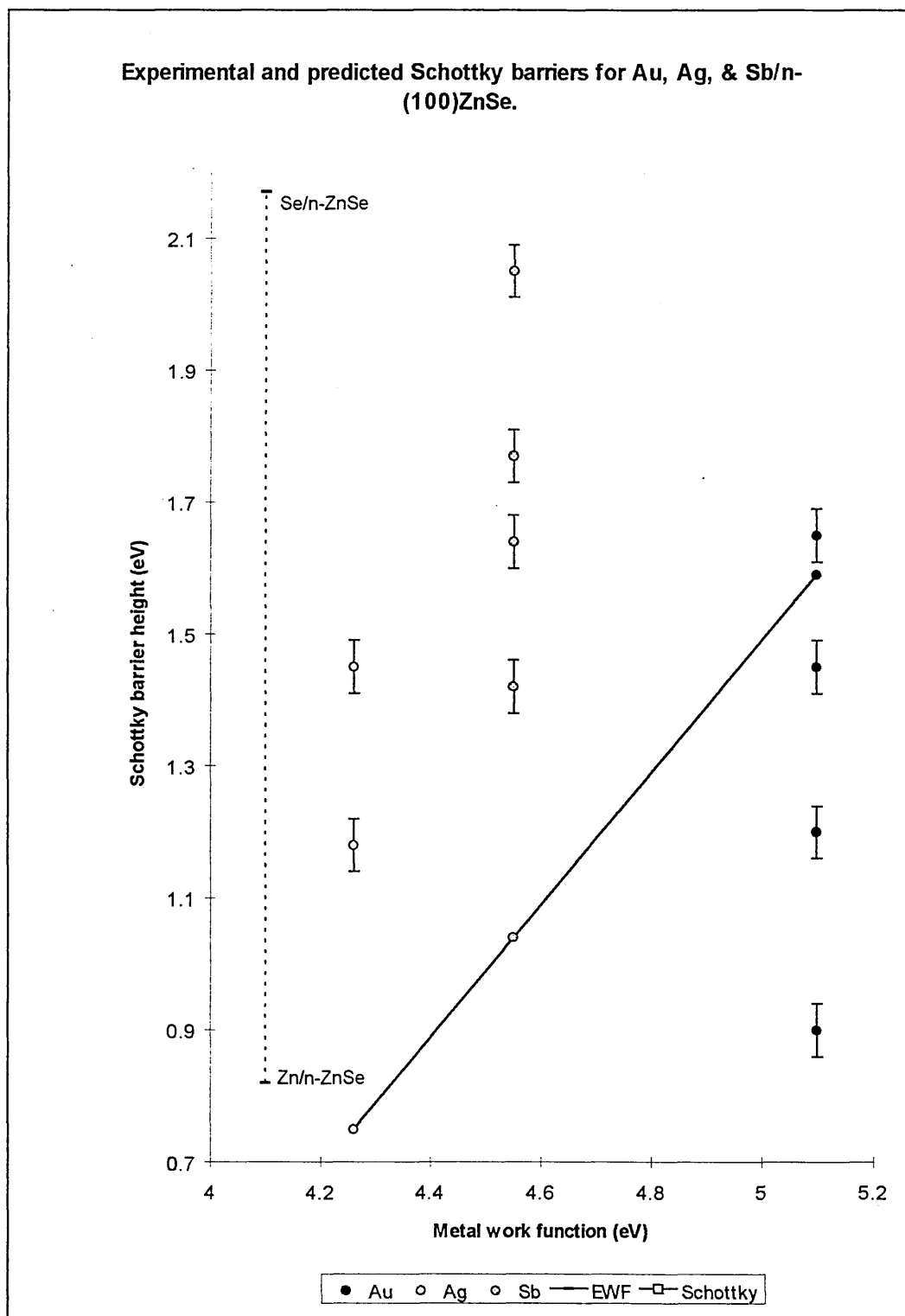


Figure 7.1 Experimental Schottky barriers for Au, Ag, Sb/n-(100)ZnSe contacts compared with predicted values from Schottky model and effective work function model.

Barrier height eV \pm 0.04	Metal	No obs
0.9	Au	8
1.2	Au	13
	Ag	15
1.45	Au	22
	Ag	16
	Sb	6
1.65	Au	9
	Sb	6
1.8	Sb	7
2.1	Sb	5

Table 7.1 Sample audit showing breakdown of barrier heights measured for metal/n-ZnSe following the $n < 1.1$ criterion.

predicted values clearly show little correlation with experimental data reflecting the idealised nature of the model and its inability to take into account interfacial phenomena.

7.2.2 Linear model.

Kurtin *et al*(1969) gave the index of interface behaviour (S) for CdTe, CdS and ZnSe as 0.3, 0.6 and 0.5 respectively. The predicted behaviour should therefore lie between the Schottky limit ($S = 1$) and the Bardeen limit ($S = 0$) following equation 1.2. This predicted linear relationship was not observed for any of the systems studied and the model can not explain the multiple Schottky barriers observed.

7.2.3 Effective work function model.

The effective work function model (EWF) of Freeouf and Woodall (1981) is one of the only models not to involve pinning of the E_F that can account for multiple Schottky barriers. Surface analysis of the etched surfaces has already demonstrated that the surface can be non-stoichiometric in terms of anion or cation composition. A metal layer formed onto such a surface could then be modified to form a compound of variable composition depending upon the degree of reactivity or the excess of cation or anion. The interfacial compound would then have an effective work function dependent upon the composition.

Applying the EWF model to the CdTe and ZnSe data results in two different scenarios to test the model. In the case of CdTe, the work function of the interfacial compound would then vary between that of Au = 5.1 eV ($\phi_b = 0.92$ eV), Te = 4.95 eV ($\phi_b = 0.72$ eV) and Cd = 4.22 ($\phi_b = 0.04$ eV). It is reasonable to then assume that the effective work function (and therefore the Schottky barrier height) of this interfacial compound or phase would not be in excess of the maximum for pure Au. The barrier height for a Au/Te compound would be between 0.92 and 0.72 eV, for Au/Cd between 0.92 and 0.04 eV, for Au/Te/Cd again between 0.92 and 0.04 eV. At first this analysis appears to fit with at least some of the data. There is good agreement with Te/CdTe ($\phi_b = 0.72$ eV) and barrier (b), for Au/CdTe $\phi_b = 0.92$ eV, which is of course the Schottky limit and could well explain barrier (c) and barrier (a) ($\phi_b = 0.64$ eV) could be explained by an amalgam of Au/Cd/Te.

Figure 7.1 shows that the limits of the EWF model could possibly account for all the observed Schottky barriers on ZnSe. The two extremes of surface composition, pure Se or pure Zn, would yield, $\phi_b = 2.17$ eV ($\phi_{Se} = 5.68$ eV Freese (1979)) and $\phi_b = 0.82$ eV ($\phi_{Zn} = 4.33$ eV Weast and Astle (1983)) respectively. The formation of discrete barriers independent of the metal employed implies that the interfacial compound responsible for the effective work function is formed without incorporating the metal overlayer. Previous

photoemission experiments by Vos *et al*(1989) have shown that Au and Ag are indeed unreactive with respect to the ZnSe surface, while no information on Sb exists. The bulk thermodynamic properties indicate that there is some interaction between the metal and semiconductor which becomes more pronounced with time, as will be discussed below. All three of these metals have yielded the same barrier height (1.45 eV Au, Ag, and Sb) although they display different interfacial reactions.

The main problem with the quantification of this model is the lack of published data for the work functions of alloys. More specifically individual systems can not be completely explained, for instance, the highest barrier of the Au/n-CdTe system, ($\phi_b = 1.10$ eV), has no explanation by this model.

7.2.4. Models of Fermi level pinning.

As discussed earlier [Sec 2.2.4] the remaining models are based upon the Bardeen limit, where the Schottky barrier height is completely independent of the metal due to surface states, effectively pinning E_F . In this context surface states are regarded as a generic term encompassing metal induced gap states (MIGS), disorder induced gap states (DIGS) and defect states (UDM).

Heine (1965) first predicted that the exponentially decaying wave functions of the metal at the semiconductor surface would induce states within the bandgap with the possibility of pinning E_F to a fixed position. The distinctions made by Louis *et al* (1981) [Sec 2.2.4.1] for different interfacial conditions appear to suggest that chemically etched covalent compounds such as CdTe (covalent relative to ZnSe and CdS), with a thin layer of oxide, would have a reduced density of states at ϕ_0 and so have a reduced ability to pin E_F . Tersoff (1984) has cautioned that MIGS have a short charge-decay length in wide gap

semiconductors such as CdS and ZnSe again leading to a decreased ability to pin E_F . Very little experimental data has been linked to the MIGS model for II-VI compounds and it seems this data is no exception; whether E_F pinning due to MIGS is possible or not it seems unlikely that this model could account for the observed multiple barriers.

The DIGS model of Hasegawa and Sawanda (1979) and Hasegawa and Ohno (1986) is applicable to contacts prepared by chemical etching, which inherently produces disorder at the interface. In this case E_F is pinned at an energy E_{H0} which lies at a charge neutrality point between acceptor and donor like states induced by interfacial disorder. The concentration of the states and therefore the ability to pin E_F is proportional to the level of disorder at the interface. The E_{H0} point for most tetrahedral semiconductors was found to lie ≈ 5.0 eV below the vacuum level (E_{VAC}), to give $\phi_b = 0.72$ eV for Au/n-CdTe and $\phi_b = 1.49$ eV for Au/n-ZnSe (the hexagonal structure of CdS prevents any such analysis). In fact these values should hold for any metal, E_{H0} being independent of the metal. Although both of these values are in good agreement with experimental data obtained for these systems this model predicts only one such barrier height, which clearly does not reflect the results.

The (UDM) of Spicer *et al* (1980) states that the Schottky barrier height is determined according to the position at which E_F is pinned by extrinsic states, introduced by metal-overlayer induced defects. Calculations performed for III-V semiconductors, namely GaAs and InP indicated the most common defects to be anti-site or anion vacancies. No experimental work has been performed by this group on II-VI compounds, which makes quantitative analysis of the model relative to the data presented impossible. The thermodynamics of defects in II-VI semiconductors are fundamentally different to III-V semiconductors due to their greater ionicity, as pointed out by Van Vechten (1975). Anion or cation vacancies are energetically more favourable than anti-site defects [Sec 3.4].

Nevertheless the initial premise that E_F is pinned by defects, be they intrinsic or extrinsic appears to offer an explanation of the multiple Schottky barrier heights observed. There is remarkable agreement between many of the defect-associated deep levels reported in the literature and the Schottky barrier heights reported for all three materials here. The DLTS experiments performed on CdTe, CdS and ZnSe resulted in the observation of several deep levels associated with anion or cation vacancies which coincide with Schottky barriers observed on these materials.

The degree of spatial inhomogeneity of the Schottky barrier height as discussed by Tung (1991) was investigated by BEEM experiments. The patchy nature of the ballistic current meant that the level of lateral inhomogeneity was difficult to assess. At this stage it is not possible to state categorically that the inhomogeneity of the ballistic current is a true reflection of inhomogeneity in thermionic current or indeed inhomogeneity at the interface. Figure 6.29 did however show that there was a definite spread in the measured barrier heights for Au/n-ZnSe of some 0.65 eV. Although this histogram was obtained over a number of contacts which showed that from contact to contact the barrier height varied it seems that macroscopic I-V measurements showing a number of barrier heights on the same slice of wafer as observed for CdTe, CdS and ZnSe imply some level of inhomogeneity. At present the best evidence for metal-semiconductor interface inhomogeneity is this macroscopic data.

7.3 Thermodynamics of metal-semiconductor interfaces.

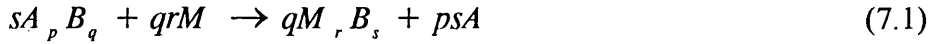
7.3.1. Introduction.

In chapter 6 the different ageing properties of the metal/ CdTe, CdS and ZnSe systems were monitored by observing I-V characteristics over several months. It was apparent that the ageing processes of the metal-semiconductor interface evolved in two stages. In the first phase the overall quality of the diode, as determined by the diode quality factor n , was maintained. There was little increase in n but the Schottky barrier height ϕ_b moved a specific discrete amount. The observed movements of ϕ_b were generally to a higher value and the Au/n-ZnSe contact of figure 6.20 exhibited this type of behaviour. The second phase of ageing was accompanied by a decline in diode quality, indicated by increases in n , reverse current, and an overall decrease in the rectification factor. The ideal Au/n-CdTe contacts of figure 6.7 were prime examples of such behaviour. The main difference between these two ageing phenomena appears to be the time taken for the contact to degrade; for Au/n-CdTe this process is immediate but takes much longer for Au/n-ZnSe.

The bulk thermodynamic properties of metal-semiconductor systems have been used in the past with some success to predict interfacial behaviour. Two common approaches have previously been adopted. The first is based upon a semiquantitative model of the heat of reaction of interfacial compounds (McGilp and McGovern (1985)). This approach was adopted by Dharmadasa *et al* (1987) to describe the metal/CdTe system and Forsyth (1989) for the metal/-CdS system. The second approach is some what simpler and is based upon the heat of formation of the most stable metal /anion compound and has been used by Vos *et al* (1989) to describe Co/ZnSe and Au/ZnSe systems.

7.3.2. Heat of reaction, ΔH_R^N

In this model the heat of reaction is calculated for a metal-anion compound or a metal-cation alloy. A semiconductor compound $A_p B_q$ can react with a metal M to form a compound $M_r B_s$ according to the equation:



The heat of reaction ΔH_R^N normalised to the unit metal atom is then given by:

$$\Delta H_R^N = (1/r)\Delta H_f^o(M_r B_s) - (s/qr)\Delta H_f^o(A_p B_q) \quad (7.2)$$

Equation (7.2) can be modified to include metal-cation alloying, ΔH_R^N then becomes;

Compound/ alloy	$\Delta H_R^N (M_r B_s)$ eVatom ⁻¹	$\Delta H_R^N (M_r B_s)+(A;M)$ eVatom ⁻¹	$\Delta H_R^N (A;M)$ eVatom ⁻¹
AuSe, Zn;Au	+1.61	+0.95	+1.10
Ag ₂ Se, Zn;Ag	+0.62	+0.475	+1.55
Sb ₂ Se ₃ , Zn;Sb	+1.88	+1.845	+1.66
AuS, Cd;Au	+3.94*	+3.51*	+1.12
AuTe ₂ , Cd;Au.	+1.90	+1.47	+0.62

Table 7.2 Semiquantitative thermodynamic data for M/AB compound A;M, alloy or compound + alloy formation. Shaded = most favourable reaction. * determined for CdS_(g)

$$\Delta H_R^N = (1/r)\Delta H_f^o(M_r B_s) - (s/qr)\Delta H_f^o(A_p B_q) + (ps/qr)\Delta H_{sol}(A;M) \quad (7.3)$$

ΔH_{sol} is the heat of solution of solute A in solvent M as defined by Niessen *et al* (1983) for the limit of infinite dilution. Using equations (7.2) and (7.3) the heats of reaction for compound and compound + alloy formation were calculated.

Assuming entropies of reaction are similar in magnitude then the more endothermic ΔH_R^N , the more energy must be supplied to induce the reaction and the less likely is that reaction. The data of table 7.2 shows that compound formation alone is thermodynamically unfavourable for all the systems studied. The relatively high ΔH_R^N values of compound, alloy and compound plus alloy formation testify to the relative stability of the metal/ZnSe interfaces, in agreement with the photoemission spectroscopy measurements of Vos *et al* (1989) [Sec 3.3.4.1]. The ΔH_R^N for the Al₂Se₂ compound and Zn₃Al alloy reaction for example is -0.38 eVatom⁻¹ which shows Al to be reactive in comparison to Au, Ag and Sb. Several groups (Vos *et al* (1989) and Chen *et al* (1994)) have reported Al reacting with the ZnSe surface releasing Zn into the Al overlayer. Although Vos and co-workers have reported Au and Ag to be unreactive, I-V measurements indicate some interfacial reaction is taking place. Over longer periods of time (up to one year) it would appear that even stable interfaces react. One problem with calculations of this type is that they do not take into account the reaction kinetics which may in fact be the main factor in determining interfacial reactivity. The predicted stability of contacts to ZnSe from table 7.2 follows the regime Ag<Au<Sb. The electrical characteristics of Sec 6.4 showed that the stability was in fact Sb<Ag<Au. Table 7.2 indicates that Au/ZnSe and Ag/ZnSe would form a compound plus an alloy. For Sb/ZnSe,

alloy formation alone is the probable reaction. Alloying of Sb/ZnSe alone may proceed more rapidly than compound formation and alloying of Au/ZnSe in tandem. Such an explanation would explain the relatively rapid decline in Sb/ZnSe contacts compared Au/ZnSe.

The results for Au/CdS and Au/CdTe can not be assessed in the same manner as only Au contacts were electrically investigated. One anomaly in the ageing of Au/CdTe can be explained by ΔH_R^N calculations. Non-ideal characteristics (usually with an interlayer) were seen to actually improve rather than degrade with time. If the surface is not composed of CdTe but a thin interfacial layer the ΔH_R^N will be modified. If the surface is composed of TeO₂ say then $\Delta H_R^N = + 1.99 \text{ eV atom}^{-1}$, which makes the reaction with the Au overlayer much less likely than the corresponding Au/CdTe reaction.

7.3.3 Heat of formation, ΔH_f° .

Compound	$\Delta H_f^\circ \text{ eV atom}^{-1}$
AuSe	-0.08
Ag ₂ Se	-0.45
Sb ₂ Se ₃	-1.32
AuS*	+2.39
AuTe ₂	-0.19

Table 7.3 Heats of formation of M/AB compounds after Kubaschewski *et al* (1993).

* determined for CdS_(g)

A basic approach in explaining the interface chemistry is simply to take the heat of formation of the most probable metal-anion compound, ΔH_f° . Table 7.3 shows that this method is in agreement with experimental observations of interface reactivity. The more positive ΔH_f° the less likely is the compound to form. In this regime the stability of contacts to ZnSe follows $\text{Sb} < \text{Ag} < \text{Au}$. This approach has been used to predict the reactivity of Co/ZnSe and Au/ZnSe interfaces by Anderson *et al* (1989) and appears to fit with the experimental observations of Chapter 6. It is also possible to explain the ageing of non-ideal Au/CdTe contacts, as ΔH_f° of $\text{Au}_2\text{O}_3 = -0.035 \text{ eVatom}^{-1}$ which is less likely to react than AuTe_2 .

7.3.4. Summary.

Both thermodynamic techniques provide a reasonable qualitative explanation of metal-semiconductor interfaces. A major drawback of either method is the lack of consideration given to the kinetics of interfacial reaction. The ageing of metal/ZnSe in particular highlights the differences between interfacial reactivity observed by photoemission techniques and the I-V performance of real metal contacts. Essentially there are two very different mechanisms of metal deposition involved; a typical photoemission experiment is performed by the successive deposition of sub-monolayer metal films, whereas metal contacts are formed by the rapid deposition of a thick layer in a matter of minutes. Influential reactions such as alloying or compound formation may then take much longer to occur in this type of interface as observed for Au/ZnSe contacts. The lack of agreement between the thermodynamic calculations and experimental observations indicates that the ageing process is influenced by kinetic considerations which may explain the two-stage ageing process

7.4 The role of defects in determining the Schottky barrier height.

7.4.1 CdTe.

Of the existing models of Schottky barrier formation the defect model as first suggested by Spicer *et al* (1979) seems to offer the closest explanation for the observed behaviour of metal contacts to the etched surfaces of CdTe, CdS and ZnSe. The inability of many of the accepted models to explain these results is a reflection on the complex nature of the contact formation process and the inherent properties of etched II-VI surfaces.

The etching process has been shown to produce non-stoichiometric surfaces, implying the removal of the cation or anion producing the respective vacancies. The results of several studies of deep levels in II-VI's was summarised in Sec 3.4. Most of the deep levels were assigned to vacancies or vacancy complexes and in many cases there is good agreement between the deep level and an observed barrier height. Table 7.4 shows observed Schottky barrier heights for the Au/n-CdTe system compared with deep levels and their assignments from the literature. Reinforcing this data are the DLTS results of Sec 6.2.5 in which three prominent levels were identified at $E_c - 0.33$, $E_c - 0.62$ and $E_c - 0.75$ eV. The possibility of the Schottky barrier height being related to the pinning of E_F by defect induced deep levels becomes apparent when these data are compared with the barrier heights of Sec 6.2.2. The barrier having $\phi_b = 0.64$ eV was repeatedly produced by etch 5 which should produce a stoichiometric surface as determined in Sec 5.2.1; such surfaces may well have vacancies of Cd or Te. Over-etching with the second stage has been shown to produce an excess of Cd implying increases in the Te vacancy population. Such a model would fit with the assignment made by Takebe *et al* (1982) of a deep level at $E_c - 0.68$ eV

Barrier height	Deep level	Assignment of level	Reference
± 0.02 eV	E_c - (eV)		
0.64	0.68	Te vacancy	Takebe <i>et al</i> (1982)
	0.64	Cd vacancy	Sitter <i>et al</i> (1982)
	0.65	Cd interstitial	Lee <i>et al</i> (1988)
0.725	0.74	Cd vacancy	Takebe <i>et al</i> (1982)
	0.72	No assignment	Gelsdorf & Schröter (1984)
	0.74	Cd vacancy	Lee <i>et al</i> (1988)
0.96	0.85	Native defect	Isett & Raychauduri (1984)
	0.965	Te vacancy	Sobiesierski <i>et al</i> (1988)
1.10	1.15	Te vacancy	Lee <i>et al</i> (1988)
	1.24	Te vacancy	Sobiesierski <i>et al</i> (1988)

Table 7.4 Observed Schottky barrier heights for Au/n-CdTe and deep levels reported for CdTe.

due to Te vacancies. However in contradiction of Takebe, Sitter *et al* (1982) have reported a deep level at E_c - 0.64 eV and assigned it to Cd vacancies. Clearly there is some confusion as to the origin of this deep level. What is important however is that two independent groups have reported the presence of a deep level, due to a vacancy, at the energy necessary to pin E_F at such a point so as to produce $\phi_b = 0.64$ eV. A second barrier of $\phi_b = 0.725$ eV was generally observed under the same etching conditions; again this barrier is in excellent agreement with deep levels reported this time due to vacancies of Cd (E_c - 0.74 eV Takebe *et al* (1982) and E_c - 0.74 eV Lee *et al* (1988)). Etch 5 should produce stoichiometric surfaces, but underexposing the sample to the second stage of the etch would lead to a Te rich (increased Cd vacancies) surface. The barrier of $\phi_b = 0.96$ eV

was generally observed after etch 1 (Te rich surface, Cd vacancies) and occasionally with etch 5 (stoichiometric surface). This barrier height is in good agreement with deep levels observed by Sobiesierski *et al* (1988) at $E_c - 0.965$ eV. Sobiesierski reported that in fact this level was due to Te vacancies as it was most intense for Cd rich surfaces. Vitomirov *et al* (1991) has reported similar barrier heights for Te rich surfaces. There does therefore appear to be no clear relation with the assignment of the deep level and the surface preparation. The deep level does however occur (as with $E_c - 0.64$ eV) at the energy necessary to pin E_F to produce $\phi_b = 0.96$ eV. The highest barrier observed for the Au/n-CdTe system of $\phi_b = 1.10$ eV was only ever observed for surfaces treated with etch 7 which were Cd rich (Te vacancies). There is a direct correlation between this barrier height and deep levels due to Te vacancies at $E_c - 1.15$ eV reported by Lee *et al* (1988).

7.4.2 CdS and ZnSe.

Information on deep levels within the wide gap materials CdS and ZnSe remains fragmentary. This is in part due to the high temperatures required to analyse levels of energies greater than $E_c - 1.0$ eV by DLTS. Of the levels reported in Sec 3.4 there is at least supportive evidence that they may be responsible for the observed discrete Schottky barriers through pinning of E_F . Two Schottky barriers were repeatedly observed for the Au/n-CdS system and one of these barriers, $\phi_b = 0.96$ eV is in excellent agreement with a deep level detected in CdS at $E_c - 0.96$ eV by Bessomi and Wessels (1980(a)). The lack of further information on the deep level and defect structures for CdS means that it is difficult to draw any further conclusions.

ZnSe, as with CdTe, demonstrates a good correlation between reported deep levels and measured Schottky barrier heights as summarised in table 7.5. The literature data

Metal	Barrier height	Deep level	Assignment	Reference
	± 0.04 eV	$E_c -$ (eV)		
Au	0.90	0.79		Karai <i>et al</i> (1991)
		0.86	Se vacancy	Bessomi & Wessels (1980)
		0.73*	Se vacancy	Raisanen <i>et al</i> (1995)
		0.83*	Se vacancy	
		0.8	No assignment	Venkatesan <i>et al</i> (1989)
Au, Ag	1.20	1.1	No assignment	Shirakawa <i>et al</i> (1980)
		1.13*	Zn vacancy	Raisanen <i>et al</i> (1995)
Au, Ag, Sb	1.45	No level		
Au, Sb	1.65	1.5 - 1.82	As impurities	Han <i>et al</i> (1992)
		1.73*	Zn vacancy	Raisanen <i>et al</i> (1995)
Sb	1.8	1.5 - 1.82	As impurities	Han <i>et al</i> (1992)
Sb	2.1	2.43*	No assignment	Raisanen <i>et al</i> (1995)
		1.95	As impurities	Han <i>et al</i> (1992)

Table 7.5. Deep levels and Schottky barrier heights for metal /n-ZnSe. * modified for temperature dependence of ZnSe bandgap (-8.0×10^{-4} eVK⁻¹ after Ruda (1992)) as original data quoted for T =90K.

complements the DLTS performed in this work on Au/n-ZnSe devices which yielded two deep levels at $E_c - 0.83$ and $E_c - 0.35$ eV. There appears to be a level native to ZnSe at $E_c - 0.85$ eV, independently reported by four groups and assigned as a Se vacancy by Bessomi and Wessels (1980(b)). This level is in excellent agreement with $\phi_b = 0.90 \pm 0.04$ eV observed for surfaces which had been etched in etch 7 for extended periods. Such etching

has been shown to lead to an enrichment of Zn accompanied by a depletion in Se and thus an increase in Se vacancies. Further reinforcing this data is the observation of this level in Au/n-ZnSe samples having $\phi_b = 0.90 \pm 0.04$ eV by DLTS [Sec 6.4.6]. Of the remaining Schottky barriers observed for ZnSe all but one has a corresponding deep level. The discrepancy between the measured Schottky barrier heights and reported deep levels for ZnSe is minimal. The levels reported by Han *et al* (1991) were associated with As impurities due to the formation of Ga_2Se_3 at the GaAs/ZnSe heterojunction. Raisanen *et al* (1995) varied the flux ratio of Se and Zn sources during the epitaxial growth of ZnSe epilayers and in this way they were able to reduce defects due to vacancies of either Se or Zn. The only Schottky barrier height measured in this work which does not have a corresponding deep level was $\phi_b = 1.45 \pm 0.04$ eV. This is the one level which was completely independent of the metal used in that it was observed for Au, Ag and Sb/n-ZnSe devices. One simple explanation of this may be that there are only two published works which have looked at in this energy range for deep levels. In these particular samples studied this level may for some reason have been omitted. It is not possible to comment further until a thorough investigation of deep levels in ZnSe appears in the literature.

7.4.3. Native defects and the Schottky barrier.

It has been shown that CdTe, CdS and ZnSe exhibit the formation of several discrete Schottky barriers. There is a strong correlation between the Schottky barrier height and deep levels within the band gap due mainly to simple vacancy defects. Spicer *et al* (1979) first suggested the significance of defects in determining E_F pinning and hence the Schottky barrier height. In the light of the preceding discussion it now seems that a modification of the defect model can be applied to the II-VI materials CdTe, CdS and ZnSe.

Although the standard of semiconductor manufacture is extremely high, no crystal structure is perfect and each sample will have a "natural" distribution of native defects. These defects which Van Vechten (1975) has shown to be predominantly vacancies will in turn modify the electronic structure of the lattice leading in some cases to deep levels within the bandgap. These defects and hence deep levels will have a distribution throughout the crystal largely dependent upon the crystal growth mechanisms. It is even feasible that there will be a surface modification of the defect structure due to the abrupt termination of the infinite three dimensional lattice. The defect density at the surface may also be modified by

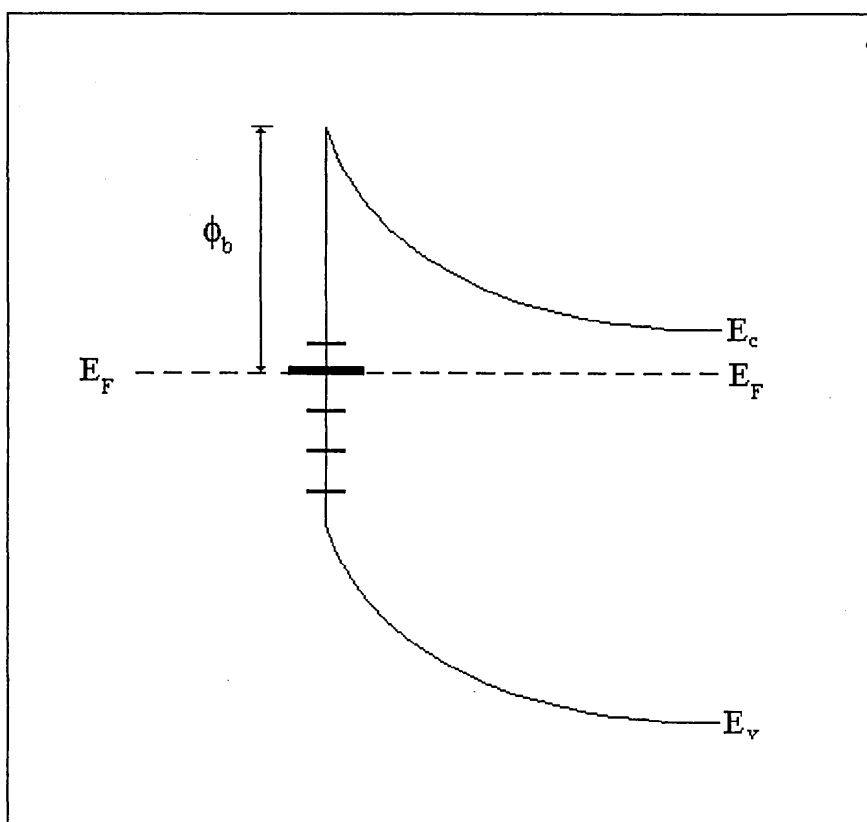


Figure 7.2 Proposed natural density of defect induced deep levels, showing E_F pinning by a high density of one particular level.

external processes such as chemical etching. For example etching CdTe with etch 2 (chromic acid) will preferentially remove Cd atoms from the top few monolayers of the sample. In turn the natural density of Cd vacancy defects will be enhanced to such a point that the Cd vacancy becomes the dominant defect, but only in the surface region. This extrinsic enhancement of the intrinsic defect levels will modify the surface electronic structure, promoting the deep level associated with Cd vacancies to be the dominant level. At sufficient densities charge transfer will occur into this level, resulting in realignment of E_F and band bending at the free semiconductor surface. As shown in figure 7.2, subsequent metal contact formation will have little effect upon the position of E_F , and the Schottky barrier height will be a function of the deep level energy rather than the metal work function. This model is essentially a modification of Spicers original defect model in which E_F was pinned due to a high density of defects which originated as the metal overlayer was formed. In these interfaces it seems that the relevant defects are present prior to metal contact formation. Although this has not been implicitly confirmed in this work Sobiesierski *et al* (1998) and Han *et al* (1992) have observed deep levels due to native defects with photoluminescence for CdTe and ZnSe respectively, with no metal layer present. The energies of the deep levels were in good agreement not only with levels measured with a metal overlayer using techniques such as DLTS but were also in good agreement with the Schottky barriers measured here. No such report of deep levels in CdS exists but given the similar behaviour of all three of these II-VI materials in terms of chemical etching and formation of several discrete Schottky barriers it seems that this theory can reasonably be extended to cover CdS.

It seems that native defects such as vacancies or vacancy impurity complexes rather than metal-induced defects act to pin E_F . However the ageing of several systems namely Au/n-ZnSe and Au/n-CdS (thermodynamically relatively stable) suggests that the metal overlayer may play a role in determining the barrier height with time. In these systems the

Chapter 8.

Conclusions and recommendations for future work.

8.1 Wet chemical etching.

Wet chemical etchants based upon aqueous reagents (with the exception of Br methanol) were applied to the surfaces of CdTe, CdS and ZnSe which were subsequently analysed by XPS. A simple chemical model was developed describing the II-VI materials as ionic semiconductors which behave as insoluble salts of strong bases and weak acids with respect to such aqueous reagents. A summary of the main conclusions of the surface analysis and the wet chemical etching of CdTe, CdS and ZnSe is given below.

- All as-received/air-exposed materials exhibited a strong signal from the O 1s photoelectron peak indicating the presence of a surface oxide layer. The composition of this surface oxide was identified as predominantly; TeO₂ for CdTe, SeO₂ for ZnSe and a combination of CdO and CdSO₄ for CdS.
- Acid etchants induced a stoichiometric excess of semiconductor anion which appeared to be in an elemental or hydrogenated state. Consequently these surfaces had a reduced oxide content.
- Alkaline etchants conversely induced a stoichiometric excess of semiconductor cation which appeared to be in an oxidised state namely, CdO for CdS, ZnO for ZnSe and a combination of TeO₂ CdO and CdTeO₃ for CdTe.

- A two stage etchant comprising an initial short acid etch phase followed by a longer alkaline etch was developed. The effect was to reduce the initial native oxide dominated surface to an anion rich one via the acid etch. Secondly the alkaline etch returned the surface to stoichiometry by removing the excess anion to leave a stoichiometric surface with a reduced oxide content.

As yet no clear relationship between a particular etchant and a specific Schottky barrier has been demonstrated. The quality of devices in terms of reducing the n value to $n < 1.1$ has been achieved for all systems primarily by reducing the surface oxide to a minimum prior to metal contact evaporation. This was best achieved by either employing etchants 1 or 2 which although they would reduce the surface oxide to a minimum would also induce an enrichment of the semiconductor anion at the surface. Stoichiometric surfaces with reduced oxide content were achieved by employing etch 5 in which chromic acid (etch 1) was applied for 30 s followed by a solution containing 0.6g NaOH + 1.0g Na₂S₂O₃ in 75ml H₂O at 90°C (etch 7) for 6 min for CdS, 4 min for ZnSe and 3 min for CdTe.

8.2 Electrical characterisation.

Chapter 6 documented the results of the electrical characterisation of metal contacts formed to etched surfaces. I-V and C-V characterisation were the primary techniques used to yield the parameters describing the Schottky barriers. DLTS was performed on selected Au/n-ZnSe and Au/n-CdTe devices. The Au/n-ZnSe interface particularly was investigated by BEEM. The key results are summarised below.

- CdTe, CdS and ZnSe all showed the formation of discrete Schottky barriers. Au/n-CdTe repeatedly gave $\phi_b = 0.64, 0.725, 0.96$ and 1.10 ± 0.02 eV. Au/n-CdS produced $\phi_b = 0.86$ and 0.96 ± 0.02 eV. Au, Ag and Sb/n-ZnSe contacts were investigated using n-ZnSe/n⁺GaAs substrate structure. The forward current

appeared to be dominated by the potential barrier at the n-ZnSe/n-GaAs heterojunction, ϕ_{HJ} . Despite the observed low currents, ZnSe as with CdTe and CdS displayed the formation of discrete Schottky barriers. Metal/n-ZnSe devices routinely had $\phi_{\text{b}} = 0.9, 1.2, 1.45, 1.65, 1.8$ and 2.1 ± 0.04 eV.

- DLTS analysis of Au/n-CdTe and Au/n-ZnSe indicated the presence of a number of deep levels at $E_{\text{c}} - 0.755, 0.62$ and 0.33 eV for Au/n-CdTe and $E_{\text{c}} - 0.83$ and 0.35 eV for Au/n-ZnSe.
- The ageing of Au/n-ZnSe and Au/n-CdS devices often followed a pattern of maintaining the diode quality factor, n while ϕ_{b} "jumped" to another one of the discrete levels reported.
- Analysis of the electrical stability of metal/II-VI contacts revealed that all devices degraded with time. A qualitative explanation of stability was achieved by considering the heat of reaction $\Delta H_{\text{R}}^{\text{N}}$, of the metal-anion and metal-cation compounds. Generally the more endothermic this value then the more stable the interface.
- BEEM images of the Au/n-ZnSe interface showed a great deal of inhomogeneity. With the limited data it was not possible to assess whether this inhomogeneity reflected a true variation in the thermionic current and hence barrier height or just a variation in the ballistic current. There was generally good agreement between the Schottky barrier height determined by BEES and that determined by I-V.

In conclusion it is apparent that the semiconductor surface preparation has a profound effect upon the subsequent electrical properties of the metal-semiconductor interface. Wet chemical treatments have been realised which can produce a reduction in the surface oxidation of the semiconductor. Formation of a metal contact to a surface of

low oxide content will then yield a device of comparable electrical quality to UHV fabricated devices. Ideal devices formed to such surfaces routinely exhibited the formation of discrete Schottky barriers, which for metal/n-ZnSe were completely independent of the metal work function ϕ_m . Deep levels observed both in this study and reported in the literature suggest that native defects within the semiconductor act to pin E_F in a manner similar to that first suggested by Spicer *et al* (1979) for metal/III-V interfaces. The wet chemical etch appears to act to modulate the natural distribution of defects so that one level in particular dominates to pin E_F , and hence establishes the Schottky barrier.

8.3 Future work.

Au contacts were investigated to CdTe and CdS due to the technological importance of this system. Time constraints meant that this study was limited to Au and for ZnSe only a limited number of metals (Au, Ag and Sb) were investigated. In order to establish the independence of the barrier height from the metal work function this range of metals should be extended to cover a wider range of work functions. Prime candidates for future work would be Pt and Pd which are relatively unreactive metals.

Given the relative importance ascribed to deep levels in this work, it would seem appropriate that a thorough study of deep level origins, activation energies and concentrations in II-VI compounds should be undertaken. At present such data is fragmentary and often contradictory. One suitable experiment may be to perform DLTS experiments on several devices on the same material to determine the role played by a specific deep levels in defining the Schottky barrier height. For example Au/n-CdTe devices have been shown to exhibit $\phi_b = 0.64$ and $\phi_b = 0.72$ eV. If the hypothesis presented here is correct then both devices would yield several deep levels but the concentration of the level at $E_c - 0.64$ eV in the lower barrier device would exceed the concentration of this level in the higher barrier device. Conversely for the

higher barrier device the concentration of a deep level at $E_c - 0.72$ would exceed this level's concentration in the lower barrier device. Such an experiment would be an important test of the theories presented in this work.

A greater understanding of the origin of deep levels be they due to native defects or to impurities would in turn lead to better control of these levels. This may then facilitate some degree of control over the Schottky barrier height. Such a possibility was suggested in this work but was far from established. For instance over-etching the ZnSe substrate to produce a Se depleted layer invariably produced $\phi_b = 0.90 \pm 0.04$ eV. This value of the Schottky barrier height is in fact within experimental error of literature reported values for deep levels due to Se vacancies of $E_c - 0.86$ eV as reported by Bessomi and Wessels (1980(b)). A long term aim should then be to control the concentration of a particular deep level at the surface region so as to act to pin E_F to produce the Schottky barrier of the desired magnitude.

Stability of metal contacts to II-VI semiconductors remains a problem which impedes the long term reliability of II-VI devices. In this work the degradation of the electrical properties with time was all too apparent and this is an area which requires a lot of work in the future. It may be that it will be necessary to compromise the short term properties of a specific device in order to improve lifetime. Such an example was shown with some of the Au/n-CdTe devices which appeared to be initially non-ideal but actually out-performed ideal devices in terms of rectification over one year. The use of suitable interlayers or reaction barriers seems to offer the possibility of increasing stability.

BEEM of metal-semiconductor interfaces is still a relatively new technique and much effort is required to fully understand the physics of electron transport from tip to base and then to relate this microscopic information to macroscopic I-V characteristics. This area now holds the key to assessing many theories of interfacial inhomogeneity

and their applicability to metal/II-VI interfaces. The advantage of BEEM is that "real" metal-semiconductor devices can be investigated with nm resolution. It has been demonstrated here that this technique is ideally suited to the analysis of metal/II-VI interfaces

8.4 Contribution to device technology.

This work offers several contributions to the field of metal/II-VI contacts which in turn will offer direct improvements to II-VI devices, including those outlined in Chapter 1. The wet chemical etchants developed in this work should improve the repeatability and reliability of metal contacts to CdTe, CdS and ZnSe primarily by a reduction of surface oxides. Similarly epitaxial growth of II-VI semiconductors relies upon growth on a clean substrate seed material and the reduction of surface oxides prior to growth is a key element of epilayer growth. The use of a suitable chemical etchant described in this work should facilitate growth by reducing the oxide layer on the substrate material as it is inserted into the vacuum growth chamber.

Control of the Schottky barrier height offers many advantages to the device physicist, for instance decreasing the Schottky barrier inherent in ohmic contacts to n and p-type ZnSe would in turn reduce specific contact resistances. This in turn would reduce the voltage required to drive a ZnSe based solid-state laser for example, thus increasing device lifetime and device efficiency. This work has shown that achieving control of the Schottky barrier is a realistic proposition provided control of defect induced deep levels can be attained. Wet chemical etching has been employed in this study to achieve some level of control over defect densities and such control has been demonstrated by other techniques. However Raisanen *et al* (1995) demonstrated that defect concentrations were related to beam pressure ratios during the MBE growth of ZnSe. Similarly Sottomayor Torres *et al* (1994) established that surface stoichiometry and hence defect levels could again be influenced by dry plasma-etching the ZnSe surface.

It is envisaged that processes such as these will be employed to modulate a particular defect, so increasing the concentration of a specific discrete deep level to pin E_F to a discrete point. An advance of this nature would yield many benefits to important II-VI devices such as photovoltaic cells and short-wavelength light emitters.

References

- Amalnerkar DP, Badrinarayanan S, Date SK and Sinha APB. (1982) Applied Physics Letters Vol 41 (3) pp270-271.
- Anderson SG, Xu F, Vos M, Weaver JH and Cheng H. (1989) Physical Review B Vol 39 (8) pp5079-5090.
- Annan RH (1993) Proceedings 23rd IEEE Photovoltaics Specialists Conference Kentucky USA.
- Asano K, Watanabe Y, Ebina A and Takahashi T. (1984) Japanese Journal of Applied Physics Vol 27 (12) pp881-890.
- Ayyar SG, Colak S, Marshall T, Khan B and Cammack D. (1990) Journal of Applied Physics Vol 68 (10) pp5226-5233.
- Bauer A, Cuberes MT, Prietsch M and Kaindl G. (1993(a)) Physical Review Letters Vol 71 (1) pp149-152.
- Bauer A, Cuberes MT, Prietsch M and Kaindl G. (1993(b)) Journal of Vacuum Science and Technology B Vol 11 (4) pp1584-1590.
- Bardeen J. (1947) Physical Review 71 pp717-727.
- Bell LD and Kaiser WJ. (1988) Scanning Microscopy Vol 2 (3) pp1231-1236.
- Besomi P and Wessels B. (1980(a)) Journal of Applied Physics Vol 51 (8) pp4305-4309.
- Besomi P and Wessels BW. (1980(b)) Electronics Letters Vol 16 (21) pp798-795.
- Binnig G, Rohrer H, Gerber CH and Weibel E. (1982) Applied Physics Letters Vol 40 (2) pp178-180.
- Bose DN, Hedge MS, Basu S and Mandal KC. (1989) Semiconductor Science and Technology Vol 4 pp866-870.
- Briggs D and Seah MP. (1990) "*Practical surface analysis- Vol 1 Auger and X-ray Photoelectron Spectroscopy*". Second Edition, Wiley

- Brillson LJ. (1978(a)) Physical Review Letters Vol40 (4) pp260-263.
- Brillson LJ. (1978(b)) Journal of Vacuum Science and Technology Vol 15 (4) pp1378-1383.
- Brillson LJ. (1979) Journal of Vacuum Science and Technology Vol 16 (5) pp1137-1142.
- Brillson LJ, Bauer RS, Bachrach RZ and McMennamin JC. (1980) Journal of Vacuum Science and Technology Vol 17 (1) pp476-480
- Brillson LJ. (1994) Surface Science 299/300 pp909-927
- Britt J and Ferekides C. (1993) Applied Physics Letters Vol 62 (22) pp2851-2852
- Brucker CF and Brillson LJ. (1981(a)) Journal of Vacuum Science and Technology Vol 18 (3) pp787-791.
- Brucker CF and Brillson LJ. (1981(b)) Journal of Vacuum Science and Technology Vol 19 (3) pp617-622
- Card HC and Rhoderick EH. (1971) Journal of Physics : D Applied Physics Vol 4 pp1589-1601.
- Chen EK and Munir ZA. (1991) Journal of Materials Science Vol 26 pp4268-4272.
- Chen W, Kahn A, Soukiassian, Mangat PS, Gaines, Ponzoni and Olego D. (1994) Journal of Vacuum Science and Technology B Vol 12 (4) pp2639-2645.
- Choi SS and Lucovsky G. (1988) Journal of Vacuum Science and Technology B Vol 6 (4) pp1198-1203.
- Chu TL and Chu SS. (1995) Solid-State Electronics Vol 38 (3) pp533-549.
- Colak S, Marshall T and Cammack D. (1989) Solid-State Electronics Vol 32 (8) pp 647-653.
- Collins RT, Kuech TF and McGill TC. (1982) Journal of Vacuum Science and Technology. Vol 21 (1) pp191-194.
- Coratger R, Beauvillain J, Ajustron F, Lacaze JC and Tremollieres C. (1991) Review of Scientific Instruments Vol 62 (3) pp830-831.
- Cowley AM, and Sze SM. (1965) Journal of Applied Physics Vol 36 pp3212-3220.

- Cowley AM. (1966) Journal of Applied Physics Vol 37 (8) pp3024-3032.
- Crowell CR and Sze SM (1967) "*Physics of Thin Films*" Editors Hass G and Thun RF. Academic Press, New York.
- Crowell CR and Roberts GI. (1969) Journal of Applied Physics Vol 40 (9) pp3726-3730.
- Davis GC, Sun TS, Buchner SP and Byer NE. (1981) Journal of Vacuum Science and Technology Vol 19 (3) pp472-476.
- Dharmadasa IM, McLean AB, Patterson MH and Williams RH. (1987) Semiconductor Science and Technology Vol 2 pp404-412.
- Dharmadasa IM, Thornton JM and Williams RH. (1989) Applied Physics Letters Vol 54 (2) pp137-139.
- Fan Y, Han J, He L, Saraie J and Gunshor RL (1993) Journal of Vacuum Science and Technology B Vol 11 (4) pp1748-1751.
- Flores F, Louis E and Yndurain F. (1973) Journal of Physics C: Solid-State Physics Vol 6 pp L465-L469.
- Forsyth NM (1989) "*A study of Schottky barriers to CdS and the CdTe:CdS heterojunction*". PhD Thesis University of Wales College Cardiff.
- Fowell AE, Williams RH, Richardson BE and Shen T-H. (1990) Semiconductor Science and Technology Vol 5 pp348-350.
- Freeouf JL and Woodall JM (1981) Applied Physics Letters Vol 39 (9) pp727-729
- Freeouf JL, Jackson TN, Laux SE and Woodall JM. (1982) Applied Physics Letters Vol 40 (7) pp634-636.
- Freese KW (1979) Journal of Vacuum Science and Technology Vol 16 (4) pp1042-1047
- Friedman DJ, Lindau I and Spicer WE. (1988) Physical Review B Vol 37 (2) pp731-739.
- Fulop G, Doty M, Meyers P, Betz J and Liu CH.(1982) Applied Physics Letters Vol 40 (4) pp327-328
- Gaines JM, Drenten RR, Haberern KW, Marshall T, Mensz P and Petruzzello J. (1993) Applied Physics Letters Vol 62 (20) pp2462-2464

- García-García J, González-Hernández and Mendoza-Alvarez JG, Cruz EL and Contreras-Puente G. (1990) *Journal of Applied Physics* Vol 67 (8) pp3810-3814.
- Gaugash P and Milnes AG. (1981) *Journal of Electrochemistry* Vol 128 (4) pp924-926.
- Gelsdorf F and Schröter W. (1984) *Philosophical Magazine A* Vol 49 (5) ppL35-L41.
- Goodman AM. (1964) *Journal of Applied Physics* Vol 35 (3) pp573-580.
- Grill C, Bastide G, Sagnes G and Rouzeyre M. (1979) *Journal of Applied Physics* Vol 50 (3) pp1375-1380.
- Guha S, Depuydt JM, Haase MA, Qiu J and Cheng H. (1993) *Applied Physics Letters* Vol 63 (23) pp3107-3109.
- Haase MA, Qiu J, DePuydt JM and Cheng H. (1991) *Applied Physics Letters* Vol 59 (11) pp1272-1274.
- Han KJ, Abbate A, Bhat IB and Das P. (1992) *Applied Physics Letters* Vol 60 (7) pp862-864.
- Häring JP, Werthen JG, Bube RH. (1983) *Journal of Vacuum Science and Technology A* Vol 1 (3) pp1469-1472.
- Hasegawa H and Ohno H. (1986) *Journal of Vacuum Science and Technology B* Vol 4 (4) pp1130-1138.
- Heine V. (1965) *Physical Review* Vol 138 (6a) pp1689-1696
- Heuken M, Höpken L and Opitz B. (1993) *Solid-State Electronics* Vol 36 (5) pp 761-766.
- Humphreys TP, Patterson MH and Williams RH (1980) *Journal of Vacuum Science and Technology* Vol 17 (5) pp886-890.
- Issett LC and Raychaudhuri PK. (1984) *Journal of Applied Physics* Vol 55 (10) pp3605-3612.
- Kaiser WJ and Bell LD. (1988) *Physical Review Letters* Vol 60 pp1406-1409.
- Kolhe S, Kulkarni SK, Nigavekar AS and Sharma SK. (1984) *Solar Energy Materials* Vol 10 (1) pp47-54.

- Kowalczyk SP, Kraut EA, Waldrop JR and Grant RW (1982) *Journal of Vacuum Science and Technology* Vol 21 pp482-491
- Kubashewski O, Alcock CB and Spencer PJ. (1993), "*Materials Thermo-chemistry*" Sixth Edition, Pergamon Press.
- Kuech TF. (1981) *Journal of Applied Physics* Vol 52 (7) pp4874-4876.
- Kurtin S, McGill TC and Mead CA. (1969) *Physical Review Letters* Vol 22 (26) pp1433-1436.
- Lang DV. (1974) *Journal of Applied Physics* Vol 45 (7) pp3023-3032.
- Lee WI, Taskar NR, Ghandhi SK and Borrego JM. (1988) *Solar Cells* Vol 24 pp279-286.
- Lepley B and Ravelet S. (1976) *Physica Status Solidi (A)* Vol 33 pp517-522
- Livingstone AW, Turvey K, Allen JW. (1973) *Solid State Electronics* Vol 16 pp351-356
- Louis E and Flores F. (1981) *Journal de Physique* Vol 42, pp1313-1325.
- Lu YC, Stahle CM, Feigelson RS and Morimoto J (1987). *Journal of Applied Physics* Vol 62 (11) pp4453-4459.
- Lu YC, Feigelson RS and Route RK. (1990) *Journal of Applied Physics* Vol 67 (5) pp2583-2590.
- Mandal KC, Basu S and Bose DN. (1987) *Journal of Physical Chemistry* Vol 91 pp 4011-4013.
- Marshall T, Colak S and Cammack D. (1989) *Journal of Applied Physics* Vol 66 (4) pp1753-1758.
- Mayajima T, Akimoto K and Mori Y. (1990) *Journal of Applied Physics* Vol 67 (3) pp1389-1392.
- McGilp JF and McGovern IT. (1985) *Journal of Vacuum Science and Technology B* Vol 3 (6) pp1641-1644.
- McLean AB, Dharmadasa IM and Williams RH. (1986) *Semiconductor Science and Technology* Vol 1 pp137-142.
- Menz PM (1994) *Applied Physics Letters* Vol 64 (16) pp2148-2150.

- Meyerhof WE. (1947) *Physical Review* Vol 71 pp727-732
- Missous M and Rhoderick EH. (1986) *Electronics Letters* 22 pp477-478
- Mott NF (1938) *Proceedings of Cambridge Philosophical Society* Vol 34 pp568-572
- Nair MTS, Nair PK, Zingaro RA, Meyers EA. (1994) *Journal of Applied Physics* Vol 75 (3) pp1557-1564.
- Nedeoglo DD, Huy Lam D and Simashkevich AV. (1977) *Physica Status Solidi (A)* Vol 44 pp83-89.
- Neumark GF, Park RM and DePuydt JM. (1994) *Physics Today*, June, pp26-32.
- Niessen AK, de Boer FR, Boom R, de Châtel PF and Mattens WCM. (1983) *CALPHAD* Vol 7 (1) pp51-70.
- Niedermann P, Quattropani L, Solt K, Maggio-Aprile I and Fischer O. (1993) *Physical Review B* Vol 48 (12) pp8833-8839.
- Ohdomari I, Kuan TS and Tu KN. (1979) *Journal of Applied Physics* Vol 50 (11) pp7020-7029
- Ohdomari I and Tu KN. (1980) *Journal of Applied Physics* Vol 51 (7) pp 3735-3739.
- Padovani FA and Stratton R. (1966) *Solid-State Electronics* Vol 9 pp695-701
- Park RM, Troffer MB, Rouleau CM, Depuydt JM and Haase MA. (1990) *Applied Physics Letters* Vol 57 pp2127-2130
- Patterson MH and Williams RH. (1978) *Journal of Physics D : Applied Physics* Vol 11 ppL83 - L86.
- Patterson MH and Williams RH (1982) *Journal of Crystal Growth* Vol 59 pp281-288.
- Pearton SJ and Ren F. (1993) *Journal of Vacuum Science and Technology B* Vol 11 (1) pp15-19.
- Pickhardt VY and Smith DL (1967) *Journal of Electrochemical Society* Vol 121 (8) pp1064-1066.
- Prior KA. (1994) *Microelectronics Journal* 25 pp631-641.

- Pritchard AA and Wagner S. (1974) *Journal of Electrochemical Society* Vol 124 pp961-962.
- Raisanen A, Brillson LJ, Franciosi A, Nicolini R, Vanzetti L and Sorba L. (1995) *Journal of Electronic Materials* Vol 24 (3) pp 163-169.
- Raychaudhuri PK. (1987) *Journal of Applied Physics* Vol 62 (7) pp3025-3028.
- Rhiger DR and Kvass RE. (1982) *Journal of Vacuum Science and Technology* Vol 21 pp168-171.
- Rhoderick EH and Williams RH. (1988) "*Metal-Semiconductor Contacts*" Second Edition, Oxford University Press.
- Ricco AJ, White HS and Wrighton MS (1984) *Journal of Vacuum Science and Technology A* Vol 2 (2) pp910-915.
- Roche A, Montes H, Brissot J, Romand M, P Josseaux and A Kirsch De Mesmaeker (1985) *Applications of Surface Science* Vol 21 pp12-28.
- Robertson DS, Shaw N and Young IM. (1978) *Journal of Material Science* Vol 13 pp199-205
- Ruda HE (1992) "*Widegap II-VI compounds for optoelectronic applications*" First Edition, Chapman and Hall, UK.
- Schottky W (1938) *Naturwiss* Vol 26 pp 843.
- Shockley and Read (1952) *Physical Review* Vol 87 pp835-842
- Shaw JL, Viturro, Brillson LJ, Kilday D, Kelly M and Magritondo C. (1988) *Journal of Vacuum Science and Technology A* Vol 6 (3) pp1579-1582.
- Shirakawa Y and Kukimoto H (1980) *Journal of Applied Physics* Vol 51 (11) pp5859-5863.
- Simpson J, Adams SJA, Wang SY, Wallace JM, Prior KA and Cavenett BC. (1992) *Journal of Crystal Growth* 117 pp134-141.
- Sitter H, Heinrich H, Lischka K and Lopez-Otero A. (1982) *Journal of Applied Physics* Vol 53 (7) pp4948-4954.

- Sobiesierski Z, Dharmadasa IM and Williams RH. (1988) Applied Physics Letters Vol 53 (26) pp2623-2625.
- Sobiesierski Z, Forsyth NM, Dharmadasa IM and Williams RH. (1990) Surface Science Vol 231 pp98-102.
- Solzbach U and Richter HJ. (1980) Surface Science Vol 97 pp191-205.
- Sottomayor Torres CM, Smart AP, Watt M, Foad MA, Tsutsui K and Wilkinson CDW. (1994) Journal of Electronic Materials Vol 23 (3) pp289-298.
- Spicer WE, Chye PW, Skeath PR, Su CY and Lindau I. (1979) Journal of Vacuum Science and Technology Vol 16 (5) pp1422-1433
- Spicer WE, Lindau I, Skeath P and Su CY. (1980) Journal of Vacuum Science and Technology Vol 17 pp1019-1027
- Spicer WE, Kendelewicz T, Newman N, Chin KK and Lindau I (1986) Surface Science Vol 168 pp240-259.
- Spicer WE, Liliental-Weber Z, Weber E, Newman N, Kendelewicz T, Coa R, McCants C Mahowald P, Miyano K and Lindau I. (1988) Journal of Vacuum Science and Technology B Vol 6 pp1245-1258
- Spitzer and Mead (1963) Journal of Applied Physics Vol 24 (10) pp3061-3072
- Sullivan JP, Tung RT, Pinto MR and Graham WR (1991) Journal of Applied Physics Vol 70 (12) pp7403-7424.
- Sullivan MV and Bracht WR. (1967) Journal of Electrochemical Society Vol 114 (3) pp295-297.
- Swank RK, Aven M and Devine JZ. (1969). Journal of Applied Physics Vol 40 (1) pp89-97.
- Takebe T, Saraie J and Mtsunami H. (1982) Journal of Applied Physics Vol 53 (1) pp457-469.
- Tam NT and Chot T. (1986) Physica Status Solidi (A) Vol 91 ppK91-K95.

- Talin AA, Williams RS, Morgan BA, Ring KM and Kavanagh KL. (1994) *Journal of Vacuum Science and Technology B* vol 12(4) pp2634-2638.
- Tarricone L (1980) *Revue Physique Applications*. Vol 15 pp1617-1623.
- Tejedor C, Flores F and Louis E. (1977) *Journal of Physics C : Solid State Physics*. Vol 10 pp2163-2177.
- Tersoff J. (1984) *Physical Review Letters* 52 pp465-468.
- Tersoff J (1985) *Physical Review B* Vol 32 (10) pp6968-6971.
- Tomitori M, Ishii S, Kuriki M and Hayakawa S. (1985) *Japanese Journal of Applied Physics* Vol 24 (11) pp1488-1492.
- Trafas BM, Meyer HM, Aldao CM Siefert RL, Vos M, Xu F and Weaver JH. (1990) *Journal of Vacuum Science and Technology A* Vol 8 (3) pp2055-2061.
- Tung RT. (1991) *Applied Physics Letters* Vol 58 (24) pp2821-2823.
- Tung RT. (1992) *Physical Review B* Vol 45 (23) pp13509-13523.
- Tyagi MS and Arora SN. (1975) *Physica Status Solidi (a)* Vol 32 pp165-172.
- Ullal HS. (1992) *Proceedings of Cadmium '92*
- Van Meirhaeghe RL, van de Walle R, Laflère WH and Cardon F. (1991) *Journal of Applied Physics* Vol 70 (4) pp2200-2203.
- Van Vechten JA. (1975) *Journal of Electrochemical Society*. Vol 122 (3) pp 423-429.
- Venkatesan S, Pierret RF, Qiu J, Kobayashi M and Gunshor RL. (1989) *Journal of Applied Physics* Vol 66 (8) pp3656-3660.
- Verity D, Bryant FJ, Scott CG and Shaw D. (1982) *Journal of Crystal Growth* Vol 59 pp234-239.
- Vitomirov IM, Chang S, Brillson LJ, Rioux DF, Sivananthan S and Faurie JP. (1991) *Journal of Vacuum Science and Technology A* Vol 9 (3) pp966-971.
- Vos M, Xu F, Weaver JH nad Cheng H. (1988) *Applied Physics Letters* Vol 53 (16) pp1530-1532.

- Vos M, Xu F, Anderson SG, Weaver JH and Cheng H. (1989) *Physical Review B* Vol 39 (15) pp10744-10752.
- Vos M, Aldao CM, Aastuen DJW and Weaver JH. (1990) *Physical Review B* Vol 41 (2) pp991-994.
- Waag A, Wu YS, Bicknell-Tassius RN and Ladwehr G. (1989) *Applied Physics Letters* Vol 54 (26) pp2662-2664.
- Wagner CD, Riggs WM, Davis LE Moulder JF and Muilenberg GE (1979) "*Handbook of X-ray Photoelectron Spectroscopy*" Perkin Elmer Corporation. Minnesota, USA.
- Wang AZ, Anderson WA and Haase MA. (1995) *Journal of Applied Physics* Vol 77 (7) pp3513-3517.
- Walton RA. (1980) *Coordinate Chemistry Review* Vol 31 pp183
- Weast RC and Astle MJ (1983) Editors "*Handbook of Chemistry and Physics*" ppE78-79, 63rd Edition. CRC Press, USA
- Webb C and Lichtensteiger M (1986) *Journal of Electron Spectroscopy and Related Phenomena* Vol 41 pp125-144.
- Williams RH, Forsyth N, Dharmadasa IM and Sobiesierski Z. (1989) *Applied Surface Science* 41/42 pp189-194.
- Williams RH. (1991) *Surface Science* 251/252 pp12-21
- Williams RH (1993) *Applied Surface Science* Vol 70/71 pp386-390
- Xu F, Vos M, Weaver JH and cheng H. (1988) *Physical Review B* Vol 38 (18) pp13418-13421.
- Zanio K (1978) "*Cadmium Telluride*". in *Semiconductors and Semimetals* (Editors Willardson RK and Beer AC) Academic Press Vol 13.

Appendix 1

A1.1 Refereed publications.

1. "Ageing effects and Auger depth profiling of Sb/n-CdTe contacts."

IM Dharmadasa, CJ Blomfield , GE Gregory & J Haigh. Semiconductor Science and Technology. (1994) Vol 9 pp185-187.

2. "Influence of chemical etching on metal contacts to II-VI compounds: CdTe and ZnSe".

IM Dharmadasa, CJ Blomfield, GE Gregory, & J Young. International Journal of Electronics. (1994) Vol 76 No5 pp961-967.

3. "Microscopic and macroscopic investigations of electrical contacts to ZnSe".

IM Dharmadasa, CJ Blomfield, GE Gregory, BC Cavenett, KA Prior and J Simpson. Surface and Interface Analysis.(1994) Vol 21 pp718-723.

4. "Structural and electrical stability of metal contacts to MBE grown CdTe layers".

P Devine, GW Matthews, D Sands, CG Scott, and M Yousaf, CJ Blomfield, IM Dharmadasa and GE Gregory. Surface Science, in press.

5. "Investigation of Au/n-ZnSe contacts by ballistic electron emission microscopy."

R Coratger, F Ajustron, J Beauvillain, I M Dharmadasa, CJ Blomfield, KA Prior, J Simpson and BC Cavenett. Physical Review B Vol51 (4) pp2357-2362.

6. "Microscopic and macroscopic investigation of electrical contacts to n-type and p-type ZnSe."

IM Dharmadasa, CJ Blomfield, R Coratger, J Simpson, KA Prior, BC Cavenett. Journal of Materials Science.in press.

7. "Chemically etched CdS, CdTe and ZnSe surfaces characterised by XPS"

CJ Blomfield, IM Dharmadasa and J Haigh. Semiconductor Science and Technology in press

8. "Discrete Schottky barriers observed for the metal/n-ZnSe(100) system."

CJ Blomfield, IM Dharmadasa, KA Prior and BC Cavenett. Journal of Crystals Growth in press.

A2 Conferences attended.

Condensed Matter and Materials Physics

Sheffield UK 15-17 December 1992

Poster: "Ageing effects and Auger depth profiling of Sb/n-CdTe contacts."

IM Dharmadasa, CJ Blomfield , GE Gregory & J Haigh.

Electronic Properties of Metal/non-metal Micro Systems

Sheffield UK August 1993.

Oral: "Electrical properties of metal/non-metal microsystems: CdTe and ZnSe".

CJ Blomfield, IM Dharmadasa, GE Gregory and J Young.

European Conference on Applications of Surface and Interface Analysis.

Catania, Sicily. 4-8 October 1993

Oral: "Microscopic and macroscopic investigations of metal contacts to ZnSe".

IM Dharmadasa, CJ Blomfield, GE Gregory, BC Cavenett, KA Prior, and J Simpson.

Condensed Matter and Materials Physics

Leeds UK 20-22 December 1993

Poster: "Surface preparation, fabrication and electrical characterisation of electrical contacts to n- and p- ZnSe". IM Dharmadasa, CJ Blomfield, PM Holland and J Young.

Poster: "SIMS imaging as a tool for the study of metal/semiconductor surfaces and interfaces". GE Gregory, CJ Blomfield and IM Dharmadasa.

Poster: XPS, AES and SIMS characterisation of etched II-VI compounds and the influence of etching on subsequent metal contacts". CJ Blomfield, GE Gregory and IM Dharmadasa.

First International Conference on Materials for Microelectronics .

Barcelona, Spain 17-19 October 1994.

Oral: "Microscopic and macroscopic investigation of electrical contacts to n-type and p-type ZnSe". IM Dharmadasa, CJ Blomfield, R Coratger, J Simpson, KA Prior, BC Cavenett.

Poster: "Chemically etched CdS, CdTe and ZnSe surfaces characterised by XPS, SAM and SIMS." CJ Blomfield, GE Gregory, IM Dharmadasa.

Poster: "SIMS imaging as a tool for the study of metal/semiconductor surfaces and interfaces." CJ Blomfield, IM Dharmadasa, GE Gregory, J Haigh.

Seventh International Conference on II-VI Compounds and Devices.

Edinburgh UK. August 13-18 1995.

Poster: "Discrete Schottky barriers observed for the metal/n-ZnSe(100) system."

CJ Blomfield, IM Dharmadasa, KA Prior and BC Cavenett.